WRC RESEARCH REPORT No. 124

BUOYANT SURFACE JETS DISCHARGED INTO A STRONG CROSSFLOW

by

Chi-Yu Lin

Edward R. Holley

and

W. Hall C. Maxwell

Department of Civil Engineering

University of Illinois at Urbana-Champaign

Urbana, Illinois 61801

FINAL REPORT

Project No. B-088-ILL

This project was partially supported by the U.S. Department of the Interior in accordance with the Water Resources Research Act of 1964, P.L. 88-379, Agreement No. 14-31-0001-5071.

UNIVERSITY OF ILLINOIS
WATER RESOURCES CENTER
2535 Hydrosystems Laboratory
Urbana, Illinois 61801

April, 1977

ABSTRACT

BUOYANT SURFACE JETS DISCHARGED INTO A STRONG CROSSFLOW

Analytical and experimental investigations were carried out for three-dimensional buoyant surface jets with strong ambient flow but without boundary attachment. A numerical model in curvilinear coordinates was developed from an integral jet analysis modified for buoyancy effects and included asymmetry of the jet.

Detailed temperature distributions were measured in the laboratory with densimetric Froude numbers (F_o) of 5, 10 and 15 and velocity ratios (R) from 2 to 13. Experimental results showed that ambient crossflows can cause significant distortion of the jet, even for R = 13. Near the exit, the lower portion of the jet is swept toward the lee side of the jet. The resulting L-shaped cross section and the associated density instability may enhance spreading on the lee side and may contribute to the subsequent formation of bimodal temperature distributions. The jet bending increases as R decreases and as F_o increases. Dilution increases with increasing F_o and decreasing R.

The model was calibrated against the entire set of measured temperatures for each run and is capable of predicting temperature distributions to an accuracy of $0.63C^{\circ}$. The agreement could probably be improved by using similarity profiles better suited to the actual jet cross sectional shape which was not known at the beginning of the research.

Lin, Chi-Yu, Edward R. Holley, and W. Hall C. Maxwell
BUOYANT SURFACE JETS DISCHARGED INTO A STRONG CROSSFLOW
Final report to the Office of Water Research and Technology, Department of Interior on Matching Grant Project B-088-ILL, April 1977.

KEYWORDS: Fluid Mechanics, *Heated Water, *Mixing, Interfaces, Rivers, *Thermal Pollution, *Thermal Stratification, *Water Temperature

FOREWORD

This report is the final report for an Office of Water Research and Technology Matching Grant project entitled "Mechanics of Heated Surface Discharges to Rivers." This project was begun in July 1974, and represented part of the principal investigators' continuing research on the fluid mechanics and transport of various types of effluents, including thermal discharges. This report is essentially the same as C. Y. Lin's doctoral thesis relating to heated surface jets. Two of the appendices were not reproduced for this printing. An additional aspect of the research is presented in Appendix III.

E. R. Holley was on leave during the first year of this project, so most of the initial formulation of the research was done under the sole supervision of W.H.C Maxwell.

Special appreciation is expressed to Professor V. J. McDonald of the Department of Civil Engineering for his designing the automatic data collection system discussed in Section 4.2.6 of this report.

TABLE OF CONTENTS

Page

LIST OF TABLES

LIST OF FIGURES

LIST OF SYMBOLS

a	horizontal distance from the jet axis to the boundary of the core region
A_r	$\frac{b_o}{h_o}$; jet aspect ratio
B	outer width of the measured temperature profile
b	width of the turbulent shear region of the jet outer part
$\bar{\bar{b}}$	characteristic width of the jet (from jet axis)
b_o	total jet width at the outfall
$B_{1/2}$	distance from the point of ΔT_m to the point on the upstream side of the jet where $\Delta T = \frac{1}{2} \Delta T_{m\ell}$
b_1, b_2	constants
c	vertical distance from the jet axis to the boundary of the core region
C^o	centigrade degrees
C_B	buoyant spreading coefficient
C_D	drag coefficient
C_i	interfacial shear stress coefficient
C_V	spreading coefficient due to velocity difference
$C_1, C_2, C_3, C_4, C_5, C_6$	constants
d	lateral distance from the furthermost measurement point on the upstream side of the jet
d_m	lateral distance from the furthermost measurement point on the upstream side of the jet to the peak of the similarity profile
E	voltage

E_B entrainment coefficient for buoyant jets

E_{NB} entrainment coefficient for nonbuoyant jets

E_s entrainment coefficient of a submerged jet

E_1, E_2 output voltages in system calibration

F_d drag force

F_o $\frac{u_o}{\sqrt{\frac{\Delta\rho_o}{\rho_a} gh}}$; densimetric Froude number at the outfall

F_r $u_m / \sqrt{[(\frac{\Delta\rho}{\rho_a})gh]}$; local densimetric Froude number

$F(\Delta T)$ objective function

$F(\phi_n)$ $-3\phi_n + 9\phi_n^{\frac{5}{2}} - 5\phi_n^4$; a similarity function for lateral velocity of nonbuoyant jets

$f(\phi)$ $(1-\phi^{3/2})^{nv}$; similarity function for jet longitudinal velocity

g gravitational acceleration

h vertical height of the turbulent shear region of the jet

$\bar{h}$ characteristic jet thickness

h_o jet thickness at the outfall

h_1, h_2, h_3 metric coefficients in curvilinear coordinates

$\vec{i}_1, \vec{i}_2, \vec{i}_3$ unit vectors in s, n and z coordinate directions

K $-d\theta/ds$; curvature of jet axis

ℓ, ℓ_ℓ lateral distance from the jet axis and the point of maximum temperature of each level, respectively, with positive being toward the upstream side of the jet

L_S, L_N, L_Z length scales in the s, n, z directions

nv	an exponent used in the similarity function for velocity
nt	an exponent used in the similarity function for temperature
P	pressure
ΔP_D	scale of dynamic pressure changes
P_d	dynamic pressure
P_h	hydrostatic pressure
P_{r_t}	turbulent Prandtl number
q_e	the volume flux per unit length into the jet
Q_1	volume flux of the outer part of the jet
q_1	volume flux per unit length into the outer part of the jet
R	u_o/u_a; velocity ratio
$\vec{r}$	position vector
$R_{a_1},..R_{a_{12}},R_c,R_d,R_e,R_f$	resistors
$R_{b_1},..R_{b_{12}}$	resistors used to represent the probes
R_e	$\frac{u_m(c+h)}{\nu}$; jet Reynolds number
R_{e_o}	$\frac{u_o h_o}{\nu_o}$; Reynolds number at the outfall
R_i	$\Delta\rho gh/(\rho_a u_m^2)$; Richardson number
s	distance along the jet trajectory
T	temperature
T_a	an arbitrary but constant ambient temperature
T_{cal}	apparent temperature in system calibration
T_o	jet temperature at the outfall

T_{ref}, T_{δ}	coefficients of true calibration curve for data acquisition
$t(\phi)$	$(1-\phi^{3/2})^{nt}$; similarity function for temperature
u,v,w	velocity components in the α, β and γ, or the n, s and z directions
u_a	ambient velocity
$(u_a)_{a+b}$	the average over the depth of the jet ($0<z<-(c+h)$) of the ambient velocity at the upstream edge of the jet ($n = a+b$)
$(u_a)_{-(c+h)}$	the average over the width of the jet ($-(a+b')<n<(a+b)$) of the ambient velocity at the bottom boundary of the jet ($z = -(c+h)$)
u_c	$(u_a)_{-(c+h)} \cos \theta$
u_d	u_s or u_c, whichever is smaller
U_F	scale of the velocity fluctuations $\tilde{u}$, $\tilde{v}$, $\tilde{w}$
u_m	velocity on jet axis
u_o	jet velocity at the outfall
u_R	$(\underline{v}^2 + \underline{u}^2)^{1/2}$
u_{rel}	$u_R - u_a \cos \theta_r$; relative velocity between the jet and the ambient flow
u_s	$(u_a)_{a+b} \cos \theta$
U_S, U_N, U_Z	scale of mean velocity components, u, v, w
v_B	lateral velocity induced by buoyancy forces
v_{bd}	lateral velocity on the upstream edge of the jet
v_e	lateral entrainment velocity on the upstream side of the jet
v_f	front velocity of a density wedge

v_{NB}	lateral velocity in nonbuoyant jet
w_{bd}	vertical velocity on the jet bottom boundary
w_e	vertical entrainment velocity on the jet bottom boundary
X,Y,Z	Cartesian coordinate
ΔT	$T-T_a$; temperature excess above an arbitrary but constant reference ambient temperature (T_a)
δT	temperature standard deviation
ΔT_c	the average over the width of the jet $(-(a+b')<n<(a+b))$ of the ambient temperature rise at the bottom boundary of the jet ($z = -(c+h)$)
ΔT_d	ΔT_s or ΔT_c, whichever is smaller
ΔT_e	measured temperature excess
ΔT_F	scale of temperature fluctuations
ΔT_M	scale of mean temperature changes
ΔT_m	temperature rise on jet axis relative to reference ambient temperature
$\Delta T_{m\ell}$	maximum temperature excess at certain measurement level
ΔT_s	the average over the depth of the jet $(0<z<-(c+h))$ of the ambient temperature rise at the upstream edge of the jet ($\eta = a+b$)
α,β,γ	orthogonal curvilinear coordinates
λ	thermal expansion coefficient
Ω	gravitational potential or ohms
δ	a quantity an order of magnitude less than unity
ρ	density of the fluid

ρ_a	ambient fluid density
$\Delta\rho$	$\rho_a-\rho$; difference between the density at the point of interest and the ambient density
$\Delta\rho_o$	initial density disparity
η	water surface elevation
τ_i	component of interfacial shear stress normal to jet axis
ϕ_n	$\frac{(n-a)}{b}$ for n>a
ϕ'_n	$\frac{-(n+a)}{b'}$ for n<-a
ϕ_z	$\frac{-(c+z)}{h}$ for z<-c
θ	angle between the jet axis and x axis
θ_o	angle between discharge channel centerline and x axis
θ_r	the angle between the directions of u_R and ambient flow
ν_o	kinematic viscosity of the jet at the outfall

Superscripts:

'	refers to the inner part of the jet
-	denotes a time average
*	denotes a dimensionless quantity
~	denotes a fluctuating quantity

Subscripts:

-	denotes depth, length or cross sectional average
B	refers to buoyant value
NB	refers to nonbuoyant value
V	refers to values due to velocity difference

1. INTRODUCTION

1.1 Definition of the Problem

Demand for electric power in the United States has been approximately doubling every ten years in the past several decades. This rate of increase is expected to continue in the future. The consequence of this situation has been to increase energy production and explore the potential for energy development from many possible sources. In calendar year 1974, approximately 84 percent of the electric power produced in this country was generated by steam electric plants, which utilized either nuclear or fossil fuel [Federal Power Commission, 1975]. Since additional suitable sites for hydroelectric development are rather limited, and since on-going research to develop acceptable and economical alternative means of large-scale energy conversion is not likely to succeed in the near future, all indications are that increases in power requirements will be met in the near future primarily by steam electric plants.

As one of the consequences of the second law of thermodynamics, conversion of energy from one form to another is always accompanied by some losses. Modern fossil-fueled electric power plants can reach a thermal efficiency of approximately 38 percent by use of very high steam temperatures and high inlet pressures [Peterson et al., 1973]. Present nuclear plants operate at an even lower thermal efficiency of about 32 percent because of safety restrictions on maximum steam temperatures [Peterson et al., 1973]. This means that about 62 percent of the heat generated from fossil-fueled power plants must be wasted. In the case of nuclear power plants, about 68 percent of the total heat generated becomes waste heat.

This large amount of heat presently must be carried away by cooling water and ultimately dissipated to the atmosphere in most situations.

Because of the rapid rise in the production of electricity and the increasing number of less-efficient nuclear power plants, disposal of waste heat from thermal power plants has become a major concern in water resources. The Water Resources Council [1968] estimated that cooling water requirements will be increased from 50 trillion gallons per year in 1968 to 100 trillion gallons per year by 1980. This will comprise about one-fifth of total fresh water runoff in the continental United States. More recently, Young and Thompson [1973] forecast that by 1980, the national freshwater withdrawls for generation of electricity will range from 3.2 billion gallons per day for low economic growth rate to 177 billion gallons per day for high economic growth rate.

The cooling systems currently employed by electric power industries can be distinguished as "closed cycle" or "open cycle" depending on whether the cooling water is recycled. In a closed cycle cooling system, the waste heat is transferred to the atmosphere by radiation, evaporation, and/or conduction through the use of cooling lakes and ponds, cooling towers, and/or spray modules. In "open cycle" or "once-through" cooling, the cooling water is taken from a water body and returned to the source with higher temperature. At sites where adequate supplies of water are available, once-through cooling systems have usually been adopted by electric power industries for disposing waste heat since this method has economical advantages over the closed cycle systems. Recently, however, new EPA guidelines [Federal Register, 1974] practically prohibit once-through cooling. The guidelines make exception only in cases where it can be clearly demonstrated that there will be no adverse environmental and

ecological effects due to thermal discharges in the receiving body of water, i.e., the body into which the cooling water is discharged.

One of the crucial aspects of understanding the effects of waste heat on the environment is the accurate prediction of how much water will be affected by the waste heat and what the resulting temperature distribution will be. This prediction, in turn, depends on an understanding of the mechanisms which influence the temperature distribution and on having a predictive tool or model which represents these mechanisms. Some aspects of the models are different depending on whether the discharge is made below the water surface or at the surface. This study is concerned with surface discharge into flowing water. There are several different types of models currently being used for predicting temperature distributions resulting from surface discharges. Three of these types of models will be discussed briefly in Section 1.3. All currently available models require empirically determined coefficients in making predictions. However, before summarizing these three types of models, the general behavior of buoyant surface jets will be discussed in Section 1.2.

1.2 Physical Processes of Buoyant Surface Jets

When heated water is discharged at the surface of a body of receiving water, velocity and temperature disparities normally exist between the effluent and the ambient water. Thus, the effluent will be considered as a turbulent buoyant surface jet.

A buoyant surface jet, as its name implies, possesses buoyancy and a free surface, both of which do not exist in a submerged nonbuoyant jet. Although the relative density differences between the effluent and the ambient flow are normally very small (on the order of 0.004 gm/cc

or less), the density differences still can have a significant effect on the behavior of buoyant surface jets as compared to nonbuoyant jets. The parameter used to assess the importance of the buoyancy effect on the jet is the densimetric Froude number (F_r), which is representative of the ratio of inertial to buoyancy forces. The mathematical definition will be given in Section 2.1.2 (Eqs. 2.2-2.3). Another parameter which is frequently used is the Richardson number which is defined in Eq. 2.2.

When $F_r \to \infty$, a jet is called nonbuoyant because buoyancy forces are negligible compared with inertial forces. Another limiting case is $F_r \to 1$. This case occurs when buoyancy forces have the same order of magnitude as inertial forces. Then inertial effects of the jet behavior are almost unnoticeable and the effluent has primarily the characteristics of a density current or a buoyancy driven flow. Unless otherwise specified, the terms "buoyant jet" or "jet" will be used to refer to a jet with moderate densimetric Froude number, i.e., $1 < F_r << \infty$. It should be noted that it is not possible for a discharge from a rectangular channel to have a densimetric Froude number less than 1. If a calculated F_r less than 1 is obtained, this is an indication that cold water intrudes into the outlet canal or outlet structure and the warm water flow will adjust itself to the critical condition of $F_r = 1$ [Harleman, 1961].

Three principal flow regions can be distinguished in a buoyant surface jet. Figure 1.1 depicts the general configuration of a buoyant surface jet in a crossflow, with the various regions of the jet and the associated physical processes being indicated in the figure. The various aspects of the jet are discussed in the next three subsections which deal with the three principal flow regions. In the analytical parts of this

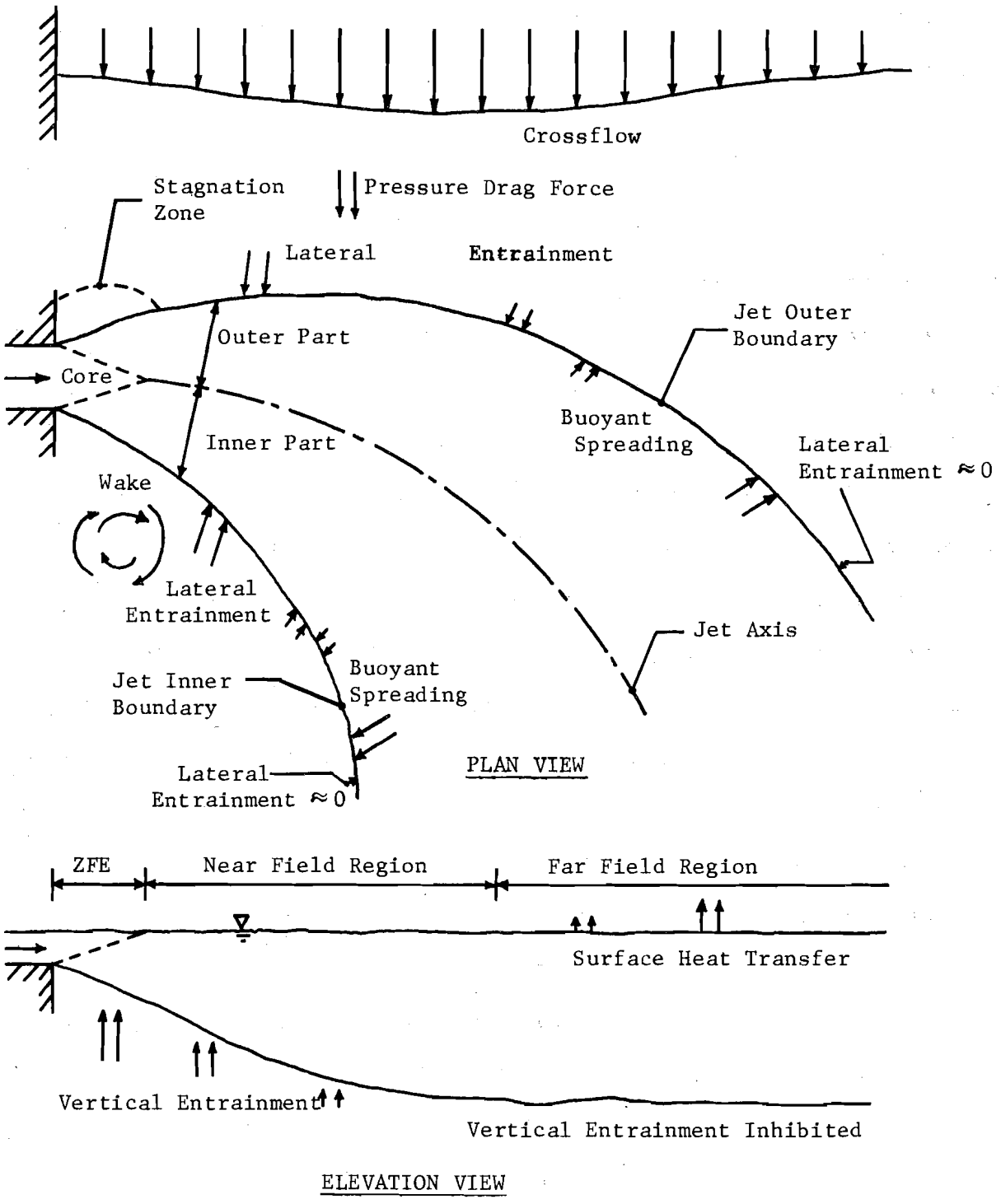

Fig. 1.1 General configuration of a buoyant surface jet

study, it is assumed that the jet does not impinge on any of the flow boundaries.

1.2.1 Zone of Flow Establishment

At the channel exit turbulence usually exists in the jet flow. The velocity distribution in the jet is usually assumed to be uniform. As the jet enters into the ambient fluid, a discontinuity of fluid velocity is created. The velocity difference between the jet and the ambient fluid creates shear which in turn generates turbulence [Dunn et al., 1975]. The turbulence is responsible for the transport of jet momentum and thermal energy and for the incorporation or "entrainment" of ambient fluid into the jet. In the immediate vicinity of the discharge outlet, unless the outlet densimetric Froude number is near unity, the jet turbulent processes are considered to be dominated by entrainment [Dunn et al., 1975].

Due to the shear and the associated turbulence, a mixing zone is created around the jet periphery. Between the mixing zone and the surface there is an undisturbed "core" region. The mixing zone grows both inward and outward with distance from the outlet and the size of the core decreases. At some distance from the outfall, the core ends and the jet centerline velocity begins to decay. Downstream of the core, the velocity profiles are often assumed to be similar. The region between the outfall and the point where the jet centerline velocity starts to decay is called the zone of flow establishment (ZFE).

Since a surface buoyant jet is warmer than the receiving water, one may also define a ZFE based on the consideration of temperature distribution. Thus the end of ZFE could be considered as the point where centerline temperature starts to decay. The turbulent diffusion coefficient

for heat is larger than eddy viscosity in buoyant jets [Policastro and Tokar, 1972]. As a consequence, the length of the ZFE is shorter if the definition is based on the temperature distribution rather than the velocity distribution. However, for convenience it is usually assumed that both velocity and temperature start to decay at the same point.

For the case of discharge into a crossflow, the effluent will be deflected in the downstream direction of the ambient flow both due to entrainment of momentum from the crossflow and due to the net pressure force on the effluent jet. The jet trajectory depends primarily on the velocity ratio R which is the ratio of initial jet velocity to the average ambient velocity. For low velocity ratios the bending of the jet in the ZFE can be significant.

In addition to causing the bending of the jet trajectory, the crossflow is also responsible for the creation of a stagnation zone on the upstream side of the jet and a wake on the lee side as shown in Fig. 1.1. Both the stagnation zone and the wake may extend beyond the ZFE and into the next region.

1.2.2 Near Field Region

The next region beyond the end of the ZFE is called the near field region (NFR). Here the effluent is influenced significantly by both the inertial forces and buoyancy forces. The velocity profiles and temperature profiles are often each assumed to be self-similar. In the initial portion of the NFR, both velocity and temperature excesses are still relatively large for moderate or large initial Froude numbers, but the jet is gradually dissipated primarily due to the entrainment of the ambient fluid. The end of the NFR and the beginning of the far field

region (Section 1.2.3) is defined as the point where the jet velocity excess (i.e., the difference between the maximum jet velocity (u_m) and the component of the ambient velocity parallel to the jet axis ($u_a \cos \theta$, where u_a is the ambient velocity and θ is the angle between u_a and the jet trajectory)) is practically dissipated so that the jet-like behavior ceases; however, the density gradients may still be significant and the effluent may not have aligned with the ambient flow (Section 1.2.3).

Buoyancy plays an important role in the NFR. On the one hand it causes an unbalanced hydrostatic pressure distribution around the jet boundary and this in turn causes lateral buoyant spreading; on the other hand it generates stable vertical density gradients which suppress turbulence and inhibit vertical entrainment.

The interaction of jet and crossflow is one of the most complicated and least understood problems in the dynamics of jets. Besides causing the bending of jet trajectory and the formation of a wake and a stagnation zone (Section 1.2.1), the crossflow may significantly distort the jet cross section (Figs. 5.1-5.4) and the common assumption of similarity for velocity and temperature distributions may not be valid.

1.2.3 Far Field Region

This research relates to the ZFE and the NFR. However, for the sake of completeness, a brief discussion is given here of the far field region (FFR) which is downstream of the NFR. Depending on the characteristics of both the jet at the outfall and the ambient flow, a maximum of four types of effluent conditions can exist at the beginning of the FFR. Since the end of the NFR is defined on the basis of the dissipation of the (magnitude of) excess velocity (i.e., $u_m \approx u_a \cos \theta$), the four possible

conditions at the beginning of the FFR are (1) density gradients are small and the effluent has already bent over and aligned with the ambient flow, (2) density gradients are small but the effluent has not yet aligned with the ambient flow, (3) density gradients are still significant but the effluent has already aligned with the ambient flow, and (4) density gradients are still significant and the effluent has not aligned with the ambient flow. It is not clear whether all of these four conditions are physically possible.

The first type of condition (i.e., small density gradients and the effluent aligned with the ambient flow) usually occurs when jets are discharged with high F_o and large R. The ambient velocity field in the FFR is practically undisturbed by the presence of the effluent. Ambient turbulent diffusion, ambient advection and surface heat loss are then the three primary mechanisms responsible for the transport of the excess heat of the effluent [Adams et al., 1975]. Most of the models for the far field region are concerned with this situation [Policastro and Paddock, 1972]. (See Section 1.3.2.)

For the second and fourth types of effluent conditions at the beginning of the FFR, the velocity excesses are dissipated ($u_m \approx u_a \cos \theta$) before the effluent becomes aligned with the ambient flow (i.e., before θ becomes zero). Then the effluent may actually be accelerated in the initial portion of the FFR because the maximum effluent velocity (u_m) must approach the ambient velocity (u_a) when the effluent is aligned with the ambient flow. This phenomenon is mathematically possible and is observed in the numerical model, but it is not clear whether it is physically possible. It is also not clear whether the third type of condition can actually occur.

1.3 Mathematical Models

The continuity equation, momentum equations, thermal energy conservation equation and equation of state constitute the basis of a mathematical model for thermal discharges. Due to the complexities of turbulent flow, those equations are impossible to solve in their exact, instantaneous forms. Some assumptions must be made in order to obtain a set of simplified governing equations which can be solved.

Numerous mathematical models for buoyant surface jets have been developed during the past ten years (1967-1977). Many of the models have been summarized by Policastro and Tokar [1972], Dunn et al. [1975], Jirka et al. [1975]. Some models were developed for a specific region by considering only the predominant factors affecting the transport of heat and momentum in that region. Others were derived in an attempt to predict the velocity and temperature distributions throughout the entire flow field.

There are three principal types of mathematical models for surface buoyant jets, namely, integral jet models, ambient diffusion models and three-dimensional numerical models. Only a brief discussion of each type of model will be presented here. More complete discussions of mathematical models can be found in reviews by Policastro and Tokar [1972], Dunn et al. [1975] and Jirka et al. [1975].

1.3.1 Integral Jet Models

Some concepts and techniques used in integral analysis of a buoyant surface jet are adapted directly from the nonbuoyant jet theory. The governing equations for the buoyant surface jets are first simplified

based on some assumptions such as hydrostatic pressure distribution, Boussinesq approximation for small density differences, fully turbulent jet flow, etc. (See Section 3.1.1.) Similarity functions for velocity and temperature distributions are then introduced into the simplified governing equations which subsequently are integrated over the cross section normal to the jet axis to yield a set of ordinary differential equations. In the model development, either entrainment or jet spreading concepts must be used to ensure a closure relation of governing equations (Jirka et al., 1975). The buoyancy effects may be incorporated into the model through the pressure-gradient terms in the momentum equations and through the considerations of buoyant spreading and the reduction of vertical entrainment (or spreading) due to density differences.

Solutions can be obtained for integral jet models with relatively much less time and expense than that required for other types of models. Some limitations of the integral jet models are (1) that they are generally valid only in the near field region, although some attempts with varying degrees of success have been made to include buoyant spreading in integral jet models, (2) that only a gross jet behavior can be obtained and (3) that it is difficult with the present models to handle boundary conditions such as unsteady ambient flow conditions and jet attachment to a solid boundary. Such limitations come mainly from the fact that in an integral approach, many physical phenomena are not actually simulated, but rather are either lumped into the entrainment, jet spreading or drag concepts or are marked by the use of similarity functions and by integration over the cross section. Because of these inherent simplifications, integral models will apparently always have definite limitations, but on the other hand,

integral models are relatively inexpensive to use and can provide useful information if the model limitations are recognized.

1.3.2 Ambient Diffusion Models

If the initial momentum and buoyancy of the effluent are either negligible or have been dissipated, the heat can be treated as a passive tracer. Then ambient turbulence, ambient advection and surface heat transfer are the primary factors influencing the transport of heat (Section 1.2.3). Models to represent these factors are called ambient diffusion models [Senshu and Wada, 1965; Edinger and Polk, 1969; Koh and Fan, 1970] and are based on the thermal energy conservation equation which is uncoupled from the hydrodynamic equations and solved by using a measured or assumed ambient velocity distribution.

Ambient diffusion models assume that transport of heat due to turbulent velocity fluctuations can be represented by eddy diffusion terms. Successful modeling hinges on the accurate specification of eddy diffusion coefficients which are functions of flow conditions. Thus the selection of those coefficients can represent a considerable problem for ambient diffusion models.

Another significant problem with the ambient diffusion models lies in the difficulty of specifying the upstream thermal boundary conditions. One way to overcome this difficulty is to subdivide the model into two parts using an ambient diffusion model in the downstream part and an integral jet model in the upstream part. The calculations from the integral model then give the upstream boundary condition for the ambient diffusion models. This, of course, is an approximation, but has been

found to be a useful approximation for some problems when judiciously applied [Jirka et al., 1975].

1.3.3 Three-dimensional Numerical Models

Some models have been developed to solve numerically the governing three-dimensional partial differential equations for the entire flow field. Usual simplifying assumptions utilized in the development of a three-dimensional numerical model include the hydrostatic assumption, rigid lid approximation for the free water surface [Dunn et al., 1975; Jirka et al., 1975] and the use of eddy viscosity and eddy diffusivity concepts. The simplified partial differential equations are transformed into finite difference forms and solved numerically. Some of the presently available three-dimensional numerical models are the ones developed by Waldrop and Farmer [1974], Paul and Lick [1974] and Rastogi and Rodi [1975], among others.

The possibility that three-dimensional numerical models can include and simulate complexities of the physical fluid flow phenomena is an advantage over other types of models. For example, in three-dimensional numerical models, unsteady ambient flow conditions and complicated boundary geometries can be handled. Also, the zone of flow establishment and the near field and far field regions can be all included in one model, and detailed hydrothermal prediction is possible. However, the use of these models is often hampered by disadvantages such as the difficulty involved in the specification of boundary conditions for velocity and pressure, uncertainty as to the choice of eddy diffusion coefficients for both energy and momentum, the need for several empirical relationships for various aspects of the flow structure, and enormous computational effort.

In fact, Jirka et al. [1975] concluded from their assessment of techniques for hydrothermal prediction that at the stage of development at that time, three-dimensional numerical models appeared highly unsatisfactory. Hence they recommended that only integral jet models be used for the prediction of temperature distributions in the near field region. Probably, improved speed and efficiency of computers will make three-dimensional numerical models more practical in the future.

1.4 Objectives of this Study

The objectives of this study are as follows:

1. to develop a three-dimensional integral jet model for the prediction of temperature distributions in the near field region for heated effluents discharged horizontally at the surface of channel flows where spatially dependent velocity and temperature fields may exist and where the velocity ratios are in the range of approximately 2 to 15 so that ambient velocity is not negligible.
2. to conduct laboratory experiments to investigate the ability of the model to predict temperature distributions.
3. to use the laboratory data to calculate one drag and two spreading coefficients in the model.

2. REVIEW OF PREVIOUS STUDIES

Considerable work on the mechanisms and modeling of heated discharges was reviewed by Krenkel and Parker [1969], Silberman and Stefan [1970], Policastro and Paddock [1972], and Benedict et al. [1974]. Several mathematical models for predicting the behavior of buoyant surface jets have also been critically reviewed by Policastro and Tokar [1972], Dunn et al. [1975] and Jirka et al. [1975]. In view of these previous reviews and an almost prohibitively large amount of literature on the subject of heated discharges, no attempt is made here to cover all of the related references. Rather, only those which contain material particularly relevant to this study will be discussed in order to establish some background for the present investigation. It is assumed that the reader is familiar with the basic concepts of turbulent jets as discussed, for example, by Albertson et al. [1950] and Abramovich [1963], and with the integral method of analyzing jet flows as discussed, for example, by Abraham [1965] and Fan [1967].

2.1 Entrainment

2.1.1 Entrainment Concept

Abraham [1972] has demonstrated for jet diffusion theory that the number of available equations based on conservation relationships is always exceeded by the number of unknown quantities for turbulent flow. This is the major obstacle in the analysis of jet problems. To obtain a closed system of equations, the rate of entrainment may be specified. Morton et al. [1956] applied the entrainment concept and integral technique

to analyze the spreading and dilution of a simple plume in a stratified environment. They proposed that the rate of entrainment was proportional to a characteristic velocity in the plume. This classic concept of entrainment can be expressed equivalently as

$$v_e = E_S u_m \tag{2.1}$$

where v_e is the entrainment velocity on the edge of the plume, E_S is the entrainment coefficient and u_m is the plume centerline velocity.

The entrainment concept has been adapted and extended to more complicated submerged jet cases by many investigators [Fan, 1967; Platten and Keffer, 1968; Hoult et al., 1969; Fox, 1970; Hirst, 1971, 1972a]. A detailed review on the entrainment mechanisms of submerged jets was given by Chan and Kennedy [1972].

It has been shown for two-dimensional pure plumes [Jirka et al., 1975] and for three-dimensional nonbuoyant jets with no curvature [Stolzenbach and Harleman, 1971] that there exists a linear relationship between the entrainment coefficient and spreading coefficient (Section 3.8.2.1). Thus entrainment and spreading concepts are in fact functionally equivalent. To achieve the closure of the governing equations (Section 3.8) either one of the concepts may be used.

2.1.2 Lateral and Vertical Entrainment

The entrainment concept has also been used extensively with some modification for buoyant surface jets. One single entrainment function (which may have one or more than one entrainment coefficients) is usually employed to characterize the entrainment process of submerged jets. However, for heated surface discharges, it is necessary to divide the entrainment process into two parts, namely, lateral entrainment and

vertical entrainment. Ellison and Turner [1959] conducted a series of laboratory experiments on the vertical entrainment of two-dimensional buoyant surface jets. They found that as the bulk Richardson number increased from approximately zero to more than about 0.8, entrainment decreased rapidly from the value observed in homogeneous fluids to almost zero. Here the bulk Richardson number is defined as

$$R_i = \frac{(\Delta\underline{\rho} g h)}{(\rho_a \underline{u}^2)} \tag{2.2}$$

where R_i = bulk Richardson number,

$\underline{u}$ = average local jet velocity,

ρ_a = ambient fluid density,

$\Delta\underline{\rho}$ = average local density difference between jet and ambient fluid,

h = local jet thickness.

The bulk Richardson number R_i is related to the densimetric Froude number $F_r=(\underline{u}/\sqrt{(\Delta\underline{\rho}/\rho_a)gh})$ by

$$R_i = \frac{1}{F_r^2} \tag{2.3}$$

Thus a significant feature of vertical entrainment is that it is suppressed by the presence of a stable density difference.

Work on the problem of buoyant surface jets discharged into a flowing ambient stream has been done by Hoopes et al. [1968], Motz and Benedict [1970], Stolzenbach and Harleman [1971], Prych [1972], Shirazi and Davis [1974] and Adams et al. [1975], among others. The entrainment concept was used by all of those investigators in one form or the other. Hoopes et al. [1968] neglected vertical entrainment and assumed that

entrainment came only from the two sides of the jet. They related entrainment solely to the jet centerline velocity. This approach is applicable when R_i is large enough that the vertical entrainment is suppressed and when there is no ambient flow or when the centerline velocity at any cross section in the jet is an order of magnitude greater than the ambient velocity [Policastro and Tokar, 1972]. Motz and Benedict [1970] also considered only lateral entrainment and assumed that the entrainment velocity was proportional to the scalar difference between the jet centerline velocity and the component of crossflow velocity parallel to the jet trajectory. The models developed by Hoopes et al. [1968] and Motz and Benedict [1970] are called two-dimensional models in that the jet thickness is assumed constant and the jet can grow only in two lateral directions, as contrasted with three-dimensional models in which the jet is allowed to spread in all three directions.

Stolzenbach and Harleman [1971] were among the first to take vertical entrainment into account. Most of the models developed subsequently by other investigators, for example, Prych [1972] and Adams et al. [1975], among others, have also considered vertical entrainment. Since the vertical entrainment function used by these three-dimensional jet models were all derived from the same source of data, only Stolzenbach and Harleman's [1971] model will be discussed.

Stolzenbach and Harleman [1971] considered both the lateral and vertical spreading of the heated surface jets discharged into a crosscurrent. First, using a similarity profile for the velocity distribution and using the experimental nonbuoyant jet spreading formula from Abramovich [1963], they solved the nonbuoyant jet case with no crossflow. This allowed the calculation of lateral entrainment coefficients, which

were then applied in the buoyant jet case based on the assumption that the buoyant jet lateral entrainment was not affected by buoyancy forces. To account for the reduction of vertical entrainment due to density differences, they used

$$\frac{E_B}{E_{NB}} = \text{EXP}\ \left(\frac{-5}{F_r^2}\right) \tag{2.4}$$

where E_B = vertical entrainment coefficient of buoyant jets,

E_{NB} = lateral or vertical entrainment coefficient of nonbuoyant jets.

Equation 2.4 was derived from the experimental data of Ellison and Turner [1959] for two-dimensional buoyant jets. With the lateral and vertical entrainment coefficients available, Stolzenbach and Harleman [1971] defined the entrainment velocity as being equal to the entrainment coefficient times the jet centerline velocity. As mentioned before, this definition is considered valid only for low ambient velocity.

2.1.3 Evaluation of Entrainment Coefficient

Using the entrainment concept to lump complex turbulent processes into a gross entrainment function has made the solution of many buoyant jet problems easier. However, a primary question arises as to the choice of the appropriate value of entrainment coefficients. These coefficients are commonly determined by fitting a model to laboratory and/or field data, hoping that the values of the coefficients obtained in this way are universal. Unfortunately no universal entrainment coefficient for surface discharges into a crossflow has yet been found.

Often a model may contain some other empirical coefficients such as drag coefficient (Section 2.4), buoyant spreading coefficient (Section 3.8.2.2), shear stress coefficient, etc., in addition to entrainment coefficient. If this is the case, one would expect that all of the coefficients are interrelated and that they should be determined simultaneously. However, no buoyant surface jet model was found which had ever had the coefficients determined in this way. Instead, evaluation of the coefficients was usually performed by fitting the model to determine one coefficient at a time while holding others at fixed constant values. This procedure may be incorrect, because the empirical coefficients normally used may not be independent of each other.

2.2 Buoyant Spreading

2.2.1 Difficulties in Modeling Buoyant Spreading

There are basic difficulties in representing buoyant spreading in an integral jet model. These problems stem from the fact that an integral model is based on the conservation of the total volume, momentum, and heat fluxes at each cross section and that this type of model was originally conceived and developed for turbulent jets. All attempts (including the present one) to include buoyant effects in integral jet models have taken the approach of modifying the established type of integral analysis. This type of modification may be valid when the buoyancy produces minor changes in the turbulent mixing and spreading patterns. However, it would appear that the presently used types of buoyancy-modified integral models have little hope of providing a high degree of accuracy in regions where the buoyant forces play a dominant role in the flow. When this condition is

reached, the effluent is in fact no longer a jet and there is really no reason to expect a modified jet model to be applicable. Thus, it should be expected that an integral analysis applied to a buoyant surface jet will probably be useful only in the region between the outlet and the section at which density forces start to play a dominant role. Downstream of this section, an analysis based primarily on density currents rather than primarily on turbulent jet behavior would probably be more reasonable.

2.2.2 Total Lateral Spreading

The normal approach for the inclusion of buoyant spreading in the total spreading is to let the lateral spreading be separated into buoyant (subscript B) and nonbuoyant (subscript NB) components as shown by the following equation [Stolzenbach and Harleman, 1971; Stefan et al., 1971; Prych, 1972; Shirazi and Davis, 1974; Adams et al., 1975]:

$$\frac{d\bar{\bar{b}}}{ds} = \frac{d\bar{\bar{b}}}{ds}\Big|_B + \frac{d\bar{\bar{b}}}{ds}\Big|_{NB} \tag{2.5}$$

where $\bar{\bar{b}}$ = characteristic width of the jet (from jet axis),

s = distance along the jet trajectory,

and $d\bar{\bar{b}}/ds$ = the rate of increase of jet width.

Here the total jet lateral spreading is assumed to be due to two independent components. This assumption ignores the fact that the interaction between entrainment and buoyancy is in fact nonlinear [Dunn et al., 1975]. Dunn et al. [1975] pointed out that Eq. 2.5 was probably valid only when one component was much larger than the other. Despite those discrepancies, Eq. 2.5 appears to be the primary formula which has been used for representing the combined effects of buoyant and nonbuoyant spreading. An

expression similar to Eq. 2.5 is also normally used for spreading in the vertical direction. Any attempt to improve Eq. 2.5 must be based on a more complete understanding than is presently available for the complex physical processes responsible for jet spreading.

The nonbuoyant component $d\bar{\bar{b}}/ds|_{NB}$ in Eq. 2.5 may be treated either from the entrainment concept or the spreading concept (Section 2.1.1). Examples of formulations of $d\bar{\bar{b}}/ds|_{B}$ from past work are presented in the next section.

2.2.3 Buoyant Spreading Formulations

Several buoyant spreading formulations have been proposed. Three examples of those formulations are the ones used by Stefan et al. [1971]:

$$\frac{d\bar{\bar{b}}}{ds}\Big|_B = \frac{C_1}{F_r} \tag{2.6}$$

by Prych [1972]:

$$\frac{d\bar{\bar{b}}}{ds}\Big|_B = \frac{C_2}{\sqrt{F_r^2-1}} \tag{2.7}$$

and by Shirazi and Davis [1974]:

$$\frac{d\bar{\bar{b}}}{ds}\Big|_B = \frac{C_3}{\sqrt{F_r^2 \frac{\bar{\bar{b}}}{\bar{\bar{h}}} - 1}} \tag{2.8}$$

where C_1, C_2, C_3 = constants,

F_r = local densimetric Froude number,

$\bar{\bar{h}}$ = characteristic jet thickness.

Equations 2.6, 2.7 and 2.8 were all derived from assuming that the buoyant spreading could be analyzed as the unsteady motion of a density wedge. Stefan et al. [1971] and Prych [1972] assumed that in a density wedge the pressure forces induced by density differences were balanced by hydrodynamic drag due to both shear and added mass effects [Koh and Fan, 1970; Adams et al., 1975; Dunn et al., 1975]. Based on this assumption, the the continuity equation and momentum equation could be solved to yield the front velocity (v_f) of a density wedge

$$v_f = C_4 \left(\frac{\Delta\rho g h}{\rho_a}\right)^{1/2} \tag{2.9}$$

where g = gravitational acceleration,

h = depth of a density wedge,

ρ_a = ambient density,

$\Delta\rho$ = density disparity between the density wedge and ambient fluid,

and C_4 = constant.

Using Eq. 2.9 and further assuming that in a jet the buoyant spreading occurred in the direction normal to the jet axis, Stefan et al. [1971] derived Eq. 2.6. Prych [1972] also used Eq. 2.9 to obtain Eq. 2.7, but unlike Stefan et al. [1971], he assumed that the jet buoyant spreading occurred in the direction normal to the jet boundary [Jirka et al., 1975].

Equation 2.7 shows that $d\bar{\bar{b}}/ds\big|_B \to \infty$ as $F_r \to 1$. This behavior is responsible for the prediction of excessive jet widths as F_r approaches unity. In view of this shortcoming, Shirazi and Davis [1974] modified Eq. 2.7 by the use of the following spreading velocity of a density wedge:

$$v_f = C_5 \left(\frac{\Delta\rho g h}{\rho_a}\right)^{1/2} \left(\frac{\bar{\bar{h}}}{\bar{\bar{b}}}\right)^{1/2} \tag{2.10}$$

where C_5 = constant and h = average thickness of the jet. Shirazi and Davis [1974] reasoned that the introduction of the factor $(\bar{\bar{h}}/\bar{\bar{b}})^{1/2}$ for the front velocity of a density wedge was to account for the effects of interfacial resistance to the lateral buoyant spreading. This resistance is important far away from the source [Koh and Fan, 1970]. This modification yielded Eq. 2.9 which gave improved predictions in most cases [Dunn et al., 1975]. However, the choice of $(\bar{\bar{h}}/\bar{\bar{b}})^{1/2}$ was based purely on physical reasoning. Since it lacked theoretical basis, it must therefore be considered somewhat arbitrary [Dunn et al., 1975; Jirka et al., 1975]. This point is considered further in Section 3.8.2.2.

2.3 Similarity Profiles

2.3.1 Validity of Similarity Profiles

The use of similarity functions to represent distributions of velocity excess and temperature disparity in the cross sections of the jets provides considerable simplification for the solution of jet problems when the integral approach is used. For submerged buoyant [Rouse et al., 1952] or nonbuoyant [Albertson et al., 1950] jets with no crossflow, it has been shown experimentally that the velocity profiles and temperature profiles are self-similar and are approximately Gaussian in form. However, for buoyant surface jets discharged into a crossflow, several factors (e.g. the presence of a free-surface boundary, the nonuniform pressure field, and the unequal rates of entrainment around the periphery of the jet cross section) may cause the usual assumption of similarity for velocity and temperature not to be valid, particularly when the crossflow velocity is of the same order of magnitude as the jet velocity. Carter [1969] performed laboratory

experiments on heated, vertical slot jets discharged perpendicular to a crossflow. He observed that the velocity and temperature profiles were not symmetrical about the jet axis (i.e. about the trajectory of maximum temperature). On the downstream side there was a recirculating eddy. The temperature in the eddy was approximately constant and was higher than the ambient temperature. On the upstream side, the velocity and temperature profiles approximated half of bell-shaped or Gaussian distributions. The asymmetrical velocity and temperature profiles and the recirculation phenomenon have also been observed by Carter et al. [1973] in the experiments of three-dimensional buoyant surface jets discharged into a crossflow.

Except for the model developed by Adams et al. [1975], none of the existing buoyant surface jet models considered the asymmetry of the velocity and temperature profiles. Adams et al. [1975] considered the jet to be asymmetrical only for that portion of the jet where bottom boundary attachment occurred.

2.3.2 Examples of Similarity Profiles

The most popular similarity profile is apparently the Gaussian distribution [Hoopes et al., 1968; Motz and Benedict, 1970; Stefan et al., 1971; Prych, 1972; Shirazi and Davis, 1974]. A "tophat" profile has also been used by several investigators [Carter, 1969; Sill, 1973; Adams et al., 1975]. Stolzenbach and Harleman [1971] used the following similarity function for velocity:

$$f(\phi) = (1-\phi^{3/2})^2 \tag{2.11}$$

where ϕ is the nondimensional lateral or vertical distance from the boundary of core region or from the jet axis in the case the cross section

is not in the ZFE. The function f, which is due to Schlichting [1968], has been used extensively by Abramovich [1963] for submerged nonbuoyant jets and has the advantage that it gives a definite jet boundary at $\phi = 1$ as contrasted with a Gaussian distribution which approaches zero asymptotically.

To describe the off-axis decay of temperature in the turbulent shear region, Stolzenbach and Harleman [1971] chose the following similarity function

$$t(\phi) = 1-\phi^{3/2} \tag{2.12}$$

Implicit in the use of Eqs. 2.11 and 2.12 is the assumption that turbulent Prandtl number (P_{r_t}) is equal to 1/2. According to Reichardt [1942], the turbulent Prandtl number (P_{r_t}) for a heated two-dimensional jet is equal to 1/2 and is greater than 1/2 for three-dimensional jets [Corrsin and Uberoi, 1950]. Thus the use of the above two functions is justified for the portion of the jet where the width of the jet is much larger than the depth. However, for the portion of the jet where the width and depth of the jet are of the same order of magnitude, the similarity functions used by Stolzenbach and Harleman [1971] may be inappropriate.

2.4 Pressure Drag Force

2.4.1 Primary Approaches

A jet discharged into a crossflow will be deflected in the direction of the crosscurrent both due to the entrainment of ambient longitudinal momentum and due to the pressure drag force [Fan, 1967]. The classical approach [Abramovich, 1963; Vizel and Mostinskii, 1965; Epshtein, 1965 and Shandorov, 1966, among others] for analyzing jet deflection is to

regard the jet as an obstruction in the flow and to examine the forces exerted on the jet by the stream. In the studies cited above, the deflection of submerged, nonbuoyant jets was considered to be due solely to the pressure drag force acting on the jet. The contribution due to entrainment of crossflow momentum was not included. A refinement of this approach was made by Fan [1967] who included entrainment as well as the pressure drag force in the momentum equation in his study on the submerged axisymmetrical buoyant jets discharged into flowing ambient fluids.

2.4.2 Various Definitions of Drag Force

For surface discharges, the jet may be regarded as an obstruction in the ambient flow as in the submerged case. Several representations of the pressure drag force have been proposed for buoyant surface jets. Carter [1969] assumed the drag force to be given by

$$F_d = \frac{1}{2} C_D \rho_a u_a^2 h \tag{2.13}$$

where ρ_a = ambient density,

u_a = ambient velocity,

h = jet thickness,

and C_D = drag coefficient.

He estimated the drag coefficient C_D from Rouse's [1957] pressure distribution on the boundary of an air jet. The results showed that C_D could be expressed as a function of velocity ratio R where $R = u_o/u_a$. Motz and Benedict [1970], on the other hand, defined the pressure drag force on the jet as

$$F_d = \frac{1}{2} C_D \rho_a u_a^2 \sin\theta\, h \tag{2.14}$$

where θ is the angle between the jet centerline and ambient current. They

also considered C_D as a function of R only. The values of C_D were determined from their experimental data.

Prych [1972] assumed that the pressure drag could be represented by the formula for form drag on a solid body [Daily and Harleman, 1966]:

$$F_d = \frac{1}{2} C_D \rho_a (u_a \sin \theta)^2 h \qquad (2.15)$$

where $u_a \sin \theta$ is the component of ambient velocity normal to the jet axis.

The diversity in the definitions of drag force is caused by the fact that different investigators use different forms of characteristic velocity. Prych [1972] defined the characteristic velocity as $u_a \sin \theta$ whereas Motz and Benedict [1970] assumed it to be $u_a \sqrt{\sin \theta}$. For these two forms the drag force approaches zero when the jet trajectory is parallel to the ambient current. Carter [1969] chose u_a as the characteristic velocity in order to obtain a behavior observed in his experiments. With vertical slot jets discharged perpendicular to a crossflow, he observed that the jet curved back toward the near shore. The use of u_a as the characteristic velocity provided a mathematical mechanism to return the jet trajectory to the near shore. The actual mechanism is a trapped vortex in the wake of the jet [Sawyer, 1960; Stoy et al., 1973].

The case of small crossflow velocity considered by Stolzenbach and Harleman [1971] and by Adams et al. [1975] implies that there is no significant pressure force on the jet (except for the case considered by Adams et al. [1975] of a jet attached to a boundary). Thus only entrainment is responsible for deflecting the jet. This condition will no longer exist if the ambient velocity is sufficiently large.

3. ANALYTICAL DEVELOPMENT

The analytical development considers a three-dimensional heated water jet discharged from a rectangular open channel at the surface of a flowing ambient stream. The ambient flow may have a spatially dependent velocity and temperature field but is assumed to have a uniform density. The analysis is developed from the basic equations of heat, mass and momentum conservation to a set of integrated equations which are solved numerically.

The procedure in simplifying the governing equations and the assumption of jet similarity profiles generally follow the framework established by Stolzenbach and Harleman [1971]. Based on the assumption of hydrostatic pressure distribution, the effects of buoyancy are incorporated through the pressure-gradient terms in the longitudinal and lateral momentum equations. Further incorporation of buoyancy effects in the lateral direction is achieved through the consideration of buoyant spreading. The progression from the nonbuoyant jet to the buoyant case is considered in the simplification of the governing equations by an order of magnitude analysis. The jet cross section is assumed to be rectangular and is divided into several regions in order to facilitate the direct inclusion of the ZFE in the analytical modeling.

In addition to the above procedures that follow the work by Stolzenbach and Harleman [1971], in the present study the model is formulated in curvilinear coordinates and the simplification of the governing equations includes the consideration of the progression from the no curvature (no crossflow) case to the case of significant curvature of the jet axis (or the significantly bent case). To obtain a

closed system of equations, the jet spreading concept is employed. The incorporation of buoyancy effects in the vertical direction is accomplished through the use of the spreading concept rather than the entrainment concept. The consequences of strong ambient currents, including the significant jet curvature, the pressure drag forces acting on the jet, the unequal lateral spreading on the two sides of the jet and the asymmetry of velocity and temperature profiles in the jet are also incorporated into the model. Assumptions of boundary conditions between regions are not necessary in the present study since all variables are continuous and the integration of governing equations may be performed directly over the entire jet cross section instead of region by region as done by Stolzenbach and Harleman [1971].

3.1 Governing Equations

3.1.1 Basic Assumptions

The basic assumptions of the analysis are:

1. The flow is steady.
2. The fluids are incompressible.
3. Specific heat is constant.
4. The jet is fully turbulent after the zone of flow establishment. This assumption implies that the jet Reynolds number is large. Thus, viscous terms and molecular diffusion terms are negligible.
5. The Boussinesq assumption of small density differences applies. Thus, variations in density are neglected in inertial terms but included in gravity terms. This assumption

also implies that density changes are linearly proportional to temperature changes.

6. The jet has positive buoyancy.

3.1.2 Governing Equations in Orthogonal Curvilinear Coordinates

With the above assumptions, the basic equations of mass, momentum and thermal energy conservation in general orthogonal curvilinear coordinates are [Rouse, 1965]:

continuity equation

$$\frac{1}{h_1 h_2 h_3}\left[\frac{\partial}{\partial\alpha}(uh_2h_3) + \frac{\partial}{\partial\beta}(vh_3h_1) + \frac{\partial}{\partial\gamma}(wh_1h_2)\right] = 0 \tag{3.1}$$

momentum equation in α-direction

$$\frac{u}{h_1}\frac{\partial u}{\partial\alpha} + \frac{v}{h_2}\frac{\partial u}{\partial\beta} + \frac{w}{h_3}\frac{\partial u}{\partial\gamma} + \frac{uv}{h_1h_2}\frac{\partial h_1}{\partial\beta} + \frac{uw}{h_1h_3}\frac{\partial h_1}{\partial\gamma} - \frac{v^2}{h_1h_2}\frac{\partial h_2}{\partial\alpha}$$

$$- \frac{w^2}{h_1h_3}\frac{\partial h_3}{\partial\alpha} = -\frac{1}{h_1}\frac{\partial}{\partial\alpha}\left(\frac{P}{\rho} + \Omega\right) \tag{3.2}$$

momentum equation in β-direction

$$\frac{u}{h_1}\frac{\partial v}{\partial\alpha} + \frac{v}{h_2}\frac{\partial v}{\partial\beta} + \frac{w}{h_3}\frac{\partial v}{\partial\gamma} + \frac{vw}{h_2h_3}\frac{\partial h_2}{\partial\gamma} + \frac{uv}{h_1h_2}\frac{\partial h_2}{\partial\alpha} - \frac{w^2}{h_2h_3}\frac{\partial h_3}{\partial\beta}$$

$$- \frac{u^2}{h_1h_2}\frac{\partial h_1}{\partial\beta} = -\frac{1}{h_2}\frac{\partial}{\partial\beta}\left(\frac{P}{\rho} + \Omega\right) \tag{3.3}$$

momentum equation in γ-direction

$$\frac{u}{h_1}\frac{\partial w}{\partial\alpha} + \frac{v}{h_2}\frac{\partial w}{\partial\beta} + \frac{w}{h_3}\frac{\partial w}{\partial\alpha} + \frac{vw}{h_2h_3}\frac{\partial h_3}{\partial\beta} + \frac{uw}{h_1h_3}\frac{\partial h_3}{\partial\alpha} - \frac{u^2}{h_1h_3}\frac{\partial h_1}{\partial\gamma}$$

$$- \frac{v^2}{h_2h_3}\frac{\partial h_2}{\partial\gamma} = -\frac{1}{h_3}\frac{\partial}{\partial\gamma}\left(\frac{P}{\rho} + \Omega\right) \tag{3.4}$$

equation of thermal energy conservation

$$\frac{1}{h_1 h_2 h_3}\left[\frac{\partial}{\partial\alpha}(uTh_2h_3) + \frac{\partial}{\partial\beta}(vTh_3h_1) + \frac{\partial}{\partial\alpha}(wTh_1h_2)\right] = 0 \qquad (3.5)$$

where α,β,γ = orthogonal curvilinear coordinates,

u,v,w = velocity components in the α, β and γ directions,

ρ = density of the fluid,

P = pressure,

g = gravitational acceleration,

T = temperature,

Ω = gravitational potential,

h_1,h_2,h_3 = metric coefficients in curvilinear coordinates.

For a particular system of coordinates there exist definite functional relationships between the metric coefficients and the coordinates. Equations 3.1-3.5 can be transformed into cylindrical, spherical, or any other orthogonal curvilinear coordinate system once the system is defined and once these metric coefficients for that particular system are known. The mathematical definitions of h_1, h_2 and h_3 are given in standard references [e.g., Rouse, 1965; Chao, 1969] and are used in the next section.

3.2 Transformation of Equations

3.2.1 Natural Coordinate System

A suitable coordinate system for bent-over jet problems is the natural coordinate system s, n and z as shown in Fig. 3.1. The natural coordinate system is a particular orthogonal curvilinear coordinate system in which s is horizontal and is along the axis of the jet, n is normal to

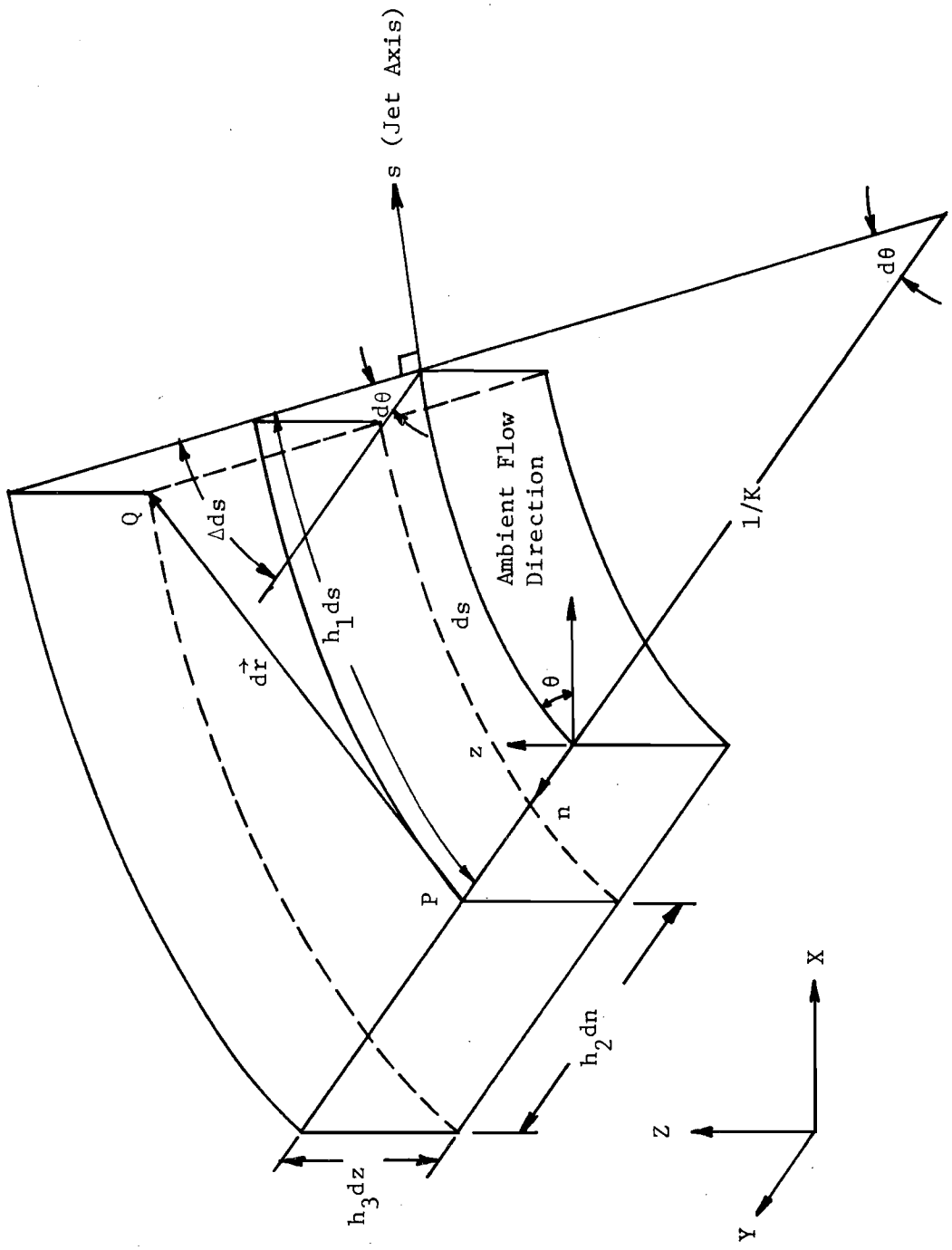

Fig. 3.1 Natural coordinate system

s in a horizontal plane and z is vertical with positive being upward. The natural coordinate system is a local system which coincides at the origin with a Cartesian coordinate system (X,Y,Z) if the effluent is perpendicular to the ambient flow.. The origin is located at the intersection of the near shoreline, the ambient free surface and the discharge channel centerline. In the Cartesian coordinate system, X is along the shoreline with positive in the ambient flow direction, Y is on the water surface and is normal to X, and Z is positive upward.

Referring to Fig. 3.1, P is a point (s,n,z) in three-dimensional space and Q is another point (s+ds, n+dn, z+dz) located an infinitesimal distance from P. The incremental vector from P to Q is

$$\vec{dr} = \frac{\partial \vec{r}}{\partial s}\, ds + \frac{\partial \vec{r}}{\partial n}\, dn + \frac{\partial \vec{r}}{\partial z}\, dz \tag{3.6}$$

The mathematical definitions of h_1, h_2 and h_3 [Chao, 1969] are

$$\begin{aligned} h_1 &= \left| \frac{\partial \vec{r}}{\partial s} \right| \\ h_2 &= \left| \frac{\partial \vec{r}}{\partial n} \right| \\ h_3 &= \left| \frac{\partial \vec{r}}{\partial z} \right| \end{aligned} \tag{3.7}$$

where $|\ |$ denotes magnitude. Let $\vec{i}_1$, $\vec{i}_2$ and $\vec{i}_3$ be unit vectors tangent to the coordinates s, n and z, respectively, at point P. Hence

$$\begin{aligned} \vec{i}_1 &= \frac{\frac{\partial \vec{r}}{\partial s}}{\left| \frac{\partial \vec{r}}{\partial s} \right|} \\ \vec{i}_2 &= \frac{\frac{\partial \vec{r}}{\partial n}}{\left| \frac{\partial \vec{r}}{\partial n} \right|} \end{aligned} \tag{3.8}$$

$$\vec{i}_3 = \frac{\frac{\partial \vec{r}}{\partial z}}{\left| \frac{\partial \vec{r}}{\partial z} \right|} \qquad (3.8)\ \text{Cont.}$$

From Eqs. 3.7 and 3.8 one obtains

$$\frac{\partial \vec{r}}{\partial s} = \vec{i}_1 h_1$$

$$\frac{\partial \vec{r}}{\partial n} = \vec{i}_2 h_2 \qquad (3.9)$$

$$\frac{\partial \vec{r}}{\partial z} = \vec{i}_3 h_3$$

Substitution of Eq. 3.9 into Eq. 3.6 yields

$$d\vec{r} = \vec{i}_1 h_1 ds + \vec{i}_2 h_2 dn + \vec{i}_3 h_3 dz \qquad (3.10)$$

which implies that $h_1 ds$, $h_2 dn$ and $h_3 dz$ are the projection of $d\vec{r}$ on the three coordinate axes s, n and z, respectively [Chao, 1969].

It is assumed that both θ which is the angle between the ambient flow direction X and the coordinate s, and K, which is the curvature of the surface n = 0 are functions of s only. From the geometry of Fig. 3.1, the differential arc length in the direction of increasing s but off the s axis is ds + Δds, while the lengths in the directions of increasing n and z are dn and dz regardless of the values of s, n, and z. Hence

$$h_1 ds = (ds+\Delta ds) = (1+nK)ds$$

$$h_2 dn = dn$$

$$h_3 dz = dz$$

or

$$h_1 = (1+nK)$$

$$h_2 = 1 \qquad (3.11)$$

$$h_3 = 1$$

where $K = -d\theta/ds$. Substituting $h_1 = 1 + nK$, $h_2 = 1$, $h_3 = 1$, $s = \alpha$, $n = \beta$ and $z = \gamma$ into Eqs. 3.1-3.5, the governing equations in the natural coordinate system are obtained:

continuity equation

$$\frac{\partial u}{\partial s} + \frac{\partial v}{\partial n} + \frac{\partial w}{\partial z} + K\frac{\partial nv}{\partial n} + K\frac{\partial nw}{\partial z} = 0 \qquad (3.12)$$

s-momentum equation

$$\frac{\partial u^2}{\partial s} + \frac{\partial uv}{\partial n} + \frac{\partial uw}{\partial z} + K\frac{\partial nuv}{\partial n} + K\frac{\partial nuw}{\partial z} + Kuv = -\frac{\partial}{\partial s}\left(\frac{P}{\rho}\right) \qquad (3.13)$$

n-momentum equation

$$\frac{\partial uv}{\partial s} + \frac{\partial v^2}{\partial n} + \frac{\partial vw}{\partial z} + K\frac{\partial nv^2}{\partial n} + K\frac{\partial nvw}{\partial z} - Ku^2 = -(1+Kn)\frac{\partial}{\partial n}\left(\frac{P}{\rho}\right) \qquad (3.14)$$

z-momentum equation

$$\frac{\partial uw}{\partial s} + \frac{\partial vw}{\partial n} + \frac{\partial w^2}{\partial z} + K\frac{\partial nvw}{\partial n} + K\frac{\partial nw^2}{\partial z} = -(1+Kn)\frac{\partial}{\partial z}\left(\frac{P}{\rho}\right) - (1+Kn)g \qquad (3.15)$$

equation of thermal energy conservation

$$\frac{\partial u\Delta T}{\partial s} + \frac{\partial v\Delta T}{\partial n} + \frac{\partial w\Delta T}{\partial z} + K\frac{\partial nv\Delta T}{\partial n} + K\frac{\partial nw\Delta T}{\partial z} = 0 \qquad (3.16)$$

In Eq. 3.16, $\Delta T = T - Ta$, temperature excess above an arbitrary but constant reference ambient temperature (T_a). Eq. 3.16 can be obtained from Eq. 3.5 using the fact that all of the derivatives of T_a are zero.

3.2.2 Mean Values

The dependent variables u, v, w, ρ, P and ΔT can be decomposed into a time average indicated by an over bar and a fluctuating component indicated by a $\tilde{}$:

$$\begin{aligned} u &= \bar{u} + \tilde{u} \\ v &= \bar{v} + \tilde{v} \\ w &= \bar{w} + \tilde{w} \\ \rho &= \bar{\rho} + \tilde{\rho} \\ P &= \bar{P} + \tilde{P} \\ \Delta T &= \Delta\bar{T} + \Delta\tilde{T} \end{aligned} \tag{3.17}$$

Substituting Eqs. 3.17 in Eqs. 3.12-3.16 and then taking the time average [Daily and Harleman, 1966] of each term yields the following set of equations:

continuity equation

$$\frac{\partial \bar{u}}{\partial s} + \frac{\partial \bar{v}}{\partial n} + \frac{\partial \bar{w}}{\partial z} + K\frac{\partial n\bar{v}}{\partial n} + K\frac{\partial n\bar{w}}{\partial z} = 0 \tag{3.18}$$

s-momentum equation

$$\frac{\partial \bar{u}^2}{\partial s} + \frac{\partial \bar{u}\bar{v}}{\partial n} + \frac{\partial \bar{u}\bar{w}}{\partial z} + K\frac{\partial n\bar{u}\bar{v}}{\partial n} + K\frac{\partial n\bar{u}\bar{w}}{\partial z} + K\overline{uv} = -\frac{\partial \overline{\tilde{u}^2}}{\partial s} - \frac{\partial \overline{\tilde{u}\tilde{v}}}{\partial n}$$

$$-\frac{\partial \overline{\tilde{u}\tilde{w}}}{\partial z} - K\frac{\partial n\overline{\tilde{u}\tilde{v}}}{\partial n} - K\frac{\partial n\overline{\tilde{u}\tilde{w}}}{\partial z} - K\overline{\tilde{u}\tilde{v}} - \frac{1}{\rho}\frac{\partial P}{\partial s} \tag{3.19}$$

n-momentum equation

$$\frac{\partial \bar{u}\bar{v}}{\partial s} + \frac{\partial \bar{v}^2}{\partial n} + \frac{\partial \bar{v}\bar{w}}{\partial z} + K\frac{\partial n\bar{v}^2}{\partial n} + K\frac{\partial n\bar{v}\bar{w}}{\partial z} - K\bar{u}^2 = -\frac{\partial \overline{\tilde{u}\tilde{v}}}{\partial s} - \frac{\partial \overline{\tilde{v}^2}}{\partial n}$$

$$-\frac{\partial \overline{\tilde{v}\tilde{w}}}{\partial z} - K\frac{\partial n\overline{\tilde{v}^2}}{\partial n} - K\frac{\partial n\overline{\tilde{v}\tilde{w}}}{\partial z} + K\overline{\tilde{u}^2} - \frac{(1+Kn)}{\rho}\frac{\partial P}{\partial n} \tag{3.20}$$

z-momentum equation

$$\frac{\partial \bar{u}\bar{w}}{\partial s} + \frac{\partial \bar{v}\bar{w}}{\partial n} + \frac{\partial \bar{w}^2}{\partial z} + K\frac{\partial n\bar{v}\bar{w}}{\partial n} + K\frac{\partial n\bar{w}^2}{\partial z} = -\frac{\partial \overline{\tilde{u}\tilde{w}}}{\partial s} - \frac{\partial \overline{\tilde{v}\tilde{w}}}{\partial n}$$

$$-\frac{\partial \overline{\tilde{w}^2}}{\partial z} - K\frac{\partial n\overline{\tilde{v}\tilde{w}}}{\partial n} - K\frac{\partial n\overline{\tilde{w}^2}}{\partial z} - \frac{(1+Kn)}{\rho}\frac{\partial P}{\partial z} - (1+Kn)g \qquad (3.21)$$

equation of thermal energy conservation

$$\frac{\partial \bar{u}\overline{\Delta T}}{\partial s} + \frac{\partial \bar{u}\overline{\Delta T}}{\partial n} + \frac{\partial \bar{w}\overline{\Delta T}}{\partial z} + K\frac{\partial n\bar{v}\overline{\Delta T}}{\partial n} + K\frac{\partial n\bar{w}\overline{\Delta T}}{\partial z} = -\frac{\partial \overline{\tilde{u}\tilde{\Delta T}}}{\partial s}$$

$$-\frac{\partial \overline{\tilde{v}\tilde{\Delta T}}}{\partial n} - \frac{\partial \overline{\tilde{w}\tilde{\Delta T}}}{\partial z} - K\frac{\partial n\overline{\tilde{v}\tilde{\Delta T}}}{\partial n} - K\frac{\partial n\overline{\tilde{w}\tilde{\Delta T}}}{\partial z} \qquad (3.22)$$

In later equations, except for fluctuating terms, the mean values will be written without an overbar for convenience.

3.2.3 Hydrostatic Pressure

The mean pressure P can be considered as the sum of dynamic pressure P_d and hydrostatic pressure P_h:

$$P = P_d + P_h \qquad (3.23)$$

The hydrostatic pressure P_h is defined as

$$P_h = -\int_{\eta}^{z} \rho g dz \qquad (3.24)$$

in which η is the elevation of the water surface. In general, the water surface in the jet is not horizontal because of the density differences within the jet [Engelund and Pedersen, 1973]. The density ρ can be expressed as

$$\rho = \rho_a - \Delta\rho \qquad (3.25)$$

where ρ_a = ambient density and $\Delta\rho$ = difference between the density at the point of interest and the ambient density. Substitution of Eq. 3.25 into Eq. 3.24 gives

$$P_h = \rho_a g(\eta - z) + \int_{\eta}^{z} \Delta\rho g dz \tag{3.26}$$

A typical temperature rise in cooling water is about 10 to 25 F^o above the ambient temperature. Over such a range of temperature, the density of the fluid may be assumed to be a linear function of temperature, and the variations of density throughout the flow field are small relative to the ambient density, as previously assumed. Thus, one may write

$$\Delta\rho = \lambda(T - T_a) = \lambda\Delta T \tag{3.27}$$

and

$$\frac{\Delta\rho}{\rho_a} << 1 \tag{3.28}$$

where λ = thermal expansion coefficient. In Eq. 3.27 $\Delta\rho$ is the density difference below ambient (Eq. 3.25) while ΔT is the temperature difference above ambient. Using Eqs. 3.23, 3.26, and 3.28, the pressure terms in the momentum equations can now be expressed as [Stolzenbach and Harleman, 1971]

$$-\frac{1}{\rho}\frac{\partial P}{\partial s} = -g\frac{\partial \eta}{\partial s} - \frac{g}{\rho_a}\int_{\eta}^{z}\frac{\partial \Delta\rho}{\partial s}dz - \frac{1}{\rho_a}\frac{\partial P_d}{\partial s} \tag{3.29}$$

$$-\frac{1}{\rho}\frac{\partial P}{\partial n} = -g\frac{\partial \eta}{\partial n} - \frac{g}{\rho_a}\int_{\eta}^{z}\frac{\partial \Delta\rho}{\partial n}dz - \frac{1}{\rho_a}\frac{\partial P_d}{\partial n} \tag{3.30}$$

and

$$-\frac{1}{\rho}\frac{\partial P}{\partial z} = -g - \frac{1}{\rho_a}\frac{\partial P_d}{\partial z} \tag{3.31}$$

after interchanging the order of integration and differentiation in

Eqs. 3.29 and 3.30 and after assuming that $\Delta\rho/\rho_a|_{z=\eta}\ \frac{\partial\eta}{\partial s}$ and $\Delta\rho/\rho_a|_{z=\eta}\ \frac{\partial\eta}{\partial n}$ are negligible.

As $z \to -\infty$ the influence of the jet becomes negligible. Thus Eqs. 3.29 and 3.30 become

$$-\frac{1}{\rho}\frac{\partial P}{\partial s}\Big|_{z\to-\infty} = 0 = -g\frac{\partial\eta}{\partial s} - \frac{g}{\rho_a}\int_{\eta}^{-\infty}\frac{\partial\Delta\rho}{\partial s}\,dz - \frac{1}{\rho_a}\frac{\partial P_d}{\partial s}\Big|_{z\to-\infty} \tag{3.32}$$

and

$$-\frac{1}{\rho}\frac{\partial P}{\partial n}\Big|_{z\to-\infty} = 0 = -g\frac{\partial\eta}{\partial n} - \frac{g}{\rho_a}\int_{\eta}^{-\infty}\frac{\partial\Delta\rho}{\partial n}\,dz - \frac{1}{\rho_a}\frac{\partial P_d}{\partial n}\Big|_{z\to-\infty} \tag{3.33}$$

if any pressure gradients associated with the ambient flow are neglected. Using Eqs. 3.32 and 3.33, η in Eqs. 3.29 and 3.30 can be eliminated [Stolzenbach and Harleman, 1971]. The results are

$$-\frac{1}{\rho}\frac{\partial P}{\partial s} = \frac{g}{\rho_a}\int_{z}^{-\infty}\frac{\partial\Delta\rho}{\partial s}\,dz - \frac{1}{\rho_a}\frac{\partial P_d}{\partial s} \tag{3.34}$$

$$-\frac{1}{\rho}\frac{\partial P}{\partial n} = \frac{g}{\rho_a}\int_{z}^{-\infty}\frac{\partial\Delta\rho}{\partial n}\,dz - \frac{1}{\rho_a}\frac{\partial P_d}{\partial n} \tag{3.35}$$

After substitution of Eqs. 3.31, 3.34 and 3.35, the foregoing momentum equations yield

s-momentum equation

$$\frac{\partial u^2}{\partial s} + \frac{\partial uv}{\partial n} + \frac{\partial uw}{\partial z} + K\frac{\partial nuv}{\partial n} + K\frac{\partial nuw}{\partial z} + Kuv = \frac{\lambda g}{\rho_a}\int_{z}^{-\infty}\frac{\partial\Delta T}{\partial s}\,dz$$
$$-\frac{1}{\rho_a}\frac{\partial P_d}{\partial s} - \frac{\partial\overline{\tilde{u}^2}}{\partial s} - \frac{\partial\overline{\tilde{u}\tilde{v}}}{\partial n} - \frac{\partial\overline{\tilde{u}\tilde{w}}}{\partial z} - K\frac{\partial n\overline{\tilde{u}\tilde{v}}}{\partial n} - K\frac{\partial n\overline{\tilde{u}\tilde{w}}}{\partial z} - K\overline{\tilde{u}\tilde{v}} \tag{3.36}$$

n-momentum equation

$$\frac{\partial uv}{\partial s} + \frac{\partial v^2}{\partial n} + \frac{\partial vw}{\partial z} + K\frac{\partial nv^2}{\partial n} + K\frac{\partial nvw}{\partial z} - Ku^2 = \frac{\lambda(1+Kn)g}{\rho_a}\int_z^{-\infty}\frac{\partial \Delta T}{\partial n}\,dz$$

$$- \frac{(1+Kn)}{\rho_a}\frac{\partial P_d}{\partial n} - \frac{\partial \overline{\tilde{u}\tilde{v}}}{\partial s} - \frac{\partial \overline{\tilde{v}^2}}{\partial n} - \frac{\partial \overline{\tilde{v}\tilde{w}}}{\partial z} - K\frac{\partial n\overline{\tilde{v}^2}}{\partial n} - K\frac{\partial n\overline{\tilde{v}\tilde{w}}}{\partial z} + K\overline{\tilde{u}^2} \tag{3.37}$$

z-momentum equation

$$\frac{\partial uw}{\partial s} + \frac{\partial vw}{\partial n} + \frac{\partial w^2}{\partial z} + K\frac{\partial nvw}{\partial n} + K\frac{\partial nw^2}{\partial z} = -\frac{(1+Kn)}{\rho_a}\frac{\partial P_d}{\partial z} - \frac{\partial \overline{\tilde{u}\tilde{w}}}{\partial s}$$

$$- \frac{\partial \overline{\tilde{v}\tilde{w}}}{\partial n} - \frac{\partial \overline{\tilde{w}^2}}{\partial z} - K\frac{\partial n\overline{\tilde{v}\tilde{w}}}{\partial n} - K\frac{\partial n\overline{\tilde{w}^2}}{\partial z} \tag{3.38}$$

In Eqs. 3.36 and 3.37 the density difference has been replaced by the temperature difference by using Eq. 3.27. The continuity equations for volume and heat are given in Eqs. 3.18 and 3.22.

3.3 Order of Magnitude Analysis

As a buoyant surface jet discharges into a river, the curvature of the jet trajectory is initially zero but the curvature may rapidly become significant near the exit due to strong river flow. The curvature then gradually becomes smaller further downstream. For heated jets discharged at small, non-zero Richardson number, the buoyancy is initially negligible relative to inertial effects and the general behavior in the ZFE is not too different from that in the nonbuoyant case [Silberman and Stefan, 1970]. As the velocity of the jet decreases with distance, the Richardson number increases and the effects of buoyancy forces will gradually become significant with respect to the inertial forces [Dunn et al., 1975]. These facts suggest that an analytical model for buoyant

surface discharges into rivers should allow for the progression of a jet from the non-buoyant case to the buoyant case with large Richardson number as well as from the no curvature (no crossflow) case to the significantly curved (or bent) case. Thus in carrying out an order of magnitude analysis the following four cases are considered:

1. Nonbuoyant jets (zero Richardson number) with no curvature.
2. Nonbuoyant jets with significant curvature.
3. Buoyant jets (large Richardson number) with no curvature.
4. Buoyant jets with significant curvature.

The results of the order of magnitude analysis for these four cases will be used to obtain governing equations which are simplified but which still contain all of the significant terms for any of the four cases. Thus, the resulting governing equations will be applicable to all four cases. (See Section 3.3.4.)

For the purpose of estimating the relative magnitude of each term in the governing equations, the following characteristic scales are introduced:

L_S, L_N, L_Z = length scale in the s, n, z directions

U_S, U_N, U_Z = scale of mean velocity components u, v, w

U_F = scale of the velocity fluctuations $\tilde{u}$, $\tilde{v}$, $\tilde{w}$

ΔP_D = scale of dynamic pressure changes

ΔT_M = scale of mean temperature changes

ΔT_F = scale of temperature fluctuations

3.3.1 Continuity Equations

First, consider the equation of continuity, which from Eq. 3.18 can be written as

$$\frac{\partial u}{\partial s} + \frac{\partial v}{\partial n} + \frac{\partial w}{\partial z} + K\frac{\partial nv}{\partial n} + K\frac{\partial nw}{\partial z} = 0$$

$$\frac{U_S}{L_S} \quad \frac{U_N}{L_N} \quad \frac{U_Z}{L_Z} \quad KU_N \qquad K\frac{L_N U_Z}{L_Z} \tag{3.39}$$

The magnitude of each term is written directly under it.

For the no crossflow case, the curvature of jet trajectory is zero. Therefore the last two terms in Eq. 3.39 are dropped. The magnitude of the velocity scale in one direction is not independent of the velocity scales of the other two directions; that is, changes in the velocities in various directions are related as indicated by the continuity equation [Hinze, 1959]. Thus the order of magnitude of the first three terms of Eq. 3.39 must be the same. Hence

$$\frac{U_S}{L_S} \sim \frac{U_N}{L_N} \sim \frac{U_Z}{L_Z} \tag{3.40}$$

where $\sim$ denotes the equivalence of the order of magnitude between two terms.

For significantly bent jets, the curvature K is assumed to have such an order of magnitude that it gives the last two terms in Eq. 3.39 the same order of magnitude as the other three terms. With this assumption, one obtains the following relations from Eq. 3.39

$$\frac{U_S}{L_S} \sim \frac{U_N}{L_N} \sim \frac{U_Z}{L_Z}$$

and $$K \sim \frac{1}{L_N} \tag{3.41}$$

Only two of the four possible cases need to be considered for the continuity equation since the density difference does not appear in Eq. 3.39.

3.3.2 Momentum Equations

In the free shear flows, the intensities $\overline{\tilde{u}^2}$, $\overline{\tilde{v}^2}$ and $\overline{\tilde{w}^2}$ are of the same order of magnitude [Hinze, 1959]. For circular [Shashidhara and Bourodimos, 1975] and two-dimensional [Mih and Hoopes, 1972] nonbuoyant jets, $\overline{\tilde{u}^2}$, $\overline{\tilde{v}^2}$ and $\overline{\tilde{w}^2}$ were found to be an order of magnitude less than the square of the mean velocity. Dornhelm et al. [1972] conducted velocity fluctuation measurements on buoyant surface jets and found that $\overline{\tilde{u}^2}$ was an order of magnitude less than the square of the mean velocity, as in the nonbuoyant case. There is a lack of information regarding the turbulence characteristics of buoyant surface jets in vertical and lateral directions. Although there exists a stabilizing density gradient in buoyant surface jets, it is assumed that both $\overline{\tilde{v}^2}$ and $\overline{\tilde{w}^2}$ are an order of magnitude less than the square of the mean velocity as in the nonbuoyant case. Hence the same scale of velocity fluctuation U_F^2 is introduced for $\overline{\tilde{u}^2}$, $\overline{\tilde{v}^2}$ and $\overline{\tilde{w}^2}$ and that $U_F^2/U_S^2 \sim \delta$, where δ is a quantity an order of magnitude less than unity. For cases with significant buoyancy, it might be reasonable to assume that $\overline{\tilde{v}^2}$ is of a smaller order of magnitude, but this possibility was not pursued because of the apparent lack of supporting data.

The assumption made in Section 3.1.1 that the jets are fully turbulent implies that each of the equations of heat and momentum conservation should retain at least one turbulence term. This requirement will be used frequently in the following order of magnitude analysis.

Table 3.1 Simplification of Momentum and Thermal Energy Conservation Equations

Nonbuoyant Jets with No Curvature

s-momentum equation

Stage	$\frac{\partial u^2}{\partial s} + \frac{\partial uv}{\partial n} + \frac{\partial uw}{\partial z} = -\frac{1}{\rho_a}\frac{\partial P_d}{\partial s} - \frac{\partial \overline{\tilde{u}}^2}{\partial s} - \frac{\partial \overline{\tilde{u}\tilde{v}}}{\partial n} - \frac{\partial \overline{\tilde{u}\tilde{w}}}{\partial z}$						
I	$\frac{U_S^2}{L_S}$	$\frac{U_S U_N}{L_N}$	$\frac{U_S U_Z}{L_Z}$	$\frac{\Delta P_D}{\rho_a L_S}$	$\frac{U_F^2}{L_S}$	$\frac{U_F^2}{L_N}$	$\frac{U_F^2}{L_Z}$
II	$\frac{U_S^2}{L_S}$	$\frac{U_S^2}{L_S}$	$\frac{U_S^2}{L_S}$	$\frac{\Delta P_D}{\rho_a L_S}$	$\frac{U_F^2}{L_S}$	$\frac{U_F^2}{L_N}$	$\frac{U_F^2}{L_Z}$
III	1	1	1	$\frac{\Delta P_D}{\rho_a U_S^2}$	$\frac{U_F^2}{U_S^2}$	$\frac{U_F^2 L_S}{U_S^2 L_N}$	$\frac{U_F^2 L_S}{U_S^2 L_Z}$
IV	1	1	1	δ	δ	1	1

n-momentum equation

Stage	$\frac{\partial uv}{\partial s} + \frac{\partial v^2}{\partial n} + \frac{\partial vw}{\partial z} = -\frac{1}{\rho_a}\frac{\partial P_d}{\partial n} - \frac{\partial \overline{\tilde{u}\tilde{v}}}{\partial s} - \frac{\partial \overline{\tilde{v}}^2}{\partial n} - \frac{\partial \overline{\tilde{v}\tilde{w}}}{\partial z}$						
I	$\frac{U_S U_N}{L_S}$	$\frac{U_N^2}{L_N}$	$\frac{U_N U_Z}{L_Z}$	$\frac{\Delta P_D}{\rho_a L_N}$	$\frac{U_F^2}{L_S}$	$\frac{U_F^2}{L_N}$	$\frac{U_F^2}{L_Z}$
II	$\frac{U_N^2}{L_N}$	$\frac{U_N^2}{L_N}$	$\frac{U_N^2}{L_N}$	$\frac{\Delta P_D}{\rho_a L_N}$	$\frac{U_F^2}{L_S}$	$\frac{U_F^2}{L_N}$	$\frac{U_F^2}{L_Z}$
III	$\frac{L_N}{L_S}$	$\frac{L_N}{L_S}$	$\frac{L_N}{L_S}$	$\frac{\Delta P_D L_S}{\rho_a U_S^2 L_N}$	$\frac{U_F^2}{L_S}$	$\frac{U_F^2 L_S}{U_S^2 L_N}$	$\frac{U_F^2 L_S}{U_S^2 L_Z}$
IV	δ	δ	δ	1	δ	1	1

z-momentum equation

Stage	$\frac{\partial uw}{\partial s} + \frac{\partial vw}{\partial n} + \frac{\partial w^2}{\partial z} = -\frac{1}{\rho_a}\frac{\partial P_d}{\partial z} - \frac{\partial \overline{\tilde{u}\tilde{w}}}{\partial s} - \frac{\partial \overline{\tilde{v}\tilde{w}}}{\partial n} - \frac{\partial \overline{\tilde{w}}^2}{\partial z}$						
I	$\frac{U_S U_Z}{L_S}$	$\frac{U_N U_Z}{L_N}$	$\frac{U_Z^2}{L_Z}$	$\frac{\Delta P_D}{\rho_a L_Z}$	$\frac{U_F^2}{L_S}$	$\frac{U_F^2}{L_N}$	$\frac{U_F^2}{L_Z}$
II	$\frac{U_Z^2}{L_Z}$	$\frac{U_Z^2}{L_Z}$	$\frac{U_Z^2}{L_Z}$	$\frac{\Delta P_D}{\rho_a L_Z}$	$\frac{U_F^2}{L_S}$	$\frac{U_F^2}{L_N}$	$\frac{U_F^2}{L_Z}$
III	$\frac{L_Z}{L_S}$	$\frac{L_Z}{L_S}$	$\frac{L_Z}{L_S}$	$\frac{\Delta P_D L_S}{\rho_a U_S^2 L_Z}$	$\frac{U_F^2}{U_S^2}$	$\frac{U_F^2 L_S}{U_S^2 L_N}$	$\frac{U_F^2 L_S}{U_S^2 L_Z}$
IV	δ	δ	δ	1	δ	1	1

Table 3.1 (cont'd) Simplification of Momentum and Thermal Energy Conservation Equations

Nonbuoyant Jets with Significant Curvature

s-momentum equation

Stage	$\frac{\partial u^2}{\partial s} + \frac{\partial uv}{\partial n} + \frac{\partial uw}{\partial z} + K\frac{\partial nuv}{\partial n} + K\frac{\partial nuw}{\partial z} + Kuv$	$= -\frac{1}{\rho_a}\frac{\partial P_d}{\partial s} - \frac{\partial \overline{\tilde{u}^2}}{\partial s} - \frac{\partial \overline{\tilde{u}\tilde{v}}}{\partial n} - \frac{\partial \overline{\tilde{u}\tilde{w}}}{\partial z} - K\frac{\partial n\overline{\tilde{u}\tilde{v}}}{\partial n} - K\frac{\partial n\overline{\tilde{u}\tilde{w}}}{\partial z} - K\overline{\tilde{u}\tilde{v}}$											
I	$\frac{U_S^2}{L_S}$	$\frac{U_S U_N}{L_N}$	$\frac{U_S U_Z}{L_Z}$	$\frac{KL_N U_S U_N}{L_N}$	$\frac{KL_N U_S U_Z}{L_Z}$	$KU_S U_N$	$\frac{\Delta P_D}{\rho_a L_S}$	$\frac{U_F^2}{L_S}$	$\frac{U_F^2}{L_N}$	$\frac{U_F^2}{L_Z}$	$\frac{KL_N U_F^2}{L_N}$	$\frac{KL_N U_F^2}{L_Z}$	KU_F^2
II	$\frac{U_S^2}{L_S}$	$\frac{U_S^2}{L_S}$	$\frac{U_S^2}{L_S}$	$\frac{U_S^2}{L_S}$	$\frac{U_S^2}{L_S}$	$\frac{U_S^2}{L_S}$	$\frac{\Delta P_D}{\rho_a L_S}$	$\frac{U_F^2}{L_S}$	$\frac{U_F^2}{L_N}$	$\frac{U_F^2}{L_Z}$	$\frac{U_F^2}{L_N}$	$\frac{U_F^2}{L_Z}$	$\frac{U_F^2}{L_N}$
III	1	1	1	1	1	1	$\frac{\Delta P_D}{\rho_a U_S^2}$	$\frac{U_F^2}{U_S^2}$	$\frac{U_F^2 L_S}{U_S^2 L_N}$	$\frac{U_F^2 L_S}{U_S^2 L_Z}$	$\frac{U_F^2 L_S}{U_S^2 L_N}$	$\frac{U_F^2 L_S}{U_S^2 L_Z}$	$\frac{U_F^2 L_S}{U_S^2 L_N}$
IV	1	1	1	1	1	1	δ	δ	δ	1	δ	1	δ

n-momentum equation

Stage	$\frac{\partial uv}{\partial s} + \frac{\partial v^2}{\partial n} + \frac{\partial vw}{\partial z} + K\frac{\partial nv^2}{\partial n} + K\frac{\partial nvw}{\partial z} - Ku^2$	$= -\frac{1}{\rho_a}\frac{\partial P_d}{\partial n} - \frac{Kn}{\rho_a}\frac{\partial P_d}{\partial n} - \frac{\partial \overline{\tilde{u}\tilde{v}}}{\partial s} - \frac{\partial \overline{\tilde{v}^2}}{\partial n} - \frac{\partial \overline{\tilde{v}\tilde{w}}}{\partial z} - K\frac{\partial n\overline{\tilde{v}^2}}{\partial n} - K\frac{\partial n\overline{\tilde{v}\tilde{w}}}{\partial z} + K\overline{\tilde{u}^2}$											
I	$\frac{U_S U_N}{L_S}$	$\frac{U_N^2}{L_N}$	$\frac{U_N U_Z}{L_Z}$	$\frac{KL_N U_N^2}{L_N}$	$\frac{KL_N U_N U_Z}{L_Z}$	KU_S^2	$\frac{\Delta P_D}{\rho_a L_N}$	$\frac{KL_N \Delta P_D}{\rho_a L_N}$	$\frac{U_F^2}{L_S}$	$\frac{U_F^2}{L_N}$	$\frac{U_F^2}{L_Z}$	$\frac{KL_N U_F^2}{L_N}$	$\frac{KL_N U_F^2}{L_Z}$	KU_F^2
II	$\frac{U_N^2}{L_N}$	$\frac{U_N^2}{L_N}$	$\frac{U_N^2}{L_N}$	$\frac{U_N^2}{L_N}$	$\frac{U_N^2}{L_N}$	$\frac{U_S^2}{L_N}$	$\frac{\Delta P_D}{\rho_a L_N}$	$\frac{\Delta P_D}{\rho_a L_N}$	$\frac{U_F^2}{L_S}$	$\frac{U_F^2}{L_N}$	$\frac{U_F^2}{L_Z}$	$\frac{U_F^2}{L_N}$	$\frac{U_F^2}{L_Z}$	$\frac{U_F^2}{L_N}$
III	$\frac{L_N}{L_S}$	$\frac{L_N}{L_S}$	$\frac{L_N}{L_S}$	$\frac{L_N}{L_S}$	$\frac{L_N}{L_S}$	$\frac{L_S}{L_N}$	$\frac{\Delta P_D L_S}{\rho_a U_S^2 L_N}$	$\frac{\Delta P_D L_S}{\rho_a U_S^2 L_N}$	$\frac{U_F^2}{U_S^2}$	$\frac{U_F^2 L_S}{U_S^2 L_N}$	$\frac{U_F^2 L_S}{U_S^2 L_Z}$	$\frac{U_F^2 L_S}{U_S^2 L_N}$	$\frac{U_F^2 L_S}{U_S^2 L_Z}$	$\frac{U_F^2 L_S}{U_S^2 L_N}$
IV	1	1	1	1	1	1	δ	δ	δ	δ	1	δ	1	δ

Table 3.1 (cont'd) Simplification of Momentum and Thermal Energy Conservation Equations

z-momentum equation

Stage	$\frac{\partial uw}{\partial s} + \frac{\partial vw}{\partial n} + \frac{\partial w^2}{\partial z} + K\frac{\partial nvw}{\partial n} + K\frac{\partial nw^2}{\partial z} = -\frac{1}{\rho_a}\frac{\partial P_d}{\partial z} - \frac{Kn}{\rho_a}\frac{\partial P_d}{\partial z} - \frac{\partial \tilde{u}\tilde{w}}{\partial s} - \frac{\partial \tilde{v}\tilde{w}}{\partial n} - \frac{\partial \tilde{w}^2}{\partial z} - K\frac{\partial n\tilde{v}\tilde{w}}{\partial n} - K\frac{\partial n\tilde{w}^2}{\partial z}$											
I	$\frac{U_S U_Z}{L_S}$	$\frac{U_N U_Z}{L_N}$	$\frac{U_Z^2}{L_Z}$	$\frac{KL_N U_N U_Z}{L_N}$	$\frac{KL_N U_Z^2}{L_Z}$	$\frac{\Delta P_D}{\rho_a L_Z}$	$\frac{KL_N \Delta P_D}{\rho_a L_Z}$	$\frac{U_F^2}{L_S}$	$\frac{U_F^2}{L_N}$	$\frac{U_F^2}{L_Z}$	$\frac{KL_N U_F^2}{L_N}$	$\frac{KL_N U_F^2}{L_Z}$
II	$\frac{U_Z^2}{L_Z}$	$\frac{U_Z^2}{L_Z}$	$\frac{U_Z^2}{L_Z}$	$\frac{U_Z^2}{L_Z}$	$\frac{U_Z^2}{L_Z}$	$\frac{\Delta P_D}{\rho_a L_Z}$	$\frac{\Delta P_D}{\rho_a L_Z}$	$\frac{U_F^2}{L_S}$	$\frac{U_F^2}{L_N}$	$\frac{U_F^2}{L_Z}$	$\frac{U_F^2}{L_N}$	$\frac{U_F^2}{L_Z}$
III	$\frac{L_Z}{L_S}$	$\frac{L_Z}{L_S}$	$\frac{L_Z}{L_S}$	$\frac{L_Z}{L_S}$	$\frac{L_Z}{L_S}$	$\frac{\Delta P_D L_S}{\rho_a U_S^2 L_Z}$	$\frac{\Delta P_D L_S}{\rho_a U_S^2 L_Z}$	$\frac{U_F^2}{U_S^2}$	$\frac{U_F^2 L_S}{U_S^2 L_N}$	$\frac{U_F^2 L_S}{U_S^2 L_Z}$	$\frac{U_F^2 L_S}{U_S^2 L_N}$	$\frac{U_F^2 L_S}{U_S^2 L_Z}$
IV	δ	δ	δ	δ	δ	1	1	δ	δ	1	δ	1

Buoyant Jets with No Curvature

s-momentum equation

Stage	$\frac{\partial u^2}{\partial s} + \frac{\partial uv}{\partial n} + \frac{\partial uw}{\partial z} = \frac{\lambda g}{\rho_a}\int_z^{-\infty}\frac{\partial \Delta T}{\partial s}dz - \frac{1}{\rho_a}\frac{\partial P_d}{\partial s} - \frac{\partial \tilde{u}^2}{\partial s} - \frac{\partial \tilde{u}\tilde{v}}{\partial n} - \frac{\partial \tilde{u}\tilde{w}}{\partial z}$								
I	$\frac{U_S^2}{L_S}$	$\frac{U_S U_N}{L_N}$	$\frac{U_S U_Z}{L_Z}$	$\frac{\lambda g \Delta T_M L_Z}{\rho_a L_S}$	$\frac{\Delta P_D}{\rho_a L_S}$	$\frac{U_F^2}{L_S}$	$\frac{U_F^2}{L_N}$	$\frac{U_F^2}{L_Z}$
II	$\frac{U_S^2}{L_S}$	$\frac{U_S^2}{L_S}$	$\frac{U_S^2}{L_S}$	$\frac{\lambda g \Delta T_M L_Z}{\rho_a L_S}$	$\frac{\Delta P_D}{\rho_a L_S}$	$\frac{U_F^2}{L_S}$	$\frac{U_F^2}{L_N}$	$\frac{U_F^2}{L_Z}$
III	1	1	1	$\frac{\lambda g \Delta T_M L_Z}{\rho_a U_S^2}$	$\frac{\Delta P_D}{\rho_a U_S^2}$	$\frac{U_F^2}{U_S^2}$	$\frac{U_F^2 L_S}{U_S^2 L_N}$	$\frac{U_F^2 L_S}{U_S^2 L_Z}$
IV	1	1	1	1	δ	δ	δ	1

n-momentum equation

Stage	$\frac{\partial uv}{\partial s} + \frac{\partial v^2}{\partial n} + \frac{\partial vw}{\partial z} = \frac{\lambda g}{\rho_a}\int_z^{-\infty}\frac{\partial \Delta T}{\partial n}dz - \frac{1}{\rho_a}\frac{\partial P_d}{\partial n} - \frac{\partial \tilde{u}\tilde{v}}{\partial s} - \frac{\partial \tilde{v}^2}{\partial n} - \frac{\partial \tilde{v}\tilde{w}}{\partial z}$							
I	$\frac{U_S U_N}{L_S}$	$\frac{U_N^2}{L_N}$	$\frac{U_N U_Z}{L_Z}$	$\frac{\lambda g \Delta T_M L_Z}{\rho_a L_N}$	$\frac{\Delta P_D}{\rho_a L_N}$	$\frac{U_F^2}{L_S}$	$\frac{U_F^2}{L_N}$	$\frac{U_F^2}{L_Z}$
II	$\frac{U_N^2}{L_N}$	$\frac{U_N^2}{L_N}$	$\frac{U_N^2}{L_N}$	$\frac{\lambda g \Delta T_M L_Z}{\rho_a L_N}$	$\frac{\Delta P_D}{\rho_a L_N}$	$\frac{U_F^2}{L_S}$	$\frac{U_F^2}{L_N}$	$\frac{U_F^2}{L_Z}$
III	$\frac{L_N}{L_S}$	$\frac{L_N}{L_S}$	$\frac{L_N}{L_S}$	$\frac{\lambda g \Delta T_M L_Z L_S}{\rho_a U_S^2 L_N}$	$\frac{\Delta P_D L_S}{\rho_a U_S^2 L_N}$	$\frac{U_F^2}{U_S^2}$	$\frac{U_F^2 L_S}{U_S^2 L_N}$	$\frac{U_F^2 L_S}{U_S^2 L_Z}$
IV	1	1	1	1	δ	δ	δ	1

Table 3.1 (cont'd) Simplification of Momentum and Thermal Energy Conservation Equations

z-momentum equation

Stage	$\frac{\partial uw}{\partial s} + \frac{\partial vw}{\partial n} + \frac{\partial w^2}{\partial z} = -\frac{1}{\rho_a}\frac{\partial P_d}{\partial z} - \frac{\partial \tilde{u}\tilde{w}}{\partial s} - \frac{\partial \tilde{v}\tilde{w}}{\partial n} - \frac{\partial \tilde{w}^2}{\partial z}$						
I	$\frac{U_S U_Z}{L_S}$	$\frac{U_N U_Z}{L_N}$	$\frac{U_Z^2}{L_Z}$	$\frac{\Delta P_D}{\rho_a L_Z}$	$\frac{U_F^2}{L_S}$	$\frac{U_F^2}{L_N}$	$\frac{U_F^2}{L_Z}$
II	$\frac{U_Z^2}{L_Z}$	$\frac{U_Z^2}{L_Z}$	$\frac{U_Z^2}{L_Z}$	$\frac{\Delta P_D}{\rho_a L_Z}$	$\frac{U_F^2}{L_S}$	$\frac{U_F^2}{L_N}$	$\frac{U_F^2}{L_Z}$
III	$\frac{L_Z}{L_S}$	$\frac{L_Z}{L_S}$	$\frac{L_Z}{L_S}$	$\frac{\Delta P_D L_S}{\rho_a U_S^2 L_Z}$	$\frac{U_F^2}{U_S^2}$	$\frac{U_F^2 L_S}{U_S^2 L_N}$	$\frac{U_F^2 L_S}{U_S^2 L_Z}$
IV	δ	δ	δ	1	δ	δ	1

equation of thermal energy conservation

Stage	$\frac{\partial u\Delta T}{\partial s} + \frac{\partial v\Delta T}{\partial n} + \frac{\partial w\Delta T}{\partial z} = -\frac{\partial \tilde{u}\Delta\tilde{T}}{\partial s} - \frac{\partial \tilde{v}\Delta\tilde{T}}{\partial n} - \frac{\partial \tilde{w}\Delta\tilde{T}}{\partial z}$					
I	$\frac{U_S \Delta T_M}{L_S}$	$\frac{U_N \Delta T_M}{L_N}$	$\frac{U_Z \Delta T_M}{L_Z}$	$\frac{U_F \Delta T_F}{L_S}$	$\frac{U_F \Delta T_F}{L_N}$	$\frac{U_F \Delta T_F}{L_Z}$
II	$\frac{U_S \Delta T_M}{L_S}$	$\frac{U_S \Delta T_M}{L_S}$	$\frac{U_S \Delta T_M}{L_S}$	$\frac{U_F \Delta T_F}{L_S}$	$\frac{U_F \Delta T_F}{L_N}$	$\frac{U_F \Delta T_F}{L_Z}$
III	1	1	1	$\frac{U_F \Delta T_F}{U_S \Delta T_M}$	$\frac{U_F \Delta T_F L_S}{U_S \Delta T_M L_N}$	$\frac{U_F \Delta T_F L_S}{U_S \Delta T_M L_Z}$
IV	1	1	1	δ	δ	1

Buoyant Jets with Significant Curvature

s-momentum equation

Stage	$\frac{\partial u^2}{\partial s} + \frac{\partial uv}{\partial n} + \frac{\partial uw}{\partial z} + K\frac{\partial nuv}{\partial n} + K\frac{\partial nuw}{\partial z} + Kuv = \frac{\lambda g}{\rho_a}\int_z^{-\infty}\frac{\partial \Delta T}{\partial s}dz - \frac{1}{\rho_a}\frac{\partial P_d}{\partial s} - \frac{\partial \tilde{u}^2}{\partial s} - \frac{\partial \tilde{u}\tilde{v}}{\partial n} - \frac{\partial \tilde{u}\tilde{w}}{\partial z} - K\frac{\partial n\tilde{u}\tilde{v}}{\partial n} - K\frac{\partial n\tilde{u}\tilde{w}}{\partial z} - K\tilde{u}\tilde{v}$													
I	$\frac{U_S^2}{L_S}$	$\frac{U_S U_N}{L_N}$	$\frac{U_S U_Z}{L_Z}$	$\frac{KL_N U_S U_N}{L_N}$	$\frac{KL_N U_S U_Z}{L_Z}$	$KU_S U_N$	$\frac{\lambda g \Delta T_M L_Z}{\rho_a L_S}$	$\frac{\Delta P_D}{\rho_a L_S}$	$\frac{U_F^2}{L_S}$	$\frac{U_F^2}{L_N}$	$\frac{U_F^2}{L_Z}$	$\frac{KL_N U_F^2}{L_N}$	$\frac{KL_N U_F^2}{L_Z}$	KU_F^2
II	$\frac{U_S^2}{L_S}$	$\frac{U_S^2}{L_S}$	$\frac{U_S^2}{L_S}$	$\frac{U_S^2}{L_S}$	$\frac{U_S^2}{L_S}$	$\frac{U_S^2}{L_S}$	$\frac{\lambda g \Delta T_M L_Z}{\rho_a L_S}$	$\frac{\Delta P_D}{\rho_a L_S}$	$\frac{U_F^2}{L_S}$	$\frac{U_F^2}{L_N}$	$\frac{U_F^2}{L_Z}$	$\frac{U_F^2}{L_N}$	$\frac{U_F^2}{L_Z}$	$\frac{U_F^2}{L_N}$
III	1	1	1	1	1	1	$\frac{\lambda g \Delta T_M L_Z}{\rho_a U_S^2}$	$\frac{\Delta P_D}{\rho_a U_S^2}$	$\frac{U_F^2}{U_S^2}$	$\frac{U_F^2 L_S}{U_S^2 L_N}$	$\frac{U_F^2 L_S}{U_S^2 L_Z}$	$\frac{U_F^2 L_S}{U_S^2 L_N}$	$\frac{U_F^2 L_S}{U_S^2 L_Z}$	$\frac{U_F^2 L_S}{U_S^2 L_N}$
IV	1	1	1	1	1	1	1	δ	δ	δ	1	δ	1	δ

Table 3.1 (cont'd) Simplification of Momentum and Thermal Energy Conservation Equations

n-momentum equation

Stage	$\frac{\partial uv}{\partial s}$	$+\frac{\partial v^2}{\partial n}$	$+\frac{\partial vw}{\partial z}$	$+K\frac{\partial nv^2}{\partial n}$	$+K\frac{\partial nvw}{\partial z}$	$-Ku^2 = \frac{\lambda g}{\rho_a}\int_z^{-\infty}\frac{\partial \Delta T}{\partial n}dz$	$+\frac{\lambda Kng}{\rho_a}\int_z^{-\infty}\frac{\partial \Delta T}{\partial n}dz$	$-\frac{1}{\rho_a}\frac{\partial P_d}{\partial n}$	$-\frac{Kn}{\rho_a}\frac{\partial P_d}{\partial n}$	$-\frac{\partial \tilde{u}\tilde{v}}{\partial s}$	$-\frac{\partial \tilde{v}^2}{\partial n}$
I	$\frac{U_S U_N}{L_S}$	$\frac{U_N^2}{L_N}$	$\frac{U_N U_Z}{L_Z}$	$\frac{KL_N U_N^2}{L_N}$	$\frac{KL_N U_N U_Z}{L_Z}$	KU_S^2	$\frac{\lambda g \Delta T_M L_Z}{\rho_a L_N}$	$\frac{\lambda KL_N g \Delta T_M L_Z}{\rho_a L_N}$	$\frac{\Delta P_D}{\rho_a L_N}$	$\frac{KL_N \Delta P_D}{\rho_a L_N}$	$\frac{U_F^2}{L_S}$	$\frac{U_F^2}{L_N}$
II	$\frac{U_N^2}{L_N}$	$\frac{U_N^2}{L_N}$	$\frac{U_N^2}{L_N}$	$\frac{U_N^2}{L_N}$	$\frac{U_N^2}{L_N}$	$\frac{U_S^2}{L_N}$	$\frac{\lambda g \Delta T_M L_Z}{\rho_a L_N}$	$\frac{\lambda g \Delta T_M L_Z}{\rho_a L_N}$	$\frac{\Delta P_D}{\rho_a L_N}$	$\frac{\Delta P_D}{\rho_a L_N}$	$\frac{U_F^2}{L_S}$	$\frac{U_F^2}{L_N}$
III	$\frac{L_N}{L_S}$	$\frac{L_N}{L_S}$	$\frac{L_N}{L_S}$	$\frac{L_N}{L_S}$	$\frac{L_N}{L_S}$	$\frac{L_S}{L_N}$	$\frac{\lambda g \Delta T_M L_Z L_S}{\rho_a U_S^2 L_N}$	$\frac{\lambda g \Delta T_M L_Z L_S}{\rho_a U_S^2 L_N}$	$\frac{\Delta P_D L_S}{\rho_a U_S^2 L_N}$	$\frac{\Delta P_D L_S}{\rho_a U_S^2 L_N}$	$\frac{U_F^2}{U_S^2}$	$\frac{U_F^2 L_S}{U_S^2 L_Z}$
IV	1	1	1	1	1	1	1	1	δ	δ	δ	δ

Stage	$-\frac{\partial \tilde{v}\tilde{w}}{\partial z}$	$-K\frac{\partial n\tilde{v}^2}{\partial n}$	$-K\frac{\partial n\tilde{v}\tilde{w}}{\partial z}$	$+K\tilde{u}^2$
I	$\frac{U_F^2}{L_Z}$	$\frac{KL_N U_F^2}{L_N}$	$\frac{KL_N U_F^2}{L_Z}$	KU_F^2
II	$\frac{U_F^2}{L_Z}$	$\frac{U_F^2}{L_N}$	$\frac{U_F^2}{L_Z}$	$\frac{U_F^2}{L_N}$
III	$\frac{U_F^2 L_S}{U_S^2 L_Z}$	$\frac{U_F^2 L_S}{U_S^2 L_N}$	$\frac{U_F^2 L_S}{U_S^2 L_Z}$	$\frac{U_F^2 L_S}{U_S^2 L_N}$
IV	1	δ	1	δ

Table 3.1 (cont'd) Simplification of Momentum and Thermal Energy Conservation Equations

z-momentum equation

Stage	$\frac{\partial uw}{\partial s} + \frac{\partial vw}{\partial n} + \frac{\partial w^2}{\partial z} + K\frac{\partial nvw}{\partial n} + K\frac{\partial nw^2}{\partial z} = -\frac{1}{\rho_a}\frac{\partial P_d}{\partial z} - \frac{Kn}{\rho_a}\frac{\partial P_d}{\partial z} - \frac{\partial \overline{\tilde{u}\tilde{w}}}{\partial s} - \frac{\partial \overline{\tilde{v}\tilde{w}}}{\partial n} - \frac{\partial \overline{\tilde{w}^2}}{\partial z} - K\frac{\partial n\overline{\tilde{v}\tilde{w}}}{\partial n} - K\frac{\partial n\overline{\tilde{w}^2}}{\partial z}$											
I	$\frac{U_S U_Z}{L_S}$	$\frac{U_N U_Z}{L_N}$	$\frac{U_Z^2}{L_Z}$	$\frac{KL_N U_N U_Z}{L_N}$	$\frac{KL_N U_Z^2}{L_Z}$	$\frac{\Delta P_D}{\rho_a L_Z}$	$\frac{KL_N \Delta P_D}{\rho_a L_Z}$	$\frac{U_F^2}{L_S}$	$\frac{U_F^2}{L_N}$	$\frac{U_F^2}{L_Z}$	$\frac{KL_N U_F^2}{L_N}$	$\frac{KL_N U_F^2}{L_Z}$
II	$\frac{U_Z^2}{L_Z}$	$\frac{U_Z^2}{L_Z}$	$\frac{U_Z^2}{L_Z}$	$\frac{U_Z^2}{L_Z}$	$\frac{U_Z^2}{L_Z}$	$\frac{\Delta P_D}{\rho_a L_Z}$	$\frac{\Delta P_D}{\rho_a L_Z}$	$\frac{U_F^2}{L_S}$	$\frac{U_F^2}{L_N}$	$\frac{U_F^2}{L_Z}$	$\frac{U_F^2}{L_N}$	$\frac{U_F^2}{L_Z}$
III	$\frac{L_Z}{L_S}$	$\frac{L_Z}{L_S}$	$\frac{L_Z}{L_S}$	$\frac{L_Z}{L_S}$	$\frac{L_Z}{L_S}$	$\frac{\Delta P_D L_S}{\rho_a U_S^2 L_Z}$	$\frac{\Delta P_D L_S}{\rho_a U_S^2 L_Z}$	$\frac{U_F^2}{U_S^2}$	$\frac{U_F^2 L_S}{U_S^2 L_N}$	$\frac{U_F^2 L_S}{U_S^2 L_Z}$	$\frac{U_F^2 L_S}{U_S^2 L_N}$	$\frac{U_F^2 L_S}{U_S^2 L_Z}$
IV	δ	δ	δ	δ	δ	1	1	δ	δ	1	δ	1

equation of thermal energy conservation

Stage	$\frac{\partial u\Delta T}{\partial s} + \frac{\partial v\Delta T}{\partial n} + \frac{\partial w\Delta T}{\partial z} + K\frac{\partial nv\Delta T}{\partial n} + K\frac{\partial nw\Delta T}{\partial z} = -\frac{\partial \overline{\tilde{u}\Delta\tilde{T}}}{\partial s} - \frac{\partial \overline{\tilde{v}\Delta\tilde{T}}}{\partial n} - \frac{\partial \overline{\tilde{w}\Delta\tilde{T}}}{\partial z} - K\frac{\partial n\overline{\tilde{v}\Delta\tilde{T}}}{\partial n} - K\frac{\partial n\overline{\tilde{w}\Delta\tilde{T}}}{\partial z}$											
I	$\frac{U_S \Delta T_M}{L_S}$	$\frac{U_N \Delta T_M}{L_N}$	$\frac{U_Z \Delta T_M}{L_Z}$	$\frac{KL_N U_N \Delta T_M}{L_N}$	$\frac{KL_N U_Z \Delta T_M}{L_Z}$	$\frac{U_F \Delta T_F}{L_S}$	$\frac{U_F \Delta T_F}{L_N}$	$\frac{U_F \Delta T_F}{L_Z}$	$\frac{KL_N U_F \Delta T_F}{L_N}$	$\frac{KL_N U_F \Delta T_F}{L_Z}$		
II	$\frac{U_S \Delta T_M}{L_S}$	$\frac{U_S \Delta T_M}{L_S}$	$\frac{U_S \Delta T_M}{L_S}$	$\frac{U_S \Delta T_M}{L_S}$	$\frac{U_S \Delta T_M}{L_S}$	$\frac{U_F \Delta T_F}{L_S}$	$\frac{U_F \Delta T_F}{L_N}$	$\frac{U_F \Delta T_F}{L_Z}$	$\frac{U_F \Delta T_F}{L_N}$	$\frac{U_F \Delta T_F}{L_Z}$		
III	1	1	1	1	1	$\frac{U_F \Delta T_F}{U_S \Delta T_M}$	$\frac{U_F \Delta T_F L_S}{U_S \Delta T_M L_N}$	$\frac{U_F \Delta T_F L_S}{U_S \Delta T_M L_Z}$	$\frac{U_F \Delta T_F L_S}{U_S \Delta T_M L_N}$	$\frac{U_F \Delta T_F L_S}{U_S \Delta T_M L_Z}$		
IV	1	1	1	1	1	δ	δ	1	δ	1		

The stage by stage derivations of the order of magnitude analysis of the momentum equations are shown in Table 3.1. In each equation the relative order of magnitude of each term is expressed in terms of the scales and is written directly below the corresponding term. The analysis begins with first dropping buoyancy terms for the nonbuoyant case and curvature terms for no crossflow case. The deduction from stage I to stage III consists of first the use of Eqs. 3.40 and 3.41 for the no crossflow case and the significantly bent case, respectively, and then the multiplication of each term by L_S/U_S^2 for all cases. The reasoning which leads from stage III to stage IV is discussed in the following sections.

3.3.2.1 Nonbuoyant Jets with No Curvature

The s-momentum equation indicates that

$$\frac{L_S}{L_N} \sim \frac{1}{\delta} \tag{3.42}$$

and/or

$$\frac{L_S}{L_Z} \sim \frac{1}{\delta} \tag{3.43}$$

in order that at least one turbulence term has the same order of magnitude as the convective terms. The n-momentum equation and the z-momentum equation indicate that any one of three combinations of L_S/L_N and L_S/L_Z, namely, $L_S/L_N \sim 1/\delta$ and $L_S/L_Z \sim 1/\delta$, $L_S/L_N \sim 1$ and $L_S/L_Z \sim 1/\delta$, or $L_S/L_N \sim 1/\delta$ and $L_S/L_Z \sim 1$, gives $\Delta P_D/(\rho_a U_S^2) \sim \delta$ and satisfies the balancing of the equations. However, the free turbulence motions considered in this case have an important property in common with the boundary-layer motions, namely that the turbulence region is narrow in the lateral and vertical directions in comparison with the longitudinal direction [Hinze, 1959].

Hence it must be true that

$$\frac{L_S}{L_N} \sim \frac{1}{\delta}$$

$$\frac{L_S}{L_Z} \sim \frac{1}{\delta} \qquad (3.44)$$

and $$\frac{\Delta P_D}{\rho_a U_S^2} \sim \delta$$

Discussion on the results for this case and the other three cases to follow is given in Section 3.3.2.5 after all four cases have been considered.

3.3.2.2 Nonbuoyant Jets with Significant Curvature

The s-momentum equation indicates that L_S/L_N and/or L_S/L_Z must be of order $1/\delta$, otherwise all the turbulence terms in the s-momentum equation would be small compared with the convective terms. If both L_S/L_N and L_S/L_Z are of order $1/\delta$, it follows from the n-momentum equation that $\Delta P_D/(\rho_a U_S^2) \sim 1$. This will lead to the result that there is no term in z-momentum equation which can balance the pressure term. Therefore, the only possible solution is

$$\frac{L_S}{L_N} \sim 1$$

$$\frac{L_S}{L_Z} \sim \frac{1}{\delta} \qquad (3.45)$$

and $$\frac{\Delta P_D}{\rho_a U_S^2} \sim \delta$$

3.3.2.3 Buoyant Jets with No Curvature

When the jet Richardson number is large, buoyancy forces become important. Since the Richardson number represents the ratio of buoyancy forces to inertial forces, one can write $\lambda g \Delta T_M L_Z / (\rho_a U_S^2) \sim 1$ or higher, for this case. The situation that $\lambda g \Delta T_M L_Z / (\rho_a U_S^2) \sim 1$ is considered first. For some turbulence terms in the s-momentum equation to be of the same order of magnitude as the convective terms, the relations shown in Eq. 3.42 and/or in Eq. 3.43 must be true. However, the n-momentum equation shows that if both $L_S/L_N \sim 1/\delta$ and $L_S/L_Z \sim 1/\delta$ are true, then there would be no terms of sufficient magnitude to balance the buoyancy term which would be of order $1/\delta$. This leads to the conclusion that $L_S/L_N \sim 1$ and $L_S/L_Z \sim 1/\delta$. The z-momentum equation indicates that $\Delta P_D / (\rho_a U_S^2) \sim \delta$.

If it is assumed that $\lambda g \Delta T_M L_Z / (\rho_a U_S^2)$ has order of magnitude higher than unity, then all the convective terms in all the three momentum equations would be small compared with the buoyancy terms. This is an indication that the characteristics of a jet would no longer exist and the type of analysis being considered in this research would not be applicable. As a consequence, the case of $\lambda g \Delta T_M L_Z / (\rho_a U_S^2)$ of order greater than unity is not considered further.

3.3.2.4 Buoyant Jets with Significant Curvature

Following the same argument as in Section 3.3.2.3, it can be shown that for the assumption of jet-like behavior to be valid, the highest possible order of magnitude for $\lambda g \Delta T_M L_Z / (\rho_a U_S^2)$ is unity.

For some turbulence terms in the s-momentum equation to be of the same order as some of the convective terms, it is again true that Eq. 3.42

and/or Eq. 3.43 must be hold. However, if both $L_S/L_N \sim 1/\delta$ and $L_S/L_N \sim 1/\delta$, then all turbulence terms on the right hand side of the n-momentum equation would be small compared with both the buoyancy terms and the convective term Ku^2, all of which would be of order $1/\delta$. Hence the solution is $L_S/L_N \sim 1$ and $L_S/L_N \sim 1/\delta$. It follows from the z-momentum equation that $\Delta P_D/(\rho_a U_S^2) \sim \delta$.

3.3.2.5 Discussion of Results of Order of Magnitude Analysis for the Momentum Equations

The results of the order of magnitude analysis of momentum equations are as follows:

1. nonbuoyant jets with no curvature

$$\frac{L_S}{L_N} \sim \frac{1}{\delta}$$

$$\frac{L_S}{L_Z} \sim \frac{1}{\delta}$$

$$\frac{\Delta P_D}{\rho_a U_S^2} \sim \delta$$

2. nonbuoyant jets with significant curvature

$$\frac{L_S}{L_N} \sim 1$$

$$\frac{L_S}{L_Z} \sim \frac{1}{\delta}$$

$$\frac{\Delta P_D}{\rho_a U_S^2} \sim \delta$$

3. buoyant jets with no curvature

$$\frac{L_S}{L_N} \sim 1$$

$$\frac{L_S}{L_Z} \sim \frac{1}{\delta}$$

$$\frac{\Delta P_D}{\rho_a U_S^2} \sim \delta$$

4. buoyant jets with significant curvature

$$\frac{L_S}{L_N} \sim 1$$

$$\frac{L_S}{L_Z} \sim \frac{1}{\delta}$$

$$\frac{\Delta P_D}{\rho_a U_S^2} \sim \delta$$

The length scale ratios L_S/L_N and L_S/L_Z can be interpreted as the inverse of the rates of jet spreading in lateral and vertical directions, respectively. In all four cases $L_S/L_Z \sim 1/\delta$, which indicates that the jet occupies a slender region in the z or vertical direction. In case 1, both L_S/L_N and L_S/L_Z are of order of $1/\delta$. This is an indication that the jet is slender in both lateral and vertical directions. This agrees with what is expected for a nonbuoyant jet with no crossflow [Hinze, 1959]. In cases 2, 3 and 4, the rate of lateral spreading is relatively high, as suggested by $L_S/L_N \sim 1$. For case 3, this high rate of spreading is apparently due to the buoyancy forces which are assumed to be important in that case.

The significant rate of lateral spreading indicated by the solution of case 2 is clearly not due to the effect of buoyancy forces since they do not exist in case 2. The assumption of significant jet curvature apparently leads to the result that $L_S/L_N \sim 1$. The relation of large curvature K to significant lateral spreading has not been investigated in detail but may be associated with centrifugal forces. It should be noted however, that the portion of the jet in which case 2 (nonbuoyant jets with significant curvature) applies and in which $L_S/L_N \sim 1$ is relatively small compared with the entire jet region. Downstream of the small region of significant curvature the jet axis will be almost aligned with the ambient flow and $L_S/L_N \sim 1$ will no longer apply. Therefore the condition that $L_S/L_N \sim 1$ in case 2 and $L_S/L_N \sim 1/\delta$ in case 1 for nonbuoyant jets with no curvature is by no means an indication that a nonbuoyant jet discharged into a strong crossflow will have a significantly greater jet width than a nonbuoyant jet with no crossflow. The result that $L_S/L_N \sim 1$ in case 4 apparently is due to the combined effects of significant jet curvature and buoyancy forces.

In all four cases $\Delta P_D/(\rho_a U_S^2) \sim \delta$. This implies that the pressure terms in s direction is negligible, but it may be important in the other two directions, as shown in Table 3.1.

3.3.3 Equation of Thermal Energy Conservation

Table 3.1 also shows the detailed derivation of the order of magnitude analysis of the thermal energy conservation equation for buoyant jet cases. For nonbuoyant jet cases the equation of thermal energy conservation is not required since ρ and T are constants.

The procedures from stage I to stage III are the same as for the momentum equations, except that the multiplication of each term is done by using $L_S/(U_S\Delta T_M)$ instead of L_S/U_S^2. In Section 3.3.2, the order of magnitude of L_S/L_Z was found to have the highest possible order of $1/\delta$ in all four cases. Hence the highest order of magnitude of the turbulent heat flux terms on the right hand side of the equation of thermal energy conservation is $\frac{U_F}{U_S}\frac{\Delta T_F}{\Delta T_M}\frac{L_S}{L_Z}$. For the turbulent heat flux terms of highest order of magnitude to balance the mean flow convective terms, it must be that [Pande and Rajaratnam, September, 1975]

$$\frac{U_F}{U_S}\frac{\Delta T_F}{\Delta T_M}\frac{L_S}{L_Z} \sim 1 \qquad (3.46)$$

or

$$\frac{U_F}{U_S}\frac{\Delta T_F}{\Delta T_M} \sim \delta$$

Using Eq. 3.46 and the corresponding scales of L_S/L_N and L_S/L_Z established in Section 3.3.2, the deduction from stage III to stage IV can be performed as shown in the table.

3.3.4 The Simplified Governing Equations

From the order of magnitude analysis, it would be possible to obtain four sets of differential equations with one set applying for each of the previously considered cases. However, for a buoyant surface jet discharged into a strong crossflow, the jet could encounter all of the four cases considered previously as it progresses from the nonbuoyant jet to the buoyant case as well as from the significantly bent case to the no crossflow case as was discussed in the beginning of Section 3.3. Therefore, no single set of differential equations obtained for one case could

adequately describe the problem of a buoyant jet discharged into a strong crossflow. Thus, the final simplified governing equations for buoyant surface jets were obtained by retaining all the terms of order unity in any one of all four cases. These resulting equations are

continuity equation

$$\frac{\partial u}{\partial s} + \frac{\partial v}{\partial n} + \frac{\partial w}{\partial z} + K\frac{\partial nv}{\partial n} + K\frac{\partial nw}{\partial z} = 0 \tag{3.47}$$

s-momentum equation

$$\frac{\partial u^2}{\partial s} + \frac{\partial uv}{\partial n} + \frac{\partial uw}{\partial z} + K\frac{\partial nuv}{\partial n} + K\frac{\partial nuw}{\partial z} + Kuv = \frac{\lambda g}{\rho_a}\int_z^{-\infty}\frac{\partial \Delta T}{\partial s}\,dz - \frac{\partial \overline{\tilde{u}\tilde{v}}}{\partial n} - \frac{\partial \overline{\tilde{u}\tilde{w}}}{\partial z} - K\frac{\partial n\overline{\tilde{u}\tilde{w}}}{\partial z} \tag{3.48}$$

n-momentum equation

$$\frac{\partial uv}{\partial s} + \frac{\partial v^2}{\partial n} + \frac{\partial vw}{\partial z} + K\frac{\partial nv^2}{\partial n} + K\frac{\partial nvw}{\partial z} - Ku^2 = \frac{\lambda(1+Kn)g}{\rho_a}\int_z^{-\infty}\frac{\partial \Delta T}{\partial n}\,dz - \frac{1}{\rho_a}\frac{\partial P_d}{\partial n} - \frac{\partial \overline{\tilde{v}^2}}{\partial n} - \frac{\partial \overline{\tilde{v}\tilde{w}}}{\partial z} - K\frac{\partial n\overline{\tilde{v}\tilde{w}}}{\partial z} \tag{3.49}$$

z-momentum equation

$$0 = -\frac{(1+Kn)}{\rho_a}\frac{\partial P_d}{\partial z} - \frac{\partial \overline{\tilde{w}^2}}{\partial z} - \frac{\partial \overline{\tilde{v}\tilde{w}}}{\partial n} - K\frac{\partial n\overline{\tilde{w}^2}}{\partial z} \tag{3.50}$$

equation of thermal energy conservation

$$\frac{\partial u\Delta T}{\partial s} + \frac{\partial v\Delta T}{\partial n} + \frac{\partial w\Delta T}{\partial z} + K\frac{\partial nv\Delta T}{\partial n} + \frac{\partial nw\Delta T}{\partial z} = -\frac{\partial \overline{\tilde{v}\Delta\tilde{T}}}{\partial n} - \frac{\partial \overline{\tilde{w}\Delta\tilde{T}}}{\partial z} - K\frac{\partial n\overline{\tilde{w}\Delta\tilde{T}}}{\partial z} \tag{3.51}$$

3.4 Assumption of Similarity Profiles

In order to integrate Eqs. 3.47-3.51, it is necessary to assume similarity profiles for the velocity and temperature distributions

perpendicular to the jet axis, but before doing that, some general characteristics of the velocity and temperature distributions need to be considered. Experiments have shown that the trajectories of maximum temperature and maximum velocity do not coincide [Kamotani and Greber, 1972]. Since the temperature distribution is of primary interest of this study, the jet axis is defined as the locus of maximum temperature, and the jet dimensions and boundaries are all defined according to the temperature distribution.

Figure 3.2 shows the coordinate definitions for a deflected surface jet. The jet axis (n=0) divides the jet cross section into two parts which will be called the inner part and the outer part. Parameters for the inner part of the jet are designated with a prime. It is assumed that the width of the core is the same in both parts so that $a' = a$. Each part of the jet is further divided into the following four possible regions as shown in Fig. 3.3:

Region 1 - the unsheared core region where velocity and temperature are uniform.

Region 2 - the vertically sheared region where velocity and temperature profiles are functions of z only.

Region 3 - the horizontally sheared region where velocity and temperature profiles are functions of n only.

Region 4 - the vertically and horizontally sheared region where velocity and temperature profiles are functions of both n and z.

In the zone of flow establishment (ZFE) the jet has eight regions, while in the near field region (NFR), the jet has only two regions, i.e., regions 4

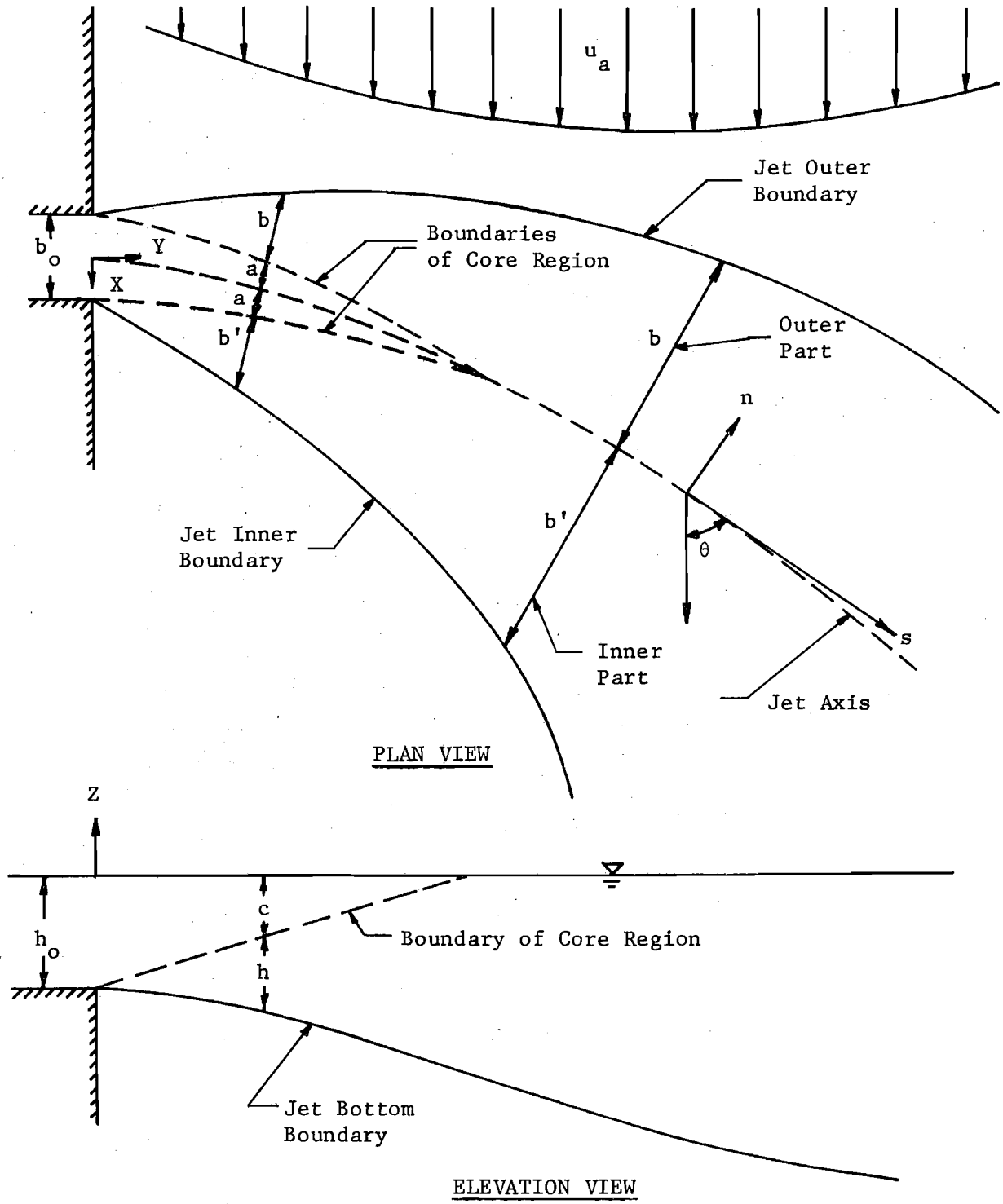

Fig. 3.2 Coordinate definitions for deflected surface jet

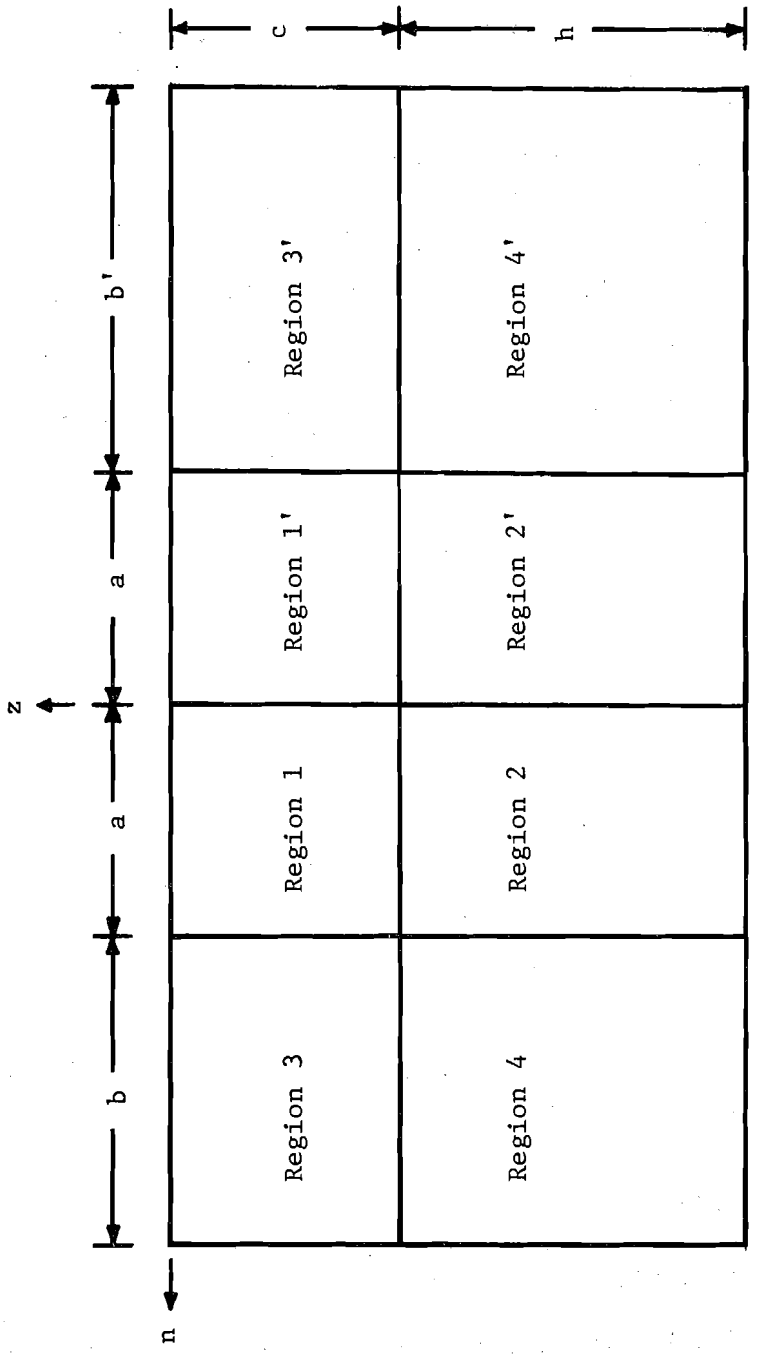

Fig. 3.3 Assumed regions of jet cross section

and 4'. During the transition of the jet from ZFE to NFR, the jet may have regions 3, 4, 3' and 4' if $a = 0$, $c \neq 0$ or regions 2, 4, 2' and 4', if $a \neq 0$, $c = 0$.

The magnitude of the free surface elevation η can be shown to be negligible [Stolzenbach and Harleman, 1971]. Thus, in specifying the range of consideration in the vertical direction, it can be assumed that $\eta = 0$.

Figure 3.4 shows the assumed similarity profiles of longitudinal velocity and temperature. The jet longitudinal velocity and temperature distributions for each region are formulated as follows and account for the fact that the ambient velocity and temperature distributions may not be uniform:

outer part of the jet

region 1: $0 < n < a, \quad -c < z < 0$

$$u = u_m$$

$$\Delta T = \Delta T_m$$

region 2: $0 < n < a, \quad -(c+h) < z < -c$

$$u = u_c + (u_m - u_c) f(\phi_z)$$

$$\Delta T = \Delta T_c + (\Delta T_m - \Delta T_c) t(\phi_z)$$

region 3: $a < n < (a+b), \quad -c < z < 0$ (3.52)

$$u = u_s + (u_m - u_s) f(\phi_n)$$

$$\Delta T = \Delta T_s + (\Delta T_m - \Delta T_s) t(\phi_n)$$

region 4: $a < n < (a+b), \quad -(c+h) < z < -c$

$$u = u_d + (u_c - u_d) f(\phi_n) + (u_s - u_d) f(\phi_z) + (u_m + u_d - u_s - u_c) f(\phi_n) f(\phi_z)$$

$$\Delta T = \Delta T_d + (\Delta T_c - \Delta T_d) t(\phi_n) + (\Delta T_s - \Delta T_d) t(\phi_z) + (\Delta T_m + \Delta T_d - \Delta T_s - \Delta T_c) \cdot t(\phi_n) t(\phi_z)$$

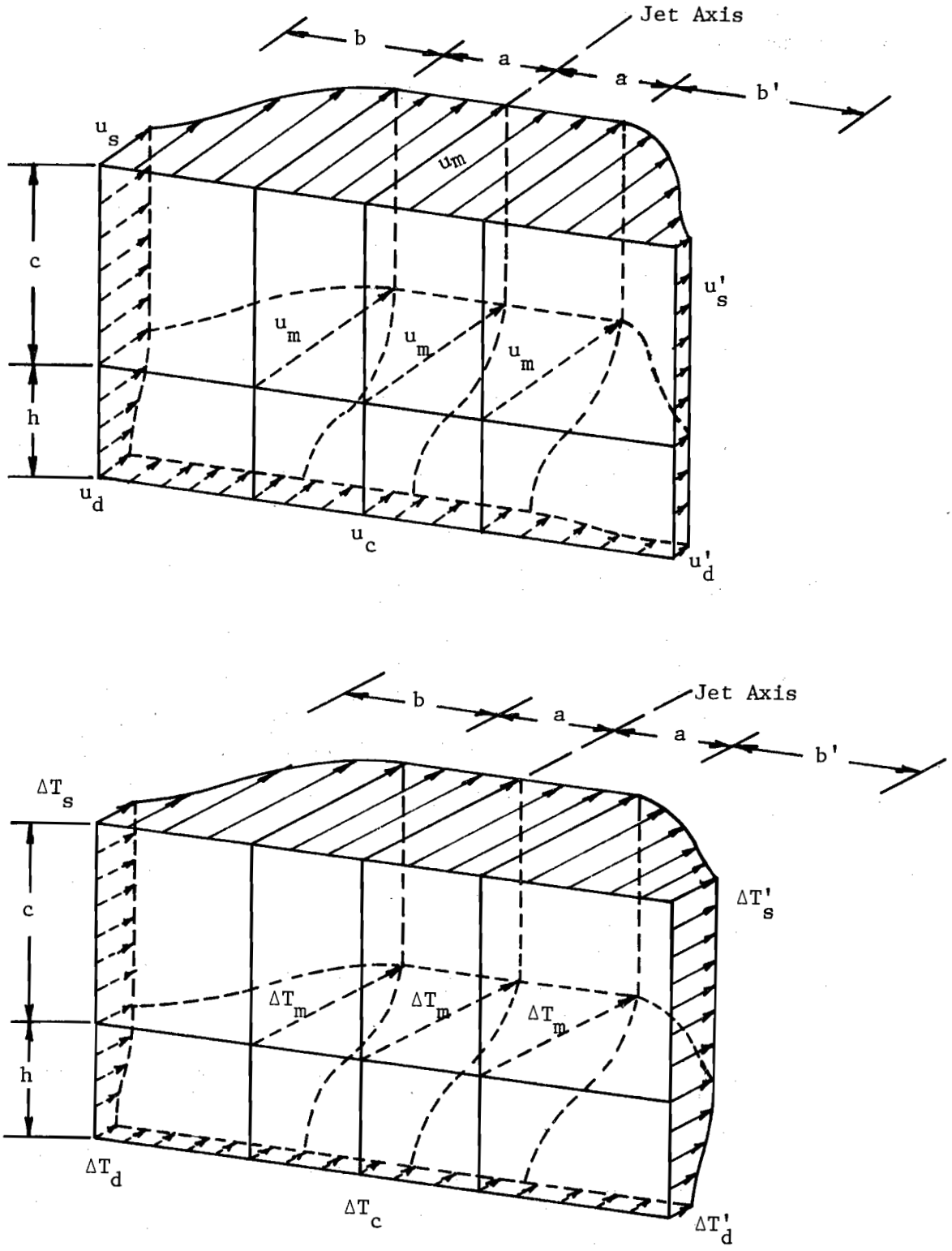

Fig. 3.4 Assumed longitudinal velocity and temperature profiles

inner part of the jet

region 1': $-a < n < 0,\ -c < z < 0$

$$u = u_m$$

$$\Delta T = \Delta T_m$$

region 2': $-a < n < 0,\ -(c+h) < z < -c$

$$u = u_c + (u_m - u_c) f(\phi_z)$$

$$\Delta T = \Delta T_c + (\Delta T_m - \Delta T_c) t(\phi_z)$$

region 3': $-(a+b') < n < -a,\ -c < z < 0$ (3.53)

$$u = u'_s + (u_m - u'_s) f(\phi'_n)$$

$$\Delta T = \Delta T'_s + (u_m - \Delta T'_s) t(\phi'_n)$$

region 4': $-(a+b') < n < -a,\ -(c+h) < z < -c$

$$u = u'_d + (u_c - u'_d) f(\phi'_n) + (u'_s - u'_d) f(\phi_z) + (u_m + u'_d - u'_s - u'_c) f(\phi'_n) f(\phi_z)$$

$$\Delta T = \Delta T'_d + (\Delta T_c - \Delta T'_d) t(\phi'_n) + (\Delta T'_s - \Delta T'_d) t(\phi_z) + (\Delta T_m + \Delta T'_d - \Delta T'_s - \Delta T'_c) \cdot t(\phi'_n) t(\phi_z)$$

In Eqs. 3.52 and 3.53,

u = jet longitudinal velocity,

ΔT = jet temperature rise above reference ambient temperature,

u_m = velocity on jet axis,

ΔT_m = temperature rise on jet axis relative to reference ambient temperature,

a, b, b', c, h = jet dimensions, assuming $a' = a$,

$f(\phi) = (1-\phi^{3/2})^{nv}$,

$t(\phi) = (1-\phi^{3/2})^{nt}$,

$\phi_n = \dfrac{(n-a)}{b}$ for $n > a$,

$$\phi_z = \frac{(-z-c)}{h} \quad \text{for} \quad z < -c$$

$$\phi'_n = \frac{(-n-a)}{b'} \quad \text{for} \quad n < -a.$$

The general form of the similarity functions f and t has been presented in Section 2.3.2. The exponents nv and nt, are assumed to be functions of only the jet aspect ratio. Reichardt [1942] performed experiments on a heated two-dimensional jet. The temperature differences were small enough that the jet was essentially non-buoyant. His measurements of velocity and temperature distributions indicated that nt/nv (or turbulent Prandtl number P_{r_t}) equalled 1/2. This supports the conclusion of Taylor [1932] based on the concept of vorticity transport for two-dimensional jets. For circular turbulent jets, the value of nt/nv is about 0.727 [Corrsin and Uberoi, 1950]. Two-dimensional and axisymmetrical jets may be considered as two extremes of three-dimensional jets. Thus, the value of nt/nv for three-dimensional jets should be between 0.5 and 0.727. In the present study, the value of nt/nv was chosen to be 0.6 and nv = 2 was used following Abramovich [1963] and Stolzenbach and Harleman [1971]. The above selection on the values of nt/nv and nv gives nt = 1.2.

The longitudinal velocities and the temperatures at the jet boundaries are represented by u_s, u_d, u_c, u'_s, u'_d, ΔT_s, ΔT_d, ΔT_c, $\Delta T'_s$ and $\Delta T'_d$ (Fig. 3.4). These quantities are considered as known and are defined as follows except that u'_s and $\Delta T'_s$ require further discussion and they will be defined later:

$u_s = (u_a)_{a+b} \cos\theta$, where $(u_a)_{a+b}$ is the average over the depth of the jet $(-(c+h)<z<0)$ of the ambient velocity at the upstream edge of the jet $(n=a+b)$ and the multiplication by $\cos\theta$ gives the component parallel to the jet axis.

$u_c = (u_a)_{-(c+h)} \cos\theta$, where $(u_a)_{-(c+h)}$ is the average over the width of the jet ($-(a+b') < n < (a+b)$) of the ambient velocity at the bottom boundary of the jet ($z=-(c+h)$) and the multiplication by $\cos\theta$ gives the component parallel to the jet axis.

ΔT_s = the average over the depth of the jet ($-(c+h) < z < 0$) of the ambient temperature rise at the upstream edge of the jet ($n=a+b$).

ΔT_c = the average over the width of the jet ($-(a+b') < n < (a+b)$) of the ambient temperature rise at the bottom boundary of the jet ($z=-(c+h)$).

$u_d = u_s$ or u_c, whichever is smaller (in Fig. 3.4, $u_c < u_s$).

$u'_d = u'_s$ or u_c, whichever is smaller (in Fig. 3.4, $u'_s < u_c$).

$\Delta T_d = \Delta T_s$ or ΔT_c, whichever is smaller (in. Fig. 3.4, $\Delta T_c < \Delta T_s$).

$\Delta T'_d = \Delta T'_s$ or $\Delta T'_c$, whichever is smaller (in Fig. 3.4, $\Delta T_c < \Delta T'_s$).

Using u_d, u'_d, ΔT_d and $\Delta T'_d$ at the lower corners of the jet boundary insures a smooth transition for ambient velocity (or ambient temperature rise) from the side boundaries to the bottom boundary of the jet.

Since the jet provides a sheltering effect on the downstream side of the jet, the ambient velocity in that protected region is smaller than that on the upstream side [Policastro and Tokar, 1972]. Thus, u'_s, the average over the depth of the jet ($-(c+h) < z < 0$) of the ambient velocity at the downstream edge of the jet ($n=a+b'$) is smaller than u_s and is somewhat arbitrarily assumed to be

$$u'_s = u_s \cos^m\left[\frac{\pi}{2}\left(\frac{\theta}{\theta_o}\right)\right] \qquad (3.54)$$

Eq. 3.54 gives $u'_s = 0$ at the exit regardless of the orientation of the

discharge, and $u_s' = u_s$ when the jet is aligned with the ambient flow. Because of the lack of data to support any other value, it was assumed that $m = 1$.

Carter [1969] conducted experiments on two-dimensional vertical slot jets discharged into a crossflow. He observed that a recirculating eddy was created on the lee side of the jet. In that eddy the temperature was higher than the ambient temperature (Section 2.3). For the two-dimensional case ambient fluids are blocked from entering into the downstream eddy region. However, for three-dimensional jets in rectangular channels as considered in this study, ambient fluids can pass underneath the jet to meet substantially all the entrainment demand on the downstream side of the jet. Therefore the temperature rise on the downstream side of the jet is not significant, as evidenced by the experimental data of this study (Section 5.1). Thus, $\Delta T_s'$ is assumed to be a known quantity and is defined as the average over the depth of the jet ($-(c+h)<z<0$) of the ambient temperature rise at the downstream edge of the jet ($n=-(a+b')$).

3.5 Boundary Conditions

The turbulent transport of heat and momentum as well as the lateral and vertical velocities on the jet boundaries have to be specified to permit the integration of the governing equations over the jet cross section.

3.5.1 Boundary Conditions on the Free Surface

It is assumed that no transfer of momentum occurs across the free surface. Hence,

$$\overline{\tilde{w}^2} = \overline{\tilde{u}\tilde{w}} = \overline{\tilde{v}\tilde{w}} = 0 \quad \text{at } z = 0 \tag{3.55}$$

Surface heat transfer to the atmosphere is assumed to be negligible in the NFR [Carter, 1969]:

$$\overline{\tilde{w}\Delta\tilde{T}} = 0 \quad \text{at } z = 0 \tag{3.56}$$

3.5.2 Boundary Conditions on the Jet Boundary

3.5.2.1 Turbulent Transfer on the Jet Boundary

The turbulent transport terms $\overline{\tilde{u}\tilde{w}}$, $\overline{\tilde{v}\tilde{w}}$ and $\overline{\tilde{w}\Delta\tilde{T}}$ are finite at the jet boundary and approach the ambient levels at sufficient distance away from the jet. When the momentum equations are integrated over the jet cross section, these turbulent transport terms give rise to Reynolds stress terms which should be evaluated on the jet boundary [Adams et al., 1975]. However, an accurate evaluation of these terms is difficult, especially because of the evolution of the jet along its trajectory [Adams et al., 1975]. Stolzenbach and Harleman [1971] assumed that there was no turbulent transfer of heat and momentum across the jet boundary. This assumption implies that the actual turbulent transport of heat and momentum at the boundaries can be artifically treated through the use of entrainment coefficient [Dunn et al., 1975]. The equivalent concept for this study is that the turbulent transfer across the jet boundaries is assumed to be taken into account in the drag and spreading coefficients, and the same assumption will be made in this study:

$$\overline{\tilde{w}^2} = \overline{\tilde{u}\tilde{w}} = \overline{\tilde{v}\tilde{w}} = \overline{\tilde{w}\Delta\tilde{T}} = 0 \quad \text{at } z = -(c+h)$$

$$\overline{\tilde{v}^2} = \overline{\tilde{u}\tilde{v}} = \overline{\tilde{v}\tilde{w}} = \overline{\tilde{v}\Delta\tilde{T}} = 0 \quad \text{at } n = a+b \text{ and } n = -(a+b') \tag{3.57}$$

3.5.2.2 Lateral and Vertical Velocity on the Jet Boundary

The entrainment velocity is assumed to be normal to the jet trajectory. Figure 3.5 shows the assumed entrainment velocity distribution on the jet boundary. The characteristic vertical entrainment velocity is w_e, whereas v_e and v_e' are the characteristic lateral entrainment velocities on the upstream side and the downstream side of the jet, respectively. The parameters w_e, v_e, and v_e' are each considered to be functions of s only, but the entrainment is also a function of n and z as shown in Fig. 3.5.

For a turbulent jet discharged into a crossflow, the kinematic boundary condition on the jet boundary must account for the fact that the fluid particles on the jet boundary possess longitudinal velocities due to crosscurrent. The lateral or vertical velocity on the boundary of a two-dimensional jet will be considered first. The results obtained from two-dimensional cases will then be extended for three-dimensional cases.

A two-dimensional vertical slot jet discharged into a coflowing ambient stream of velocity u_a is shown in Fig. 3.6. The jet is symmetrical; therefore, the primed parameters are equal to their non-primed counterparts. The continuity equation for this two-dimensional case is

$$\frac{\partial u}{\partial s} + \frac{\partial v}{\partial n} = 0 \tag{3.58}$$

Integration of Eq. 3.58 over the upper part of the jet ($0 \leq n \leq a+b$) yields

$$v_{bd} = -\frac{d}{ds}\int_0^{a+b} u\,dn + u_s \frac{d(a+b)}{ds} \tag{3.59}$$

where v_{bd} = lateral velocity on the jet boundary,

u_s = ambient velocity component parallel to the jet trajectory. For the two-dimensional jet considered here $u_s = u_a$.

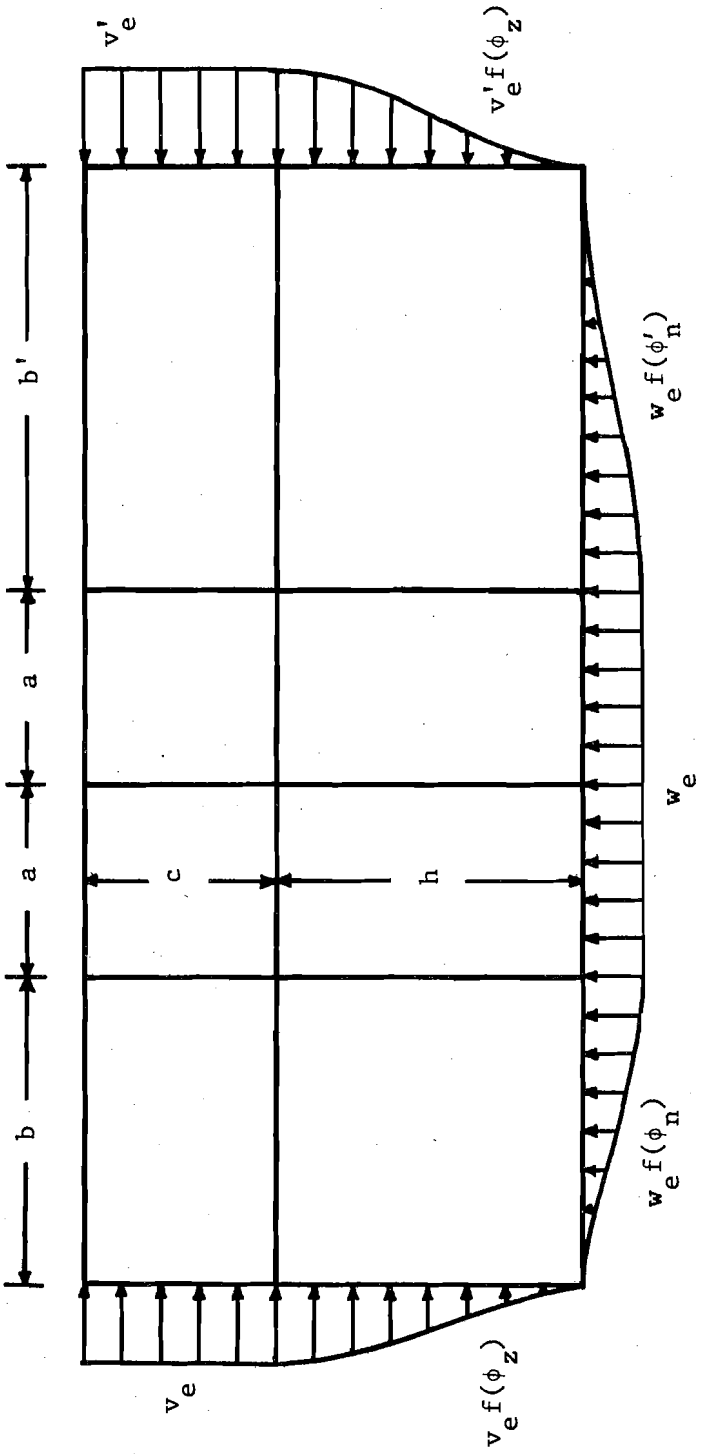

Fig. 3.5 Assumed entrainment velocity distributions

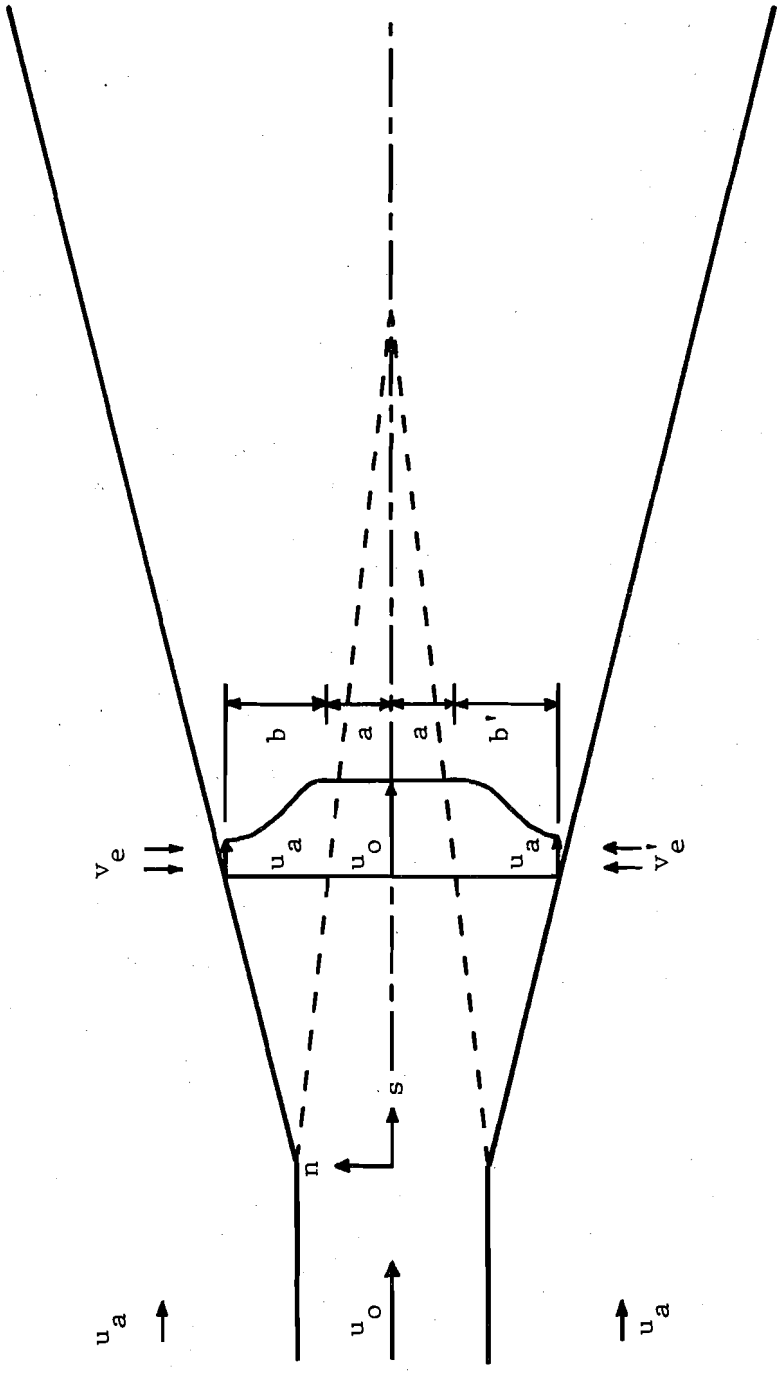

Fig. 3.6 Two-dimensional vertical-slot jet in coflowing ambient stream (Plan View)

The first term on the right hand side of Eq. 3.59 is, by definition, the entrainment velocity v_e. Hence Eq. 3.59 may be written as

$$v_{bd} = - v_e + u_s \frac{d(a+b)}{ds} \tag{3.60}$$

If Eq. 3.58 is integrated over the lower part of the jet ($0 \geq n \geq -a-b'$) one obtains

$$v'_{bd} = v'_e - u_s \frac{d(a+b')}{ds} \tag{3.61}$$

where v'_{bd} = lateral velocity on the jet boundary $n = - a - b'$. Similarily, for a horizontal two-dimensional slot jet discharged into a coflowing ambient stream as shown in Fig. 3.7, the vertical velocity on the jet boundary can be derived by integrating the continuity equation over the depth. The result can be written as

$$w_{bd} = w_e - u_c \frac{d(c+h)}{ds} \tag{3.62}$$

where w_{bd} = vertical velocity on the jet bottom boundary $z = - (c+h)$,

u_c = ambient velocity component parallel to the jet trajectory. For the case shown in Fig. 3.7, $u_c = u_a$.

Equations 3.60-3.62 indicate that the lateral or vertical velocity on the jet boundary is equal to the difference between the entrainment velocity and the spreading velocity of the jet boundary which is defined as the product of the slope of the jet boundary and the ambient velocity component parallel to the jet trajectory. Extension of this definition to the three-dimensional case leads to the following expressions for the lateral and vertical velocity on the boundary of a three-dimensional jet with crossflow:

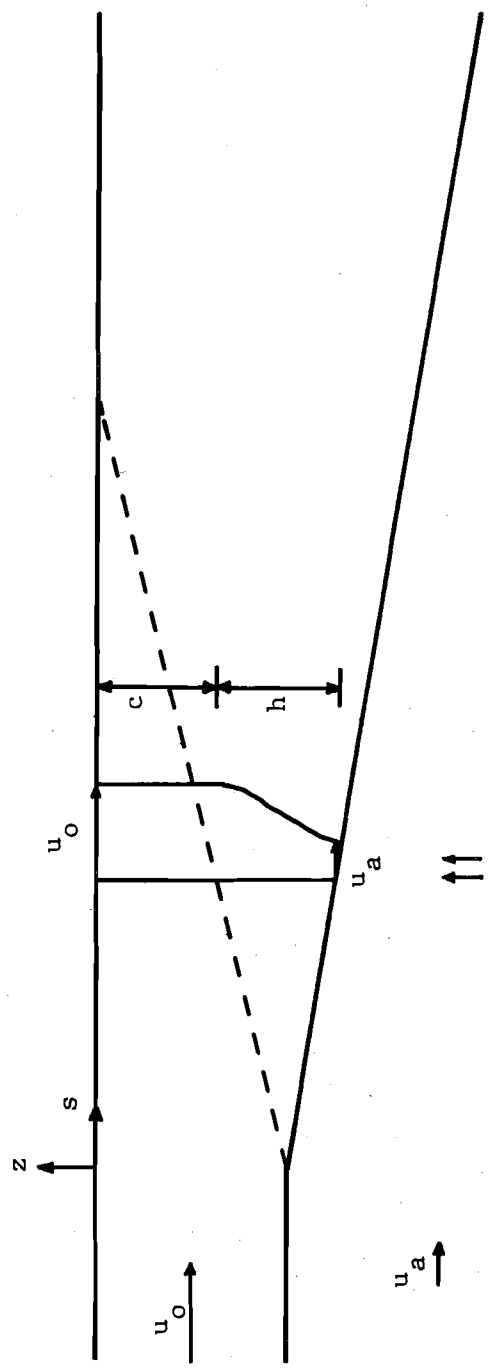

Fig. 3.7 Two-dimensional horizontal-slot jet in coflowing ambient stream

at $z = -(c+h)$:

$$w = w_e - u_c \frac{d(c+h)}{ds} \qquad \text{for } 0 < n < a$$

$$w = w_e f(\phi_n) - [u_d+(u_c-u_d)f(\phi_n)] \frac{d(c+h)}{ds} \qquad \text{for } a < n < (a+b) \tag{3.63}$$

$$w = w_e - u_c \frac{d(c+h)}{ds} \qquad \text{for } -a < n < 0$$

$$w = w_e f(\phi'_n) - [u'_d+(u_c-u'_d)f(\phi'_n)] \frac{d(c+h)}{ds} \qquad \text{for } -(a+b') < n < -a$$

at $n = a+b$:

$$v = -v_e + u_s \frac{d(a+b)}{ds} \qquad \text{for } -c < z < 0$$

$$v = -v_e f(\phi_z) + [u_d+(u_s-u_d)f(\phi_z)] \frac{d(a+b)}{ds} \qquad \text{for } -(c+h) < z < -c \tag{3.64}$$

at $n = -(a+b')$:

$$v = v'_e - u'_s \frac{d(a+b')}{ds} \qquad \text{for } -c < z < 0$$

$$v = v'_e f(\phi_z) - [u'_d+(u'_s-u'_d)f(\phi_z)] \frac{d(a+b')}{ds} \qquad \text{for } -(c+h) < z < -c \tag{3.65}$$

3.6 Lateral Velocity Distribution Over the Jet Cross Section

To allow the integration of the momentum equations over the jet cross section, the lateral velocity distribution within the cross section must be specified. It is assumed that the lateral velocity v is equal to

$$v = v_{NB} + v_B \tag{3.66}$$

where v_{NB} = lateral velocity in nonbuoyant jet,

v_B = lateral velocity induced by buoyancy forces.

Eq. 3.66 is tantamount to Eq. 2.5. Therefore, the discussion in Section 2.2.2 regarding the reason for the assumption of Eq. 2.5 and the limitations of it are all equally applicable to Eq. 3.66. Only two terms in the momentum equations require the specification of lateral velocity

distribution over the jet cross section during the integration, namely, Kuv in the s-momentum equation and $\partial uv/\partial s$ in the n-momentum equation. Experience has shown that the various assumptions which are made in formulating expressions for v_{NB} and v_B do not have a significant effect on the overall results from the momentum equations.

3.6.1 Lateral Velocity of Nonbuoyant Jets

It is not possible to formulate the lateral velocity distribution for a three-dimensional jet without the prior knowledge of the longitudinal and vertical velocity distributions. For two-dimensional and axisymmetrical jets without crossflow, the formulation of the lateral velocity distribution is possible since the longitudinal velocity distributions are well established experimentally. If one considers that two-dimensional and axisymmetrical jets are two extremes of three-dimensional jets, an approximate formulation of the lateral velocity distribution for a three-dimensional nonbuoyant jet may be obtained from those two extreme cases.

The maximum velocity on the axis of a two-dimensional jet downstream of the ZFE is inversely proportional to the square root of the distance [Abramovich, 1963]. From this fact and the assumption that the longitudinal velocity distributions are similar, Abramovich [1963] showed that the lateral velocity distribution for a two-dimensional jet with no crossflow was

$$v_{NB} = u_m C_6 \left[\phi_n f(\phi_n) - \frac{1}{2}\int_0^{\phi_n} f(\phi_n)\, d\phi_n\right] \tag{3.67}$$

where v_{NB} = lateral velocity distribution of nonbuoyant jets,

u_m = longitudinal velocity on the jet axis,

C_6 = constant,

$f(\phi_n)$ = velocity similarity function,

$\phi_n = \frac{n}{b}$.

Assuming that $f(\phi_n) = (1-\phi_n^{3/2})^2$, Eq. 3.67 yields

$$v_{NB} = u_m C_6 (\frac{1}{2}\phi_n - \frac{8}{5}\phi_n^{5/2} + \frac{7}{8}\phi_n^4) \tag{3.68}$$

At the jet boundary $\phi_n = 1$ and v_{NB} is equal to $-\frac{9}{40} u_m C_6$. This is the lateral velocity on the jet boundary and will be called v_{bd}. To extend the use of Eq. 3.68 for two-dimensional jets in a crossflow, it is assumed that the lateral velocity distributions are similar with respect to v_{bd} regardless of the ambient velocity. Thus a general lateral velocity distribution for a two-dimensional nonbuoyant jet may be obtained by substituting $u_m C_6 = -(\frac{40}{9}) v_{bd}$ into Eq. 3.68 to give

$$v_{NB} = v_{bd}(-\frac{40}{9})(\frac{1}{2}\phi_n - \frac{8}{5}\phi_n^{5/2} + \frac{7}{8}\phi_n^4) \tag{3.69}$$

The axial velocity downstream of the ZFE for a round nonbuoyant jet with no ambient flow is inversely proportional to longitudinal distance [Abramovich, 1963]. Applying the same considerations as in the formulation of Eq. 3.67 for two-dimensional jets, Abramovich [1963] showed that v_{NB} for a round nonbuoyant jet with no crossflow could be expressed as

$$v_{NB} = u_m C_6 [\phi_n f(\phi_n) - \frac{1}{\phi_n} \int_0^{\phi_n} f(\phi_n)\phi_n d\phi_n] \tag{3.70}$$

Following the same procedure as for the two-dimensional case one obtains the general lateral velocity distribution for round nonbuoyant jet as

$$v_{NB} = v_{bd}(-\frac{70}{9})(\frac{1}{2}\phi_n - \frac{10}{7}\phi_n^{5/2} + \frac{4}{5}\phi_n^4) \tag{3.71}$$

The lateral velocity distribution of a three-dimensional nonbuoyant jet with crossflow is assumed to be equal to the average of Eqs. 3.69 and 3.71 so that

$$v_{NB} = v_{bd} F(\phi_n) \tag{3.72}$$

where $$F(\phi_n) = -3\,\phi_n + 9\,\phi_n^{5/2} - 5\,\phi_n^{4} \tag{3.73}$$

Constant coefficients in $F(\phi_n)$ have been rounded off to integers. Equation 3.73 is assumed to be valid for $a < n < (a+b)$ (regions 3 and 4), and for $-(a+b') < n < -a$ (regions 3' and 4') with ϕ_n replaced by ϕ_n'. The value of v_{NB} is taken to be zero in $-a < n < a$ (regions 1, 2, 1' and 2').

3.6.2 Lateral Velocity Induced by Buoyancy Forces

To complete Eq. 3.66, v_B, the lateral velocity induced by buoyancy forces, is approximated in this section. It is assumed that v_B is zero at the jet axis and varies linearly up to its maximum at the edge of the jet at which it equals $u_m \frac{db}{ds}\big|_B$; the buoyant spreading $\frac{db}{ds}\big|_B$ will be formulated later (Section 3.8.2.2). The assumptions relative to v_B lead to

$$v_B = u_m \frac{db}{ds}\Big|_B \frac{n}{(a+b)} \tag{3.74}$$

The expression for v_B in terms of jet flow characteristics will be given after $db/ds\big|_B$ has been obtained. (See Section 3.8.2.2.)

3.7 Comments on the Integration of Governing Equations over Jet Cross Section

On the basis of the previous definitions, assumptions, and derivations, the continuity equation, the s and z momentum equations and

the equation of thermal energy conservation may be integrated over the jet cross section. The integrated z momentum equation is trivial because of the assumption of hydrostatic pressure distribution. Integration of the n momentum equation over the jet cross section requires additional considerations because the entrainment velocity distributions assumed in Section 3.5.2.2 do not represent the actual velocities of the ambient fluids as they are drawn into the jet stream, and hence should not be used to describe the momentum flux in the n direction.

In the present study, the n momentum equation is integrated over the jet cross section following the method used by Stolzenbach and Harleman [1971]. It is assumed that the flow outside the jet is irrotational. Integrating Eq. 3.49 over the jet cross section and then applying Stoke's theorem and the Bernoulli equation, one obtains

$$\iint_A \frac{\partial uv}{\partial s}\,dndz - \int_C Ku^2 dndz - \iint_A \frac{\lambda(1+Kn)g}{\rho_a}\int_z^{-\infty}\frac{\partial \Delta T}{\partial n}\,dz'dndz = \int_C (1+Kn)\cdot \left[\frac{1}{2}(w^2-v^2)dz + vwdn\right] \tag{3.75}$$

where $\iint_A$ and $\int_C$ denote surface and line integrals, respectively. The terms on the left hand side of Eq. 3.75 may be integrated over the jet cross section using the boundary conditions specified in Section 3.5, since these integrations do not require the use of boundary conditions specified by Eqs. 3.63-3.65. The right hand side of Eq. 3.75 can be evaluated separately by applying Blasius's theorem [Vallentine, 1967] for two-dimensional flow past a porous cylinder of any cross section with a sink inside. The result is [Stolzenbach and Harleman, 1971]

$$\int_C \left[\frac{1}{2}(w^2-v^2)dz + vwdn\right] = - q_e u_a \sin\theta \qquad (3.76)$$

where q_e is the volume flux per unit length into the cylinder. A negative sign on the right hand side of Eq. 3.76 is introduced because in the present study $u_a \sin\theta$ is in the negative n direction. The assumed cylinder has no curvature; therefore K on the right hand side of Eq. 3.75 is set equal to zero. The final integrated n momentum equation is obtained by substituting Eq. 3.76 into Eq. 3.75 and by adding a pressure drag term into Eq. 3.75 to account for the fact that K is not actually zero and that the flow outside the jet is not truly irrotational. Integration of the pressure drag term will give rise to a drag coefficient C_D which will be evaluated from experimental data.

3.8 Closure Relations

A system of equations does not have a unique solution unless the number of independent equations equals the number of unknowns. The closure problem of the equations is examined in this section.

The unknowns are:

1. geometric parameters

   a, b, b', c, h, X, Y, θ — 8

2. velocities

   u_m, v_e, v_e', w_e — 4

3. temperature

   ΔT_m — 1

total 13

The governing equations are:

1.	integrated continuity equation	1
2.	integrated s-momentum equation	1
3.	integrated n-momentum equation	1
4.	integrated thermal energy conservation equation	1
5.	geometric relations	
	$\frac{dX}{ds} = \cos\theta$	
	$\frac{dY}{ds} = \sin\theta$	2
	total	6

Thus, seven additional relations are needed in order to obtain a closed system of equations. Two of these relations can be established among the three entrainment velocities; the remaining five necessary relations can be obtained from the expressions for jet spreading. Their derivations are presented in the following subsections.

3.8.1 Entrainment Velocities

The entrainment velocities in both the vertical direction and the lateral direction are assumed to be proportional to the scalar difference between the local jet centerline velocity (u_m) and the components of the crossflow velocity parallel to the jet trajectory (u_s, u_s' and u_c) as was done by Motz and Benedict [1970]. It is further assumed that the lateral entrainment is not affected by the buoyancy forces while the reduction of the vertical entrainment due to density gradient effects can be expressed by Eq. 2.4. Based on these assumptions, the following expressions can be written

$$v_e = E_{NB}(u_m - u_s) \tag{3.77}$$

$$v'_e = E_{NB}(u_m - u'_s) \tag{3.78}$$

$$w_e = E_B(u_m - u_c) = E_{NB}(u_m - u_c)\ \mathrm{EXP}(-5/F_r^2) \tag{3.79}$$

where E_{NB} = entrainment coefficient for nonbuoyant jets

E_B = entrainment coefficient for buoyant jets

Eq. 3.79 is based on Eq. 2.4. From Eqs. 3.77-3.79 the following expressions for v'_e and w_e in terms of v_e are obtained

$$v'_e = \frac{v_e(u_m - u'_s)}{(u_m - u_s)} \tag{3.80}$$

$$w_e = v_e\ \mathrm{EXP}(-5/F_r^2)\ \frac{(u_m - u_c)}{(u_m - u_s)} \tag{3.81}$$

Thus v'_e and w_e may be eliminated from the governing equations by using Eqs. 3.80 and 3.81. The number of unknowns is then reduced to 11.

3.8.2 Spreading in the Near Field Region

The growth of a heated jet is assumed to be due to the following two independent factors:

1. the velocity difference between the jet and the ambient fluid.
2. the buoyancy forces due to the density difference between the jet and the ambient fluid.

The velocity difference between the jet and the ambient fluid generates shear which in turn causes entrainment and turbulent diffusion. Density differences will cause buoyant spreading which increases the jet lateral spreading while decreasing the jet thickness. Buoyant spreading is

assumed to cause only a change of the jet configuration but not the mass flux of the jet. Jet spreading due to each factor will be derived separately and the overall spreading will then be assumed to be a linear combination of these effects.

3.8.2.1 Jet Spreading due to Velocity Difference

Based on the mixing length theory, Abramovich [1963] has shown that for a turbulent jet in a coflowing external stream, the spreading rate for a non-buoyant jet has the following form:

$$\frac{db}{ds}\Big|_V = C_V \frac{(u_m - u_a)}{(u_m + u_a)} \tag{3.82}$$

where u_a = velocity of the coflowing stream,

C_V = coefficient of jet spreading due to the velocity difference between the jet and the ambient flow,

s = streamwise coordinate,

b = jet width (from the axis),

u_m = velocity on the jet axis.

The subscript V in Eq. 3.84 is used to denote terms related to the behavior of the jet due to the velocity difference between the jet and the ambient flow. Bowley and Sucec [1969] extended the use of Eq. 3.82 to the spreading of a turbulent jet in the presence of a crossflow. They reasoned that at any section along the jet trajectory, the jet may be treated as if it were coflowing with an external parallel stream whose velocity is $u_a \cos\theta$, which is the component of the crossflow velocity parallel to the jet trajectory. Using this concept, the lateral spreading of the jet outer part due to velocity difference may be expressed as

$$\left.\frac{db}{ds}\right|_V = C_V \frac{u_m - u_s}{u_m + u_s} \tag{3.83}$$

and for the spreading of the jet inner part,

$$\left.\frac{db'}{ds}\right|_V = C_V \frac{u_m - u'_s}{u_m + u'_s} \tag{3.84}$$

where b = the width of jet outer part,

b' = the width of jet inner part,

$u_s = (u_a)_{a+b} \cos\theta$,

$u'_s = u_s \cos\left[\frac{\pi}{2}\left(\frac{\theta}{\theta_o}\right)\right]$.

Equations 3.83 and 3.84 are assumed to be valid for both buoyant and non-buoyant jets.

As mentioned previously, the rate of increase of the jet thickness will be reduced because of the density currents which result from the presence of the density difference. However, independent of and in addition to the density-current effect, the density differences also suppress the turbulence and thereby cause a reduction in the vertical entrainment and vertical spreading. This is the effect which the exponential term in Eq. 3.79 represents. Since there exists a linear relationship between the entrainment coefficient and the spreading coefficient [Stolzenbach and Harleman, 1971; Jirka et al., 1975], the spreading of the jet due to velocity difference in the vertical direction can be shown from Eq. 3.79 to be

$$\left.\frac{dh}{ds}\right|_V = C_V \, \mathrm{EXP}\left(\frac{-5}{F_r^2}\right) \frac{(u_m - u_c)}{(u_m + u_c)} \tag{3.85}$$

where $u_c = (u_a)_{-(c+h)} \cos\theta$. The value of C_V based on the temperature boundaries of jets with strong crossflow are not available in the literature. They will be evaluated empirically in Section 5.3.2.

3.8.2.2 Jet Spreading due to Buoyancy Forces

The order of magnitude analysis of the n momentum equation for both buoyant jet cases shown in Table 3.1 shows that

$$\left(\frac{L_N}{L_S}\right)^2 \sim \frac{\lambda g \Delta T_M}{\rho_a} \frac{L_Z}{U_S^2} - \frac{U_F^2}{U_S^2} \frac{L_N}{L_Z} \tag{3.86}$$

In Eq. 3.86, it is assumed that

$$\frac{L_N}{L_S} = \left.\frac{db}{ds}\right|_B, \text{ rate of lateral spreading due to buoyancy forces,}$$

$$\frac{\lambda g \Delta T_M}{\rho_a U_S^2} = R_i = \frac{1}{F_r^2}, \text{ Richardson number,}$$

$$\frac{U_F^2}{U_S^2} \frac{L_N}{L_Z} = \frac{\tau_i}{\rho_a u_m^2} \frac{b}{h},$$

τ_i = component of interfacial shear stress normal to jet axis. The interface is assumed to coincide with the jet bottom boundary.

Figure 3.8 shows schematically the components of jet velocity. The interfacial shear τ_i for the outer part of the jet can be expressed as

$$\tau_i = \frac{C_i}{8} \rho_a u_{rel}^2 \frac{v}{u_R} \tag{3.87}$$

where u_{rel} = relative velocity between the jet and the ambient flow,

C_i = interfacial shear stress coefficient,

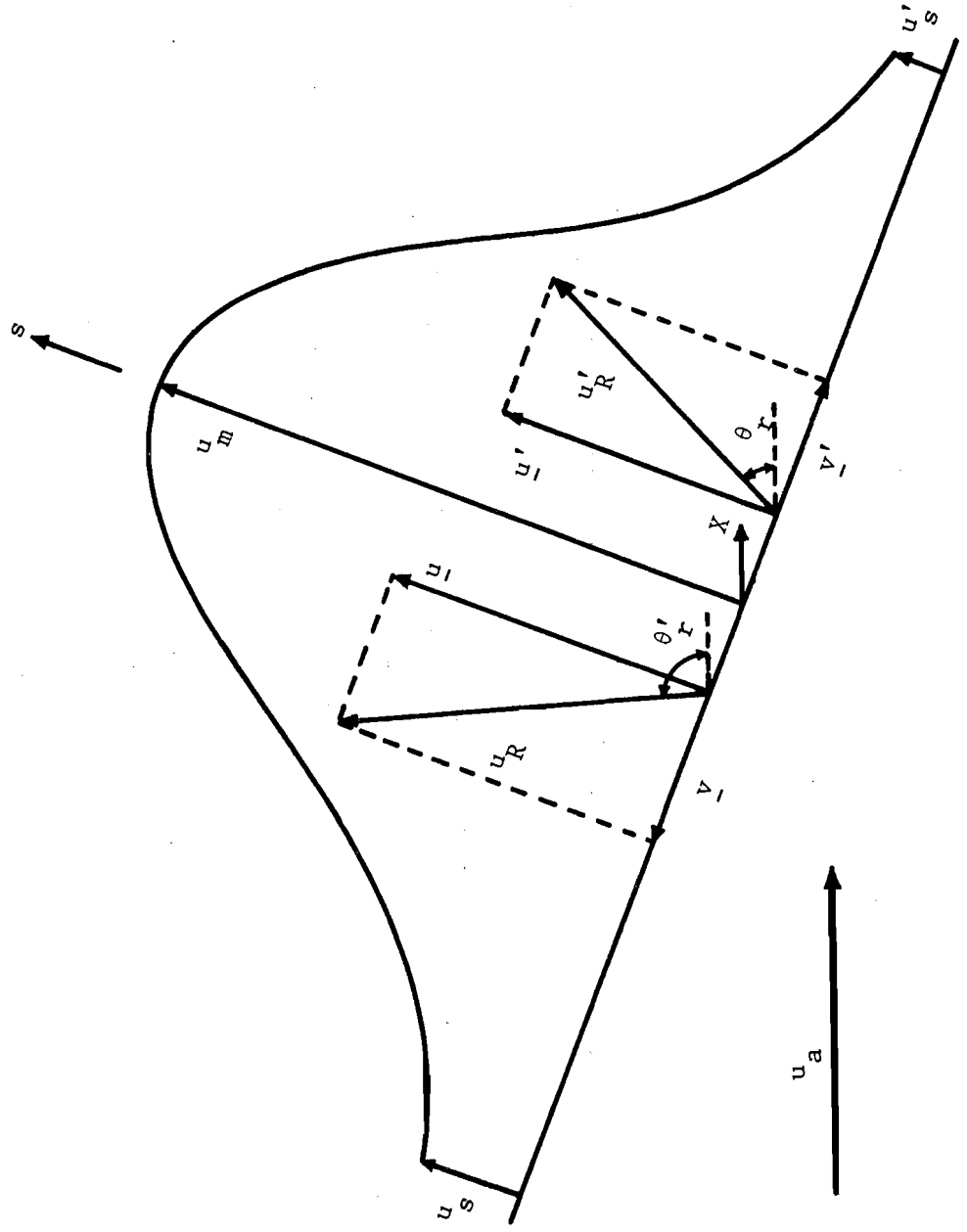

Fig. 3.8 Components of jet velocity

$\underline{v}$ = average lateral velocity over the jet outer part,

$u_R = (\underline{v}^2+\underline{u}^2)^{1/2}$,

$\underline{u}$ = average longitudinal jet velocity over the outer part.

The relative velocity u_{rel} is given by

$$u_{rel} = u_R - u_a \cos\theta_r = [(\underline{u}^2+\underline{v}^2)^{1/2} - u_a \cos\theta_r] \tag{3.88}$$

where θ_r = the angle between u_R and the X-axis. Equations 3.86-3.88 may be combined to yield the lateral spreading of the outer part of the jet due to buoyancy forces. The result is

$$\frac{db}{ds}\Big|_B = C_B\{\frac{1}{F_r^2} - \frac{C_i}{8u_m^2}[(\underline{u}^2+\underline{v}^2)^{1/2} - u_a \cos\theta_r]^2 \frac{\underline{v}}{u_R}\frac{b}{h}\}^{1/2} \tag{3.89}$$

Note that a buoyant spreading coefficient C_B is introduced in Eq. 3.89 so that an equality may replace the proportionality in Eq. 3.86. Following the same procedure, the corresponding equation for the inner part of the jet can be obtained:

$$\frac{db'}{ds}\Big|_B = C_B\{\frac{1}{T_r^2} - \frac{C_i}{8u_m^2}[(\underline{u}'^2+\underline{v}'^2)^{1/2} - u_a \cos\theta'_r]^2 \frac{\underline{v}'}{u'_R}\frac{b'}{h}\}^2 \tag{3.90}$$

The buoyant spreading coefficient C_B will be obtained empirically in Section 5.3.3.3. The interfacial shear stress coefficient C_i will be evaluated from the following equations derived by Sherenkov et al. [1971] from the data of several investigators

$$C_i = 1.28(R_e F_r^2)^{-0.54} \qquad \text{for } R_e F_r^2 > 500 \tag{3.91}$$

$$C_i = 38.72(R_e F_r^2)^{-0.9} \qquad \text{for } R_e F_r^2 < 150 \tag{3.92}$$

where R_e is the jet Reynolds number. At $150 < R_e F_r^2 < 500$ a non-single-valued relation between C_i and $R_e F_r^2$ was observed [Sherenkov et al., 1971]. The value of C_i for $150 < R_e F_r^2 < 500$ is then taken to be the average value obtained from Eqs. 3.91 and 3.92. There is considerable lack of agreement among the results of various investigators concerning the relation of C_i to R_e and F_r. Fortunately, for the NFR, the calculated behavior of the jet is not strongly influenced by C_i.

The total rates of lateral spreading db/ds and db'/ds are obtained by adding $db/ds\big|_V$ (Eq. 3.83) to $db/ds\big|_B$ (Eq. 3.89), and by adding $db'/ds\big|_V$ (Eq. 3.84) to $db'/ds\big|_B$ (Eq. 3.90). Thus the number of available equations increases to 8.

With the jet lateral spreading derived, the changes of the jet thickness due to buoyant spreading ($dh/ds\big|_B$) can be obtained from the consideration of mass conservation. The derivation of $dh/ds\big|_B$ will be done in Section 3.8.3.3 to obtain a general form valid for both the ZFE and the NFR.

In the NFR (downstream of the ZFE) both a and c are zero. The number of unknowns thus reduces to 9 and the rate of vertical spreading is the only remaining relation required for the closure of the governing equations in the NFR. The rate of vertical spreading is considered in Section 3.8.3.3.

3.8.2.3 Lateral Velocity due to Buoyancy

With $db/ds\big|_B$ available, the formulation of v_B, the lateral velocity induced by buoyancy forces in Section 3.6.2, may be completed by substituting Eq. 3.89 into Eq. 3.74. However, in view of the inherent uncertainty involved in the assumptions of Eq. 3.66 and Eq. 3.74 itself,

the complications introduced by inclusion of the effects of shear stresses in the derivation of v_B seem unjustified. Thus, with the effects due to shear stresses neglected, v_B can be shown to be

$$v_B = C_B\sqrt{\lambda\Delta T_m g(c+h)/\rho_a}\,\frac{n}{(a+b)} \tag{3.93}$$

3.8.3 Spreading in the Zone of Flow Establishment

In the zone of flow establishment (ZFE), the jet velocity and temperature distributions undergo a transition from their initial distributions at the outfall to similarity profiles. Some experimental work has been done concerning the length and shape of the ZFE for round nonbuoyant jets [Albertson et al., 1950; Sami et al., 1967] and more recently by Stefan et al. [1975] for buoyant surface jets. Figure 3.9 shows the idealized velocity and temperature distributions within the ZFE. Since heat is diffused laterally faster than momentum [Dunn et al., 1975], the temperature profile has a shorter core and greater half-width than the velocity profile.

Theoretical analysis of the ZFE is difficult because neither the velocity nor the temperature profiles within this zone follow similarity relations. Some investigators [Hoopes et al., 1968; Stefan et al., 1971] have simply neglected this zone. Then, similarity profiles which assume the flow to be fully developed have been applied beginning at the exit. Others [Motz and Benedict, 1970; Prych, 1972] established a semiempirical relation between the length of the ZFE and the angle between the jet and the crossflow at the end of the ZFE. The dimensions of the jet at the end of ZFE were estimated from the continuity and momentum equations. This

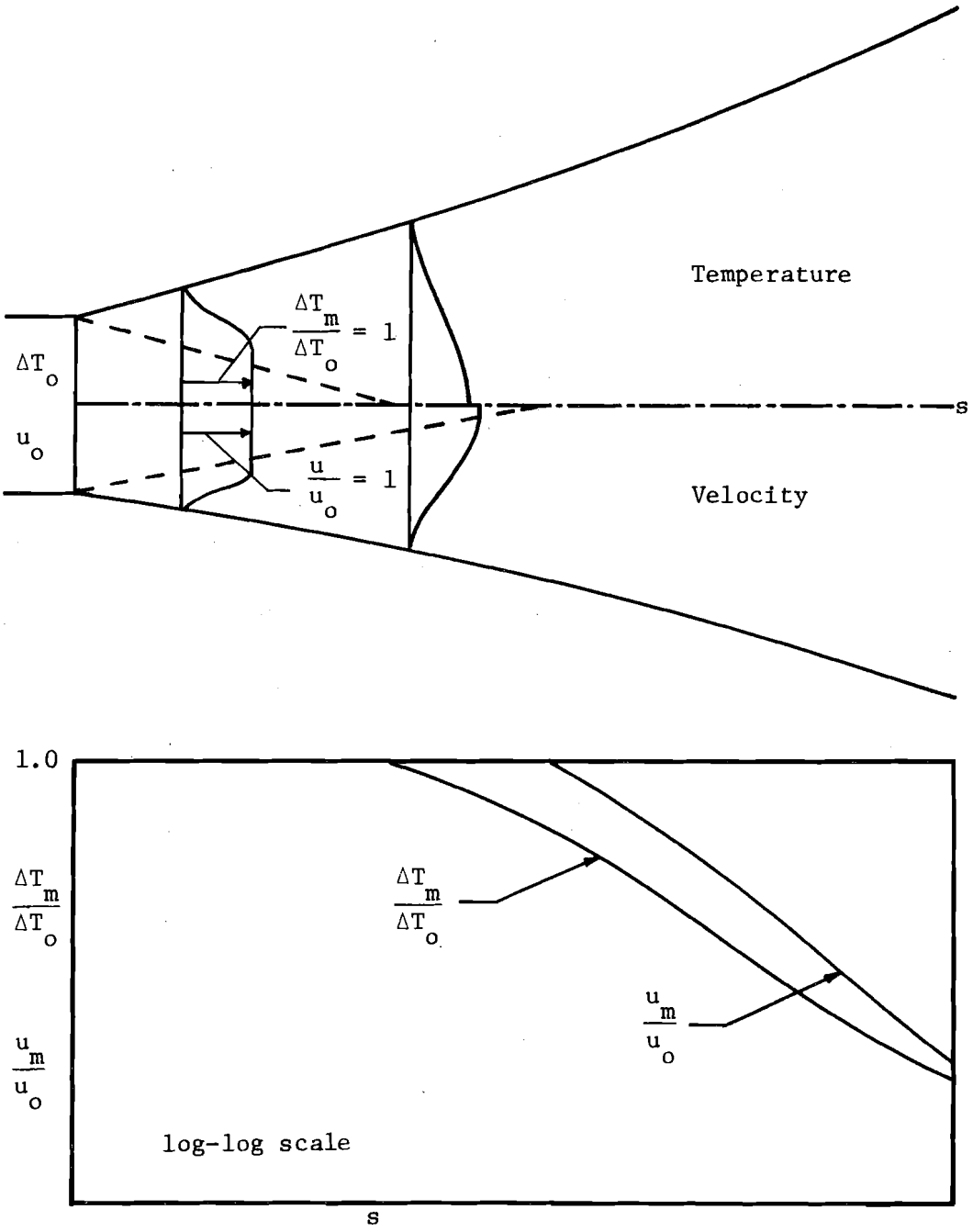

Fig. 3.9 Idealized velocity and temperature profiles in ZFE

estimated information at the end of the ZFE was then used as the initial input data to start the solution of the integrated equations.

An attempt to predict the physical properties within the ZFE by analytical modeling has been done by Hirst [1972b] for round turbulent jets. The model developed by Stolzenbach and Harleman [1971] is believed to be the first one among heated surface jet models which directly includes the ZFE in the analytical modeling.

In the present study, the velocity and temperature profiles in the shear layer within the ZFE are assumed to be similar (Section 3.4). The spreading of the jet in the ZFE is also assumed to be due to both the velocity difference and the buoyancy forces, as in the NFR. Thus one may write

$$\frac{da}{ds} = \frac{da}{ds}\Big|_V + \frac{da}{ds}\Big|_B \tag{3.94}$$

$$\frac{db}{ds} = \frac{db}{ds}\Big|_V + \frac{db}{ds}\Big|_B \tag{3.95}$$

$$\frac{db'}{ds} = \frac{db'}{ds}\Big|_V + \frac{db'}{ds}\Big|_B \tag{3.96}$$

$$\frac{dc}{ds} = \frac{dc}{ds}\Big|_V + \frac{dc}{ds}\Big|_B \tag{3.97}$$

$$\frac{dh}{ds} = \frac{dh}{ds}\Big|_V + \frac{dh}{ds}\Big|_B \tag{3.98}$$

The subscripts B and V are used to denote terms related to the behavior of the jet due to buoyancy forces and the velocity difference between the jet and the ambient flow, respectively. To achieve the closure of the governing equations in the ZFE, it is necessary to formulate the rates of jet spreading da/ds, db/ds, db'/ds, dc/ds and dh/ds.

3.8.3.1 Spreading in Lateral Direction

In the ZFE, the total lateral spreading of the outer part of the jet due to buoyancy forces consists of $da/ds|_B$ and $db/ds|_B$. From Eq. 3.89,

$$\frac{da}{ds}|_B + \frac{db}{ds}|_B = \text{LBS} \tag{3.99}$$

where $\text{LBS} = C_B\{\frac{1}{F_r^2} - \frac{C_i}{8u_m^2}[(\underline{u}^2+\underline{v}^2)^{1/2} - u_a\cos\theta_r]^2 \frac{\underline{v}}{u_R}\frac{(c+h)}{(a+b)}\}^{1/2}$

LBS and similar terms below refer to single quantities as defined.
In order to relate $da/ds|_B$ and $db/ds|_B$ separately to LBS, it is assumed that $\frac{da}{ds}|_B/\frac{db}{ds}|_B = \frac{a}{b}$. This assumption leads to the following relations

$$\frac{da}{ds}|_B = \frac{a}{(a+b)}\,\text{LBS} \tag{3.100}$$

$$\frac{db}{ds}|_B = \frac{b}{(a+b)}\,\text{LBS} \tag{3.101}$$

Following the same approach, one obtains

$$\frac{db'}{ds}|_B = \frac{b'}{(a+b')}\,\text{LBS}' \tag{3.102}$$

where $\text{LBS}' = C_B\{\frac{1}{F_r^2} - \frac{C_i}{8u_m^2}[(\underline{u}'^2+v'^2)^{1/2} - u_a\cos\theta'_r]^2 \frac{\underline{v}'}{u'_R}\frac{(c+h)}{(a+b')}\}^{1/2}$

The rates of jet spreading $db/ds|_V$ and $db'/ds|_V$ have been formulated previously (Eqs. 3.83 and 3.84). The formulations of db/ds and db'/ds are thus completed.

3.8.3.2 Velocity and Temperature Distributions in the Core

It has been assumed implicitly in Section 3.4 that (1) the boundaries of the temperature and velocity profiles concide with each other

and (2) heat is diffused laterally faster than momentum (in that nv > nt). One may intuitively set $d\Delta T_m/ds = 0$ and $du_m/ds = 0$ for the ZFE to generate two implicit formulas for the spreading of the core da/ds and dc/ds. However, this is an inconsistent approach if b is assumed to be the same for ΔT and u as in Eqs. 3.52 and 3.53 since this would imply a violation of the conservation principle unless the same similarity profile is used for both velocity and temperature. To overcome this problem, it was decided to relax the condition that $d\Delta T_m/ds = 0$ in the core and put only

$$\frac{du_m}{ds} = 0 \qquad \text{(ZFE only)} \tag{3.103}$$

The result is that ΔT_m decreases in the core, but this is somewhat consistent with the concept that heat diffuses faster than momentum in the jet.

3.8.3.3 Spreading in Vertical Direction

The volume flux of the jet outer part may be shown to be

$$Q_1 = u_m(c+hI_1)(a+bI_1) + hu_c(1-I_1)(a+bI_1) + bu_s(1-I_1)(c+hI_1) + bhu_d(1-I_1)^2 \tag{3.104}$$

where Q_1 = volume flux of the jet outer part. Taking the derivative of Eq. 3.104 with respect to s and then applying Eqs. 3.94-3.98, one obtains

$$\frac{dQ_1}{ds} = q_1 = [(c+hI_1)(a+bI_1)\frac{du_m}{ds} + h(1-I_1)(a+bI_1)\frac{du_c}{ds} + b(1-I_1)(c+hI_1)\frac{du_s}{ds} + bh(1-I_1)^2\frac{du_d}{ds} + \frac{da}{ds}\Big|_V BSA + \frac{db}{ds}\Big|_V BSB + \frac{dc}{ds}\Big|_V BSC + \frac{dh}{ds}\Big|_V BSH] + [\frac{da}{ds}\Big|_B BSA + \frac{db}{ds}\Big|_B BSB + \frac{dc}{ds}\Big|_B BSC + \frac{dh}{ds}\Big|_B BSH] \tag{3.105}$$

where q_1 = volume flux per unit length into the outer part of the jet,

$$BSA = u_m(c+hI_1) + hu_c(1-I_1),$$

$$BSB = u_m(c+hI_1)I_1 + hu_c(1-I_1)I_1 + u_s(1-I_1)(c+hI_1) + hu_d(1-I_1)^2,$$

$$BSC = u_m(a+bI_1) + bu_s(1-I_1),$$

$$BSH = u_m(a+bI_1)I_1 + u_c(1-I_1)(a+bI_1) + bu_s(1-I_1)I_1 + bu_d(1-I_1)^2.$$

Since buoyant spreading does not contribute to the change of volume flux, the buoyant terms in Eq. 3.105 must cancel each other so that

$$\frac{da}{ds}\Big|_B BSA + \frac{db}{ds}\Big|_B BSB + \frac{dc}{ds}\Big|_B BSC + \frac{dh}{ds}\Big|_B BSH = 0 \qquad (3.106)$$

This equation can be solved for $dh/ds|_B$ and combined with the results from Eq. 3.107. (The terms in the first pair of square brackets on the right hand side of Eq. 3.105 must be equal to q_1.) In a completely analogous fashion, the following equation is obtained for the inner part of the jet:

$$\frac{da}{ds}\Big|_B BSA + \frac{db'}{ds}\Big|_B BSB' + \frac{dc}{ds}\Big|_B BSC' + \frac{dh}{ds}\Big|_B BSH' = 0 \qquad (3.107)$$

where $BSB' = u_m(c+hI_1)I_1 + hu_c(1-I_1)I_1 + u_s'(1-I_1)(c+hI_1) + hu_d'(1-I_1)^2$

$$BSC' = u_m(a+b'I_1) + b'u_s'(1-I_1)$$

$$BSH' = u_m(a+b'I_1)I_1 + u_c(1-I_1)(a+b'I_1) + b'u_s'(1-I_1)I_1 + b'u_d'(1-I_1)^2$$

Similar to Eq. 3.106, Eq. 3.107 can be solved for $dh/ds|_B$ for the inner part. Then the change of depth due to buoyant spreading ($dh/ds|_B$) is taken to be the average value of $dh/ds|_B$ from Eqs. 3.106 and 3.107. The result is

$$\frac{dh}{ds}\Big|_B = [\frac{db}{ds}\Big|_B BSB + \frac{db'}{ds}\Big|_B BSB' + 2\,\frac{da}{ds}\Big|_B BSA + \frac{dc}{ds}\Big|_B (BSC + BSC')]/(BSH + BSH') \qquad (3.108)$$

The value of $dc/ds\big|_B$ is obtained from the assumption that the buoyant spreading does not change the volume flux within the core. Hence $2u_o ca$ is not altered by buoyancy and

$$\frac{dc}{ds}\Big|_B = -\frac{c}{a}\frac{da}{ds}\Big|_B = -\frac{c}{(a+c)}\,LBS \tag{3.109}$$

The rate of vertical spreading due to velocity difference $dh/ds\big|_V$ and the total rate of vertical spreading in the core dc/ds can be obtained from Eqs. 3.85 and 3.103. Thus the formulations of dh/ds and dc/ds are completed.

3.8.3.4 Width of Core

The last relation needed to achieve a closure of the governing equations is obtained from the work by Stefan et al. [1975]. From a measurement of detailed temperature profiles in the ZFE, they obtained

$$\frac{s}{a} = 12.1\, A_r^{0.46}\, e^{-0.9R}\left(1 + \frac{0.5F_o - 1.5}{0.4F_o}\right) \tag{3.110}$$
$$e$$

By differentiating Eq. 3.111, one obtains

$$\frac{da}{ds} = \frac{1}{12.1}\, A_r^{-0.46}\, e^{0.9R}\left(\frac{e^{0.4F_o}}{0.4F_o + 0.5F_o - 1.5}\right) \tag{3.111}$$
$$e$$

At the end of the core, a and c may not become zero simultaneously. To treat such cases, it is assumed that the value of da/ds (or dc/ds) at the end of the core remains the same until a (or c) goes to zero.

Figure 3.10 illustrates the nature of the velocity and temperature distributions when Eqs. 3.103 and 3.111 are used within the ZFE. The temperature on the jet axis starts to decay at the exit and the velocity

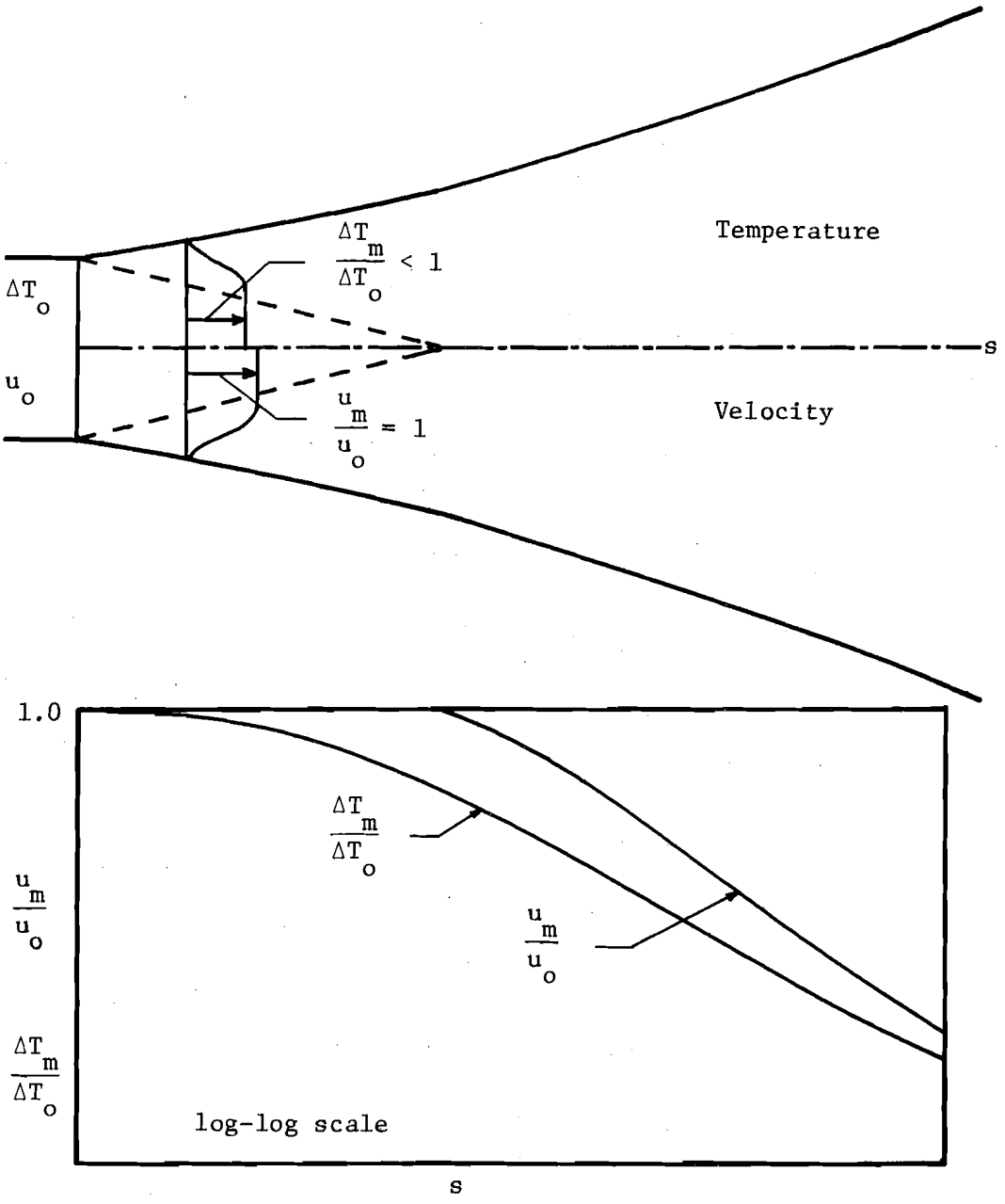

Fig. 3.10 Assumed velocity and temperature distributions in the ZFE

and temperature distributions have the same dimension in both the shear layer and the core. This discrepancy is considered to have little effect on the overall jet prediction.

3.9 Summary and Solution Procedure

A mathematical jet model has been developed from the three-dimensional, time-averaged equations of mass, momentum and energy conservation. The fluids were considered as incompressible and the viscous terms and molecular terms were assumed to be negligible. An order of magnitude analysis was performed in order to drop insignificant terms from the equations. Integration of the resulting governing equations over the jet cross section using similarity relations for velocity and temperature yields four nonlinear ordinary differential equations as shown in Appendix I. The closure relations of the governing equations were examined and the additional needed relations were obtained. The closed system of equations is as follows:

1. 4 nonlinear ordinary different equations derived from the conservation of mass, momentum and thermal energy and rearranged in the following forms suitable for integration

$$\frac{du_m}{ds} = G_u \tag{3.112}$$

$$\frac{d\Delta T_m}{ds} = G_t \tag{3.113}$$

$$\frac{d\theta}{ds} = G_\theta \tag{3.114}$$

$$v_e = G_e \tag{3.115}$$

where G_u, G_t, G_θ and G_e are functions of u_m, ΔT_m, θ, v_e, a, b, ..., etc.

2. 5 jet spreading expressions

$$\frac{da}{ds} = \frac{1}{12.1} A_r^{-0.46} e^{0.9R} \left(\frac{e^{0.4F_o}}{e^{0.4F_o}+0.5F_o-1.5}\right) \tag{3.116}$$

$$\frac{db}{ds} = C_V \frac{(u_m-u_s)}{(u_m+u_s)} + \frac{b}{(a+b)} LBS \tag{3.117}$$

$$\frac{db'}{ds} = C_V \frac{(u_m-u'_s)}{(u_m+u'_s)} + \frac{b'}{(a+b')} LBS' \tag{3.118}$$

$$\frac{dc}{ds} = \frac{dc}{ds}\Big|_V - \frac{c}{(a+b)} LBS \tag{3.119}$$

$$\frac{dh}{ds} = C_V \frac{(u_m-u_c)}{(u_m+u_c)} EXP\left(\frac{-5}{F_r^2}\right) + \frac{dh}{ds}\Big|_B \tag{3.120}$$

where $dh/ds|_B$ is given by Eq. 3.108. Equation 3.119 does not have an explicit form. The value of dc/ds is obtained from the solution of the nonlinear equation $G_u = 0$ for the core.

3. 2 geometric relations

$$\frac{dX}{ds} = \cos\theta \tag{3.121}$$

$$\frac{dY}{ds} = \sin\theta \tag{3.122}$$

Equations 3.112-3.122 have no closed form solution and numerical integration is required. First each variable is normalized with initial values using

u_o, $\sqrt{b_o h_o}$ and ΔT_o respectively as characteristic velocity, length and temperature. The dimensionless equations are solved simultaneously by using fourth order Runge-Kutta formulas [IBM, 1970] to carry out step by step integration. The initial conditions at $\overset{*}{s} = s/\sqrt{b_o h_o} = 0$ are

$$\overset{*}{a} = \frac{a}{\sqrt{b_o h_o}} = \frac{b_o}{2\sqrt{b_o h_o}} = 0.5\sqrt{A_r}$$

$$\overset{*}{b} = \frac{b}{\sqrt{b_o h_o}} = 0$$

$$\overset{*}{b'} = \frac{b'}{\sqrt{b_o h_o}} = 0$$

$$\overset{*}{c} = \frac{h_o}{\sqrt{b_o h_o}} = \frac{1}{\sqrt{A_r}}$$

$$\overset{*}{h} = \frac{h}{\sqrt{b_o h_o}} = 0 \qquad (3.123)$$

$$\overset{*}{u}_m = \frac{u_m}{u_o} = 1$$

$$\Delta\overset{*}{T}_m = \frac{\Delta T_m}{\Delta T_o} = 1$$

$$\overset{*}{X} = \frac{X}{\sqrt{b_o h_o}} = 0$$

$$\overset{*}{Y} = \frac{Y}{\sqrt{b_o h_o}} = 0$$

where * is used to denote the nondimensional variables. The results of the numerical integration of these equations are compared with the data in Section 5.4.

4. EXPERIMENTAL PROGRAM

4.1 Objectives of Experiments

The main objectives of the experiments were to test the ability of the proposed model (Chapter 3) to predict the temperature distributions in the near field region and to obtain data for calculating the drag coefficient C_D, the spreading coefficient due to velocity difference C_V and the buoyant spreading coefficient C_B.

4.2 Experimental Apparatus

The arrangement of the experimental apparatus is shown in Fig. 4.1. Experiments were performed in a rectangular flume 140 feet long, 6 feet wide and 4 feet deep. The flume has plexiglass sidewalls and a painted steel bed. Observations and measurements were taken from a probe carriage (Section 4.2.5) and from a personnel carriage, both of which were mounted on the rails along the top of the flume walls.

4.2.1 Ambient Water Supply System

Ambient flow was supplied from a constant head tank and distributed evenly across the flume by a 4-in. diameter diffuser resting on the flume bed. The ambient water depth was controlled by an adjustable weir at the downstream end of the flume.

A filter made of layers of rubberized hair was fitted into the flume about 18 feet downstream from the diffuser in order to minimize disturbance of the flow. To check the uniformity of the ambient flow, velocity measurements at several cross sections in the experimental measurement area without jet flow were done using a Kent Miniflo type 265

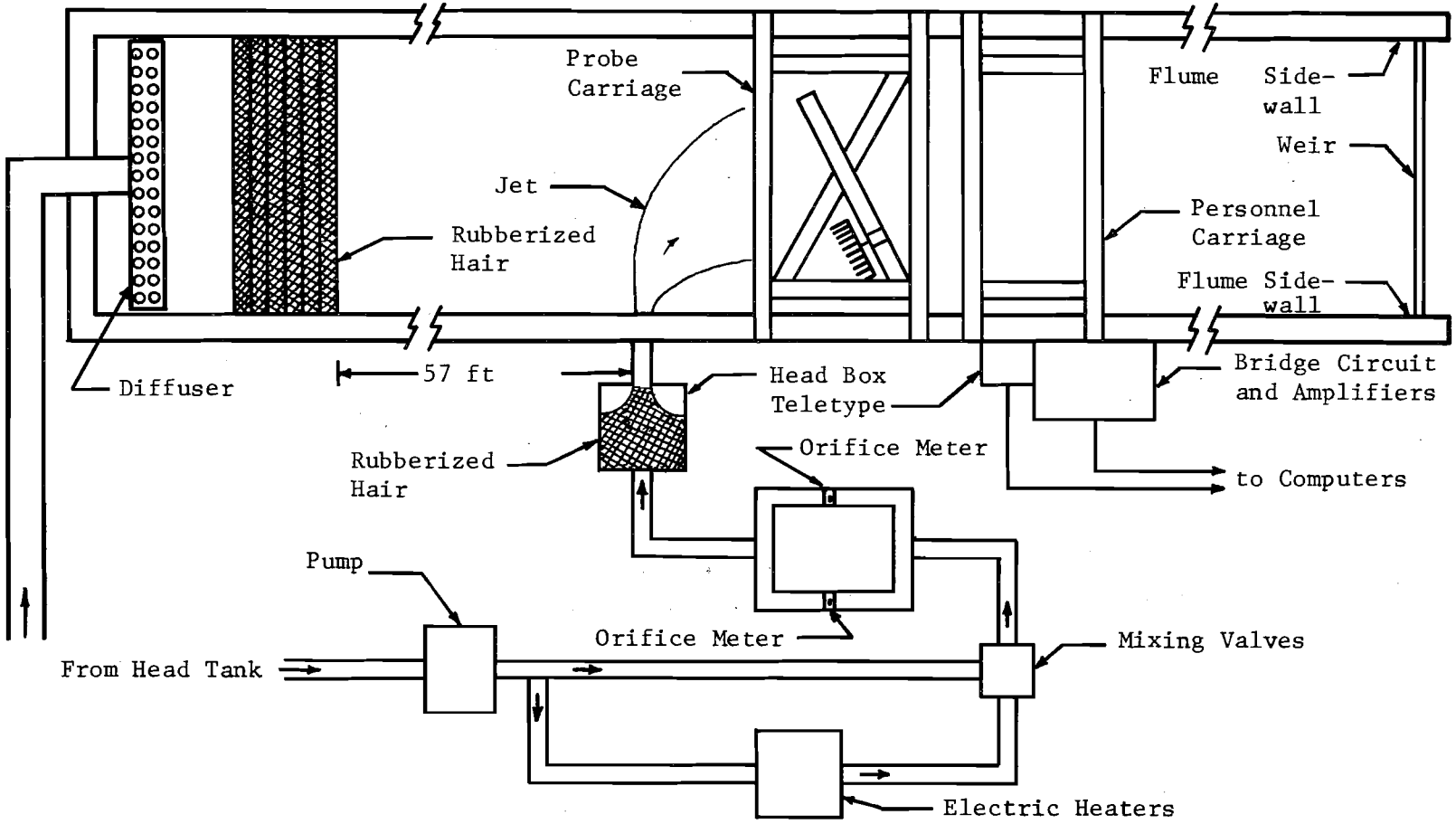

Fig. 4.1 Plan view of experimental setup

miniature propeller meter. By trial and error, the thickness of the rubberized hair filter was adjusted until a laterally uniform velocity distribution (except for sidewall effects) was obtained in the experimental area. The velocity distributions in the vertical direction indicated that the boundary layer was fully developed.

4.2.2 Heated Water Supply System

Heated water was supplied from two A. O. Smith Corp. 40.5 KW, 480 volt electric heaters capable of delivering up to 0.0624 cfs at a temperature of 11C^{o} above ambient. A 1-1/2 HP Gorman-Rupp self-priming centrifugal pump was placed in the supply line from the head tank to provide additional head to help overcome head losses in the heating system. The heated water and a cold water supply were introduced into two ITT Lawler PX-9700 thermostatic mixing valves. The mixing valves were found to be capable of controlling the outlet temperature to $\pm$ 0.5C^{o} of the setting. The discharge of the fully mixed warm water was measured with either one of two different sizes of orifice meters installed in the branched pipelines (Fig. 4.1). For low discharge, the orifice meter having the smaller diameter was used, and vice versa.

4.2.3 Warm Water Injection System

Warm water was discharged into the flume from an injection system located about 75 feet from the diffuser at the upstream end of the flume. This length was provided to assure boundary layer development upstream of the effluent point. Figure 4.2 is a photograph of the warm water injection system. Two 3/4-in. thick plywood sheets with concentric circular openings of 11-1/2 in. and 14 in. diameters were glued together

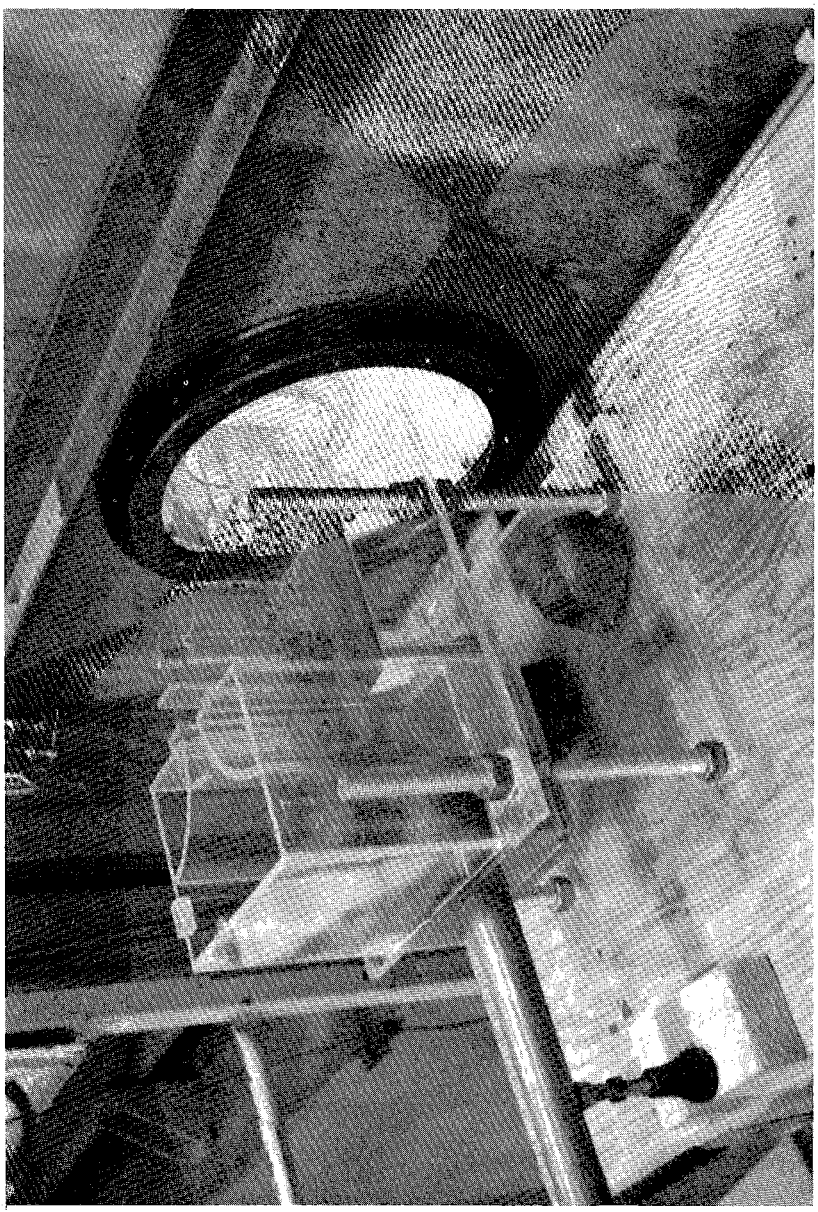

Fig. 4.2 The warm water injection system

to replace one of the plexiglass sidewall panels. The openings in the plywood were used to hold disc 1 (Fig. 4.3) which was made of plexiglass and which had an eccentric opening to accommodate the port disc, which was also made of plexiglass (Fig. 4.4). Metal rings were used to fasten disc 1 to the plywood plate and to fasten the port disc to disc 1. Grooves cut on the surfaces of both disc 1 and the port disc were fitted with o-rings to prevent leaking.

A head box which provided a smooth transition from pressurized pipe flow to open channel flow for the warm water was bolted to the port disc as shown in Fig. 4.2. An essentially uniform temperature distribution at the exit was achieved by covering the head box and the injection channel with foam rubber to insulate it.

The injection system described above offered a high degree of versatility in adjusting the elevation of the effluent channel bed in a range from 0.35 feet to 0.69 feet above the flume bed by rotating disc 1 and the port disc.

4.2.4 Thermistor Probes

The temperature distributions in the jet were measured using YSI 701 thermistor probes having a time constant of 9 seconds and an accuracy and interchangeability of $\pm$ 0.15C^{o} within a -30^{o}C to + 100^{o}C range. The tip of the probe has a nominal diameter of 3/16 in. In these experiments, the probes were individually calibrated. Twelve thermistor probes were used in the experiments. One of these was used to monitor the temperature in the ambient flow (probe 11) and another one was used to monitor the temperature at the jet exit (probe 12). The remaining ten probes were

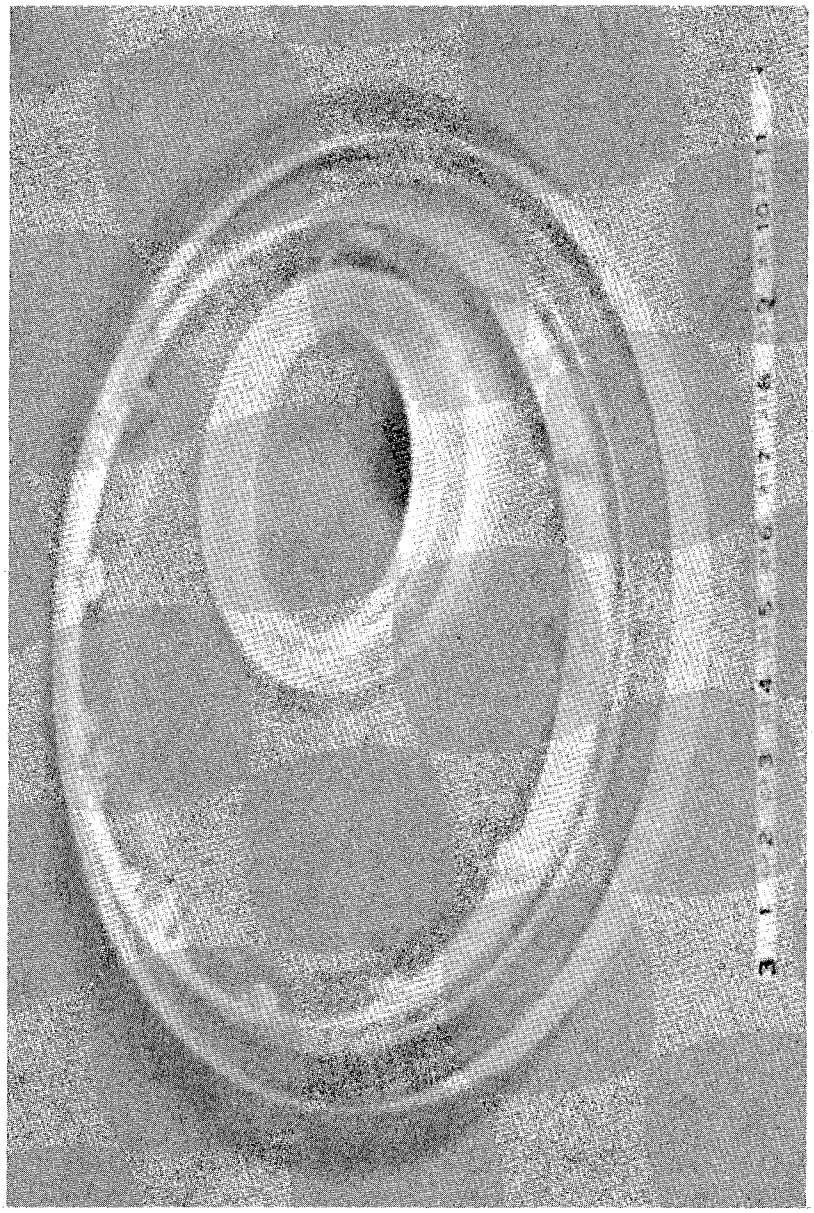

Fig. 4.3 Disc 1

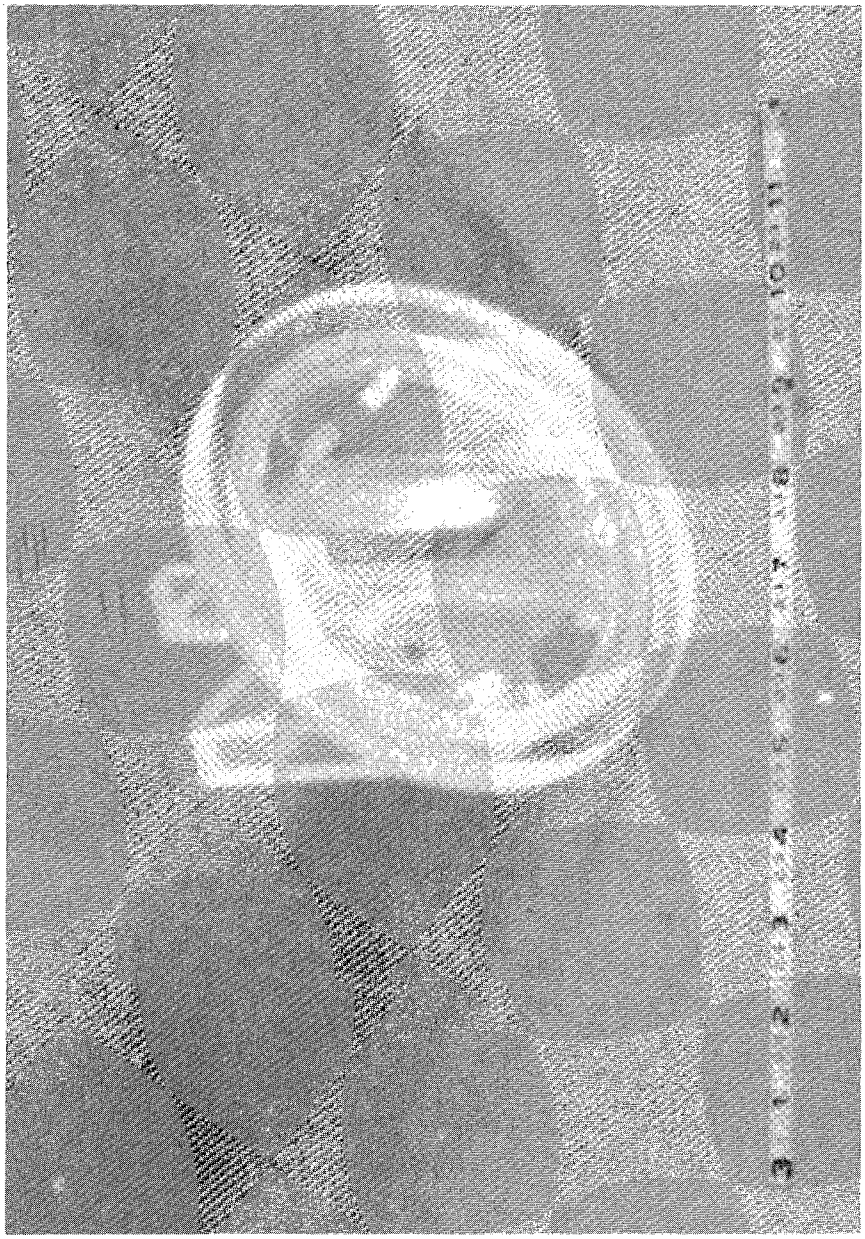

Fig. 4.4 The port disc

mounted on a rake to measure the temperature distributions over the jet cross section.

4.2.5 Probe Carriage

The probe carriage was made of aluminum angles and was essentially a box frame (Fig. 4.5) mounted on wheels at the top of the flume walls. The rake with the ten thermistors was supported by a point gage mounted on a horizontal arm across the bottom of the box frame. The arm was hinged at one end so that the arm was free to move horizontally. By rotating the horizontal arm, the probes on the rake could be placed at an angle from 0 to 90^{o} relative to the ambient flow. The result was a probe carriage constructed in such a way to enable the probes to be positioned longitudinally by rolling the carriage along the flume, to be moved vertically by using the point gage and to be rotated horizontally by moving the arm. Thus, the measurement cross section could be set approximately normal to the jet axis at any position along the trajectory.

4.2.6 Data Acquisition System

Figure 4.6 shows a flow chart of the data acquisition system. Each of the twelve thermistor probes was a part of a Wheatstone bridge circuit. The output of the bridge went to an Analog/Digital (A/D) converter, which provided the input readings for two Spiras 65 computers which were linked together to increase storage capacity. A teletype at the flume was used for control of the computers and for required data inputs.

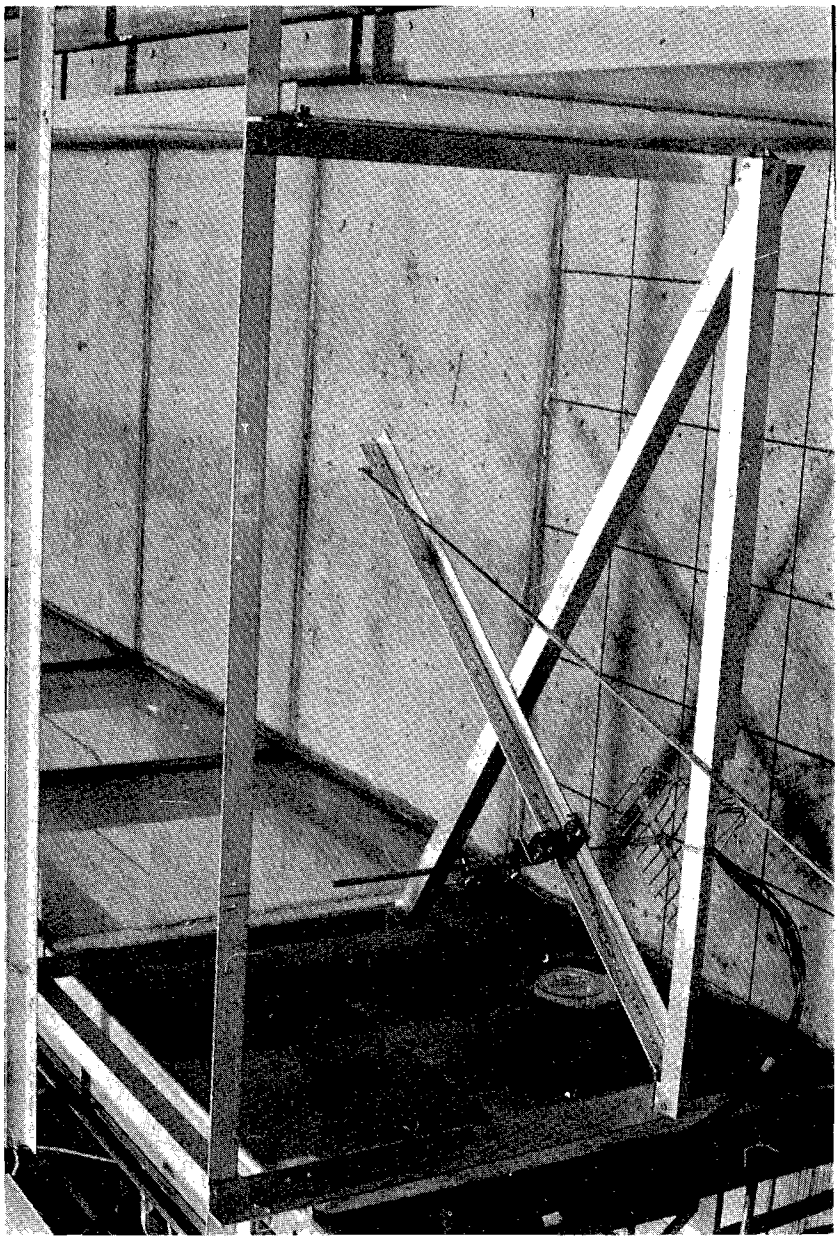

Fig. 4.5 The probe carriage

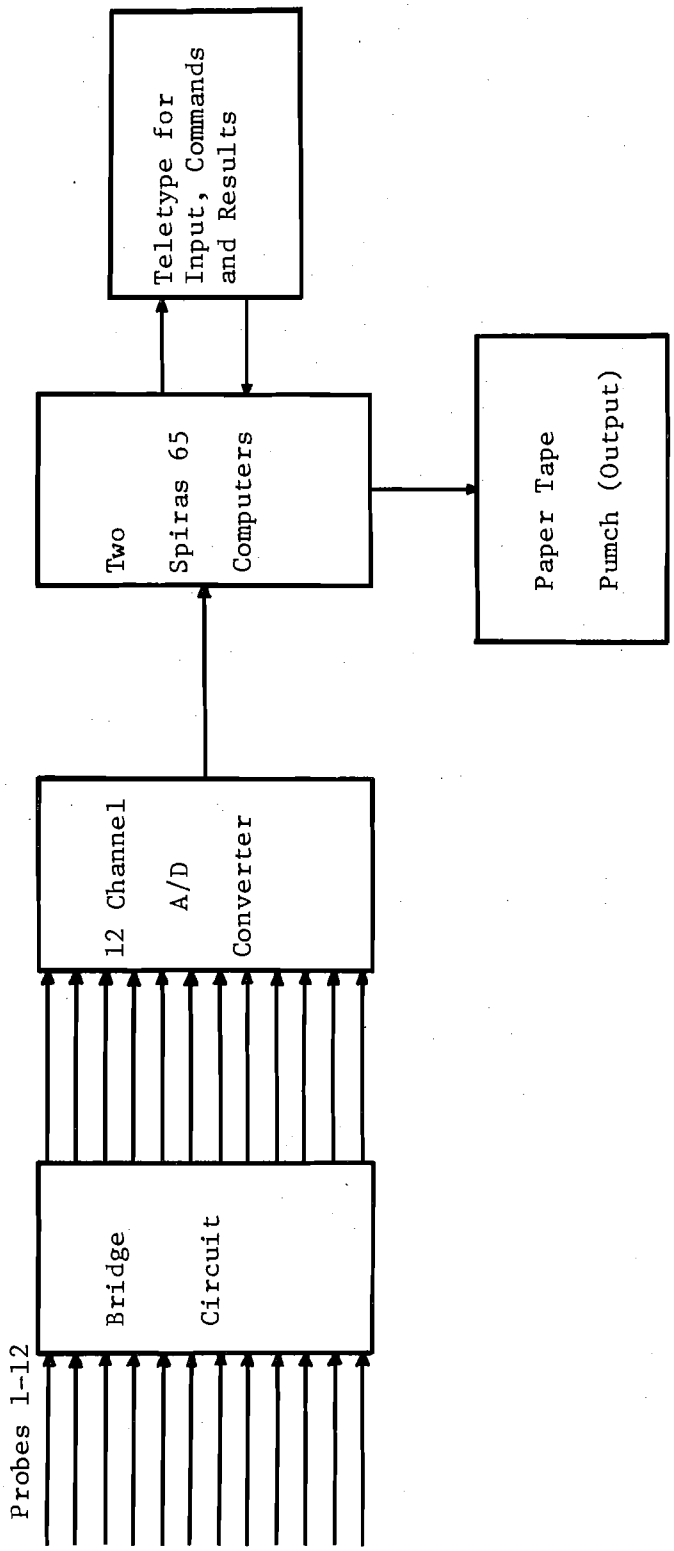

Fig. 4.6 Data acquisition system

4.2.6.1 Bridge Circuit

The bridge circuit is shown in Fig. 4.7. Switches A_j (j=1,2,...,12) and B were used to put the bridge circuit in either the calibration or the sampling mode as discussed below.

The calibration part of the bridge (R_c, R_d, R_e, R_f, R_g) was designed to calibrate the system (amplifiers and A/D converter) on the assumption that the tolerances on the thermistor interchangeability were sufficiently small for the thermistors to be considered to be identical so that they would not need calibrating. (It was later decided to calibrate the probes individually as discussed in Section 4.2.6.2.) R_d was 2848 ohms to correspond to the nominal thermistor resistance at 24.26°C and R_c was 3619 ohms so that the parallel resistance of R_c and R_d with switch B closed corresponded to a nominal 34.64°C.

To calibrate the system, SW A was placed in the calibrate position for each probe so that the output of the calibration part of the bridge was fed into each of the 12 differential amplifiers. With SW B open, the calibration bridge was balanced. The zero setting of each of the amplifiers was adjusted to give an output voltage (E_1) near zero. The computer read this output voltage to correspond to 24.26°C. Then, SW B was closed and the gain of each amplifier was adjusted to give an output voltage (E_2) of about 8 volts. This voltage was selected to allow at least 1 volt margin during the experiments to prevent over-driving of the amplifiers. The output voltage was read by the computer to correspond to 34.64°C. This procedure provided a system calibration curve as shown in Fig. 4.8.

The system calibration curve in Fig. 4.8 can be written as

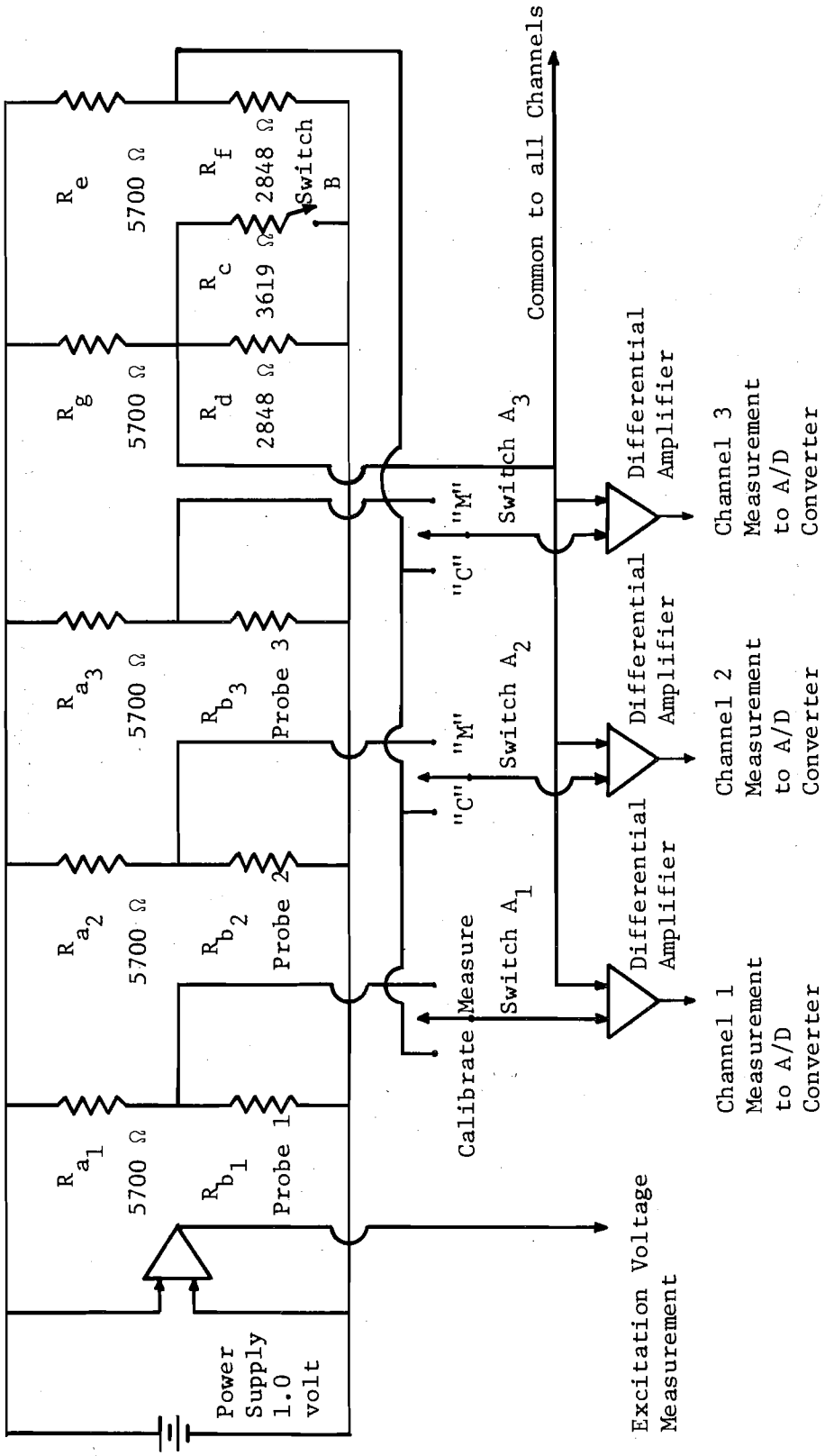

Fig. 4.7 Bridge circuit

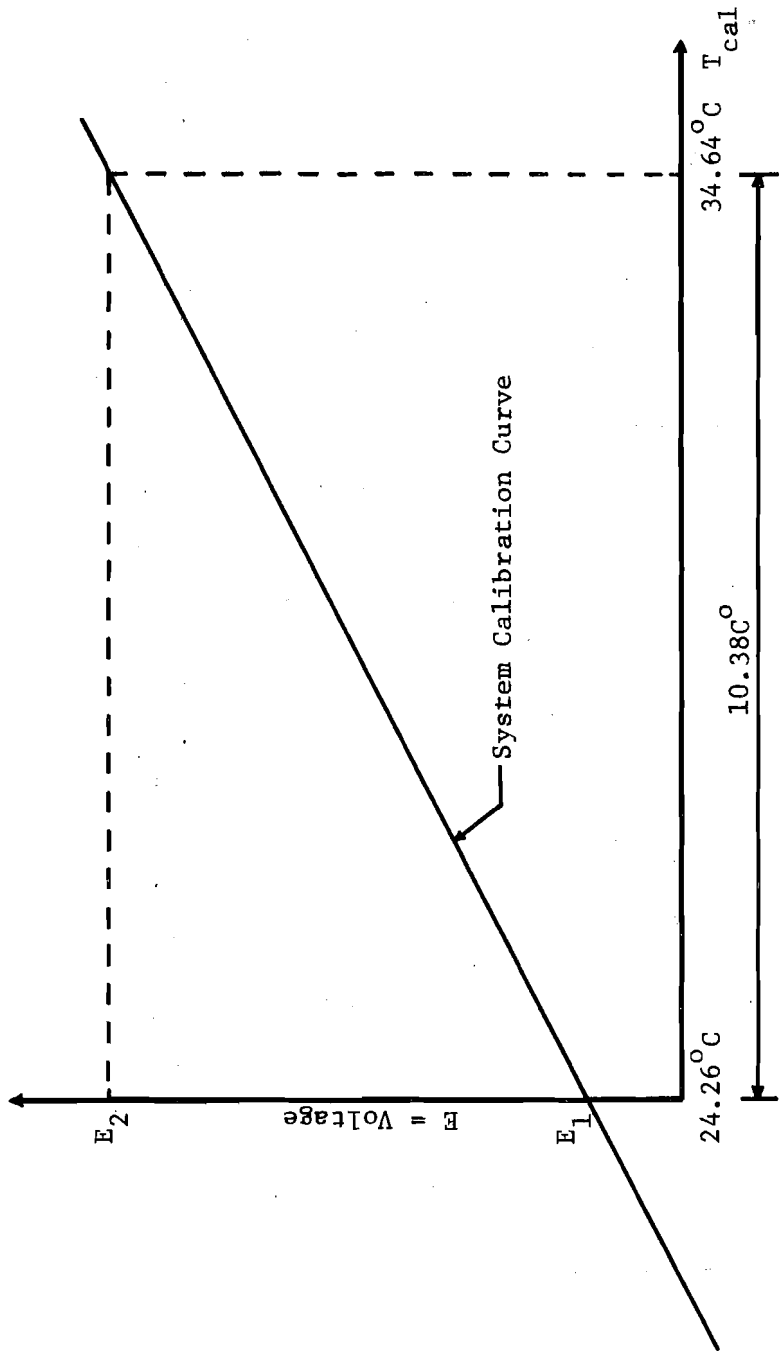

Fig. 4.8 System calibration curve

$$T_{cal} = 24.26 + 10.38 \frac{(E-E_1)}{(E_2-E_1)} \tag{4.1}$$

where T_{cal} = apparent temperature in system calibration,

E = output voltage.

4.2.6.2 Calibration of Probes

As mentioned above, after the bridge circuitry was built it was decided to calibrate each probe individually. A constant temperature bath was used for this purpose. All twelve probes together with a mercury thermometer were put into the constant temperature bath. The water was then successively heated and cooled five or six times at roughly $2C^{o}$ intervals from $25^{o}C$ to $35^{o}C$. With SW B open and SW A_1 through A_{12} set to "measure", the computer read the 12 thermistors at each of the constant temperature settings assuming that the previously obtained calibration curves were correct. The temperature readings on the mercury thermometer were also recorded and used for reference. The average of the 12 thermistors was used as the true temperature (T).

The temperature deviations (δT) were defined as

$$\delta T = T_{cal} - T \tag{4.2}$$

and were computed for each of the probes at each temperature level. It was found that for each probe the plots of δT versus T were practically straight lines. A least-square curve fitting was used to obtain

$$\delta T = b_1 + b_2 T \tag{4.3}$$

for each probe where b_1 and b_2 are constants for each probe. From Eqs. 4.1-4.3 the true calibration curve was obtained as

$$T = T_{ref} + T_{\delta} \frac{(E-E_1)}{(E_2-E_1)} \tag{4.4}$$

where $$T_{ref} = \frac{(24.26-b_1)}{(1+b_2)}$$

$$T_{\delta} = \frac{10.38}{(1+b_2)}$$

In general, T_{ref} and T_{δ} were different for each probe. T_{ref} is the temperature for each probe corresponding to R_d in the calibration bridge and T_{δ} is the change in temperature for each probe corresponding to the change in calibration resistance when SW B is closed. T_{ref} and T_{δ} were read into the computer after each calibration.

4.2.6.3 Data Collection Procedures

When SW B was open and SW A_1 through A_{12} were set to "measure", the bridge circuit was said to be at the sampling mode. Resistors R_{a_j}, R_{b_j} (j=1,2,...12), R_c and R_d would then constitute a Wheatstone bridge which was designed to be balanced at 24.26°C. In other words, $R_{a_j}/R_{b_j} = R_c/R_d$, with R_{b_j} equal to the resistance specified by the manufacturer for probe j at 24.26°C. Any temperature different from 24.26°C at probe j would change the probe resistance R_{b_j} and cause the bridge circuit to become unbalanced. A voltage signal would be produced accordingly. This voltage was amplified by a differential amplifier to the range suitable for the A/D converter. The temperature reading were sampled at 0.01 second intervals and then averaged over a specified time interval of 90 seconds. A teletype was used to control the computers and to input the sampling and averaging period, the calibration coefficients T_{ref} and T_{δ}, and geometric information on the carriage, rake, and horizontal arm positions. The geometric input data were used to compute the X, Y and Z coordinates of probes 1-10. The resulting temperature measurements and probe positions

were then printed out by the teletype for immediate inspection and were punched on paper tapes for subsequent analysis.

4.3 Experiment Parameters

For the assumed similarity profiles, the dependent variables of a buoyant surface jet discharged into a crossflow consist of the maximum velocity u_m, the maximum temperature excess ΔT_m and the geometric parameters of the jet a, b, b', c, h and θ. These dependent variables depend on the characteristics of both the jet and the ambient flow and on the distance from the outlet (s). Assuming that the ambient velocity and temperature are uniform over the depth and that the flow is steady and uniform, the ambient flow is characterized by the average crossflow velocity u_a and the ambient temperature T_a (or ambient density ρ_a). Assuming that the jet has a uniform velocity and temperature at the outlet which is a rectangular, the characteristics of the jet can be represented by the jet width and depth at the outlet, b_o and h_o, the discharge angle θ_o, the initial jet velocity u_o, the outlet temperature T_o (or the initial jet density ρ_o) and the kinematic viscosity ν_o of the jet at the exit. The distance from the outlet (s) together with the parameters characterizing the ambient flow and the jet at the outlet as cited above, are called the independent variables.

The independent variables can be grouped into the following dimensionless parameters:

outlet densimetric Froude number:

$$F_o = \frac{u_o}{\sqrt{\Delta\rho_o g h_o/\rho_a}}$$

outlet Reynolds number:

$$R_{e_o} = \frac{u_o h_o}{\nu_o}$$

velocity ratio:

$$R = \frac{u_o}{u_a}$$

and distance from the outlet:

$$\frac{s}{\sqrt{b_o h_o}}$$

The aspect ratio A_r and the discharge angle θ_o are not included in the independent dimensionless parameters because only one discharge geometry was used throughout this study.

The dependent variables can also be reduced to dimensionless forms. Then, the relationship among the dimensionless variables can be expressed as

$$\left[\frac{u_m}{u_o}; \frac{\Delta T_m}{T_o}; \frac{a}{\sqrt{b_o h_o}}; \frac{b}{\sqrt{b_o h_o}}; \frac{b'}{\sqrt{b_o h_o}}; \frac{c}{\sqrt{b_o h_o}}; \frac{h}{\sqrt{b_o h_o}}; \theta\right]$$

$$= \text{functions}\left[F_o, R_{e_o}, R, \frac{s}{\sqrt{b_o h_o}}\right] \qquad (4.5)$$

Table 4.1 gives a summary of the run parameters for each experiment. A discharge angle (θ_o) of 90^o, an initial jet dimension of 1 in. by 1 in. and an ambient flow depth of 0.77 feet at the experimental measurement area were used for all of the experiments. Selection of run parameters such as initial jet velocity u_o and crossflow velocity u_a for each run was based on the prelimary calculations of the desired values of the outlet

Table 4.1 Summary of Experimental Runs

Run No.	u_o $\frac{ft}{sec}$	u_a $\frac{ft}{sec}$	T_a ^oC	ΔT_o C^o	$\frac{\Delta\rho_o}{\rho_a} \times 10^3$	F_o	$R_{e_o} \times 10^{-4}$	$\frac{u_o}{u_a}$
1	0.43	0.10	23.41	10.49	3.04	4.79	0.45	4.33
2	1.30	0.10	23.47	9.84	2.83	14.97	1.34	13.0
3	0.87	0.10	23.15	10.14	2.91	9.86	0.89	8.67
4	0.43	0.17	22.03	10.25	2.81	4.99	0.44	2.60
5	0.87	0.17	22.53	10.19	2.85	9.91	0.88	5.19
6	1.30	0.17	20.65	10.50	2.76	15.11	1.29	7.78
7	1.30	0.23	21.16	10.14	2.70	15.27	1.29	5.58
8	0.87	0.23	20.91	10.69	2.83	9.95	0.86	3.72
9	0.43	0.23	19.47	10.85	2.76	5.03	0.42	1.86
10	1.30	0.30	17.01	11.72	2.76	15.11	1.21	4.33
11	0.87	0.30	17.85	11.61	2.84	9.93	0.82	2.89

densimetric Froude number F_o and the velocity ratio R under the constraints of the capacity of the experimental facilities.

A relative density difference of 0.0028, corresponding to a temperature difference of about $10C^o$, was selected for all the experiments. This choice of density difference was intended to give outlet densimetric Froude numbers of 5, 10 and 15 when the jet exit velocities were 0.433, 0.867 and 1.30 ft/sec, respectively. However, since the warm water was recirculated and since there was heat buildup due to the pump, it was not possible to keep the density difference constant during the experiment. As a consequence, the outlet densimetric Froude numbers were based on the average density differences during the experiments and were off at most 4 percent from the nominal values.

For $\underline{u}_a$ = 0.30 ft/sec, only two experiments were performed. A third experiment was started for $\underline{u}_a$ = 0.30 ft/sec, u_o = 0.433 ft/sec and $F_o \approx 5$, but was not completed because it was found that the jet contacted the near sidewall almost immediately after the exit. This situation was beyond the scope of this investigation.

4.4 Experimental Procedure

Before each experiment, the desired run parameters u_o and $\underline{u}_a$ were selected. The weir at the downstream end of the flume was adjusted to give an ambient flow depth of 0.77 feet in the measurement area for a desired ambient discharge.

There was always a spatial temperature variation within the sump water before the experiment began. Therefore, before temperature data were taken it was necessary to run the pump for at least half an hour in order to mix the sump and to reduce the temperature variations in the ambient

water. For the establishment of a steady state condition in the jet flow, the warm water supply system was also turned on for at least half an hour before any data were taken.

A computer program was read into the computers to control the functioning of the data acquisition system. The bridge circuit was first placed at the calibration mode to obtain the system calibration curve. The desired sampling time of 90 seconds and the coefficients T_{ref} and T_{δ} of the probe calibration curves (Eq. 4.4) were read from teletype to the computers. The bridge circuit was then turned to the sampling mode to check the temperature difference between the ambient flow and the jet flow at the outlet. The mixing valves were adjusted if necessary until the desired temperature difference was obtained. The probe calibration curves were also checked at this stage to insure that they were still valid. This was accomplished by moving the probe rake away from the jet region into the ambient flow and then taking temperature measurements. If there were significant differences (greater than $0.10C^{o}$) among the probes in the ambient flow (probes 1-11), the probes were re-calibrated.

Before taking temperature measurements for each cross section, dye was injected into the jet to help visually position the rake approximately normal to the jet trajectory. The teletype automatically printed out the temperature data after each set of samplings of the 12 probes. These temperature data were used to decide where to place the probes next and to monitor the ambient and outfall temperatures. The surface temperatures were measured with the centers of the probes about 0.14 in. below water surface.

Each run covered four cross sections and consisted of about 600 to 800 measurement points. (See Appendix II.) An entire experiment took about 8 hours.

5. PRESENTATION AND DISCUSSION OF RESULTS

This chapter gives (1) a presentation and discussion of the measured temperature distributions for a typical run, (2) the data reduction techniques which were developed to give a systematic means of obtaining necessary information from the experimental data, (3) the method and the results of evaluation of the empirical coefficients C_V, C_D, and C_B which are used in the mathematical model, and (4) a comparison of the experimental results with calculations from the numerical model.

5.1 Measured Temperature Distributions

The experimental data of all runs are presented in Appendix II. Figures 5.1-5.4 show the measured temperature distributions for the four measurement cross sections of a typical experiment, namely, Run 1. (The cross section numbers increase in the downstream direction along the jet trajectory. See Figs. 5.22-5.31 for the locations of the measurement cross sections of each run.) At each cross section, $\overset{*}{d}$ in Figs. 5.1-5.4 is the nondimensional lateral distance from the furthermost measurement point on the upstream side of the jet.

Significant asymmetry of the temperature profiles due to cross-flow can be seen from these figures. The temperature profiles are asymmetrical at every level; also for each cross section the point of maximum temperature excess moves toward the lee side of the jet with increasing depth. (See also Figs. 5.7-5.17 and the accompanying discussion in Section 5.2.3.1.)

In Fig. 5.4, it is seen that as the distance from the outlet increased, the temperature distributions below the water surface became

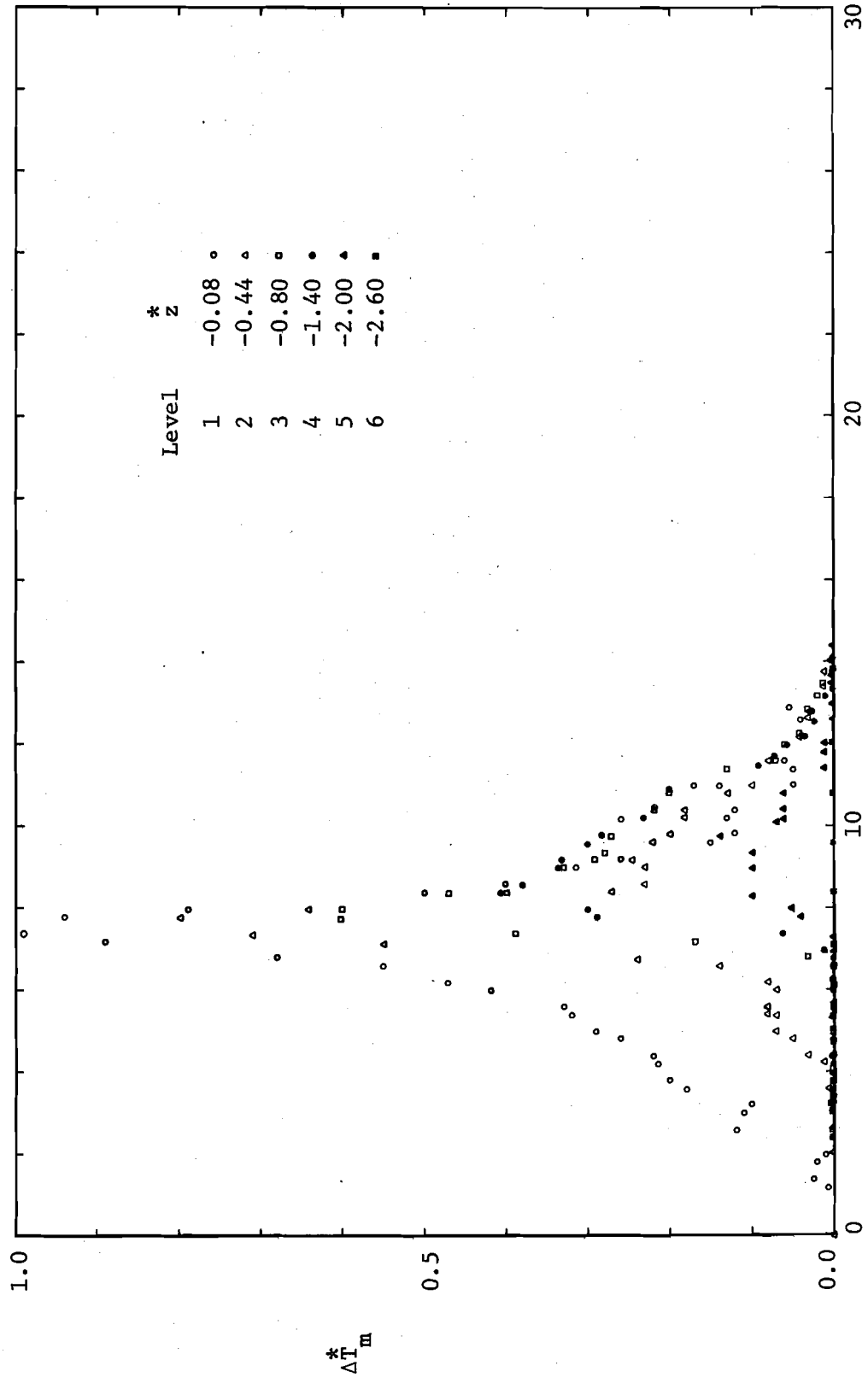

Fig. 5.1 Measured nondimensional temperature distributions at section 1, Run 1

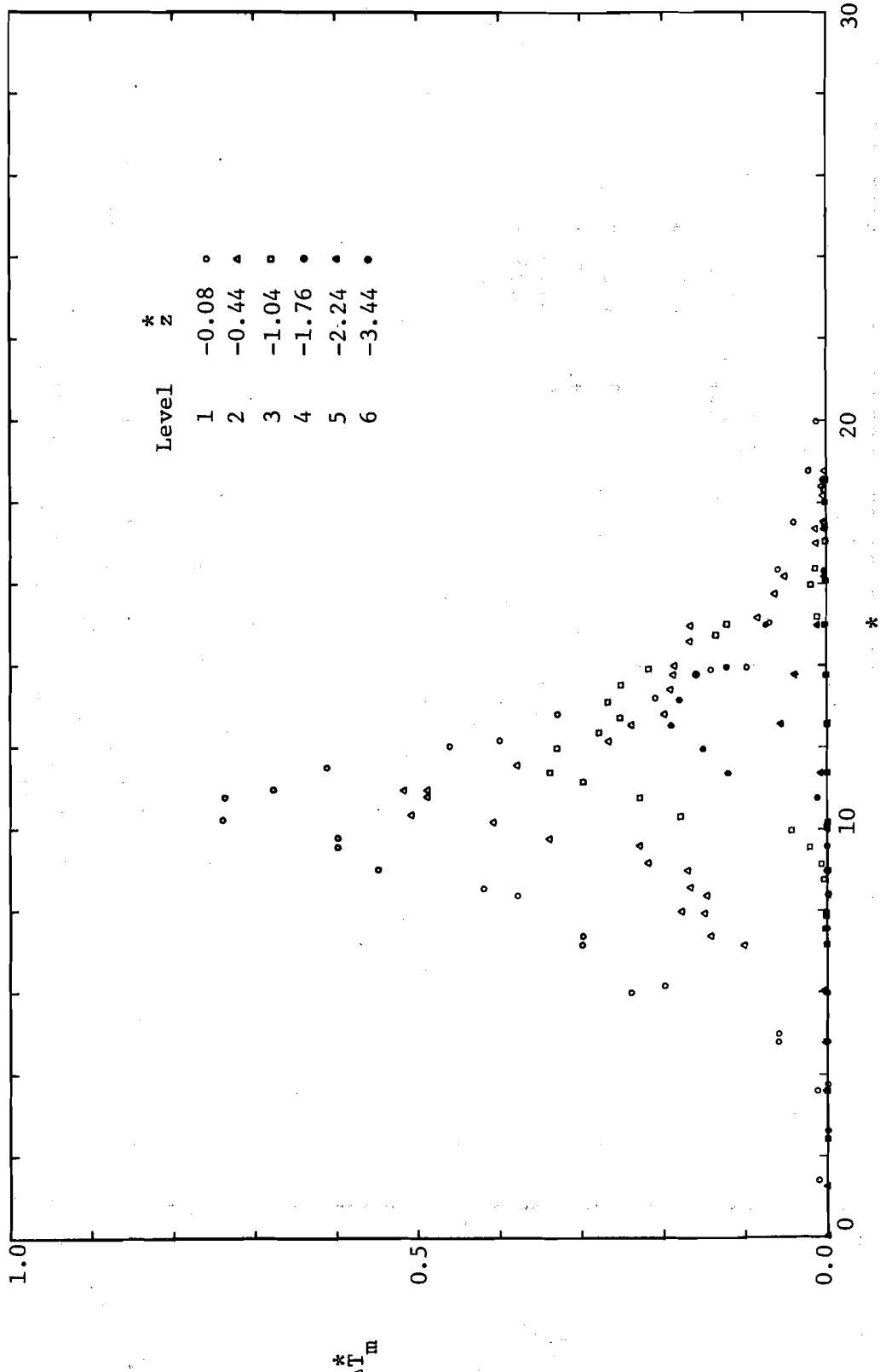

Fig. 5.2 Measured nondimensional temperature distributions at section 2, Run 1

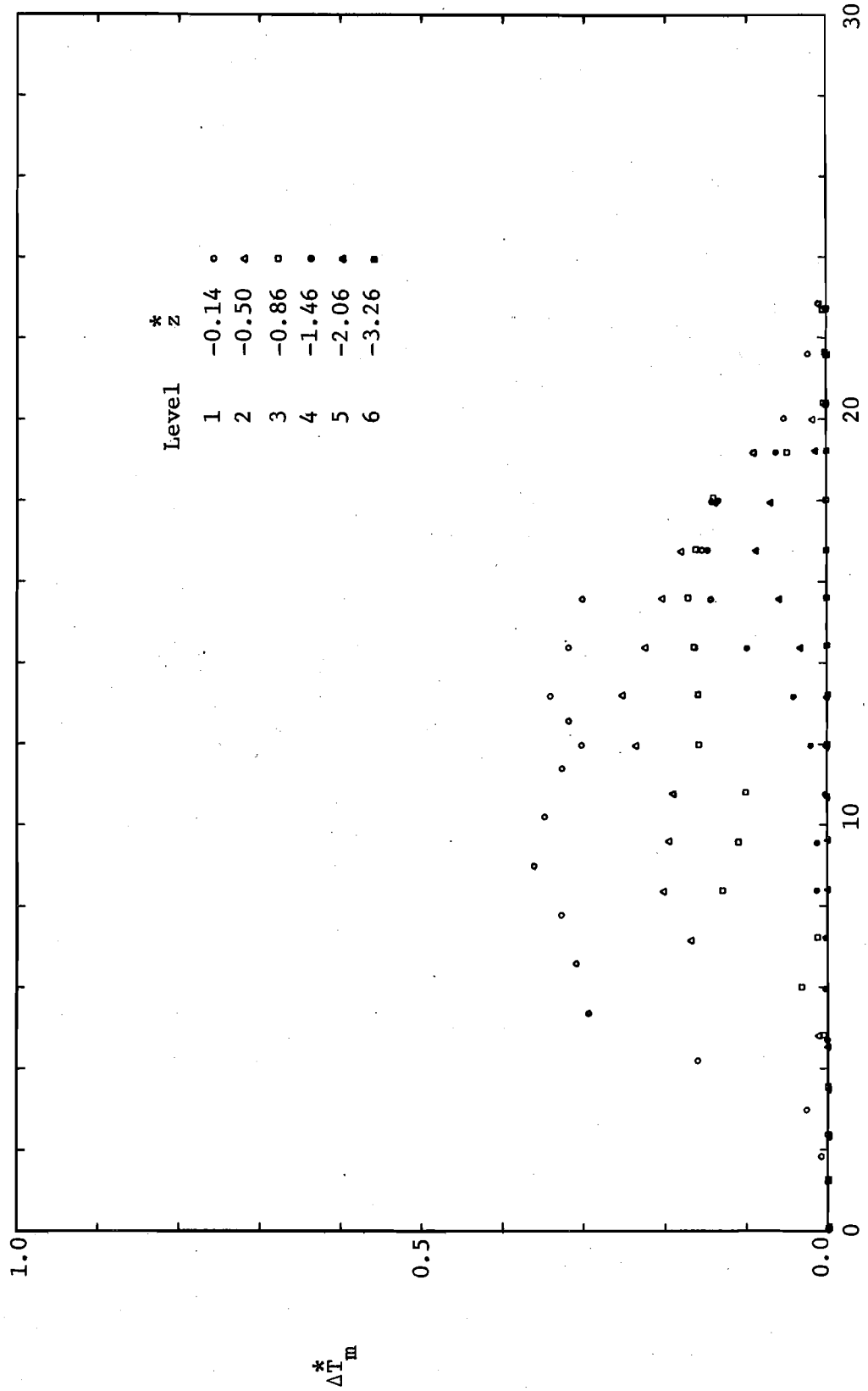

Fig. 5.3 Measured nondimensional temperature distributions at section 3, Run 1

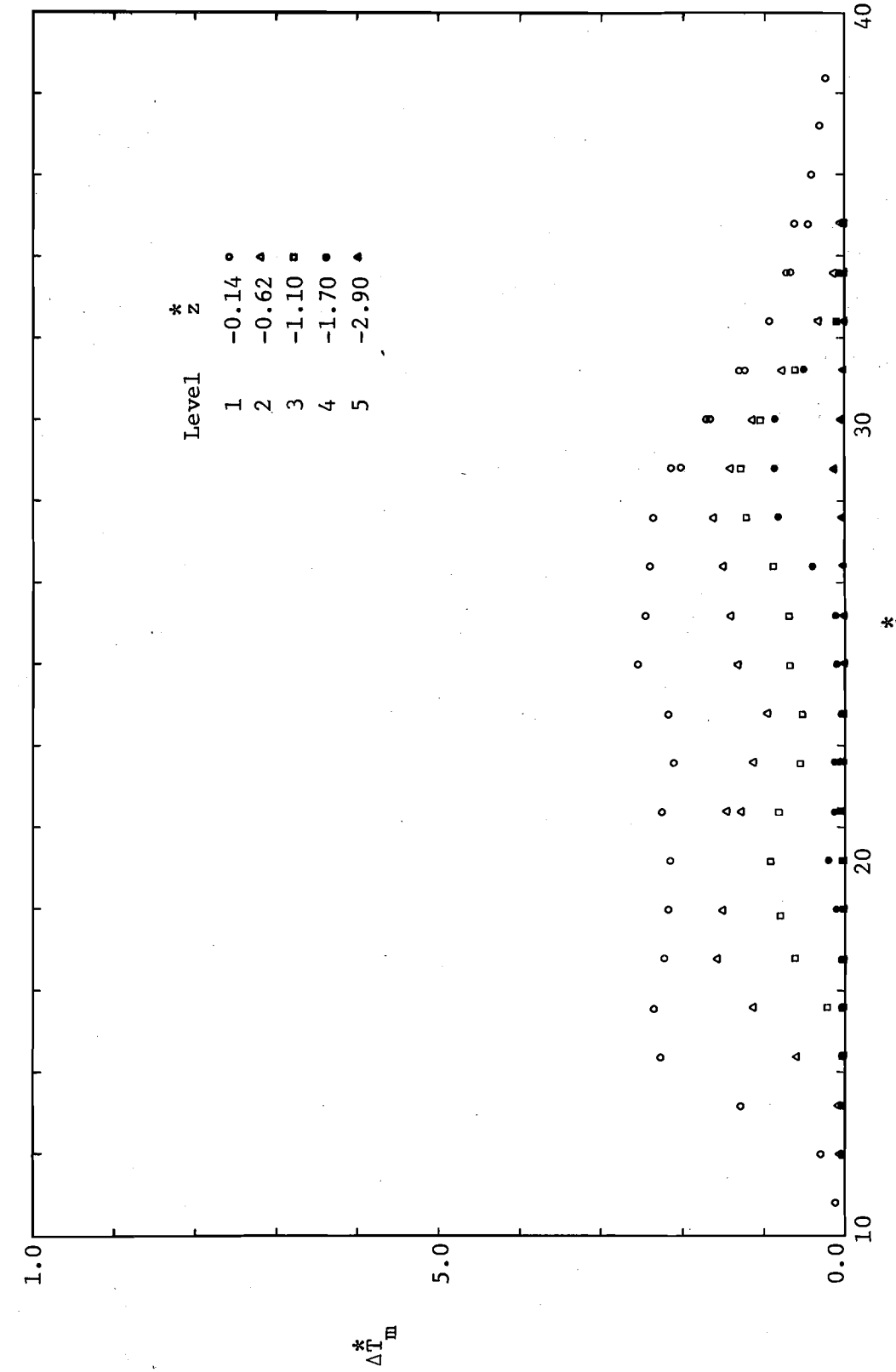

Fig. 5.4 Measured nondimensional temperature distributions at section 4, Run 1

bimodal. This phenomenon could be observed as a nearly clear streak along the center of some jet flows into which dye was injected for visualization purposes. The bimodal temperature distributions could conceivably be a result of the higher buoyant forces associated with the higher temperatures in the middle if the higher buoyant forces caused a rising tendency in the central part of the jet and created a secondary current which tended to split the jet into two parts as the jet spread out. This type of behavior was observed near the exit in Prych's [1970] experiments with coflowing buoyant discharges over the full depth of open channel flows. However, the bimodal nature of the temperature distributions disappeared rather rapidly in his experiments. No bimodal distributions were observed in the experiments of Weil and Fischer [1974] with coflowing buoyant discharges or in the experiments of Pande and Rajaratnam [September, 1975] for surface buoyant jets with no ambient flow. These results would tend to indicate that secondary, density-induced currents were not present and therefore may not be the cause of the bimodal behavior observed in the present experiments. Another possible mechanism for this behavior is mentioned in Section 5.2.3.1.

In Fig. 5.1, the lateral temperature gradients near the edges of the jet at cross section 1 nearest the exit were much smaller than expected based on jet spreading. This difference was considered to be due to the temperature built-up in the wake of the jet and in the zone where the ambient flow stagnated against the upstream side of the jet near the outlet.

5.2 Optimal Fitting of Temperature Distributions to Similarity Functions for Each Cross Section

A systematic method was developed to obtain parameters such as jet width, location of maximum temperature, etc., from the experimental data. This was done by the optimal fitting of the assumed similarity function for the temperature distribution to the data for each level (i.e. each value of z) at each cross section. An influence coefficient algorithm [Becker and Yeh, 1972] was used for this fitting and allowed the extraction of jet characteristics from the experimental data. This algorithm is an easily implemented procedure for the identification of parameters embedded in a set of governing equations defining a system. It was assumed that the temperature similarity functions were valid over the measurement cross sections even though the sections were not exactly normal to the jet axis. Thus the temperature distributions over the measurement cross section could be represented by

$$\Delta T = \Delta T_m (1-\phi_z^{1.5})^{1.2} \; (1-\phi_n^{1.5})^{1.2} \tag{5.1}$$

(See Eqs. 3.52-3.53, Section 3.4.) For all of the data, the largest deviation of the measurement cross section from the normal to the axis was 20^o and the average deviation was 8^o. Equation 5.1 can be viewed as the combination of the following two equations

$$\Delta T = \Delta T_{m\ell} (1-\phi_n^{1.5})^{1.2} \tag{5.2}$$

and

$$\Delta T_{m\ell} = \Delta T_m (1-\phi_z^{1.5})^{1.2} \tag{5.3}$$

where $\Delta T_{m\ell}$ = the maximum temperature excess at certain level. Equations 5.2 and 5.3 show that the optimal fittings of temperature distributions may

be separated into two consecutive steps: first the fitting of the measured temperature profile at each level to Eq. 5.2 and then the fittings of the maximum temperature excess of each level to Eq. 5.3 which gives the variation of the maximum temperature with depth.

5.2.1 Lateral Temperature Profiles at Each Level

The parameters obtained by the fitting of the temperature profile for each level to the similarity function were the jet widths and location of the maximum temperature, i.e., $\overset{*}{B}$, $\overset{*}{B}'$ and $\overset{*}{d}_m$. As illustrated in Fig. 5.5, $\overset{*}{B}$ and $\overset{*}{B}'$ were the nondimensional outer width and inner width, respectively, along the measurement section, and $\overset{*}{d}_m$ was the nondimensional distance from the furthermost measurement point on the upstream side of the jet to the peak of the similarity profile. All length dimensions were non-dimensionalized by dividing by $\sqrt{b_o h_o}$, which was equal to 1 in. for all experiments. The maximum temperature excess for the similarity profile was assumed to be known and was taken as the maximum measured temperature excess. This assumption greatly reduced the computational effort and caused negligible differences in the results for the typical profiles which were fitted to the similarity function both by letting $\Delta T_{m\ell}$ be a parameter to be optimized and by assuming $\Delta T_{m\ell}$ to be known. The equation which describes the asymmetrical similarity profile may be written from Eq. 5.2 as

$$\Delta T = \Delta T_{m\ell}\left[1-\left(\frac{\overset{*}{d}_m-\overset{*}{d}}{\overset{*}{B}}\right)^{1.5}\right]^{1.2} \qquad \text{for } \overset{*}{d} \leq \overset{*}{d}_m$$

$$= \Delta T_{m\ell}\left[1-\left(\frac{\overset{*}{d}-\overset{*}{d}_m}{\overset{*}{B}'}\right)^{1.5}\right]^{1.2} \qquad \text{for } \overset{*}{d} \geq \overset{*}{d}_m \tag{5.4}$$

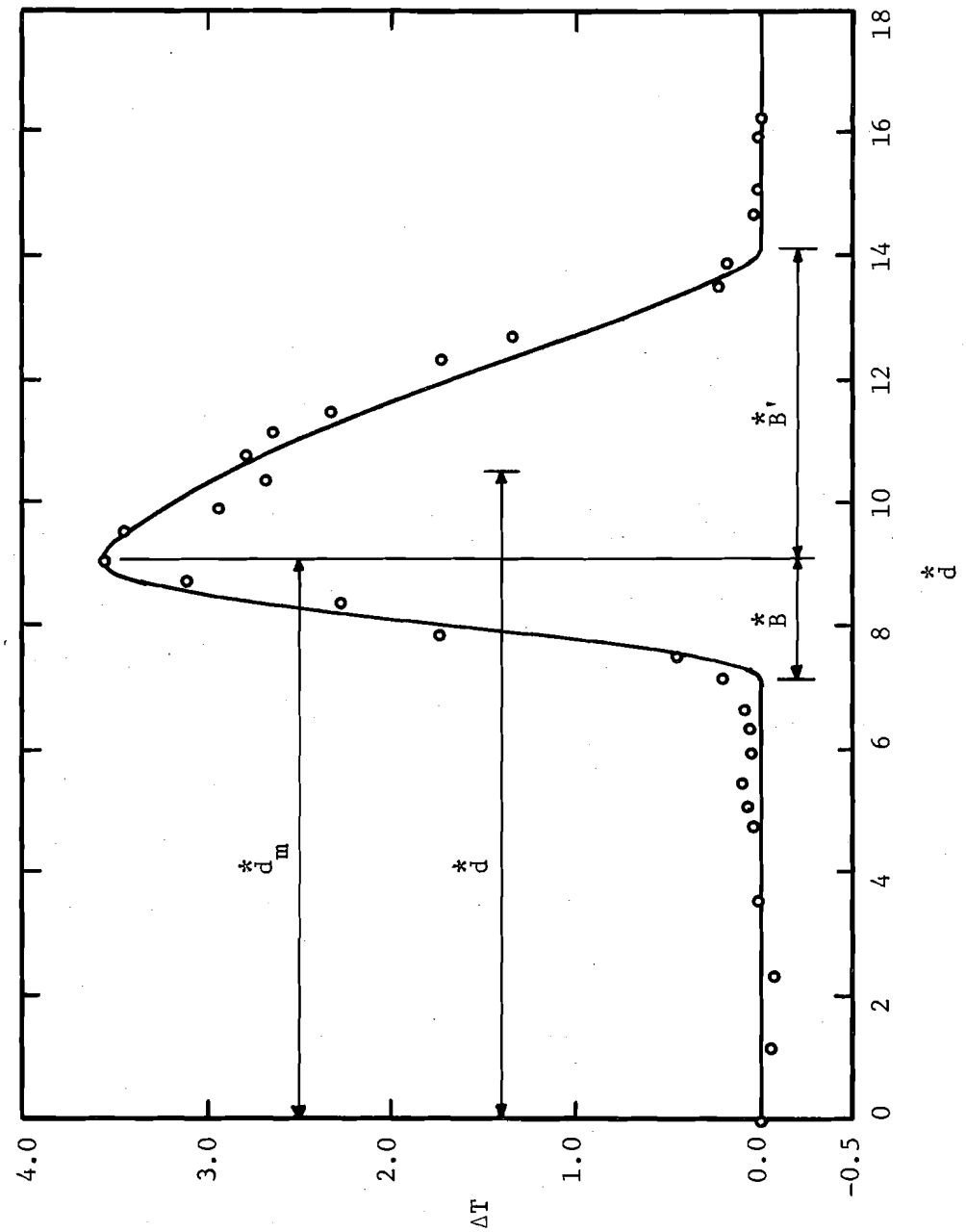

Fig. 5.5 Optimal fitting of lateral temperature profile at level 3 of section 2, Run 1

The algorithm objective is to minimize the objective function which is the sum of the squares of the differences between the computed temperature excesses from Eq. 5.4 and the measured temperature excesses from the experiment. The objective function may be expressed as

$$F(\Delta T) = \sum_{j=1}^{N} (\Delta T^j - \Delta T_e^j)^2 \tag{5.5}$$

where $F(\Delta T)$ = objective function to be minimized

ΔT_e = measured temperature excess

ΔT = computed temperature excess

$j = 1,2,\ldots,N$, index denoting the number of temperature measurement

The algorithm started with the initial estimates of the parameters $\overset{*}{B}$, $\overset{*}{B}'$ and $\overset{*}{d}_m$. Equation 5.4 was then solved for ΔT at the measurement points and the objective function was evaluated. The parameters $\overset{*}{B}$, $\overset{*}{B}'$ and $\overset{*}{d}_m$ were optimized by minimizing the objective function. The procedure was iterated as necessary until an error criterion was satisfied. The error criterion which was used in these calculations and in the other similar calculations to be discussed later was that the incremental changes in all of the parameters should be less than 5%. A detailed step-by-step computational procedure for the algorithm has been given by Becker and Yeh [1972]. Figure 5.5 shows the results of a typical fitting of lateral temperature profile.

Occasionally, when the measured temperature distributions deviated too much from the assumed similarity profiles or when the measured temperature excess values were on the order of magnitude of the accuracy of the measurement, the computational procedure did not converge to an optimum. This situation usually occurred at the temperature profiles

near the bottom boundary of the jet where the magnitudes of the temperature excesses were small. If convergence could not be obtained from the optimization, $\overset{*}{B}$, $\overset{*}{B}'$ and $\overset{*}{d}_m$ were obtained by the following method. A smooth curve was first fitted by eye through the data points of temperature measurement. The peak of the curve determined the position and the value of the maximum temperature excess. The value of $\overset{*}{B}$ was taken as 1.732 times $\overset{*}{B}_{1/2}$, which is the distance from the point of maximum temperature excess to the point on the upstream side of the jet where $\Delta T = 0.5\ \Delta T_{m\ell}$. This procedure is based on the fact that the similarity profile described by Eq. 5.4 gives $\overset{*}{B}_{1/2} = \overset{*}{B}/1.732$, $\overset{*}{B}'$ could be obtained in a similar fashion.

If the temperature distributions over the cross section were bimodal, the entire cross section was not included in the data analysis because the similarity function was no longer valid. Also, some of the individual temperature measurements (usually in sections 1 and 2, see Appendix II) were excluded from the profile-fitting process if it appeared that the measured values were the result of temperature build-up in the wake or in the stagnation zone. The model could not take this build-up effect into account.

5.2.2 Vertical Temperature Profiles

The influence coefficient algorithm was also used for optimal fitting of Eq. 5.3 to the measured maximum temperature excess for each level. Equation 5.3 may be rewritten as

$$\Delta T_{m\ell} = \Delta T_m \left[1-\left(\frac{-\overset{*}{h}-\overset{*}{z}}{\overset{*}{h}}\right)^{1.5}\right]^{1.2} \qquad \text{for } \overset{*}{h} \leq -\overset{*}{z}$$

$$= 0 \qquad \text{for } \overset{*}{h} > -\overset{*}{z} \qquad (5.6)$$

The parameters chosen for evaluation were the maximum temperature excess on the surface, ΔT_m, and the nondimensional depth of the jet $\overset{*}{h}$. The use of Eq. 5.6 implicitly assumed that the points of maximum temperature excess for each level were aligned vertically.

Equation 5.5 may also be used to represent the objective function for the optimal fitting of vertical temperature profiles, provided that ΔT and ΔT_e are interpreted as the computed (from Eq. 5.6) and measured maximum temperature excesses at a certain level j. Figure 5.6 shows the results of fitting a typical vertical temperature profile. There was consistently a significant discrepancy between the measured and the computed maximum surface temperature excess as shown in Fig. 5.6. It was found that the measured ΔT_m (at the surface) was usually about 0.5 to 1.0C^o higher than the computed ΔT_m. This discrepancy, as will be shown later in this chapter, is one of the main things that makes the prediction of the maximum temperature decay difficult.

5.2.3 Results of Evaluation of Jet Characteristics from Experimental Data

The results from the optimal fitting of the measured temperature distributions to the similarity functions are summarized in the following sections in terms of the configurations of jet temperature boundaries, the trajectories, the depths and the maximum temperature decay.

5.2.3.1 Configurations of Jet Temperature Boundaries

Figures 5.7-5.17 show the configurations of jet temperature boundaries and the location of $\Delta T_{m\ell}$ for all runs. In the figures, $\overset{*}{\ell}$ is the nondimensional lateral distance from the jet axis, with positive being toward the upstream side of the jet. The patterns are all alike except for

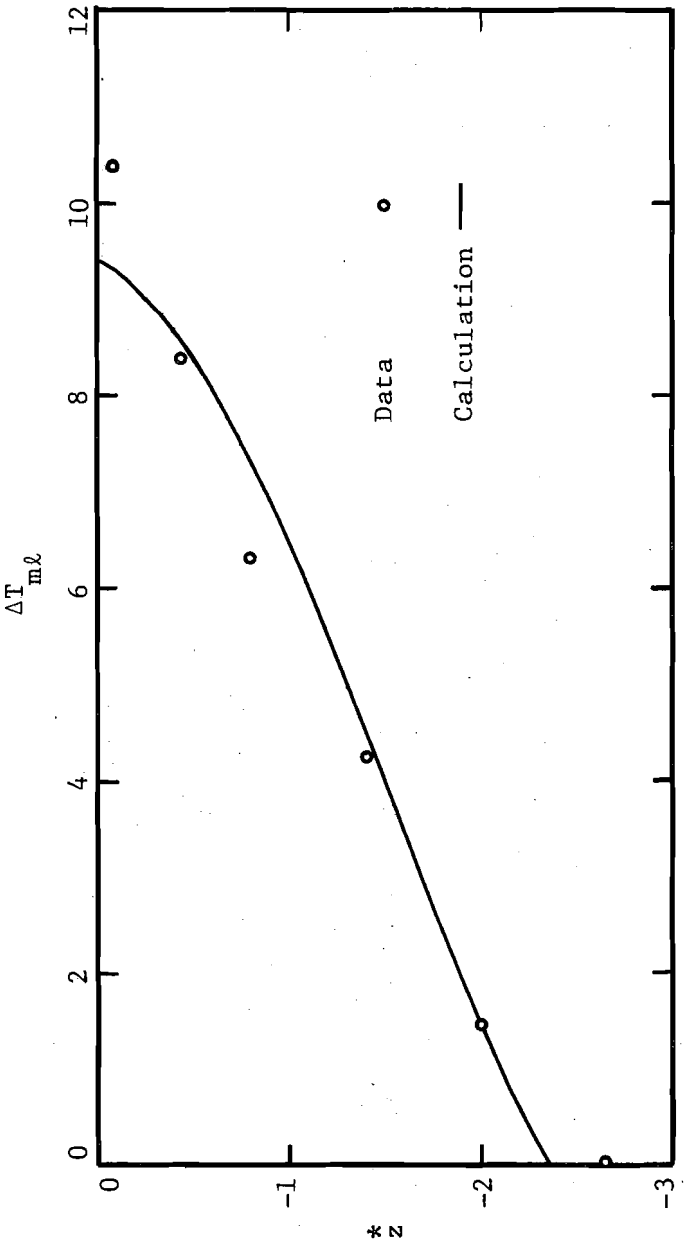

Fig. 5.6 Optimal fitting of vertical temperature profile at section 1, Run 1

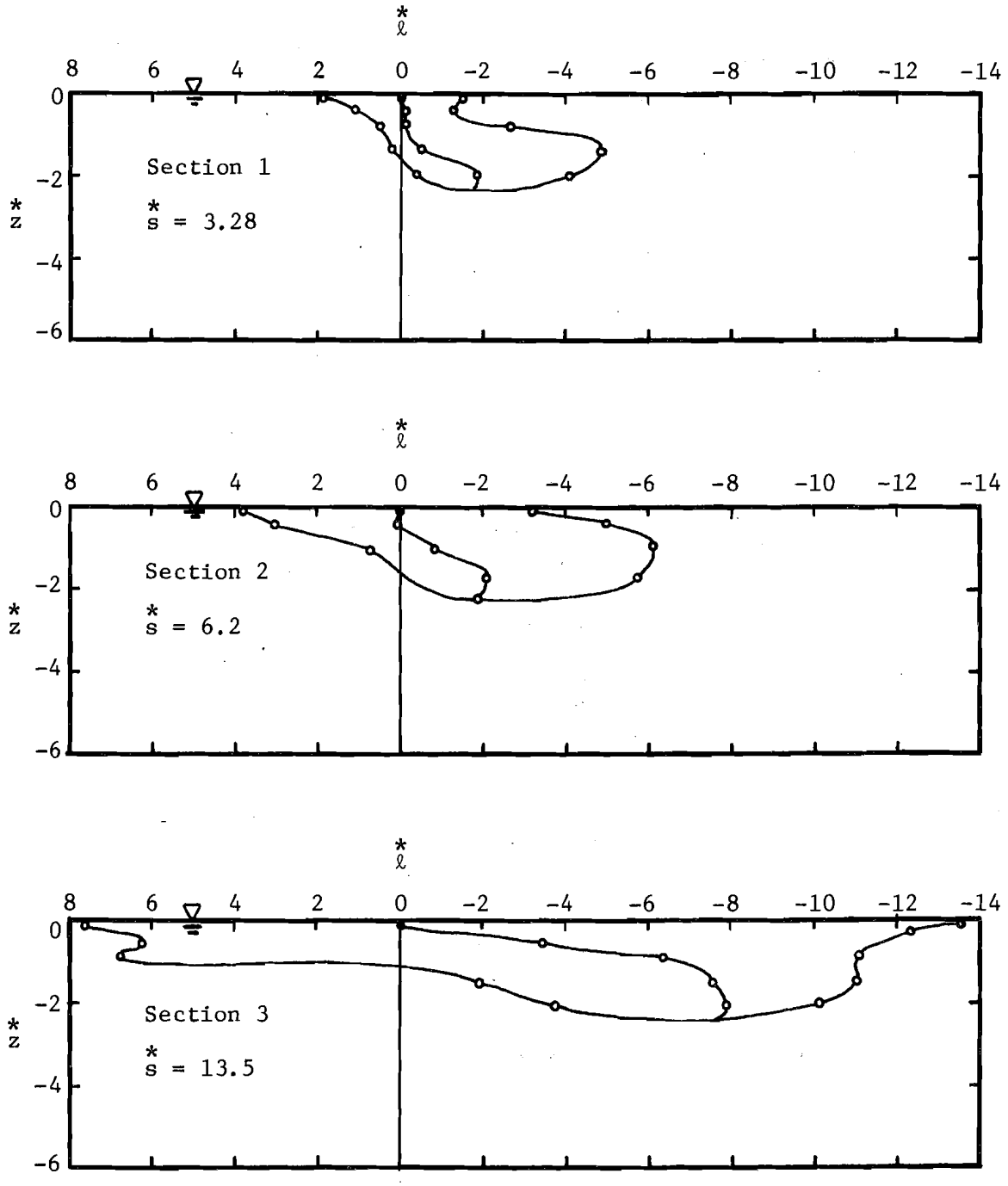

Fig. 5.7 Configuration of jet temperature boundaries for Run 1 ($F_o = 4.79$, $u_o/u_a = 4.33$)

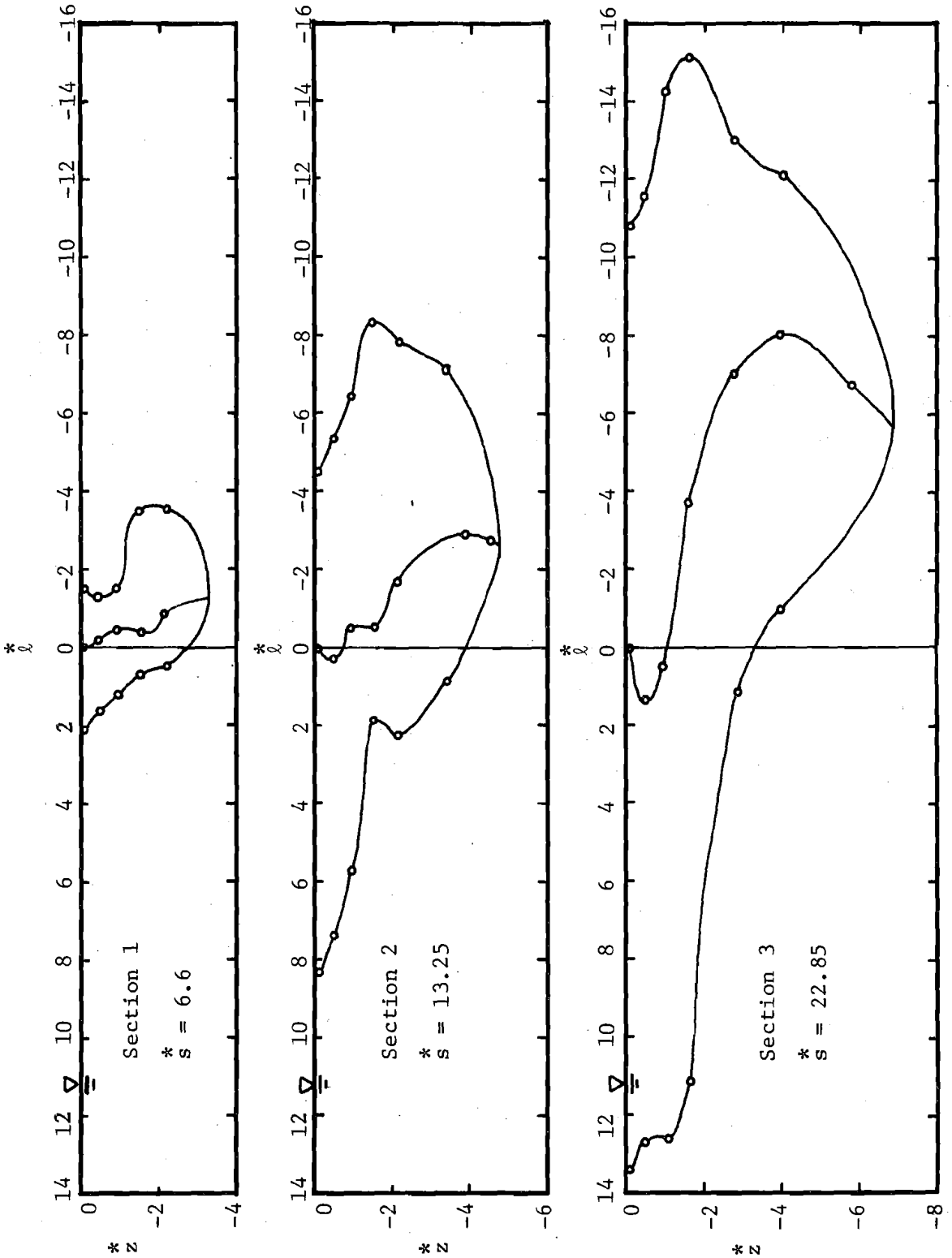

Fig. 5.8 Configuration of jet temperature boundaries for Run 2 (F_o = 14.97, u_o/u_a = 13.00)

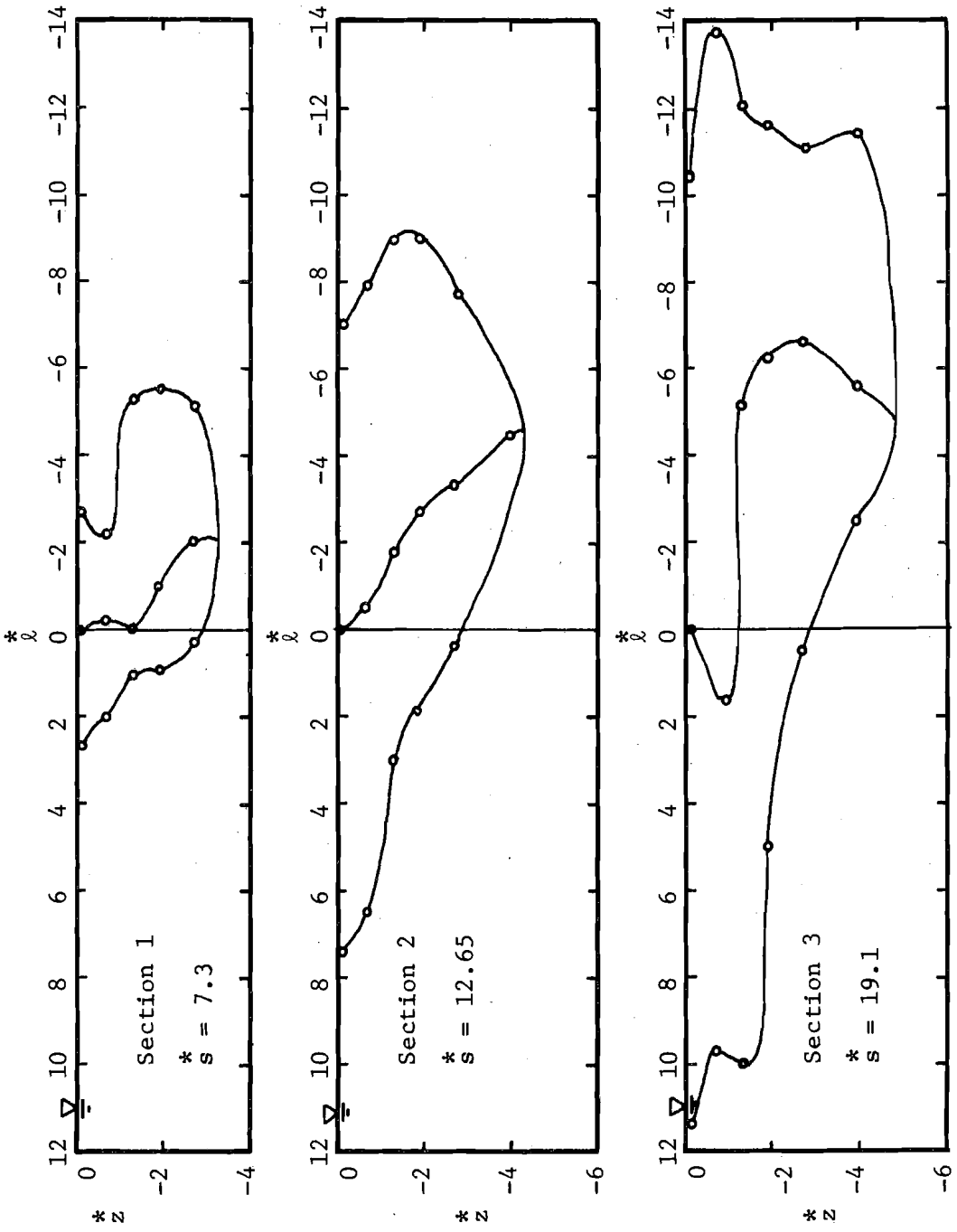

Fig. 5.9 Configuration of jet temperature boundaries for Run 3 (F_o = 9.86, u_o/u_a = 8.67)

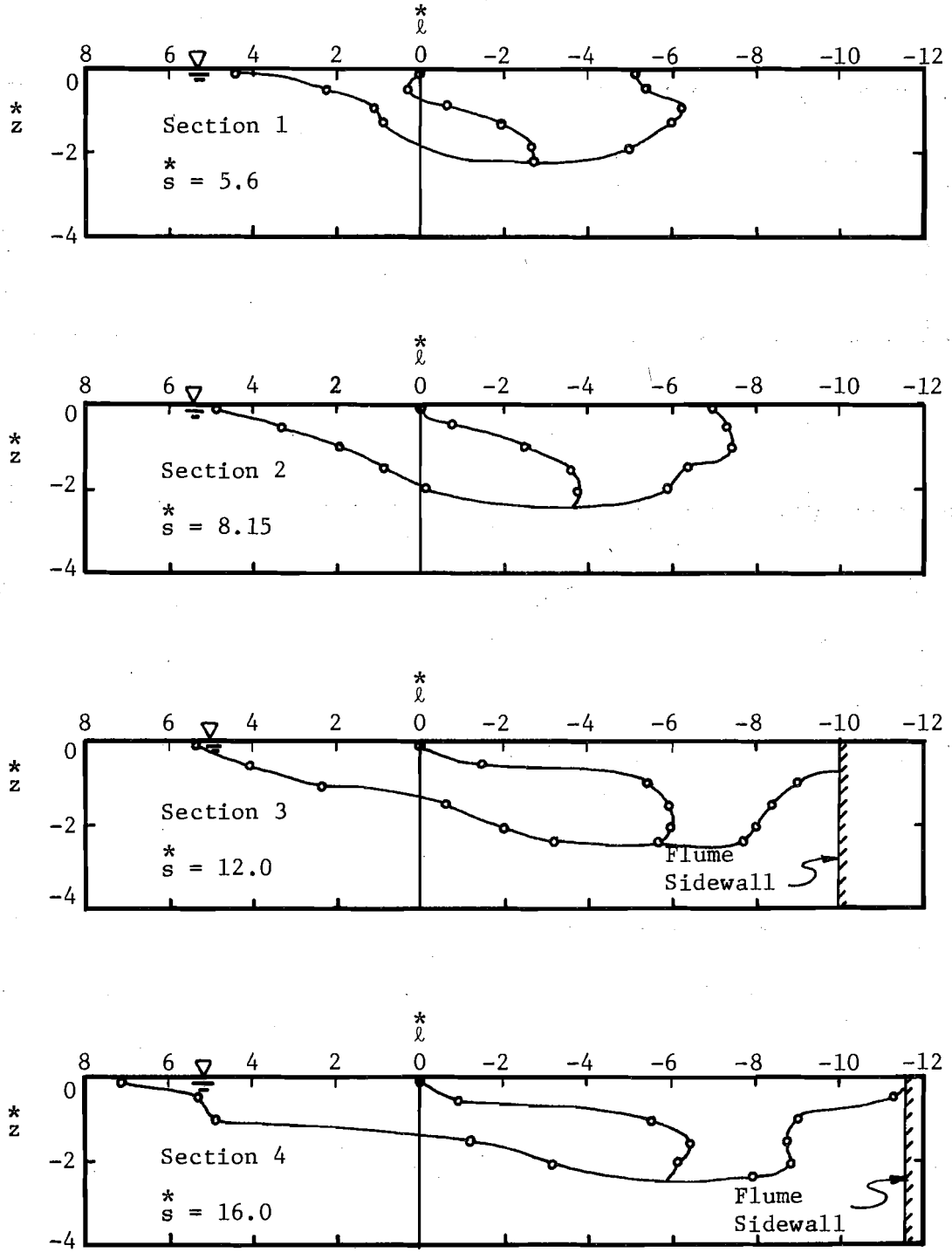

Fig. 5.10 Configuration of jet temperature boundaries for Run 4 ($F_o = 4.99$, $u_o/u_a = 2.60$)

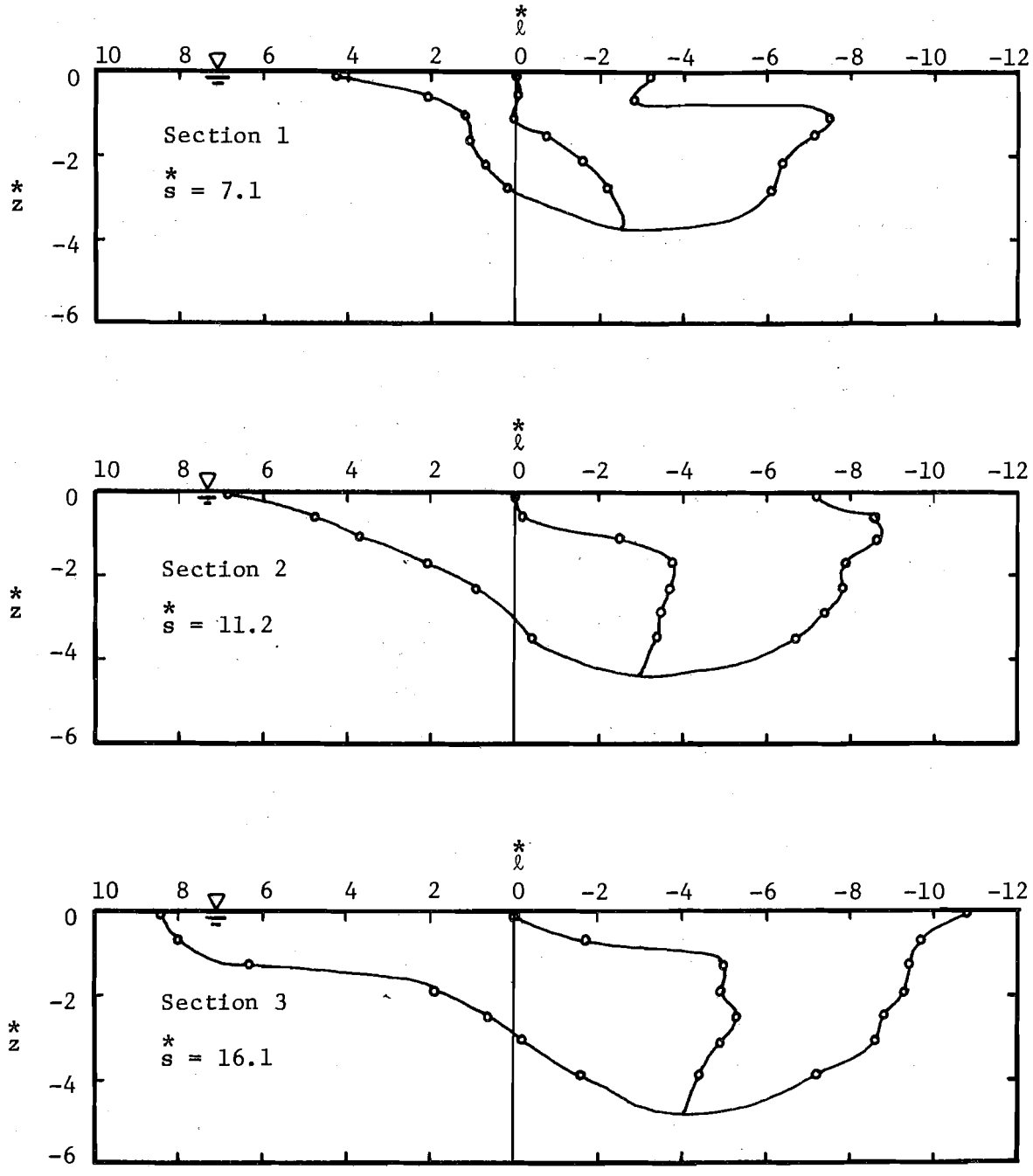

Fig. 5.11 Configuration of jet temperature boundaries for Run 5 ($F_o = 9.91$, $u_o/u_a = 5.19$)

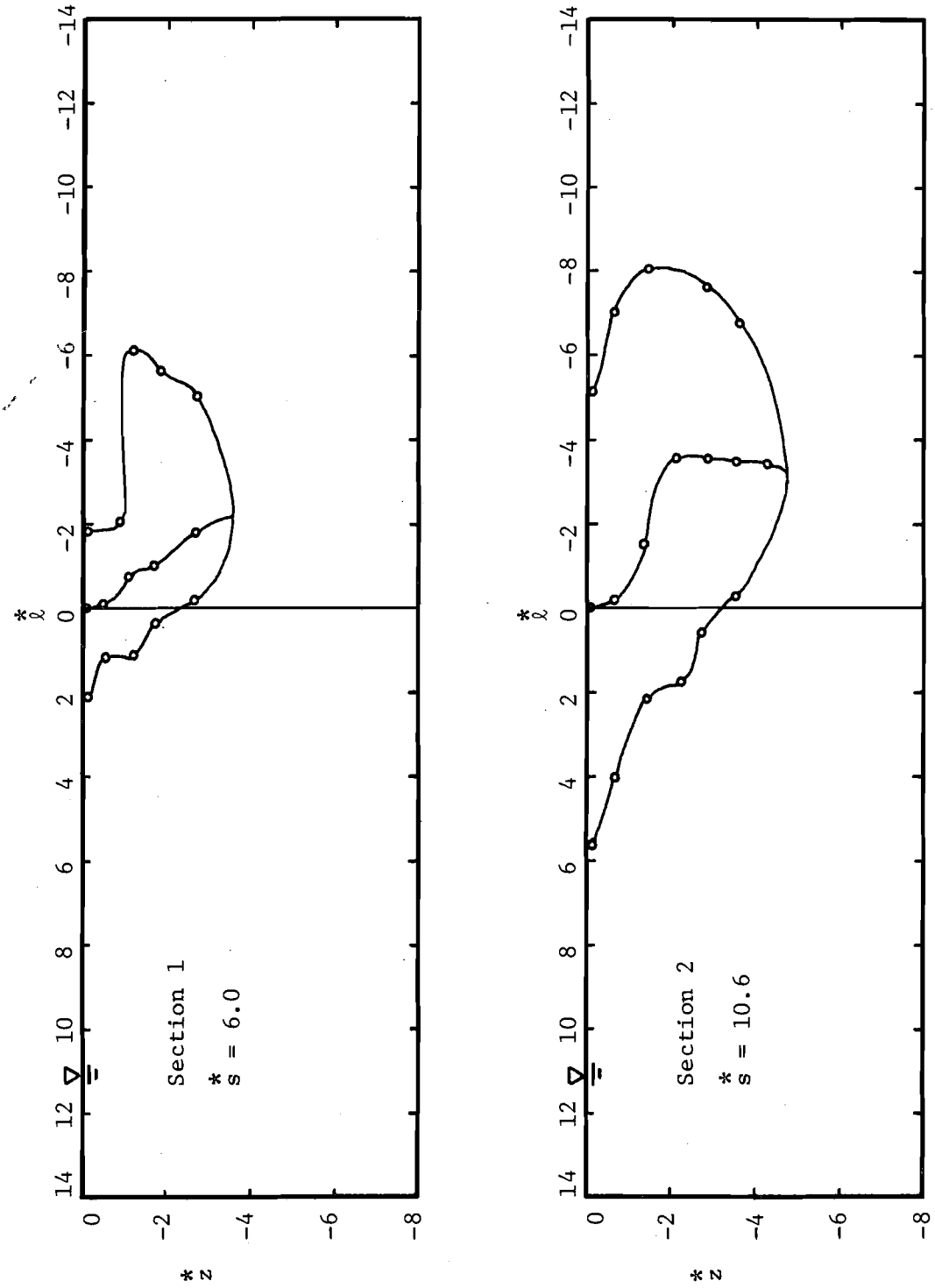

Fig. 5.12 Configuration of jet temperature boundaries for Run 6 (F_o = 15.11, $u_o/\underline{u_a}$ = 7.78)

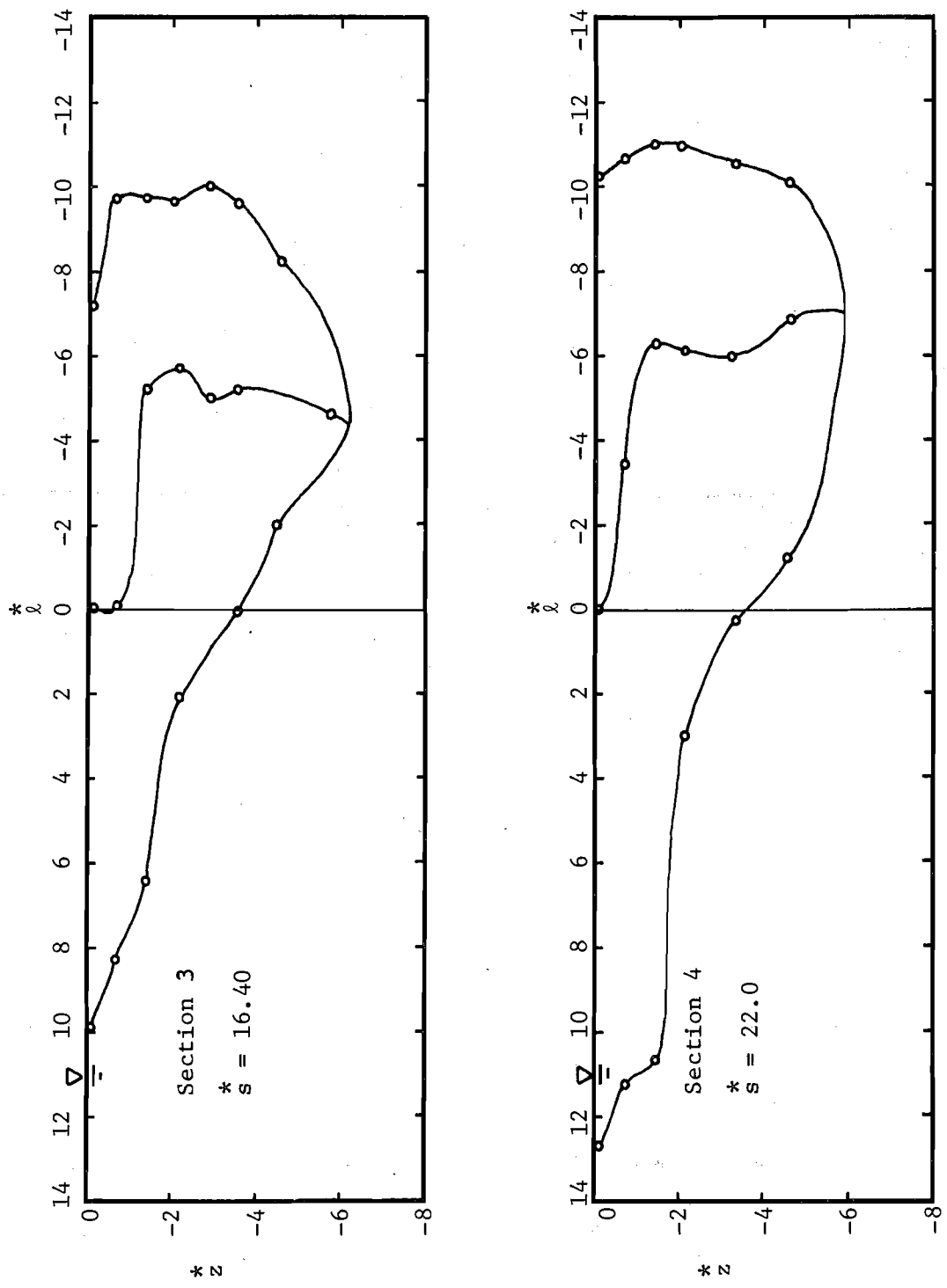

Fig. 5.12 (cont'd) Configuration of jet temperature boundaries for Run 6 (F_o = 15.11, u_o/u_a = 7.78)

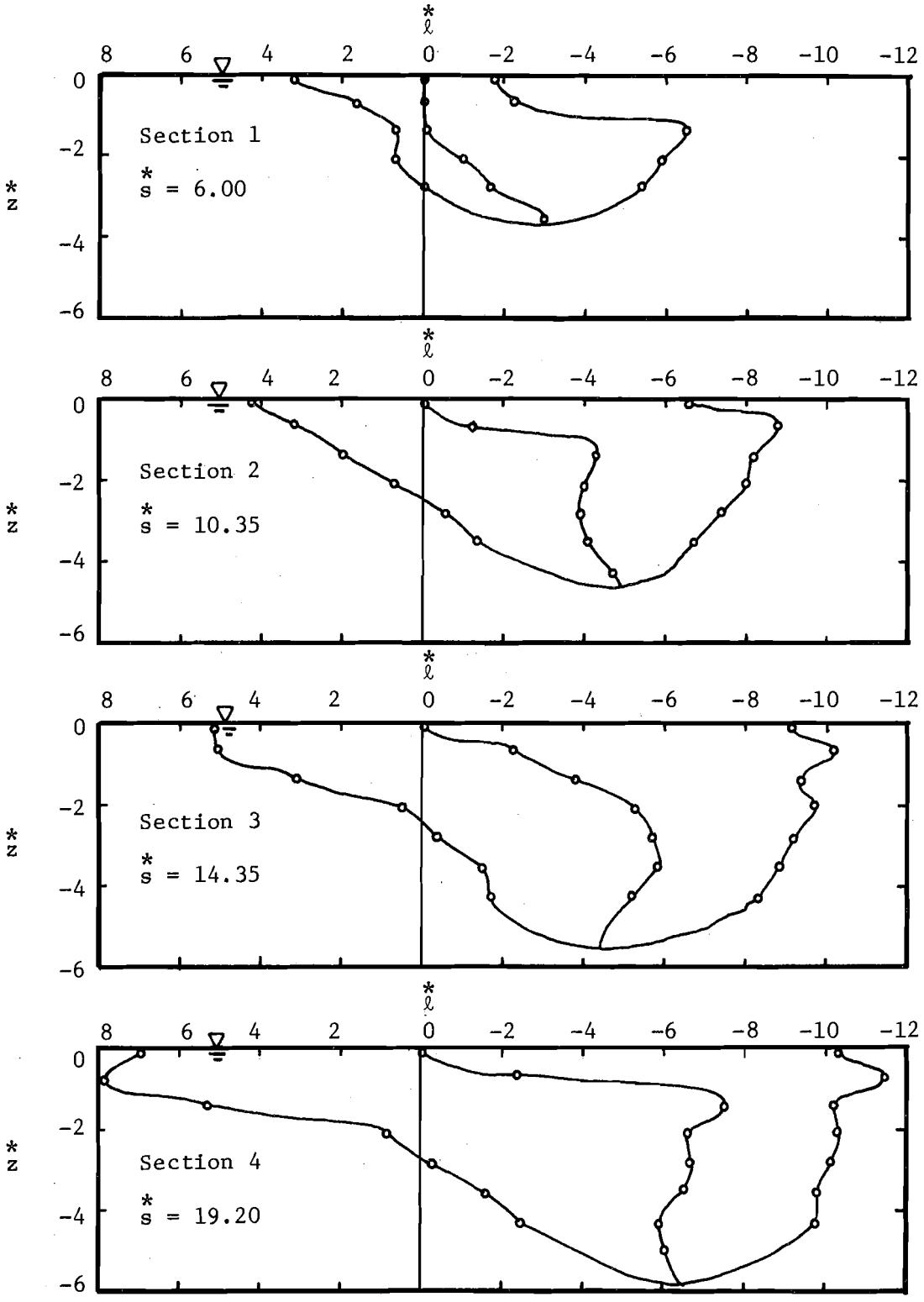

Fig. 5.13 Configuration of jet temperature boundaries for Run 7 ($F_o = 15.27$, $u_o/u_a = 5.58$)

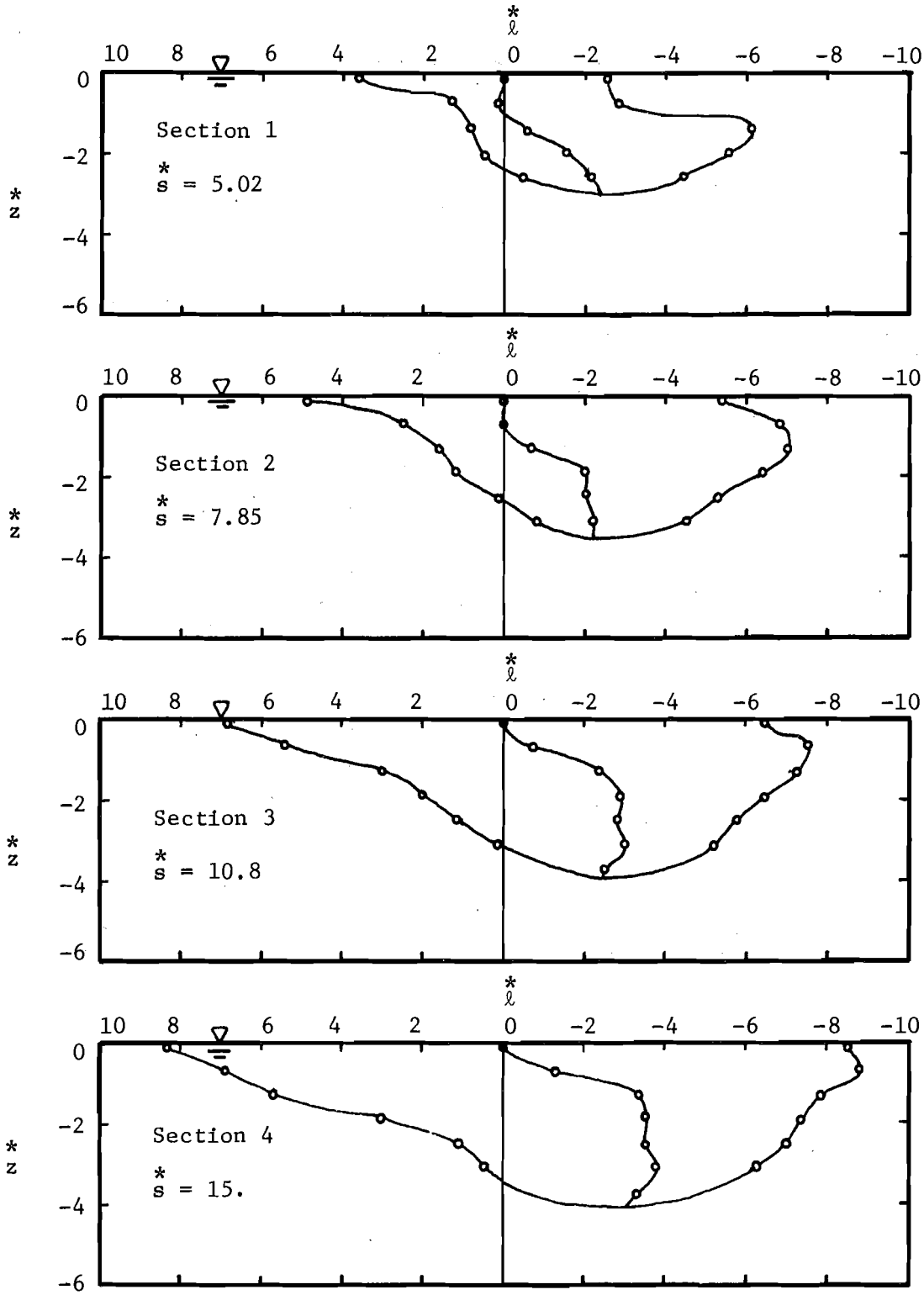

Fig. 5.14 Configuration of jet temperature boundaries for Run 8 (F_o = 9.95, u_o/u_a = 3.72)

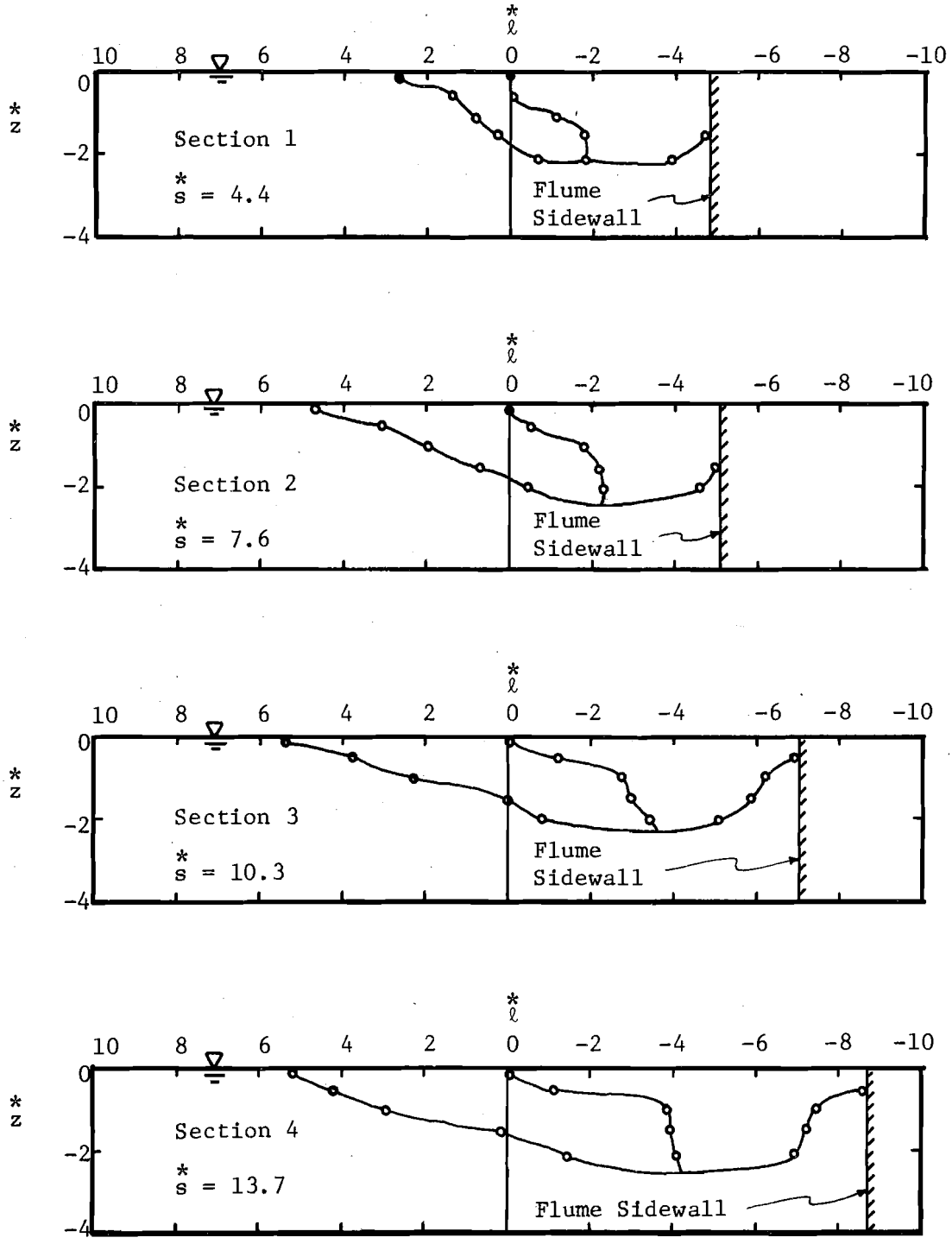

Fig. 5.15 Configuration of jet temperature boundaries for Run 9 (F_o = 5.03, u_o/u_a = 1.86)

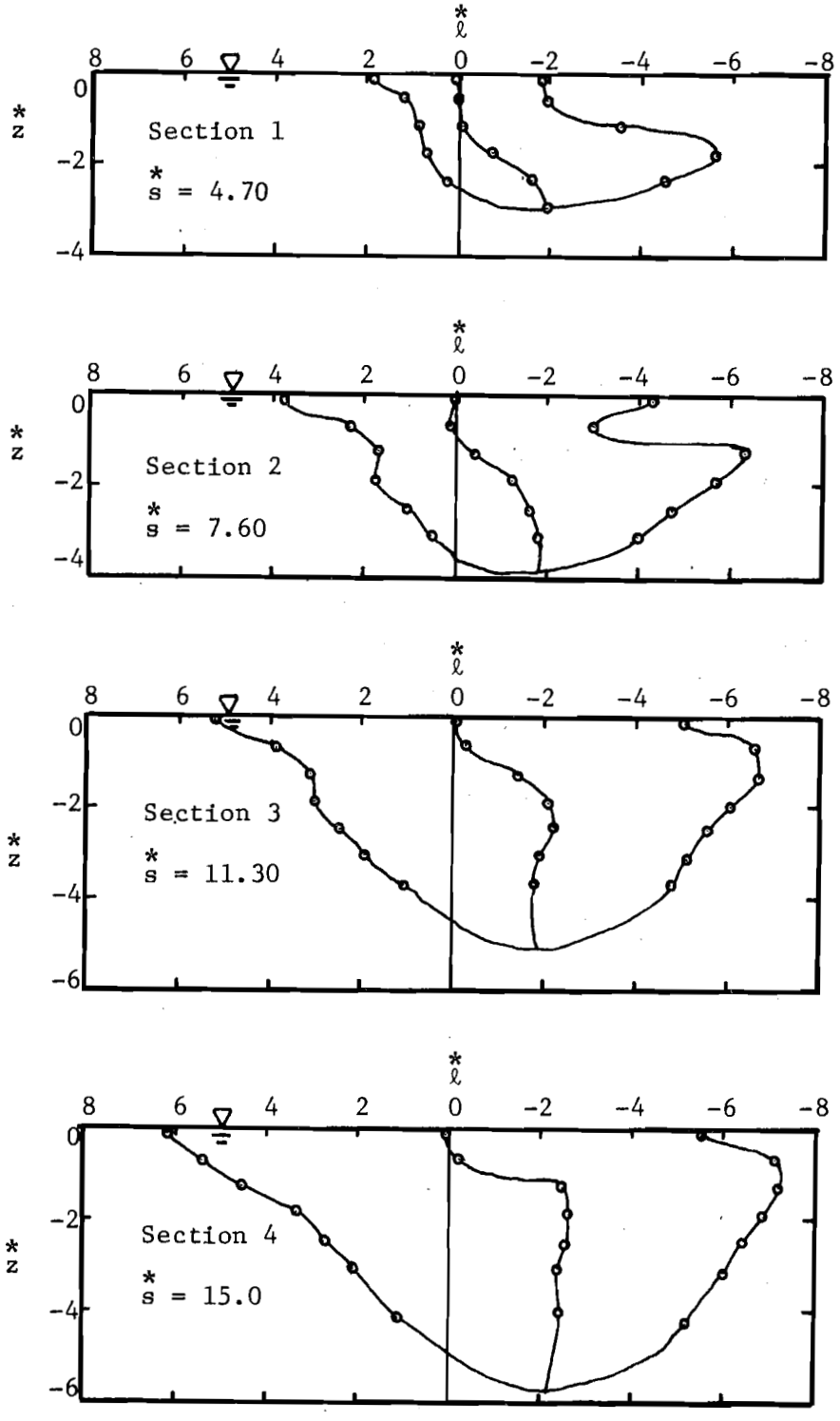

Fig. 5.16 Configuration of jet temperature boundaries for Run 10 (F_o = 15.11, u_o/u_a = 4.33)

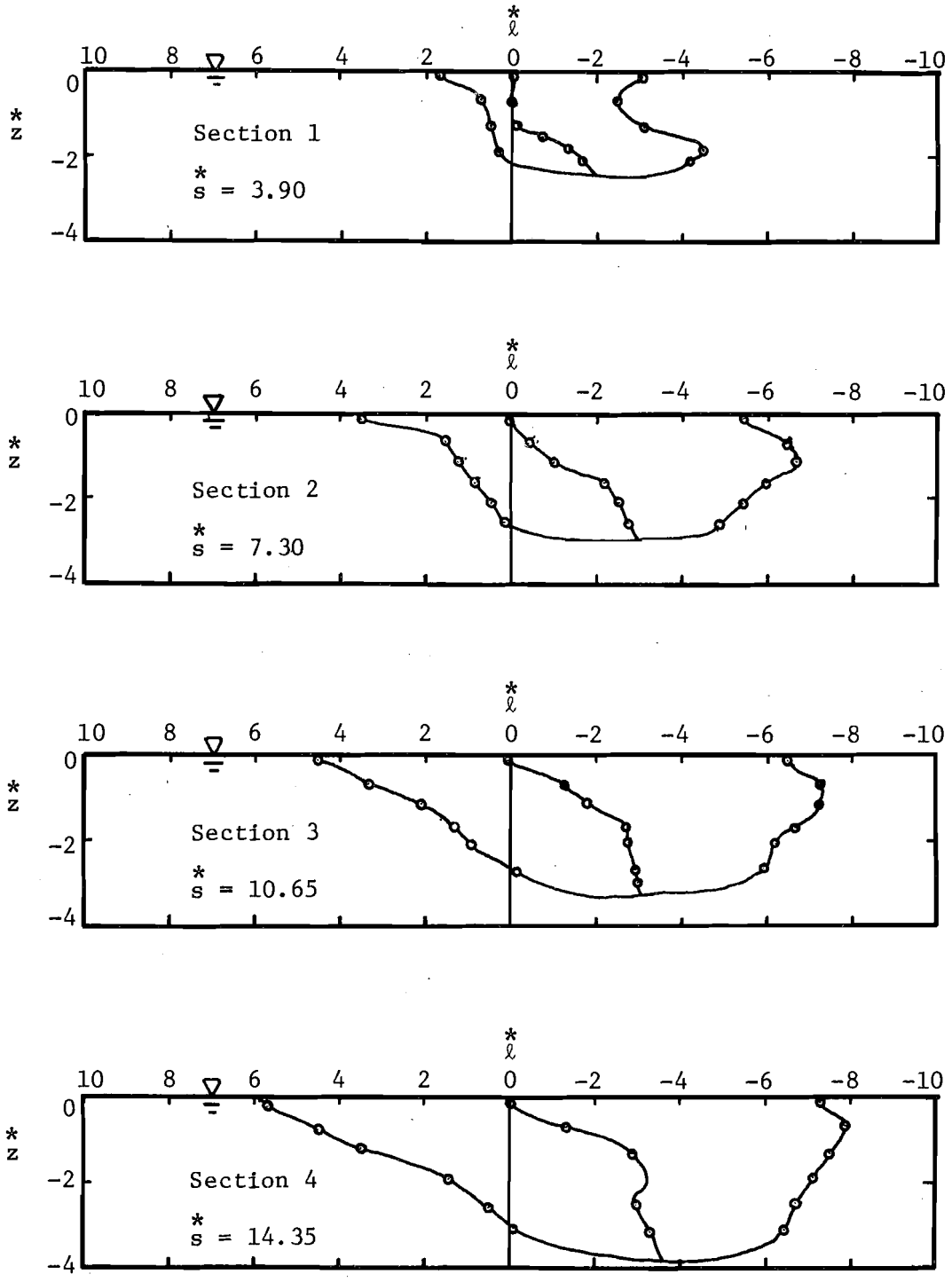

Fig. 5.17 Configuration of jet temperature boundaries for Run 11 ($F_o = 9.93$, $u_o/u_a = 2.89$)

Runs 4 and 9 which have sidewall attachment. At cross section 1 of all runs except Runs 4 and 9, the lower portion of the jet was swept toward the lee side of the jet and the jet became L-shaped. With the formation of the L-shaped profile, some of the jet fluid would be underneath the ambient fluid which has higher density than the jet. This created an unstable situation and would tend to create a density current with part of the jet rising toward the surface. The secondary flow created in this way could enhance the spreading in the lee side of the jet and could help to explain the dependence for C_V on R as discussed in Section 5.3.3.1. Also, such a secondary flow might help to trigger the apparent tendency for the jet to divide longitudinally into two parts as mentioned in Section 5.1.

At cross sections 3 or 4 for all runs the jet became wider at the surface, apparently due to the results of buoyant spreading. The observed spreading of the jet increased with decreasing F_o and with increasing velocity ratio R. At the cross sections closer to the exit, $\overset{*}{B}'$ was much larger than $\overset{*}{B}$. However, at cross sections further downstream from the exit, $\overset{*}{B}$ and $\overset{*}{B}'$ were approximately equal to each other.

Figures 5.8 and 5.9 for u_o/u_a = 13.0 and 8.67 illustrate that the asymmetry of jet configuration due to crossflow can be as significant for large values of u_o/u_a (i.e., for small crossflows) as for strong crossflows (compare Fig. 5.17 for u_o/u_a = 2.89). This demonstrates that the usual assumption of symmetrical temperature distributions for small crossflow cases may be invalid.

5.2.3.2 Measured Jet Trajectories

Figure 5.18(a) illustrates the effects of velocity ratio and initial Froude number F_o on the bending of the jet. The amount of jet

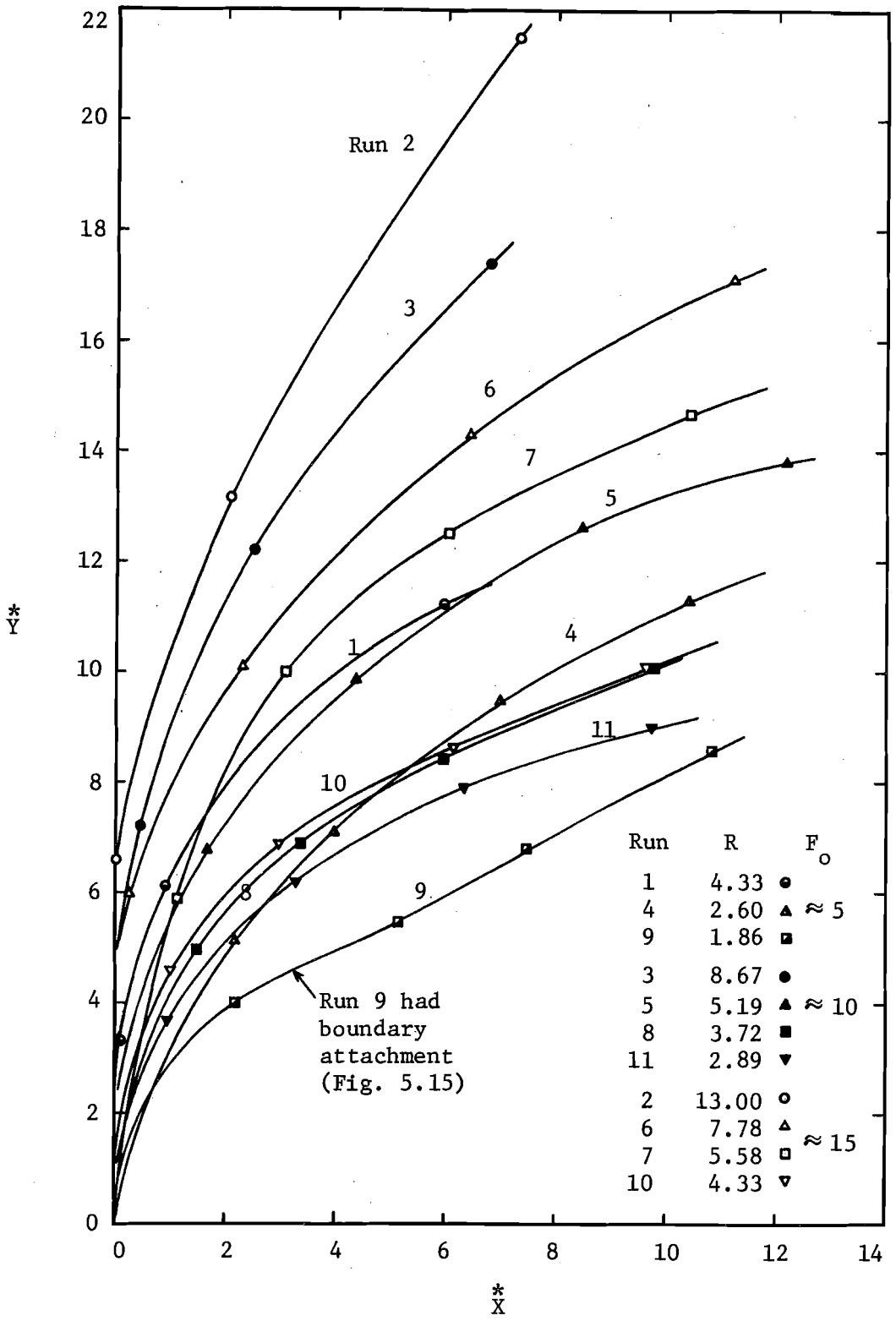

Fig. 5.18(a) Measured jet trajectories

bending in the downstream direction increases as the velocity ratio decreases. Bending is also greater for jets with higher F_o, because they spread more vertically (Section 5.2.3.3), creating a greater area on which pressure drag forces can act [Dunn et al., 1975]. This is shown, for example, by the trajectories of Runs 1 and 10.

Figure 5.18(b) shows the measured trajectories non-dimensionalized with respect to the velocity ratio R and the square root of the initial jet cross sectional area. Runs 4 and 9 were omitted because of boundary attachment. The slopes of the normalized trajectories are essentially the same for all runs. There may be some slight variation of the intercept of lines with F_o. This variation was of the same order of magnitude as expected experimental scatter and was not investigated in detail. The line

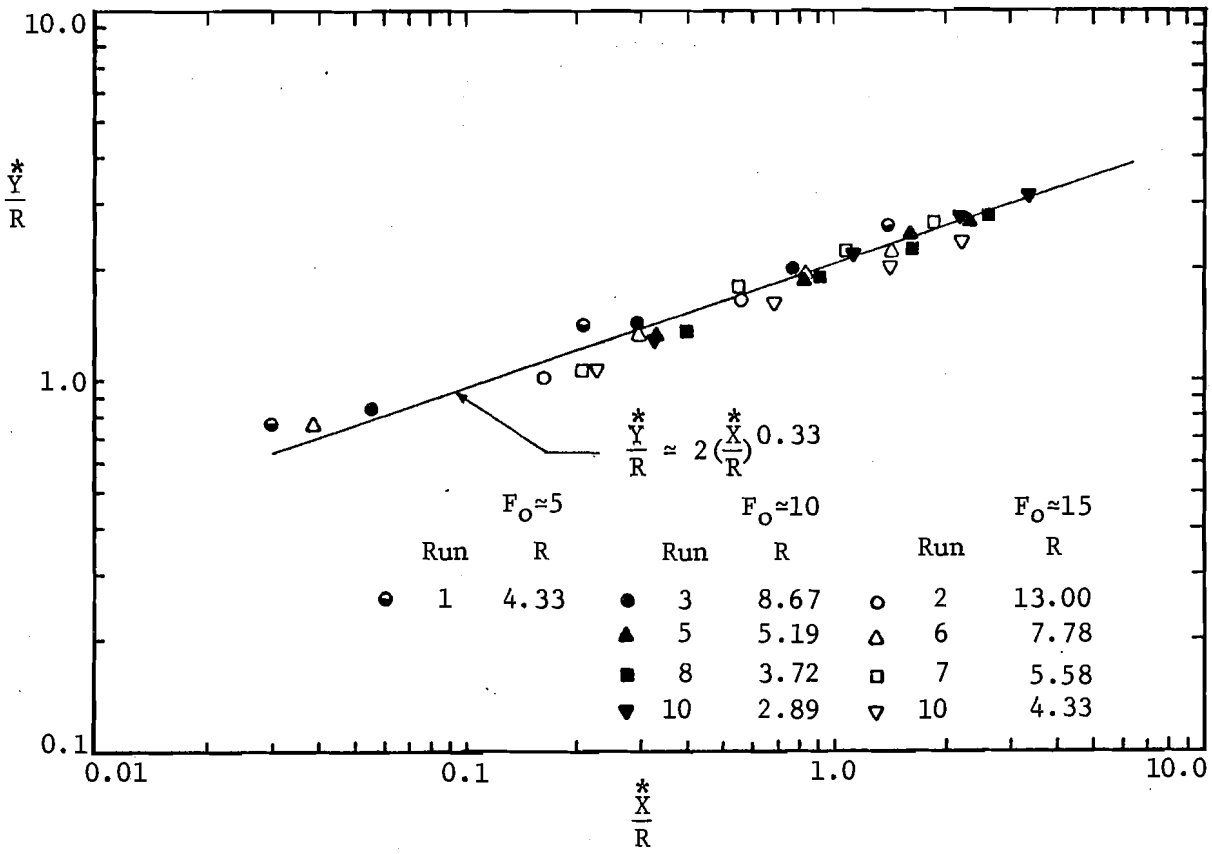

Fig. 5.18(b) Measured jet trajectories

in Fig. 5.18(b) is a visual best fit line. Although it is not obvious that the situation investigated by Chan et al. [1976] is analogous to the present problem, it may be observed that the slope in Fig. 5.18(b) is approximately the same as that for the far field as defined by Chan et al. [1976] for submerged, nonbuoyant jets in crossflows.

5.2.3.3 Measured Jet Depths

The measured depths of the jets along the trajectories are shown in Fig. 5.19. The nondimensional distance along the jet axis, $\overset{*}{s}$, was obtained graphically from the trajectories shown in Fig. 5.18(a). For runs 1, 2, 3 and 5, the temperature distributions at cross section 4 were bimodal and were not included in the calculation of the C's and were not fitted to the numerical model. Thus, in order to obtain the values of $\overset{*}{s}$ at cross section 4 for these runs, the jet trajectory was extrapolated from sections 1, 2, and 3 to section 4.

Figure 5.19 shows the maximum thickness of the jet is apparently a function primarily of F_o for constant θ_o and aspect ratio. Figure 5.19 also shows that the nondimensional maximum jet depth $\overset{*}{h}_{max}$ is given approximately by

$$\overset{*}{h}_{max} \approx \frac{F_o}{2} \tag{5.7}$$

in the range of F_o values of these experiments, assuming that the experiments for F_o = 10 and 15 did reach the maximum depths. Equation 5.7 is based only on jets with aspect ratio equal to unity and $\theta_o = 90^o$.

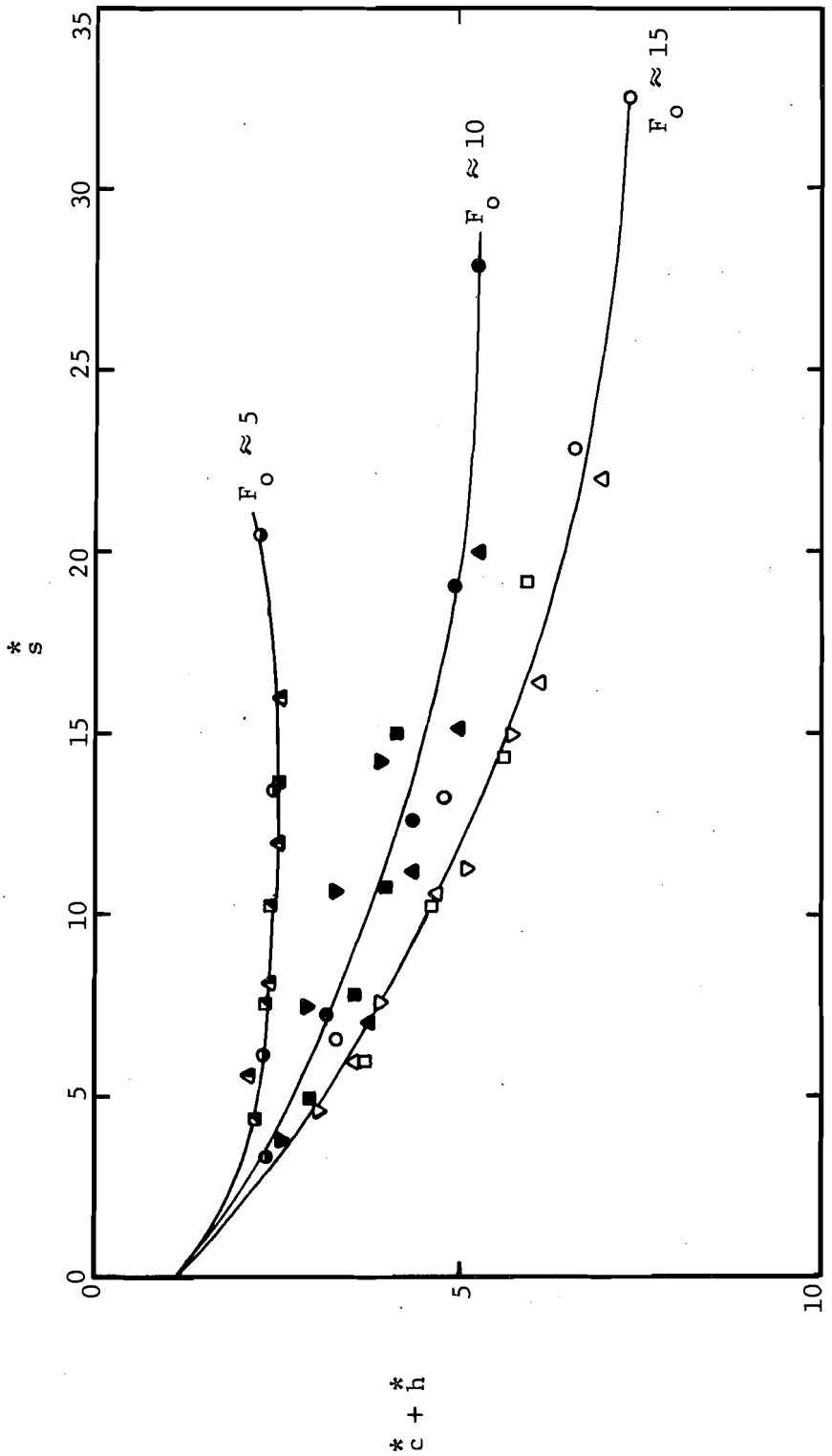

Fig. 5.19 Measured jet depths

5.2.3.4 Measured Maximum Temperature Decay

The measured maximum temperature excess of each cross section was plotted in Fig. 5.20 to show the maximum temperature decay along the jet axis. The average slope of the maximum temperature decay is about 0.9 suggesting that in the range of variables covered in these experiments, the jet behaves very much like a three-dimensional jet.

Figure 5.20 shows that at a given distance downstream from the outfall ($\overset{*}{s}$), Run 10 ($F_o \approx 15$, $u_o/\underline{u_a} = 4.33$) gives a lower value of $\Delta\overset{*}{T}_m$ than Run 1 ($F_o \approx 5$, $u_o/\underline{u_a} = 4.33$). This is an example of the general trend that dilution increases with increasing F_o. Dilution is also generally greater for cases with lower velocity ratio. This can be seen by comparing the data of the runs with the same nominal value of F_o in Fig. 5.20. At the same $\overset{*}{s}$ the run with lower velocity ratio generally gives a lower value of $\Delta\overset{*}{T}_m$ than the run with higher velocity ratio, since entrainment is enhanced by ambient crossflow.

5.3 Calculation of Empirical Coefficients C_V, C_D and C_B

It is common practice to evaluate the empirical coefficients in a jet model by matching computed information from the model to a limited amount of measured information such as measured jet widths, depths, trajectories and temperature decay along the jet axis. The most appropriate type of matching of the model and the data depends to some degree on the purpose for which the model was developed and the use which is to be made of the model. In this study, it was decided to calculate the empirical coefficients C_V, C_D and C_B by matching the computed temperature excesses to

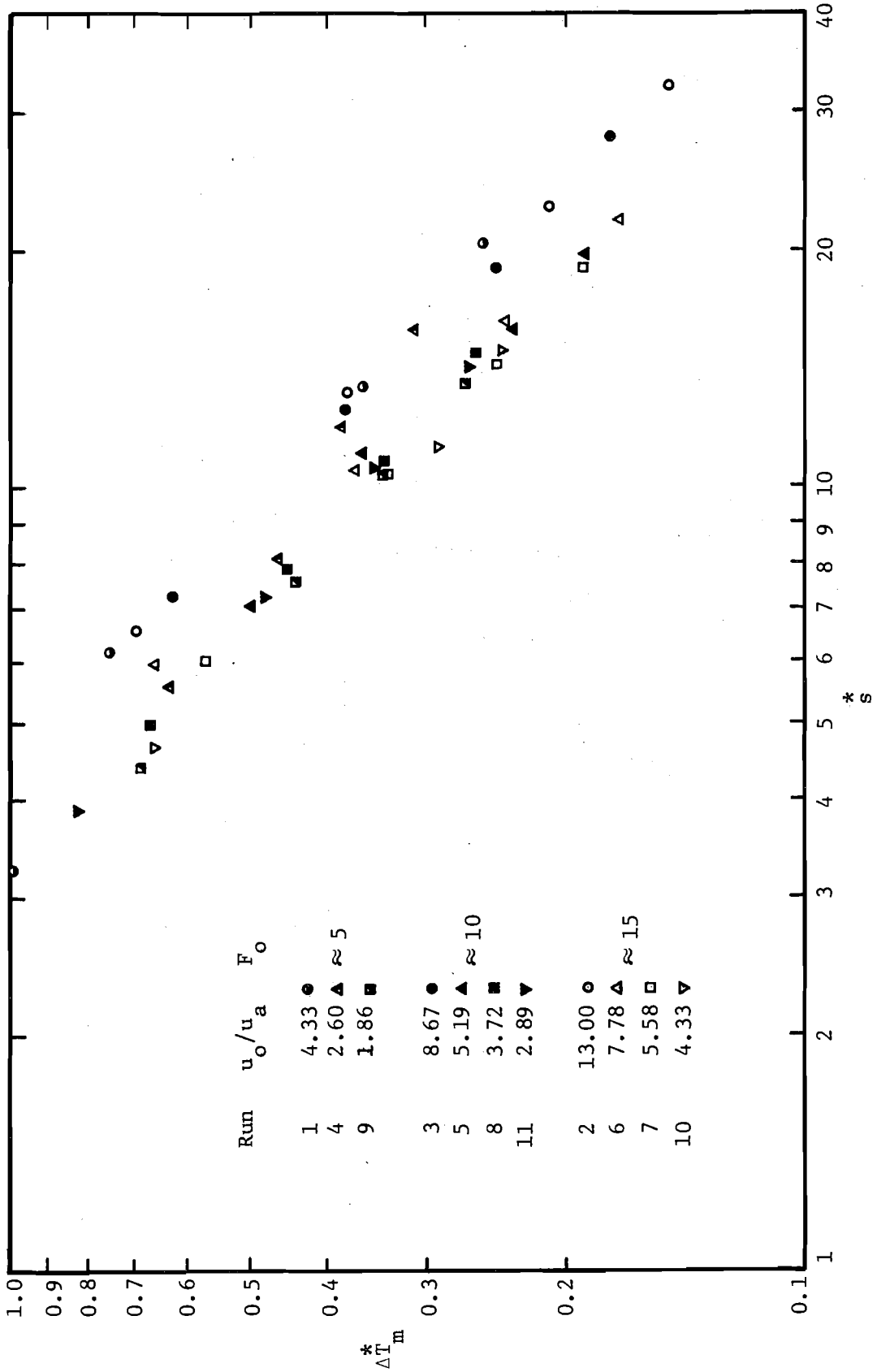

Fig. 5.20 Measured maximum temperature decay

all of the measured temperature excesses (with the exception of a relatively small number of measurements excluded for reasons given in Section 5.3.2).

5.3.1 Optimal Objective Function

The influence coefficient algorithm was again used in the calculation of coefficients C_V, C_D and C_B. The objective function which was minimized in the calculation was the sum of the squares of the differences between the computed temperature excesses from the numerical model and the measured temperature excesses from the experiments. Equation 5.5 may be used to represent the objective function of the calculation, provided ΔT is defined as the temperature excess computed from the model for each measurement point and N is the number of temperature measurements used in the calculation.

5.3.2 Calculation Procedure

In order to reduce the difficulty of matching the distorted temperature distributions with the similarity profiles assumed in the model, the temperature profile at each level below the water surface was shifted horizontally in the measurement plane such that the point of maximum temperature excess at each level below the water surface fell directly below the maximum temperature at the free surface. Temperature measurements for which any one of the following conditions applied were not included in the calculation:

1. The measured temperature excesses were apparently affected by the temperature built-up in the wake or in the stagnation zone near the discharge point.

2. The temperature distributions were bimodal. In this case, the temperature measurements at the entire cross section were excluded from calculation.
3. The calculated u_m was less than the calculated u_s, where u_s is the component of the ambient velocity parallel to the jet axis.

Both the individual temperature measurements and the entire measurement cross sections which were not used in the calculation were identified in Appendix II.

The calculation procedure was similar to that for the identification of $\overset{*}{B}$, $\overset{*}{B}'$ and $\overset{*}{d}_m$ as given in Section 5.2.1. However, there was significantly more computational effort involved in evaluating C_V, C_D and C_B, because it was necessary to solve the jet model (Eqs. 3.112-3.122) instead of Eq. 5.4 in order to obtain ΔT. The computation was further complicated by the fact that the jet model gave only the characteristics of the jet at each computational step, and the computed jet cross sections did not necessarily pass through the measurement points. Therefore, the calculated temperature corresponding to each measurement point was obtained by linear interpolation between the two closest calculation cross sections. To insure the validity of linear interpolation, the maximum nondimensional step size in the model computation was limited to 2.0 and the maximum nondimensional temperature drop was restricted to 0.05.

Experience showed that the initial estimates of the parameters are important in convergence of the calculations. Initial values for all parameters which were low but still within the feasible range of values generally had a better chance of convergence than high initial values. High estimates for each parameter tends to force the calculations toward

still higher values of the parameters. This situation was observed by Becker and Yeh [1972].

Occasionally, convergence to a minimum $F(\Delta T)$ was reached but the value of the objective function appeared to be too large to represent a true optimum. It was possible that this occurred because a local minimum of $F(\Delta T)$ had been reached. Therefore, in evaluating C_V, C_D and C_B, it was necessary to try different sets of initial estimates of the parameters for each run to determine if the various calculations converged to same values of C_V, C_D and C_B. The values of the parameters were taken to be the set of parameters which gave the smallest value of $F(\Delta T)$. This type of calculation is a standard and accepted method of evaluating coefficients but it does not necessarily lead to the true optimum values of C_V, C_D and C_B.

5.3.3 Results of Calculation

The values of C_V, C_D and C_B obtained for the various runs are shown in Table 5.1. Run 9 was not used in the calculation because it was found that the jet attached to the sidewall at every measurement cross section. Figure 5.21 shows the plots of the calculated values of C_V, C_D and C_B versus the inverse of the velocity ratio 1/R. The discussion of Fig. 5.21 is presented in the following sections.

5.3.3.1 Coefficient of Spreading Due to Velocity Difference, C_V

C_V, the coefficient of spreading due to velocity difference, appears to be function of the velocity ratio R only, as its definition would imply. C_V increases as 1/R increases. Extrapolation of the data trend to $1/R = 0$ gives $C_V = 0.20$. This value is lower than the spreading coefficient for two-dimensional nonbuoyant jets with no crossflow, which is

Table 5.1. Empirical Results from Fitting of Numerical Model to the Data

Run	1	2	3	4	5	6	7	8	9	10	11
F_o	4.79	14.97	9.86	4.99	9.91	15.11	15.27	9.95	5.03	15.11	9.93
$R = u_o/u_a$	4.33	13.00	8.67	2.60	5.19	7.78	5.58	3.72	1.86	4.33	2.89
$1/R = u_a/u_o$	0.23	0.08	0.12	0.39	0.19	0.13	0.18	0.27	0.54	0.23	0.35
C_V	0.69	0.46	0.54	0.71	0.68	0.59	0.63	0.73	-	0.65	0.78
C_D	0.45	1.08	0.56	0.56	0.70	1.05	2.16	0.82	-	1.50	1.00
C_B	0.33	0.06	0.06	1.19	0.35	0.43	0.51	0.70	-	0.85	1.20
σ_T	0.9	0.53	0.51	0.62	0.54	0.50	0.62	0.60	-	0.67	0.83

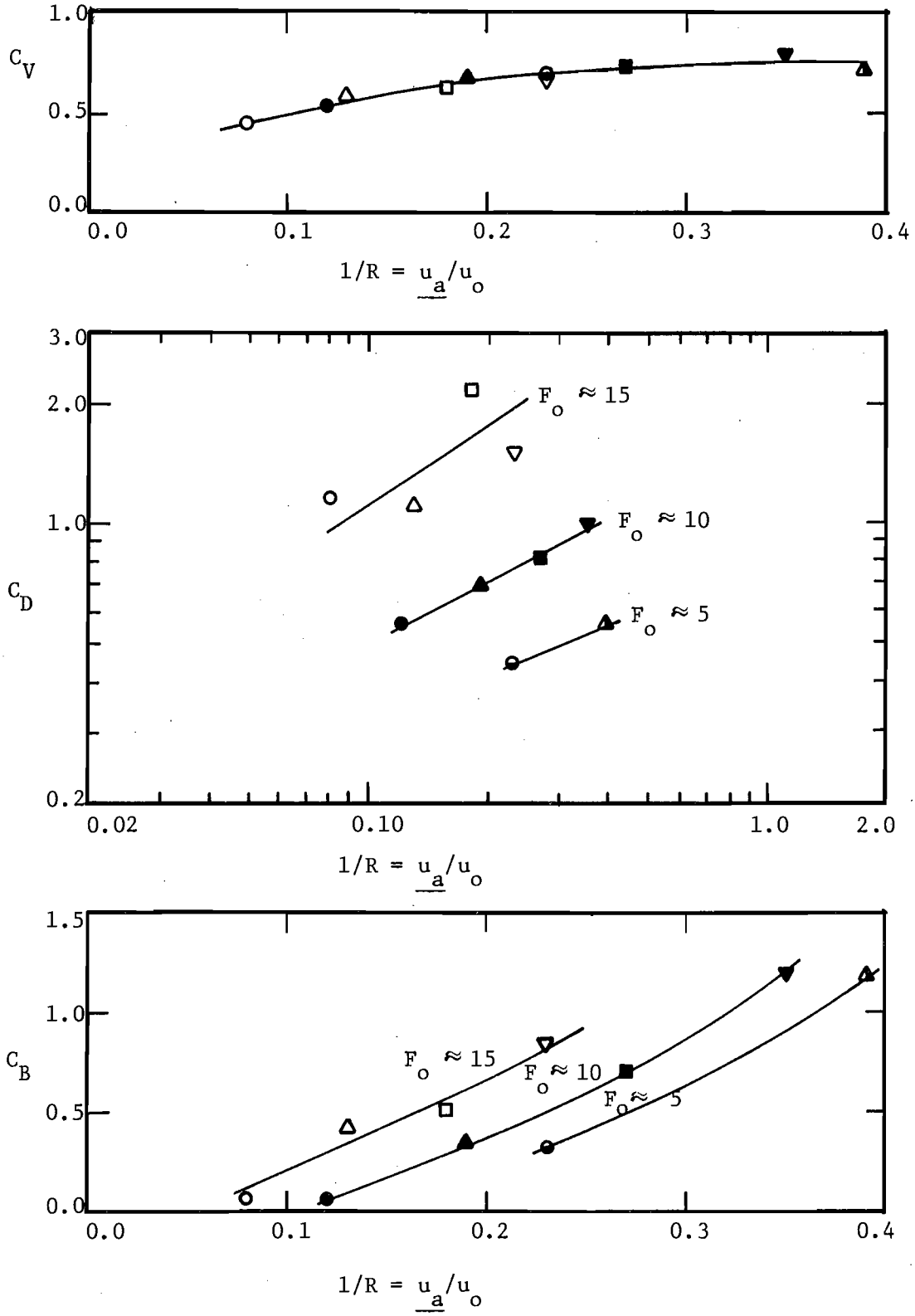

Fig. 5.21 Variation of C_V, C_D and C_B with F_o and R

about 0.236 [Newman, 1967], but is slightly higher than 0.193, the spreading coefficient for nonbuoyant round jets without crossflow [Newman, 1967]. At least part of the dependence of C_V on 1/R may be explained by the development of the L-shaped cross section as discussed in Section 5.2.3.1.

5.3.3.2 Drag Coefficient C_D

Figure 5.21 shows that the values of C_D increase as 1/R increases and as the Froude number F_o increases. The trend is the same as that for submerged jets [Ger and Holley, 1974]. It appears that the only available calibrated C_D values for buoyant surface jets in the literature are those obtained by Motz and Benedict [1970]. A direct comparison of C_D values from the present work with those of Motz and Benedict is not possible since different objective functions and different definitions of the drag coefficient were used.

The numerical model computations showed that for Runs 2, 6, 7 and 10 with $F_o \approx 15$, the lengths of the NFR were much longer than the region which the experiments had covered. In other words, for these runs all four measurement cross sections were relatively crowded into the initial portion of the NFR. Thus the true C_D values were difficult to obtain from these experimental results. This could be the reason that a relatively large scatter of C_D values was obtained for runs with $F_o \approx 15$.

5.3.3.3 Buoyant Spreading Coefficient C_B

The buoyant spreading coefficient C_B varied from 0.06 to 1.20 for the cases studied. The value of C_B increased as the initial densimetric Froude number (F_o) increased and as the inverse of velocity ratio (1/R) increased.

There are essentially no other C_B values for buoyant surface jets with crossflow for comparison with the C_B values obtained in this study. However, there are values for C_4 (Eq. 2.9). The following discussion shows the mathematical relationship between C_B and C_4. The effect of interfacial shear stress on the buoyant spreading was found to be negligible for the range of investigation covered in this study. Thus Eq. 3.89 may be simplified to

$$\frac{db}{ds}\Big|_B = \frac{C_B}{F_r} = C_B \frac{\sqrt{\frac{\Delta\rho}{\rho_a} gh}}{u_m} \tag{5.9}$$

Eq. 3.74 shows that $v_B = u_m \frac{db}{ds}\Big|_B$ at the edge of the jet. Therefore, from Eq. 5.9 one obtains

$$v_B = C_B \sqrt{\frac{\Delta\rho}{\rho_a} gh} \tag{5.10}$$

By comparing Eq. 5.10 with Eq. 2.9 one sees that v_B and C_B are in fact equal to v_f and C_4 respectively. Based on some previous experiments with density currents, Weil and Fischer [1974] suggested that the value of $C_4 \approx 1$ be used for the range of $\Delta\rho$ usually encountered in the powerplant heated discharges. Further discussion on the differences in values of C_B and C_4 is given in Section 5.4.2.2.

Figure 5.21 shows that as 1/R approached zero, the values of C_B for all levels of F_o became zero. This is apparently a questionable conclusion since buoyant spreading does occur in a buoyant surface jet with no crossflow. For the convenience of presentation, further discussion of this matter is also presented in Section 5.4.2.2.

5.4 Comparison of the Theoretical and Experimental Results

5.4.1 Temperature Distributions

The standard deviation (σ_T) between the measured temperatures and the calculations for the optimum coefficients for each run may be evaluated from the following equation

$$\sigma_T = \sqrt{\frac{F(\Delta T)_{min}}{N}} \tag{5.10}$$

where $F(\Delta T)$ = objective function defined by Eq. 5.5,

N = number of temperature measurements used for the calculation.

The average σ_T for all runs was found to be about $0.63^{o}C$. The value for each run is shown in Table 5.1. However, it should be recalled that this accuracy was obtained by shifting of the measured temperature distributions below the water surface toward the jet axis (Section 5.3.2).

5.4.2 Jet Characteristics

The comparison of the numerical and experimental results on jet trajectories, widths, depths and maximum temperature are shown in Figs. 5.22-5.31. In these figures the experimental jet boundaries are shown as the measured surface widths determined from the similarity functions as described in Section 5.2.1. It should be recalled that the objective of the calculations to obtain the coefficients C_V, C_D and C_B was to match the numerical model to the entire set of measured temperature distributions, not just to the jet characteristics (widths, depths, etc.) which are compared in this section. The model assumed a rectangular cross section since the model was developed before the experimental results were

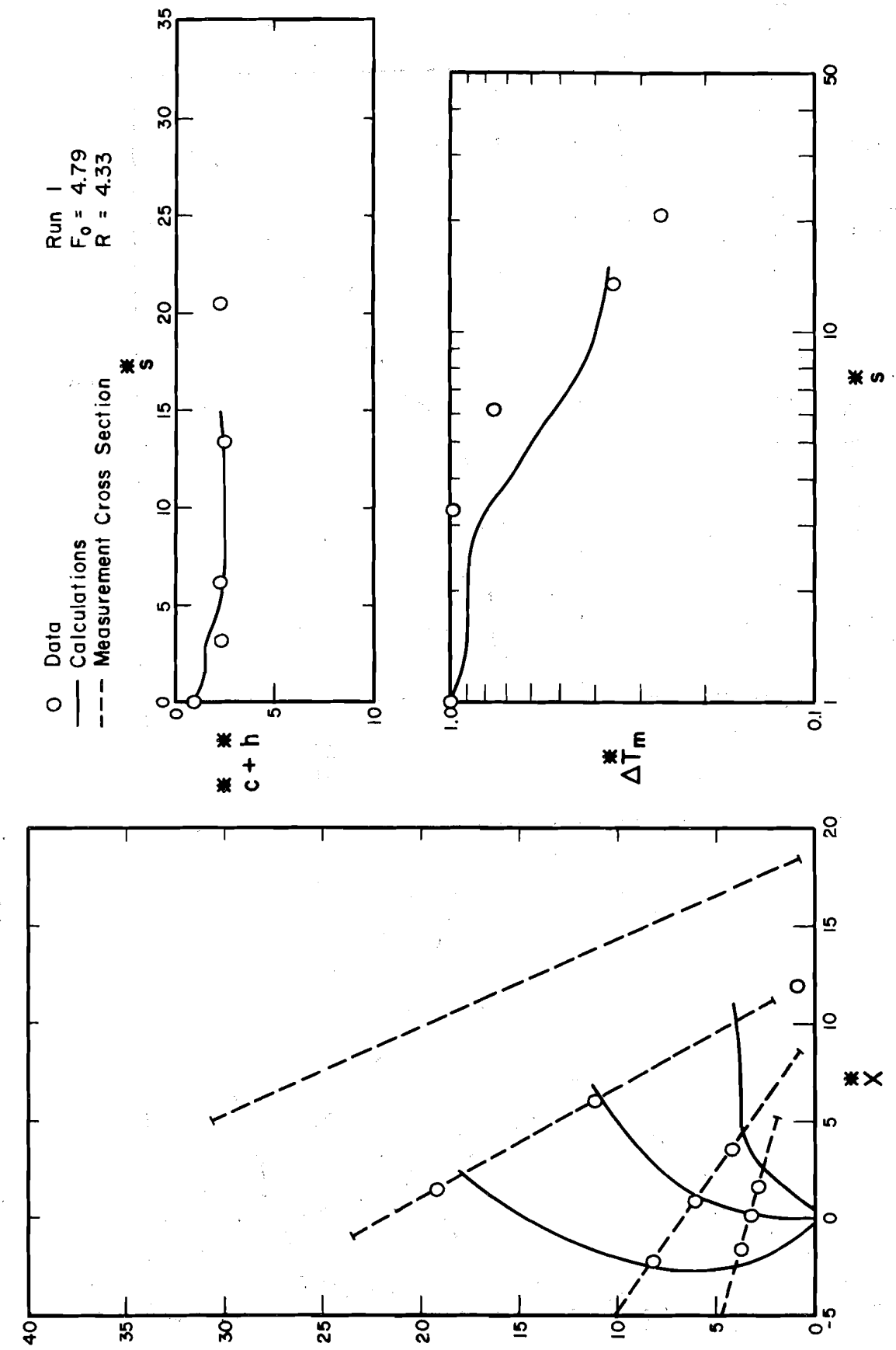

Fig. 5.22 Comparison of measured and calculated jet widths, trajectories, depths, and maximum temperatures for Run 1

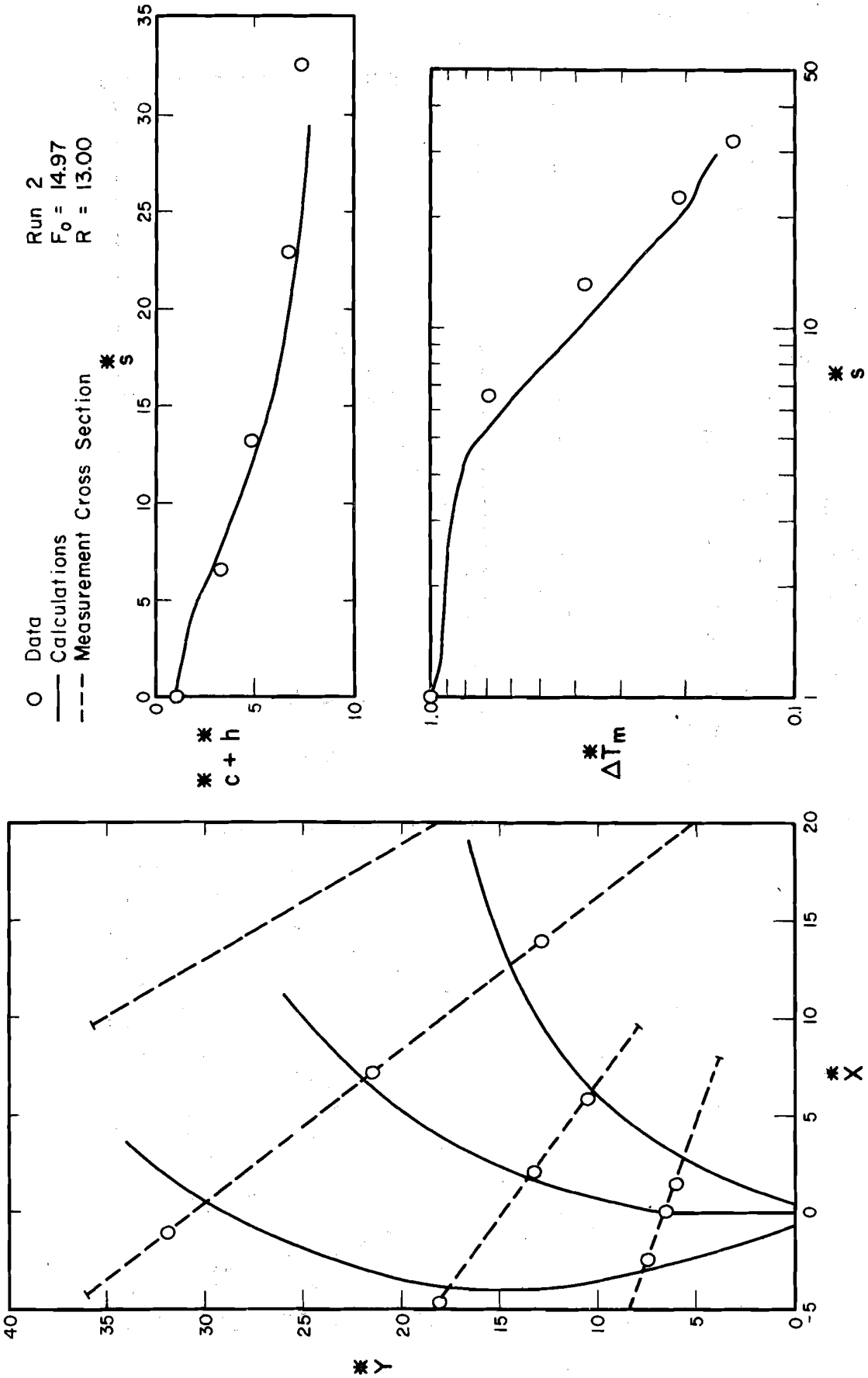

Fig. 5.23 Comparison of measured and calculated jet widths, trajectories, depths, and maximum temperatures for Run 2

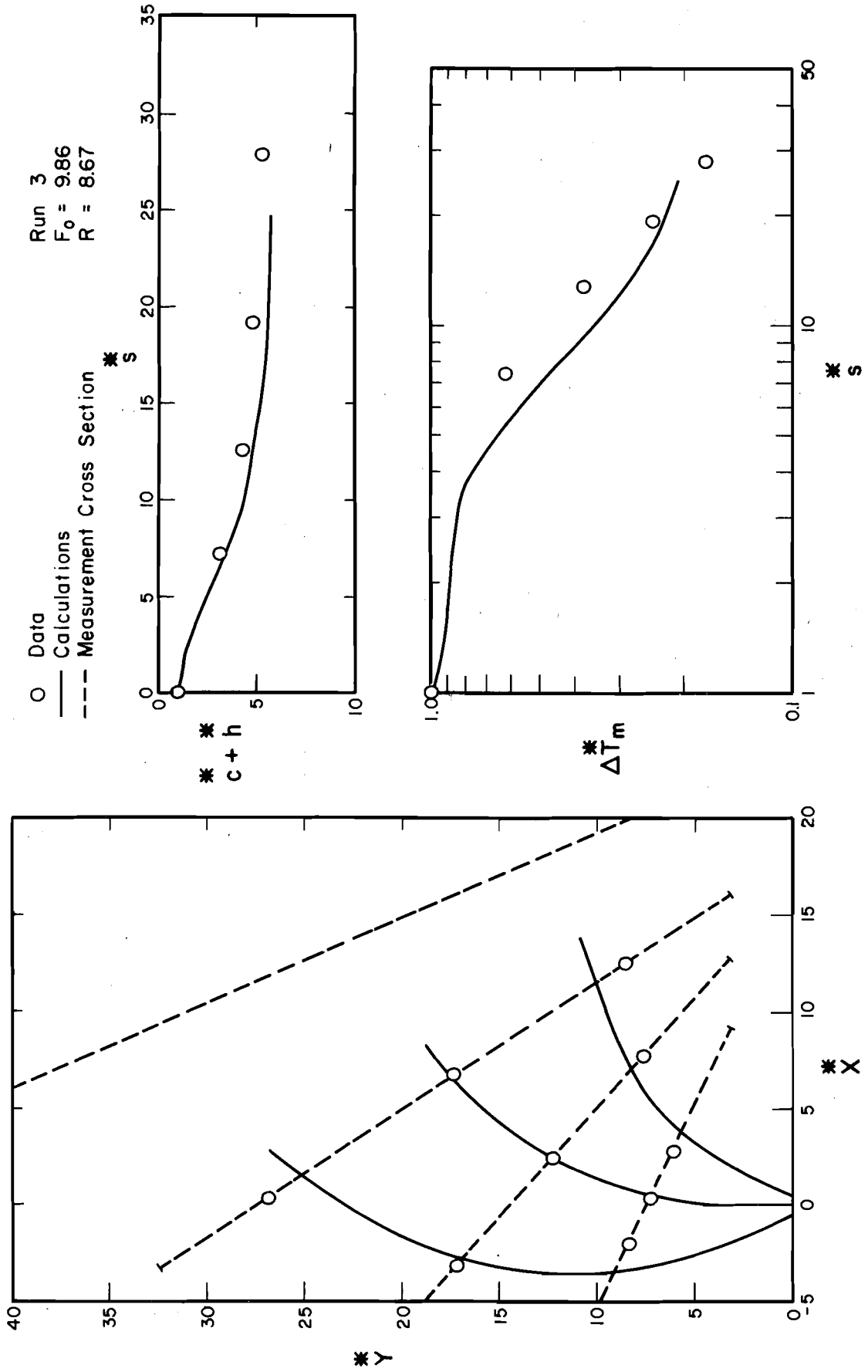

Fig. 5.24 Comparison of measured and calculated jet widths, trajectories, depths, and maximum temperatures for Run 3

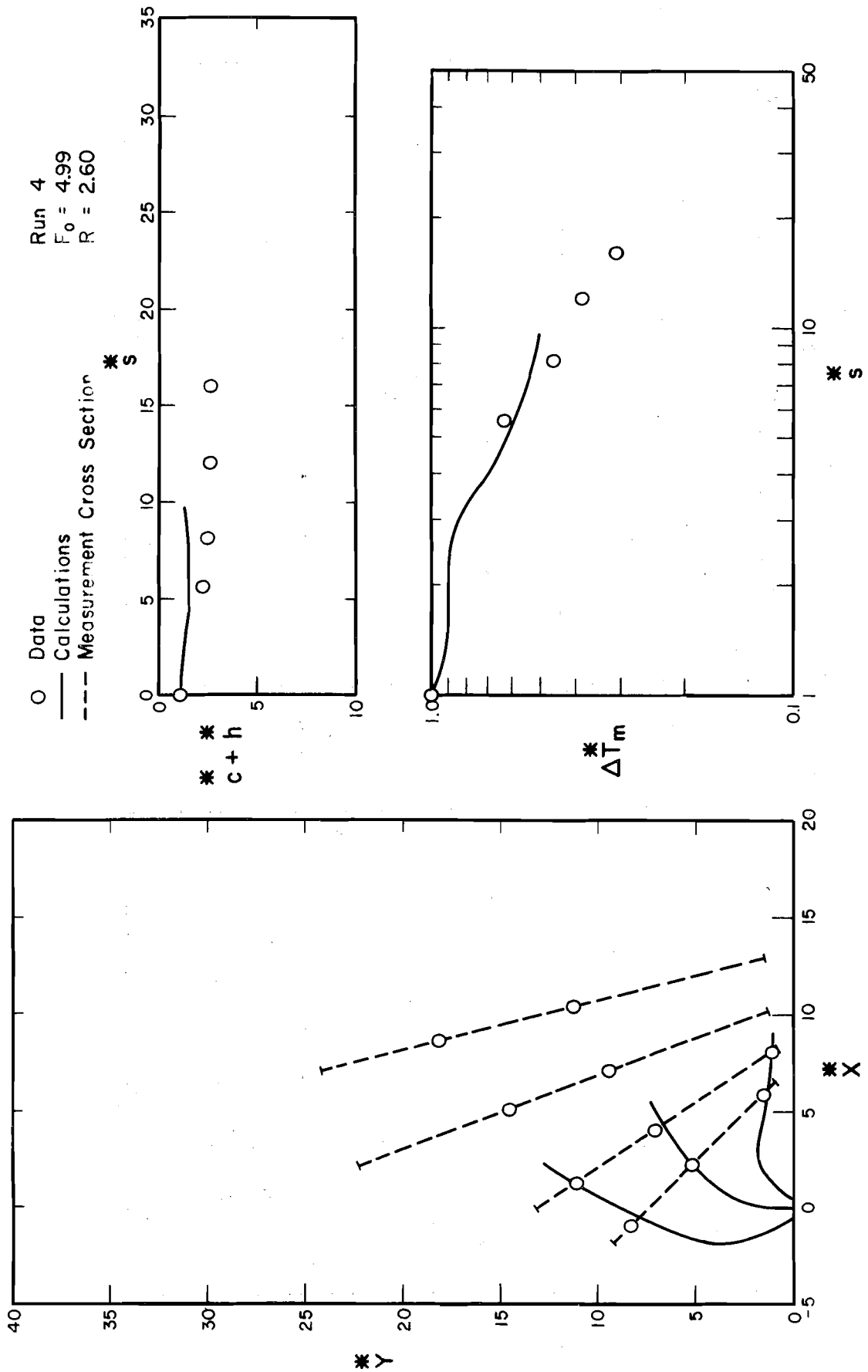

Fig. 5.25 Comparison of measured and calculated jet widths, trajectories, depths, and maximum temperatures for Run 4

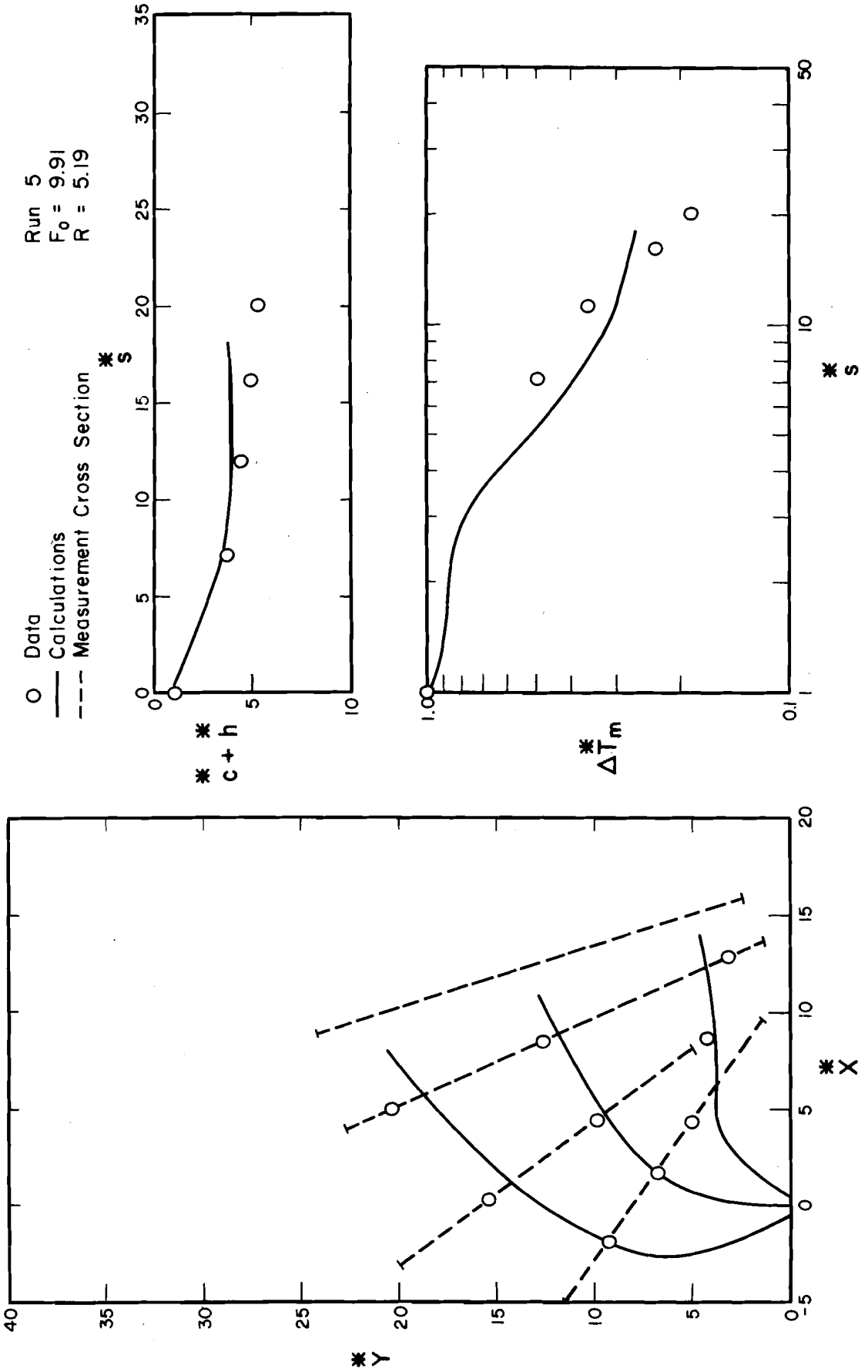

Fig. 5.26 Comparison of measured and calculated jet widths, trajectories, depths, and maximum temperatures for Run 5

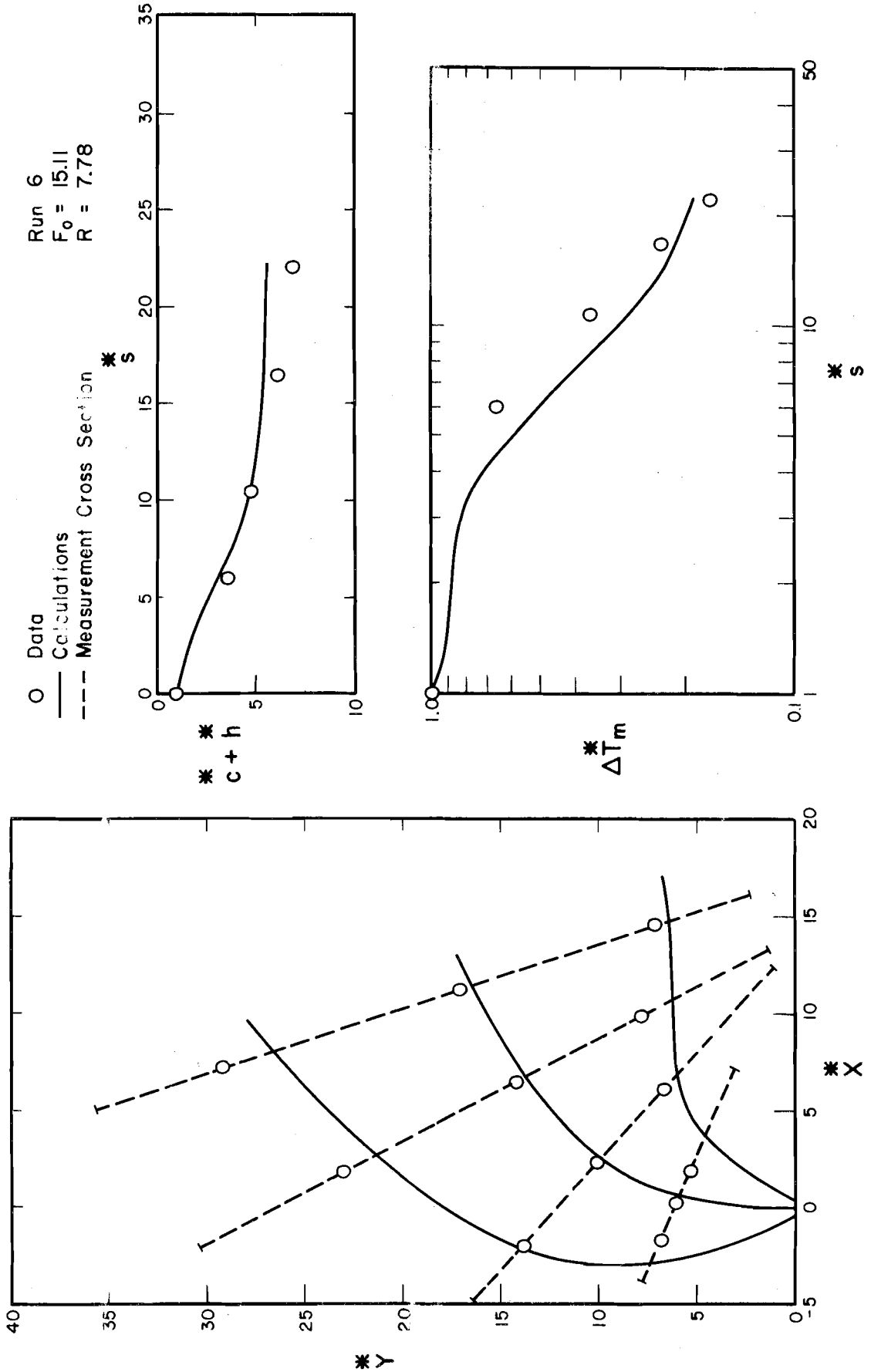

Fig. 5.27 Comparison of measured and calculated jet widths, trajectories, depths, and maximum temperatures for Run 6

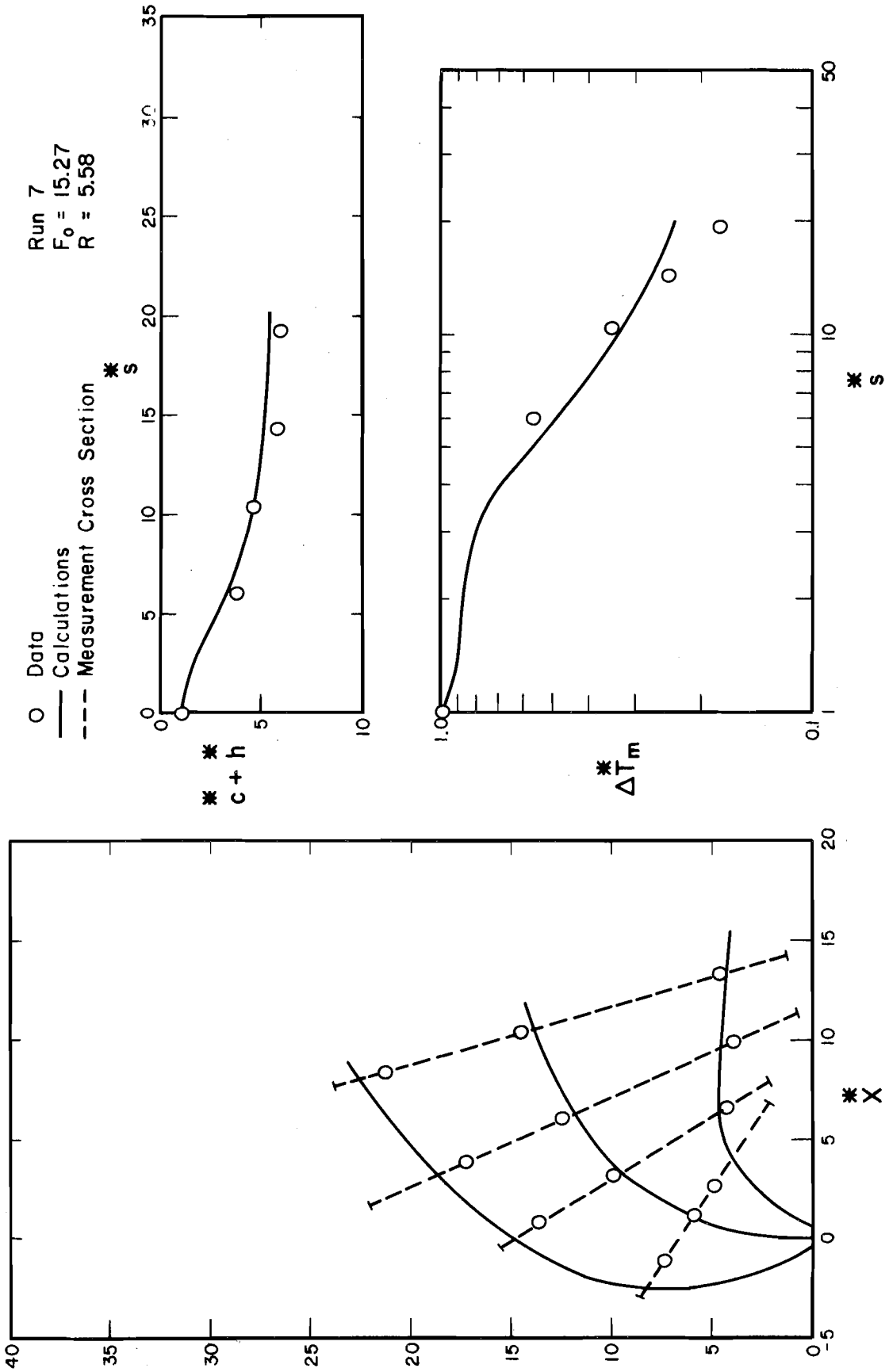

Fig. 5.28 Comparison of measured and calculated jet widths, trajectories, depths, and maximum temperatures for Run 7

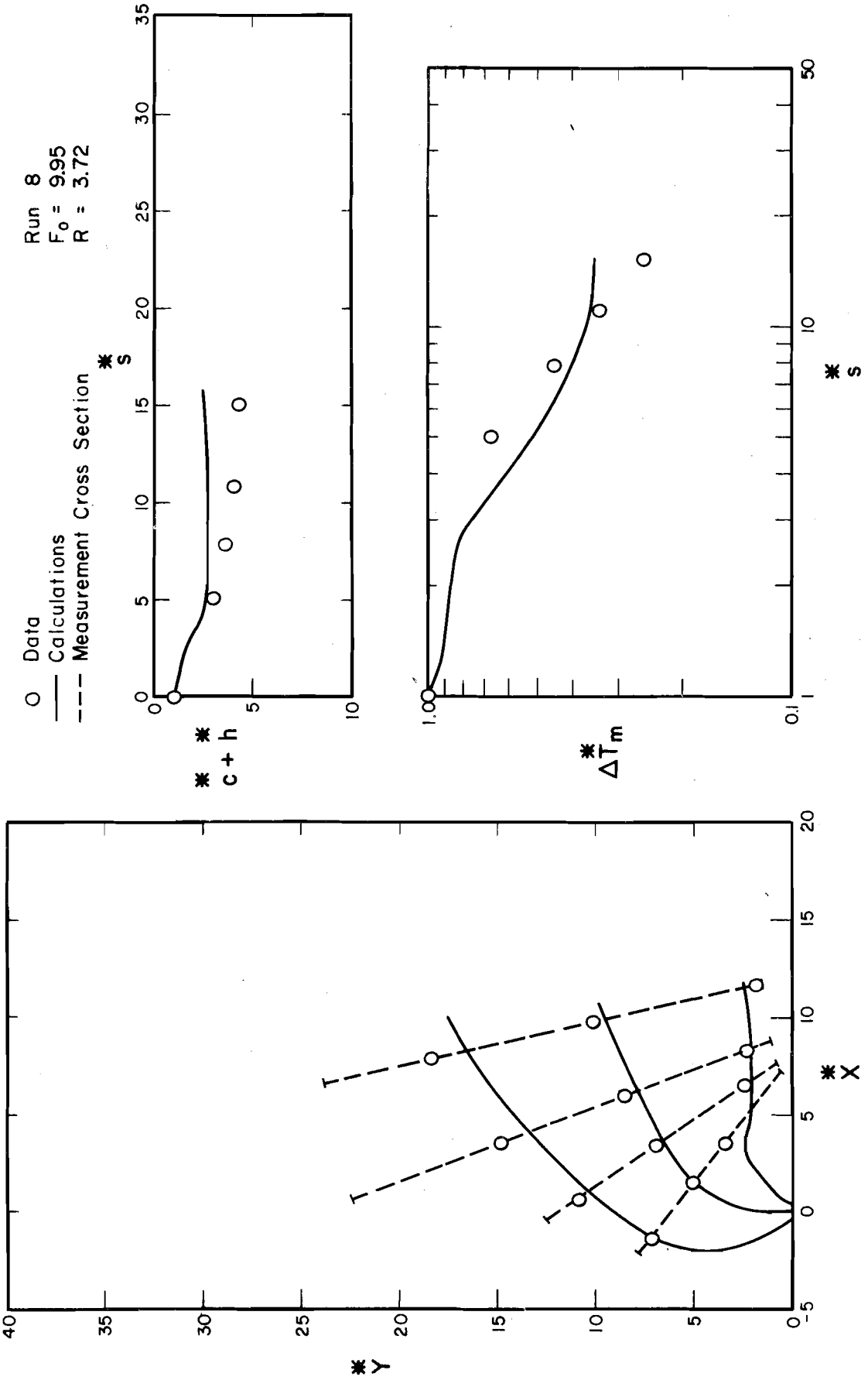

Fig. 5.29 Comparison of measured and calculated jet widths, trajectories, depths, and maximum temperatures for Run 8

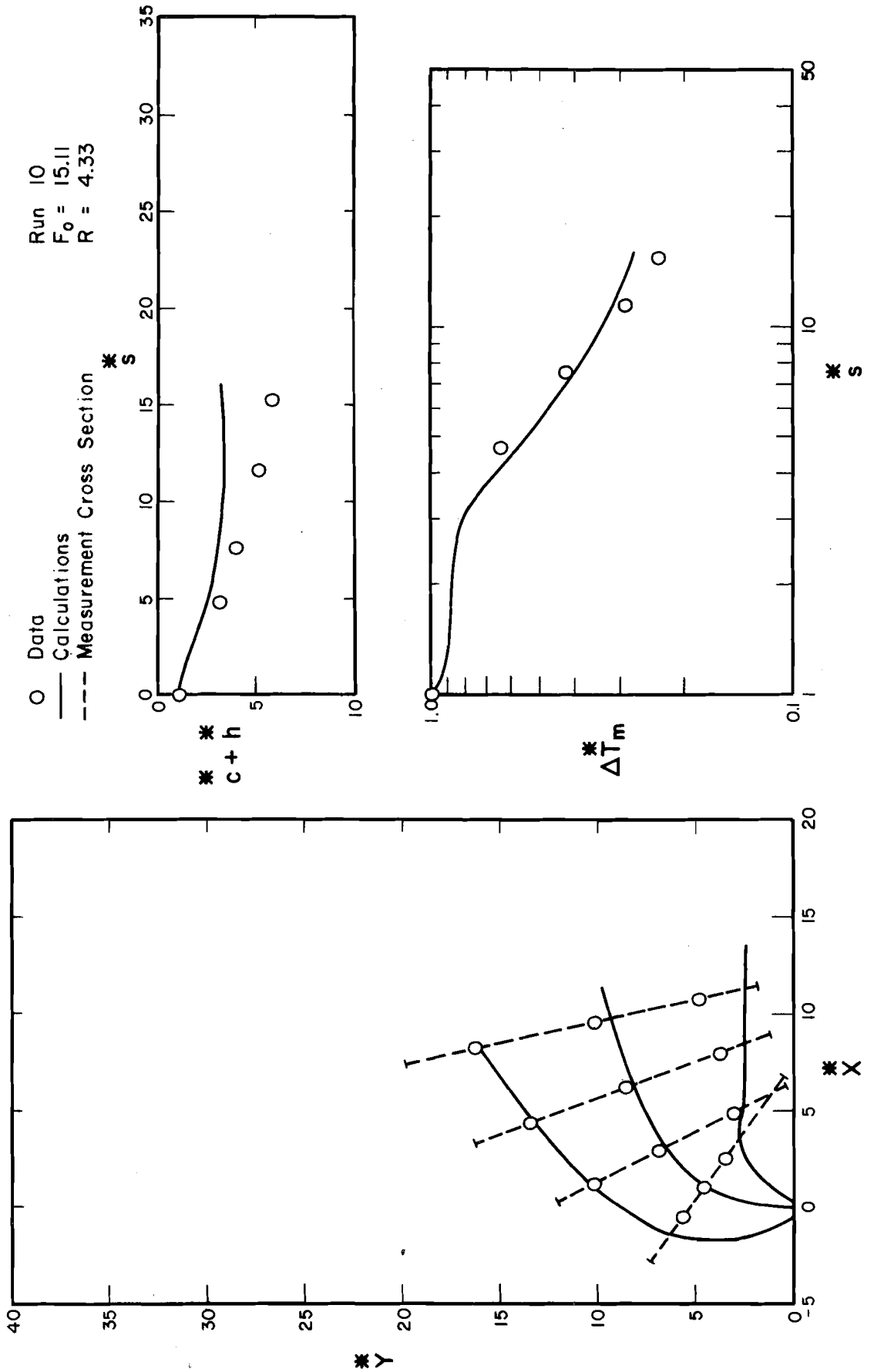

Fig. 5.30 Comparison of measured and calculated jet widths, trajectories, depths, and maximum temperatures for Run 10

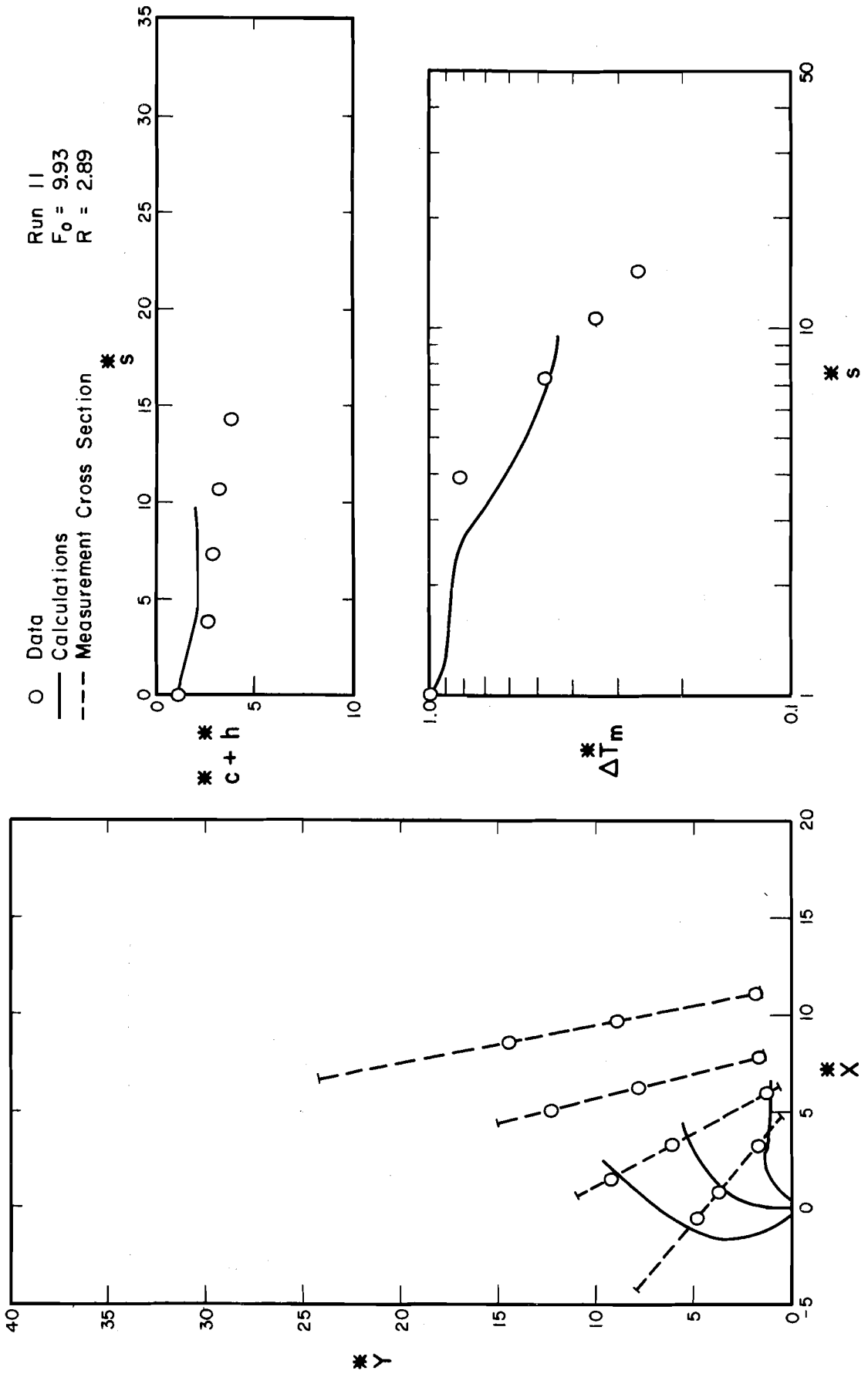

Fig. 5.31 Comparison of measured and calculated jet widths, trajectories, depths, and maximum temperatures for Run 11

available. The C's were obtained as those values which gave the best fit of the calculated temperatures to the entire set of measured temperatures for each run. No doubt, different values of the C's would have been obtained and a better representation of the measured widths, depths, etc. would have been obtained if the assumed cross-sectional shape and similarity functions had been more representative of the actual situation or if the model had been fitted to just the jet width, depth, and maximum temperature.

5.4.2.1 Jet Trajectories

The overall agreement between the predicted and the measured jet trajectories are considered to be good except for Runs 4 and 11. The velocity ratios ($R = u_o/u_a$) for Runs 4 and 11 were small. Model computations for these two cases showed that the jets bent rapidly in the downstream direction due to strong crossflow. The condition that $u_m \leq u_s$ was reached upstream of the cross-section 3 in the calculations. Thus for Runs 4 and 11 only the first two cross sections were used in the calculation of the coefficients. The large deviation between the computed and the measured jet trajectories for Runs 4 and 11 is apparently due to the insufficient data used to obtain the C's.

5.4.2.2 Jet Widths

It is difficult to give a comparison between the computed and the observed jet widths because the observed jet widths vary significantly in the vertical direction at each cross section (Figs. 5.7-5.17). The overall agreements between the computed and measured jet widths are

considered to be satisfactory, if the observed surface widths are taken to be the representative measured widths.

Further comparison of the jet widths can be made by examining Fig. 5.32 which shows several examples of the computed jet boundaries at the measurement cross-sections and the modified experimental jet temperature boundaries (obtained by shifting the measured temperature profiles horizontally below the surface to give vertical alignment of the maximum temperatures, as discussed in Section 5.3.2). In the figure, ℓ_ℓ^* is the nondimensional lateral distance from the point of maximum temperature of each level, with positive being toward the upstream side of the jet. Fig. 5.32 (a) and (b) show typical comparisons between the computed jet boundaries and the modified experimental jet boundaries at cross-sections near the exit. The inner width (right side) of the jet is predicted fairly well, from the standpoint of the calculation objective of this study. However, the model predicts outer widths which are too large. At cross sections near the exit, buoyant spreading is negligible for moderate and large initial Froude numbers. The jet lateral spreading is represented in the model by Eqs. 3.83 and 3.84. Eq. 3.83 (or 3.84) was originally used by Abramovich [1963] for jet spreading with coflowing ambient fluid, but has not been tested in the cases with the presence of a crossflow. The component of ambient velocity normal to the jet axis and the (partial) stagnation of the ambient flow against the upstream side of the jet are not taken into account in Eqs. 3.83 and 3.84 and may significantly affect the lateral spreading, especially near the outlet where θ is near 90°. The fact that the model gives a better prediction of the inner widths near the exit is to be expected because the component

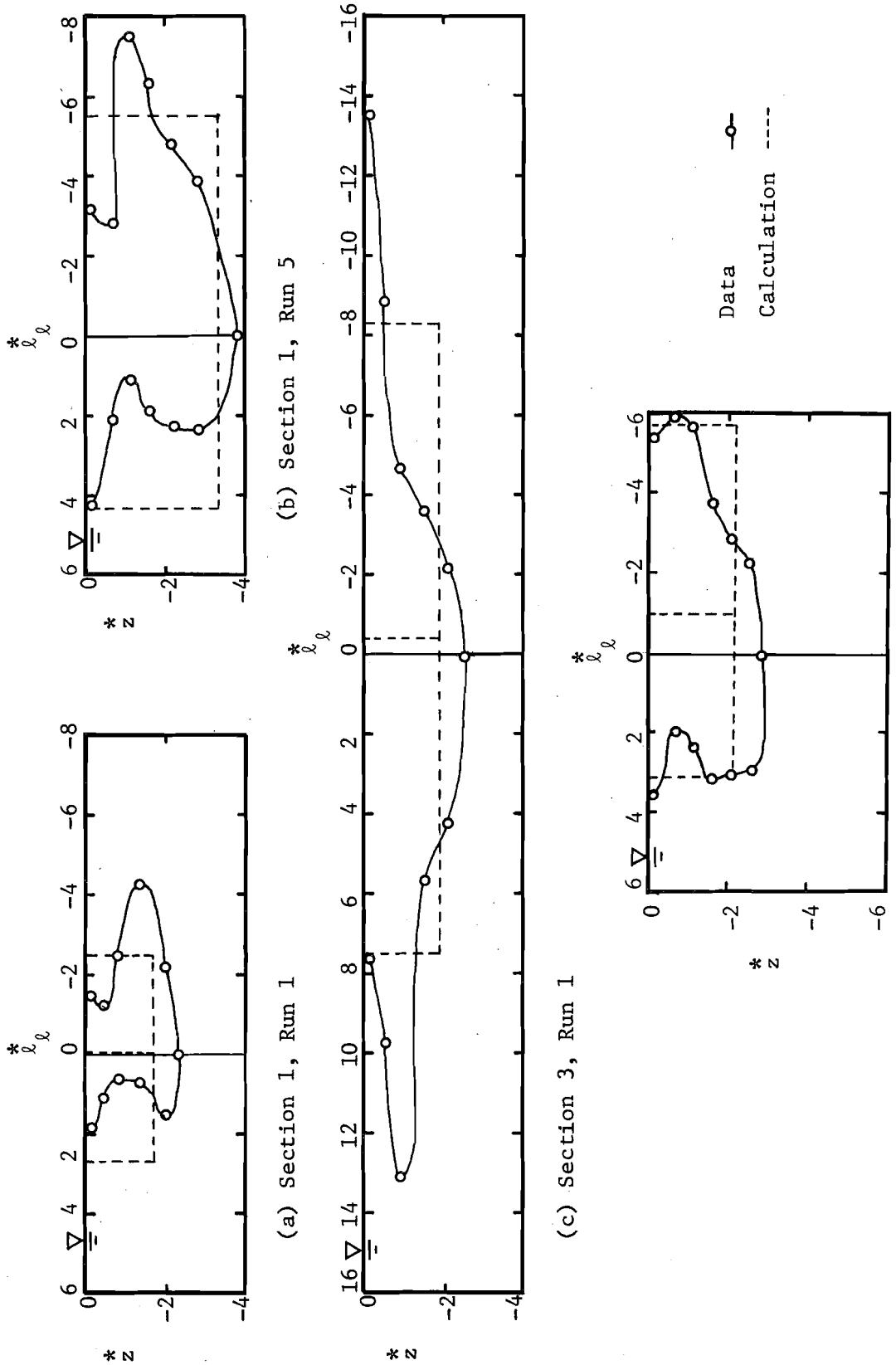

Fig. 5.32 Comparison between the computed jet boundaries and the modified experimental jet boundaries

of ambient velocity normal to the jet axis is practically zero on the right side of the jet near the exit.

The comparison between the computed and the modified experimental jet temperature boundaries shown in Fig. 5.32 (c) is typical for cross sections further downstream from the exit in Runs 1, 2, 3, 5, 6, 7 and 8. Due to buoyant spreading, a thin layer of warm water is formed on each side of the jet as shown in Fig. 5.32 (c). These thin parts of the jet have minor effects in the calculation of the coefficients because of the low temperature excess and small affected area. The optimum fitting therefore gave cross sections which were much narrower than the maximum modified experimental jet widths (which are not necessary on the surface after modification of the measured distributions). The thin parts of the jet were thus substantially disregarded in the calculations. Therefore, the calculated C_B values for Runs 1, 2, 3, 5, 6, 7 and 8 are considered to be lower than what they should be to represent the total width.

On the other hand, the computed jet widths agree much better with the maximum modified experimental jet widths at cross sections further downstream from the exit in Runs 4, 10 and 11, which have the lowest velocity ratios (u_o/u_a) among the runs with the same F_o. This behavior can be explained as follows: Strong crossflow greatly restricts the lateral buoyant spreading of the jet in the downstream part of the NFR, as can be seen by comparing the observed jet widths of the various runs with the same F_o but with different R values. As a consequence, the thin parts of the jet which cause the inaccuracies in the prediction of the widths for the cases discussed above were relatively small for Runs 4, 10 and 11. Thus, the model satisfactorily predicted the jet

widths of Runs 4, 10 and 11 and the calculated C_B values for these runs were close to unity, were in general agreement with the approximate value of C_4 quoted in Section 5.3.3.3, and were higher than the values for other runs with higher velocity ratios. Figure 5.32(d) shows an example of good agreement between the computed jet widths and the maximum modified experimental jet widths.

As 1/R approaches zero, the lateral buoyant spreading will no longer be subjected to the restriction imposed by the ambient flow. Thus thin parts of the jet are formed to the full extent, but are practically ignored in the calculations of the C's. This is probably why the calculated C_B values indicate that C_B approaches zero for no crossflow cases (Section 5.3.3.3).

In Runs 1, 4-8 and 10-11, at the locations where jet curvatures are significant (usually around cross sections 1 and 2), both the calculated and the experimental jet boundaries show a significant increase on the rate of spreading on the lee side of the jet. This confirms the results obtained in Section 3.3.2.5 that when jet curvature is large, significant lateral spreading will occur.

5.4.2.3 Jet Depths

The model successfully predicts the jet depths for Runs 1, 2, 3, 5, 6 and 7. However, there are large differences between the computed and the measured jet depths for Runs 4, 8, 10 and 11. The discrepancies between the computed and the measured jet depths follow a definite trend; they increase with decreasing F_o and velocity ratio R. The discrepancies could be due to the improper formulation of Eq. 3.85 for $dh/ds\big|_v$ which involves the local Froude number and the velocity ratio. In Eq. 3.85,

$EXP(-5/F_r^2)$ and $(u_m-u_c)/(u_m+u_c)$ were introduced to account for the reduction in the vertical spending due to density differences and ambient flow, respectively. The exponential term ($EXP(-5/F_r^2)$) was derived from the experimental data for two-dimensional surface buoyant jets discharged into non-flowing ambient fluids [Ellison and Turner, 1959], while $(u_m-u_c)/(u_m+u_c)$ was obtained for coflowing cases [Abramovich, 1963]. Apparently the reduction of the vertical spreading due to the combined effects of density differences and crossflow was not properly represented by the use of the product of $EXP(-5/F_r^2)$ and $(u_m-u_c)/(u_m+u_c)$.

The characteristic velocity used in F_r in $EXP(-5/F_r^2)$ was u_m instead of the maximum velocity excess (u_m-u_s). When (u_m-u_s) was used as characteristic velocity in F_r, the jet depth decreased rapidly after the jet had reached its maximum depth. This was not in agreement with the measurements. The use of u_m in F_r gave a longer persistence of nearly constant jet depth after the maximum depth was reached. It is not entirely clear what the mechanisms are that are responsible for maintaining an essentially constant jet depth in the presence of buoyant spreading of the jet downstream of the point of maximum depth. The questionable definition of F_r may have helped to compensate for the inaccuracies in Eq. 3.85 or for the effects of ambient turbulence. Further discussion of ambient turbulence is given in the next section.

5.4.2.4 Maximum Temperature Decay

The predictions of maximum temperature decay are best for runs with $F_o \approx 15$, i.e., Runs 2, 6, 7 and 10. The discrepancies in the predictions of jet widths and depths are naturally related to the predictions of maximum temperature decay. Furthermore, the assumed similarity profile

is a specific factor which invariably caused deviations between the measured and computed maximum temperatures. In the optimal fittings of vertical temperature profiles (Section 5.2.2), it was found that the measured maximum surface temperature excess at each cross section was generally about 0.5 to 1.0C^{o} higher than ΔT_m at the surface computed from Eq. 5.6. The predictions of the maximum temperature decay could probably be improved, by using a different similarity function for the temperature profiles.

In the model development, it was assumed that the velocity difference between the jet and the ambient flow and the associated entrainment and turbulent mixing were the only mechanisms responsible for reducing maximum temperature. Therefore, as u_m approached u_s, the velocity difference and the associated mechanisms approached zero. The result was the flattening of the computed maximum temperature decay as illustrated in Figs. 5.22-5.31, particularly for runs with low F_o and R. The log-log plots of the measured ΔT_m^* versus s^*, however, show no sign of flattening within the range the measurements. Experimental results obtained by Weil and Fischer [1974] and Shirazi et al. [1974] have shown that increases in ambient turbulence can significantly increase the rate of decay of the maximum temperature. Ambient turbulence diffusion is not included in the present model and may be responsible for the rate of temperature decay being higher than the model predicts. As mentioned previously, the ambient turbulent diffusion may also contribute to the jet remaining at nearly constant depth downstream of the point of maximum depth.

5.4.2.5 Core Region

Extrapolation of the data on Fig. 5.20 to $\Delta T_m^* = 1$ shows that the end of the core is at approximately $s^* = 3$ to 5. The model computations showed that the end of the NFR to be at s^* as small as 10, with the length of the NFR increasing with increasing R and F_o. Thus, it can be seen that the core may occupy a significant portion of the NFR and should therefore be included in the analysis.

6. CONCLUSIONS AND RECOMMENDATIONS

Analytical and experimental investigations of three-dimensional buoyant surface jets discharged into strong crossflow with no boundary attachment have been carried out. Detailed temperature distributions were measured for a range of values of F_o, the initial densimetric Froude number, and R, the ratio of the initial jet velocity to the average ambient velocity. All measurements were made for a square (1 in. by 1 in.) jet discharging at 90^o to an ambient flow which was 0.77 ft deep. The various conditions investigated are summarized in Table 4.1. For each run, approximately 200 individual temperature measurements were made at each of four cross sections approximately normal to the jet trajectory. A numerical model was developed based on an integral jet analysis modified for buoyancy effects. The model is similar to previous models in some respects; however, because of the expected behavior of jets discharged into relatively high-velocity crossflows in rivers, the present model was developed in curvilinear coordinates to account for rapid curvature of the jet trajectory and the model included asymmetry of the velocity and temperature profiles in the jet. In addition, the representation of buoyant spreading has been modified somewhat from previous studies. The model does not consider boundary attachment of the jet.

The results obtained in various phases of this study lead to the following conclusions:

1. Ambient crossflows cause significant distortion on the jet temperature distributions, even for the case with R = 13. Therefore, the usual assumption of symmetrical temperature distributions for small crossflow cases may not be valid.

2. The component of ambient velocity normal to the jet axis greatly restricts the spreading of the outer (upstream) part of the jet. At cross sections near the exit, inner (downstream) widths are much larger than outer widths. At cross sections further downstream from the exit where the component of ambient velocity normal to the jet axis is small, the differences between the inner and outer widths are not significant.

3. At cross sections near the exit, the lower portion of the jet is swept toward the lee side of the jet and the jet becomes L-shaped. The formation of the L-shapred profile and the associated density instability could create a secondary current. This current may in turn enhance the spreading on the lee side of the jet and may contribute to the apparent tendency for the jet to divide longitudinally into two parts.

4. The analytical work predicts and the experiments verify that when the jet curvature is large, significant lateral spreading occurs.

5. The maximum thickness or depth of the jet is a function of F_o only. The maximum jet depth is equal to 0.5 F_o for the cases investigated.

6. The jet bending in the downstream direction increases as the velocity ratio decreases. Bending is also greater for jets with higher F_o, because these jets spread more vertically, creating a greater area on which pressure drag forces can act.

7. Dilution increases with increasing F_o. Dilution is also generally greater for cases with lower velocity ratios since entrainment is enhanced by the ambient crossflow.

8. Strong crossflow may produce a situation in which the magnitude of jet velocity excess has been dissipated but the density gradients are still significant, and the jet axis has not yet aligned with the

ambient flow. The jet is then accelerated in the downstream direction by the crossflow as the jet continues to become aligned with the flow.

9. By matching the observed temperature distributions to the numerical model, the empirical coefficients C_V, C_D and C_B were evaluated. In determining the coefficients, the model was fitted to all of the temperature measurements, not just to characteristics of the jet such as trajectory, width, and maximum temperature. Using the values obtained for C_V, C_D and C_B, the model is capable of predicting temperature distributions to an accuracy (standard deviation) of about $0.63C^o$ on the average.

10. The overall agreement between the computed and the measured jet trajectories, widths and depths are considered to be good. There are large differences between the computed and the observed maximum temperature excesses, primarily because the model was fitted to all of the temperature measurements and because the assumed similarity profile is not the best suited function for the actual temperature distributions.

11. Ambient turbulent diffusion apparently becomes significant as the maximum jet velocity u_m approaches the component of the crossflow velocity parallel to the jet axis, u_s.

12. It is important to include the ZFE in the analysis, particularly for the cases with low initial densimetric Froude number and low velocity ratio.

Based on the results and conclusions obtained in this study the following investigations are recommended:

1. A more representative jet cross section, such as a bell-shaped cross section, should be used in order to give better prediction of jet characteristics.

2. Similarity functions for both vertical and horizontal temperature distributions must be sought in order to improve the predictions, particularly the prediction of the maximum temperature decay.

3. Detailed study on the effect of crossflow on the jet lateral spreading and the combined effect of crossflow and density differences on the jet vertical spreading could provide better information for the formulation of jet spreading functions.

4. Effects of aspect ratio and initial discharge angle on the behavior of buoyant surface jet discharged into strong crossflow should be studied.

REFERENCES

Abraham, G., "Horizontal Jets in Stagnant Fluid of Other Density," J. of the Hydraulics Division, ASCE, Vol. 91, No. HY4, July, 1965, pp. 139-153.

Abraham, G., "Jets and Plumes Issuing into Stratified Fluid," International Symposium on Stratified Flows, Novosibirsk, 1972, Published by ASCE, 1973, pp. 4-31.

Abramovich, G. N., The Theory of Turbulent Jets, The M.I.T. Press, M.I.T. Cambridge, Massachusetts, 1963, 671 pp.

Adams, E. E., Stolzenbach, K. D. and Harleman, D.R.F., "Near and Far Field Analysis of Buoyant Surface Discharges into Large Bodies of Water," R. M. Parsons Laboratory for Water Resources and Hydrodynamics, Dept. of Civil Engineering, MIT, Report No. 205, August, 1975, 267 pp.

Albertson, M. L., Dai, Y. B., Jensen, R. A. and Rouse, H., "Diffusion of Submerged Jets," Transactions, Am. Soc. of Civil Eng., Vol. 115, 1950, pp. 639-697.

Becker, L. and Yeh, W. W.-G., "Identification of Parameters in Unsteady Open Channel Flows," Water Resources Research, 8(4), 1972, pp. 956-965.

Benedict, B. A., Anderson, J. L. and Yandell, E. L., Jr., "Analytical Modeling of Thermal Discharges: A Review of the State of the Art," Argonne National Laboratory, ANL/ES-18, April 1974, 321 pp.

Bowley, W. W. and Sucec, J., "Trajectory and Spreading of a Turbulent Jet in the Presence of a Crossflow of Arbitrary Velocity Distribution," ASME Paper No. 69-GT-33, 1969, 8 pp.

Carter, H. H., "A Preliminary Report on the Characteristics of a Heated Jet Discharged Horizontally into a Transverse Current, Part I - Constant Depth," Tech. Report No. 61, Chesapeake Bay Inst., The Johns Hopkins Univ., Baltimore, Md., November, 1969, 36 pp.

Carter, H. H., Schiemer, E. W. and Regier, R., "The Buoyant Surface Jet Discharging Normal to an Ambient Flow of Various Depths," Technical Report 81, Chesapeake Bay Institute, The Johns Hopkins University, February, 1973, 64 pp.

Chan, D.T.L., Lin, J. T. and Kennedy, J. F., "Entrainment and Drag Forces of Deflected Jets," J. of the Hydraulics Division, ASCE, Vol. 102, No. HY5, May, 1976, pp. 615-635.

Chan, T. L. and Kennedy, J. F., "Turbulent Nonbuoyant or Buoyant Jets Discharged into Flowing or Quiscent Fluids," Iowa Institute of Hydraulics Research, The University of Iowa, Rep. No. 140, 1972, 153 pp.

Chao, B. T., Advanced Heat Transfer, University of Illinois Press, 1969, 459 pp.

Corrsin, S. and Uberoi, M. S., "Further Experiments on the Flow and Heat Transfer in a Heated Turbulent Air Jet," 36th Annual Report, NACA, TP 998, 1950, pp. 859-875.

Daily, J. W. and Harleman, D.R.F., Fluid Dynamics, Addison-Wesley, 1966, 454 pp.

Dornhelm, R., Nouel, M. and Wiegel, R. L., "Velocity and Temperature in Buoyant Surface Jet," J. of the Power Division, Vol. 98, No. PO1, June, 1972, pp. 29-45.

Dunn, W. E. Policastro, A. J. and Paddock, R. A., "Surface Thermal Plumes: Evaluation of Mathematical Models for the Near and Complete Field," Argonne National Laboratory, Center for Environmental Studies, 1975, 397 pp.

Edinger, J. E. and Polk, E. M., Jr., "Initial Mixing of Thermal Discharge into a Uniform Current," Report No. 1, National Center for Research and Training in the Hydrologic and Hydraulic Aspects of Water Pollution Control, Vanderbilt Univ., Nashville, Tenn., October, 1969, 45 pp.

Ellison, T. H. and Turner, J. S., "Turbulent Entrainment in Stratified Flows," Journal of Fluid Mechanics, Vol. 6, 1959, pp. 423-448.

Engelund, F. and Pedersen, F. B., "Surface Jet at Small Richardson Numbers," J. of the Hydraulics Division, ASCE, Vol. 99, No. HY3, March, 1973, pp. 405-416.

Epshtein, A. M., "Shape of Turbulent Jet Axis in an Unbounded Horizontal Cross Flow," J. of Engineering Physics, Vol. 9, No. 4, 1965, pp. 303-306.

Fan, Loh-Nien, "Turbulent Buoyant Jets into Stratified or Flowing Ambient Fluids," Report No. KH-R-15, W. M. Keck Lab. of Hydraulics and Water Resources, Calif. Inst. of Tech., Pasadena, Calif., June, 1967, 196 pp.

Federal Power Commission, 1974 Annual Report, U.S. Government Printing Office, Washington, D.C., 1975.

Federal Register, "Proposed Effluent Limitations Guidelines and Standards," Environmental Protection Agency, Vol. 39, No. 43, Part III, Washington, D.C., March 4, 1974.

Fox, D. G., "Forced Plume in a Stratified Fluid," J. of Geophysical Research, Vol. 75, No. 33, November 1970, pp. 6818-6835.

Ger, A. M. and Holley, E. R., "Turbulent Jets in Crossing Pipe Flow," Hydraulic Engineering Series No. 30, Department of Civil Engineering, University of Illinois at Urbana-Champaign, August, 1974, 197 pp.

Harleman, D.R.F., "Stratified Flow," Section 26, Handbook of Fluid Dynamics, Edited by Streeter, V. L., McGraw-Hill Book Company, 1961.

Hinze, J. O., Turbulence, McGraw-Hill Book Company, Inc., 1959, 586 pp.

Hirst, E. A., "Analysis of Round, Turbulent Buoyant Jets Discharged to Flowing Stratified Ambients," Report 4685, Oak Ridge National Laboratory, 1971, 37 pp.

Hirst, E. A., "Buoyant Jets with Three-Dimensional Trajectories," J. of Hydraulics Division, ASCE, Vol. 98, No. HY11, November, 1972a, pp. 1999-2014.

Hirst, E. A., "Zone of Flow Establishment for Round Buoyant Jets," Water Resources Research, Vol. 8, No. 5, October, 1972b, pp. 1234-1246.

Hoopes, J. A., Zeller, R. W. and Rohlich, G. A., "Heat Dissipation and Induced Circulations from Condenser Cooling Water Discharges into Lake Monona," Dept. of Civil Engineering, University of Wisconsin, Report No. 35, 1968.

Hoult, D. P., Fay, J. A. and Forney, L. J., "A Theory of Plume Rise Compared with Field Observations," J. of Air Pollution Control Association, Vol. 19(9), 1969, pp. 585-590.

IBM Application Program, GH20-0205-4, Version III, 1970, 454 pp.

Jirka, G. H., Abraham, G. and Harleman, D.R.F., "An Assessment of Techniques for Hydrothermal Prediction," Final Report to U.S. Atomic Energy Commission, R. M. Parsons Laboratory for Water Resources and Hydrodynamics, Dept. of Civil Engineering, MIT, Report No. 203, 1975, 403 pp.

Kamotani, Y. and Greber, I., "Experiments on a Turbulent Jet in a Cross Flow," AIAA Journal, Vol. 10, No. 11, Nov. 1972, pp. 1425-1429.

Koh, R.C.Y. and Fan, L. N., "Mathematical Models for the Prediction of Temperature Distributions Resulting from the Discharge of Heated Water in Large Bodies of Water," EPA Water Pollution Control Res. Series 16130 DWO, 1970, 219 pp.

Krenkel, P. A. and Parker, F. L., "Thermal Pollution: Status of the Art," Report No. 3, National Center for Research and Training in the Hydrologic & Hydraulic Aspects of Water Pollution Control, Vanderbilt Univ., Nashville, Tenn., December, 1969.

Mih, W. C. and Hoopes, J. A., "Mean and Turbulent Velocities for Plane Jet," J. of the Hydraulics Division, ASCE, Vol. 98, No. HY7, July, 1972, pp. 1275-1294.

Morton, B. R., Taylor, G. I. and Turner, J. S., "Turbulent Gravitational Convection from Maintained and Instantaneous Sources," Proceedings, Royal Soc. of London, Vol. 234A, No. 1196, January, 1956, pp. 1-23.

Motz, L. H. and Benedict, B. A., "Heated Surface Jet Discharged into a Flowing Ambient Stream," Department of Environmental and Water Resources Engineering, Vanderbilt University, Nashville, Tenn., Report No. 4, August, 1970, 207 pp.

Newman, B. G., "Turbulent Jets and Wakes in a Pressure Gradient," Fluid Mechanics of Internal Flow, Edited by Sovran, G., Elsevier Publishing Company, Amsterdam, 1967, pp. 170-209.

Pande, B.B.L. and Rajaratnam, N., "An Experimental Study of Heated Surface Discharges into Quiescent Ambients," Department of Civil Engineering, The University of Alberta, September, 1975, 75 pp.

Pande, B.B.L. and Rajaratnam, N., "A Similarity Analysis of Heated Surface Discharges into Quiescent Ambients," Report No. HY-1975-TPR1, Department of Civil Engineering, The University of Alberta, May, 1975, 70 pp.

Paul, J. F. and Lick, W. J., "A Numerical Model for a Three-Dimensional, Variable-Density Jet," School of Engineering, Case Institute of Technology, Case Western Reserve University, Ref. FTAS/TR 73-9, 1974.

Peterson, D. E., Bailey, G. F., Engstrom, S. L., and Schrotke, P. M., "Thermal Effects of Projected Power Growth: The National Outlook," Hanford Engineering Development Laboratory, Prepared for the U.S. Atomic Energy Commission, Division of Reactor Development and Technology, July, 1973, 87 pp.

Platten, J. L. and Keffer, J. F., "Entrainment in Deflected Axisymmetric Jets at Various Angles to the Stream," University of Toronto, Mechanical Engineering Department, UTME-TP-6808, 1968.

Policastro, A. J. and Paddock, R. A., "Analytical Modeling of Heated Surface Discharges with Comparisons to Experimental Data: Interim Report No. 1," Argonne National Laboratory, Center for Environmental Studies, November 1972, 59 pp.

Policastro, A. J. and Tokar, J. V., "Heated-Effluent Dispersion in Large Lakes: State-of-the-Art of Analytical Modeling. Part 1. Critique of Model Formulations," Report No. ANL/ES-11, Argonne National Laboratory, January, 1972, 374 pp.

Prych, E. A., "Effects of Density Differences on Lateral Mixing in Open-Channel Flows," Report No. KH-R-21, W. M. Keck Lab. of Hydraulics and Water Resources, Calif. Inst. of Tech., Pasadena, Calif., May, 1970, 225 pp.

Prych, E. A., "A Warm Water Effluent Analysed as a Buoyant Jet," Sverigas Meteorologiska Och Hydrologiska Institut, Serie Hydrologi, No. 21, Stockholm, Sweden, 1972.

Rastogi, A. K. and Rodi, W., "Three-Dimensional Calculation of Heat and Mass Dispersion in Open Channel Flows," Proceedings, 3rd National Heat and Mass Transfer Conference, Bombay, December, 1975.

Reichardt, H., "Gesetzmässigkeiten der frein Turbulenz," VDI-Forschungsheft 414 (1942), 2nd ed. 1951 (as quoted by Schlichting [1968]).

Rouse, H. (ed.), Advanced Mechanics of Fluids, John Wiley & Sons, 1965, 444 pp.

Rouse, H., "Diffusion in the Lee of a Two-Dimensional Jet," 9th Congress International de Mechanique Appliquee, Vol. 1, 1957, pp. 307-312.

Rouse, H., Yih, C. S., and Humphreys, H. W., "Gravitational Convection from a Boundary Source," Tellus, Vol. 4, 1952, pp. 201-210.

Sami, S., Carmody, T. and Rouse, H., "Jet Diffusion in the Region of Flow Establishment," J. of Fluid Mechanics, Vol. 27, Part 2, 1967, pp. 231-252.

Sawyer, R. A., "The Flow Due to a Two-Dimensional Jet Issuing Parallel to a Flat Plate," J. of Fluid Mechanics, Vol. 9, Part 4, 1960, pp. 543-560.

Schlichting, H., Boundary-Layer Theory, Translated by J. Kesten, Sixth Edition, McGraw-Hill Book Company, Inc., 1968, 748 pp.

Senshu, S. and Wada, A., "Thermal Diffusion of Cooling Water into the Stratified Sea Basin," Proceedings of the 11th Congress of the International Association for Hydraulic Research, Leningard, Vol. 2, Paper No. 2.2, 1965.

Shandorov, G. S., "Calculation of a Jet Axis in a Drifting Flow," NASA-TT-F-10638, December 1966, 6 pp.

Shashidhara, N. S. and Bourodimos, E. L., "Turbulence and Diffusion Investigations in a Submerged Axisymmetric Water Jet," Water Resources Bulletin, Vol. 11, No. 1, February, 1975, pp. 77-96.

Sherenkov, I. A., Netjukhailo, A. P. and Telezhkin, E. D., "Research Investigation of Transfer Process in Two-Dimensional Stratified Flow," Proc. 14th Congress, IAHR, Paper A-26, Paris, 1971, pp. 217-225.

Shirazi, M. A. and Davis, L. R., "Workbook of Thermal Plume Prediction--Vol. 2, Surface Discharges," Environmental Protection Technology Series, U.S. Environmental Protection Agency, Corvallis, Oregon, Report No. EPA-R2-72-0056, 1974, 430 pp.

Shirazi, M. A., McQuivey, R. S., and Keefer, T. N., "Heated Water Jet in Coflowing Turbulent Stream," J. of the Hydraulics Division, ASCE, Vol. 100, No. HY7, July, 1974, pp. 919-934.

Silberman, E. and Stefan, H., "Physical (Hydraulic) Modeling of Heat Dispersion in Large Lakes: A Review of the State of the Art," Argonne National Laboratory, Center for Environmental Studies, ANL/ES-2, August 17, 1970.

Sill, S., "Studies of a Heated, Turbulent Jet in a Shallow, Bounded Waterway," Ph.D. Thesis, Virginia Polytechnic Institute and State University, Aerospace Studies, 1973, 231 pp.

Stefan, H. Bergstedt, L. and Mrosla, E., "Flow Establishment and Initial Entrainment of Heated Water Surface Jets," U.S. Environmental Protection Agency, Report No. EPA-660/3-75-014, May, 1975, 141 pp.

Stefan, H., Hayakawa, N. and Schiebe, F. R., "Surface Discharge of Heated Water," U.S. Environmental Protection Agency, Report No. 16130 FSU, 1971.

Stolzenbach, K. and Harleman, D.R.F., "An Analytical and Experimental Investigation of Surface Discharges of Heated Water," M.I.T. Hydrodynamics Laboratory Technical Report No. 135, February, 1971, 212 pp.

Stoy, R. L., Stenhouse, M. H. and Hsia, A., "Vortex Containment of Submerged Jet Discharge," J. of the Hydraulics Div., ASCE, 99, HY9, 1973, pp. 1585-1597.

Taylor, G. I., "The Transport of Vorticity and Heat through Fluids in Turbulent Motion," Proc. Roy. Soc. A135, 1932, pp. 685-705.

Vallentine, H. R., Applied Hydrodynamics, Plenum Press, 1967, 295 pp.

Vizel, Ya. M. and Mostinskii, I. L., "Deflection of a Jet Injected into a Stream," J. of Engineering Physics, Vol. 8, No. 2, February 1965, pp. 190-163.

Waldrop, W. R. and Farmer, R. C., "Thermal Plumes from Industrial Cooling Water," 24th Heat Transfer and Fluid Mech. Institute, 1974.

Water Resources Council, "The Nation's Water Resources," U.S. Government Printing Office, Washington, D.C., 1968.

Weil, J. and Fisher, H. B., "Effect of Stream Turbulence on Heater Water Plumes," J. of the Hydraulics Division, ASCE, Vol. 100, No. HY7, July, 1974, pp. 951-970.

Young, H. P. and Thompson, R. G., "Forecasting Water Use for Electric Power Generation," Water Resources Research, Vol. 9, No. 4, August, 1973, pp. 800-807.

APPENDIX I. INTEGRATED EQUATIONS OF MASS, MOMENTUM, AND THERMAL ENERGY CONSERVATION

APPENDIX II. EXPERIMENTAL DATA

Note: These two appendices were omitted from this report at the request of the Water Resources Center. The appendices were included in C. Y. Lin's 1977 doctoral thesis, "Buoyant Surface Jets Discharged into a Strong Crossflow." Copies of the thesis are available from University Microfilms International, Ann Arbor, Michigan. Copies of the appendices or punched computer cards or magnetic tape containing the temperature measurement data can also be obtained on special request by writing to the second author, E. R. Holley.

APPENDIX III

SENSITIVITY OF TWO-LAYERED STRATIFIED FLOW INTERFACE GEOMETRY TO RELATIVE DISCHARGES IN THE LAYERS

by

W. Hall C. Maxwell
Associate Professor of Civil Engineering

April, 1977

ABSTRACT

A closed form solution for the geometry of the interface between two moving fluids of different density and finite depth is obtained. Emphasis is on the arrested thermal wedge when the interface is defined in such a way that the vertically-averaged velocity in the upper layer is non-zero. There are three solution forms depending on the nature of the roots of a cubic equation. The solution is useful in a variety of situations. For example, in the analysis of arrested thermal wedges the interface is often defined so that the net discharge in the upper layer is zero. It is difficult to measure in the laboratory the low velocities that exist in the upper layer with sufficient accuracy to permit location of the interface according to this definition. The wedge is usually defined using a temperature (or density) profile and may therefore have a non-zero net discharge. The solution presented permits an assessment of the error introduced by assuming that this net discharge is negligible. It is shown that such a presumption may lead to serious error.

KEY WORDS: density stratification, fluid flow, hydrodynamics, mathematics, mechanics, stratified flow, temperature, thermal pollution, thermoelectric power generation.

NOTE: A summary of the information contained in this Appendix is available in the following publication:

W. Hall C. Maxwell, "Interface Geometry for Two-Layered Stratified Flow," Proc. ASCE, Journal of the Hydraulics Division, Vol. 103, No. HY2, Feb. 1977, pp. 183-189.

NOTATION

The following symbols are used in this appendix:

A = coefficient defined by Eq. 7.

a = coefficient defined by Eq. 22.

B = coefficient defined by Eq. 8.

b = coefficient defined by Eq. 23.

C = coefficient defined by Eq. 9.

$C_Q = q_1/q_2$

c = subscript indicating critical condition.

D = coefficient defined by Eq. 10.

E = coefficient defined by Eq. 11.

F = coefficient defined by Eq. 13.

$F_o = u_o/(gh\Delta\rho/\rho)^{1/2}$, a densimetric Froude no.

f = Darcy-Weisbach friction factor for bed.

f_i = Darcy-Weisbach friction factor for interface.

G = coefficient defined by Eq. 14.

g = acceleration of gravity.

H = coefficient defined by Eq. 15.

$h = h_1+h_2$, constant flow depth.

h_1 = depth of upper layer.

h_2 = depth of lower layer.

I = integral defined by Eq. 4.

I_1 = integral defined by Eq. 16.

I_2 = integral defined by Eq. 19.

$i = (-1)^{1/2}$

k = coefficient defined by Eq. 18.

L = coefficient defined by Eq. 21.

M = coefficient defined by Eq. 24.

N = coefficient defined by Eq. 25.

q_1 = discharge per unit width in upper layer.

q_2 = discharge per unit width in lower layer.

R = coefficient defined by Eq. 33.

S = coefficient defined by Eq. 34.

u_o = average velocity of undisturbed flow.

X = coefficient defined by Eq. 29.

x = distance along interface in downstream direction.

Y = coefficient defined by Eq. 30.

z = $1-\eta$, dimensionless depth of upper layer.

z_i = roots of Eq. 20 with $i = 1,6$

α = f_i/f

$\Delta\rho$ = difference between layer fluid densities.

η = h_2/h, dimensionless depth of lower layer.

η_c = critical value of η, satisfying Eq. 3.

ρ = density of upper fluid.

ϕ = angle defined by Eq. 36.

SENSITIVITY OF TWO-LAYERED STRATIFIED FLOW INTERFACE GEOMETRY TO RELATIVE DISCHARGES IN THE LAYERS

by

W. Hall C. Maxwell
Associate Professor of Civil Engineering

INTRODUCTION

There are several flow situations involving density difference between two different regions of fluid in which density gradients in the vertical direction are far in excess of those in the horizontal direction. Examples include a layer of warm water overlying a layer of cool water in the vicinity of a thermal power plant cooling water discharge outlet; a salt water intrusion beneath a layer of fresh water; or an oil spill on the surface of a river or stream. In developing a mathematical representation of such flows a common simplification is to schematize the flow as two distinct, homogeneous layers. This of course may be extended readily to more than two layers. In such a layered schematization the position of the interface may be defined in a variety of ways, particularly for experimental convenience. These include, for example, the position at which the density is equal to the average value for the two layers (5), the position at which the density gradient is a maximum (6), the middle of the diffusion zone (1), or the position which yields zero average velocity in an arrested layer (8). For example, in the case of an arrested wedge of warm water overlying cooler water in the vicinity of a power plant cooling water discharge outlet the interface is commonly defined such that the vertically averaged velocity in the warm upper layer is zero, unless recirculation is occurring between the power plant cooling water outlet and intake via the upper layer. In the latter case the discharges in both layers are non-zero. There are numerous other situations in which the

discharges in both layers are non-zero, for example thermally driven exchange flows (3), exchange flows as a result of differences in salt concentration (4), and buoyancy driven side-arm circulations (2) to name a few.

In the particular case of laboratory measurements of arrested thermal wedges (having no recirculation) it is generally not possible to measure the very low velocities in the arrested layer with sufficient accuracy to permit location of the interface according to the definition that the average velocity in the arrested layer is zero. Rather, because of the relative ease with which accurate temperature traverses may be made, one of the alternative definitions involving fluid density is adopted. As a consequence the vertically averaged velocity of the arrested layer of the laboratory study may be non-zero, although it will generally be quite small. It is common then to proceed to use the data in conjunction with an analytical model which assumes that the discharge is zero on the presumption that the solutions for interface geometry will be quite insensitive to small variations in the discharge coefficient based on the ratio of the discharges in the two layers. It will be shown herein that such a presumption may lead to serious error.

An additional circumstance in which there may be an interest in solutions for which discharge in the arrested layer is non-zero involves situations where an attempt is made to take into account entrainment by breaking the flow into a succession of short longitudinal reaches with small constant net discharges in the arrested layer, the discharge changing from reach to reach.

In summary then, there are a variety of situations for which there may be an interest in solutions for interface geometry when the arrested layer has a small average velocity. Of particular interest to the

laboratory researcher is the sensitivity of such solutions to errors in the determination of some of the input parameters in the laboratory. In the following the solution for two-layered stratified flow developed by Bata (1), utilizing the analysis of Schijf and Schönfeld (9) will be utilized as an aid in assessing such sensitivity.

Adapting a two-layer schematization and utilizing the analysis by Schijf and Schönfeld (9), Bata (1) showed that the interface geometry for a two-dimensional flow situation was obtained from:

$$\frac{-\frac{1}{F_o^2}\eta^3(1-\eta)^3 - (\eta-1)^3 + C_Q^2\eta^3}{\alpha(1-\eta+C_Q\eta)^2 + (1-\eta)^3}\, d\eta = \frac{f}{8}\, d\left(\frac{x}{h}\right) \qquad (1)$$

in which h_1 = depth of upper layer; h_2 = depth of lower layer, $h = h_1+h_2$; $\eta = h_2/h$; f_i = Darcy-Weisbach friction factor for the interface; f = Darcy-Weisbach friction factor for the bed; $\alpha = f_i/f$; q_1 = discharge rate per unit width in the upper layer; q_2 = discharge rate per unit width in the lower layer; $C_Q = q_1/q_2$; u_o = average velocity of the undisturbed flow upstream from the end of the arrested thermal layer; ρ = density of the upper fluid; $(\rho+\Delta\rho)$ = density of the lower fluid; $F_o = u_o/(gh\Delta\rho/\rho)^{1/2}$, a densimetric Froude number; and x is the distance measured from a fixed point to any variable point on the interface in the downstream direction.

In the determination of the interface form critical depth is defined to be that for which the tangent to the interface is normal to the channel bottom so that:

$$\frac{d(x/h)}{d\eta} = 0 \qquad (2)$$

Using the subscript c to denote the critical condition Eq. 1 then yields

$$\frac{1}{F_o^2} = \frac{C_Q^2}{(1-\eta_c)^3} + \frac{1}{\eta_c^3} \tag{3}$$

In the physically real range $0<\eta_c<1$, and for $C_Q \neq 0$, there are two critical depths for a given densimetric Froude number. The interface extends between these, the upper critical depth and the lower critical depth. Integration of Eq. 1 begins at the upper critical depth and proceeds to some intermediate value, until the limit of lower critical depth is reached. Alternatively the sign of x may be changed and the integration may then proceed in the opposite direction.

Bata (1), assuming that the resistance coefficients did not vary with x, integrated Eq. (1) for the limiting cases $C_Q = 0$ and $C_Q = 1$. The former is the arrested thermal wedge with the interface selected to give zero average velocity in the wedge. Bata (1) recommended that numerical integration of Eq. 1 be used in the range $0<C_Q<1$ because of the complexity of the general solution. However, as has been noted above there are often circumstances for which the general solution is of greater interest than the limiting cases. The purpose of the present article is to present the general solution to Eq. 1, briefly outlining the method by which it is obtained.

DERIVATION

Defining I as

$$I = \int \frac{-\frac{1}{F_o^2}\eta^3(1-\eta)^3 + (1-\eta)^3 + C_Q^2\eta^3}{\alpha(1-\eta+C_Q\eta)^2 + (1-\eta)^3}\, d\eta \tag{4}$$

and making the substitution

$$(1-\eta) = z \tag{5}$$

yields:

$$I = -\frac{1}{F_o^2}\int \frac{z^6 - 3z^5 + 3z^4 - Az^3 + 3Bz^2 - 3Bz + B}{z^3 + Cz^2 + Dz + E}\,dz \tag{6}$$

in which

$$A = 1 + F_o^2 C_Q^2 - F_o^2 \tag{7}$$

$$B = F_o^2 C_Q^2 \tag{8}$$

$$C = \alpha(1-C_Q)^2 \tag{9}$$

$$D = 2\alpha C_Q(1-C_Q) \tag{10}$$

$$E = \alpha C_Q^2 \tag{11}$$

Dividing the numerator of Eq. 6 by the denominator results in:

$$I = -\frac{1}{F_o^2}\int [z^3 - (3+C)z^2 + \{3-D+C(3+C)\}z + (3D-A-E+2CD-3C-3C^2-C^3) + \frac{F(z^2+Gz+H)}{z^3+Cz^2+Dz+E}]\,dz \tag{12}$$

in which

$$F = 3B - 3D + 3E + 2CE - 6CD + AC + D^2 - 3C^2D + 3C^2 + 3C^3 + C^4 \tag{13}$$

$$G = -\frac{1}{F}(3B + 3E - 2DE + 3CE + 3D^2 + C^2E - AD + 2CD^2 - 3CD - 3C^2D - C^3D) \tag{14}$$

$$H = \frac{1}{F}(B - 3DE + AE + E^2 - 2CDE + 3CE + 3C^2E + C^3E) \tag{15}$$

The first four terms of Eq. 12 present no difficulty and may be readily integrated. The last term requires some further consideration. Let

$$I_1 = \int \frac{3z^2 + 3Gz + 3H}{z^3 + Cz^2 + Dz + E}\, dz \tag{16}$$

$$= \int \frac{3z^2 + 2Cz + D}{z^3 + Cz^2 + Dz + E}\, dz + (3G-2C) \int \frac{z+k}{z^3 + Cz^2 + Dz + E}\, dz$$

$$= \ell n\,(z^3 + Cz^2 + Dz + E) + (3G-2C)\, I_2 \tag{17}$$

in which

$$k = \frac{3H - D}{3G - 2C} \tag{18}$$

and

$$I_2 = \int \frac{z + k}{z^3 + Cz^2 + Dz + E}\, dz \tag{19}$$

Consider now the roots of

$$z^3 + Cz^2 + Dz + E = 0 \tag{20}$$

From Ref. 7, p. 318 the nature of the roots depends on the sign of

$$L = \left(\frac{\alpha C_Q^2}{2}\right)^2 - \left[\frac{\alpha C_Q(1-C_Q)}{3}\right]^3 \tag{21}$$

Inspection of Eq. 21 indicates that L changes sign in the interval $0<C_Q<1$. For $L>0$ there is one real root and two conjugate complex roots (7)

$$\text{Let } a = D - C^2/3 \tag{22}$$

$$b = 2C^3/27 - CD/3 + E \tag{23}$$

$$M = (-b/2 + L^{1/2})^{1/3} \tag{24}$$

and

$$N = (-b/2 - L^{1/2})^{1/3} \tag{25}$$

The roots of Eq. 20, z_1, z_2 and z_3 are given by

$$z_1 = M+N - C/3 \tag{26}$$

$$z_2 = -(M+N)/2 - C/3 + i\sqrt{3}(M-N)/2 \tag{27}$$

and

$$z_3 = -(M+N)/2 - C/3 - i\sqrt{3}(M-N)/2 \tag{28}$$

in which $i = (-1)^{1/2}$

$$\text{Let } X = -(M+N)/2 - C/3 \tag{29}$$

$$\text{and } Y = \sqrt{3}(M-N)/2 \tag{30}$$

Then

$$I_2 = \int \frac{z+k}{(z-z_1)(z-X-iY)(z-X+iY)}\,dz \tag{31}$$

$$= \int \left(\frac{-2R}{z-z_1} + \frac{R(2z-2X)}{z^2-2Xz+X^2+Y^2} + \frac{2RS}{z^2-2Xz+X^2+Y^2}\right) dz$$

$$= -2R\,\ell n\,(z-z_1) + R\,\ell n\,(z^2-2Xz+X^2+Y^2) + 2RS\int \frac{dz}{(z-X)^2+Y^2}$$

$$= R\,\ell n\left(\frac{z^3 + Cz^2 + Dz + E}{(z-z_1)^3}\right) + \frac{2RS}{Y}\arctan\left(\frac{z-X}{Y}\right) \tag{32}$$

in which

$$R = \frac{1}{2}\,\frac{k+z_1}{2Xz_1 - z_1^2 - X^2 - Y^2} \tag{33}$$

$$\text{and} \quad S = \frac{(X+k)z_1 - Xk - X^2 - Y^2}{k+z_1} \tag{34}$$

For L = 0 Eq. 24 and Eq. 25 show that M=N so that Y=0 and there are three real roots of Eq. 20 given by Eqs. 26, 27 and 28 with $z_2 = z_3 = X$. Then

$$I_2 = \int \frac{z+k}{(z-z_1)(z-X)^2}$$

$$= R \ell n \left(\frac{z^3 + Cz^2 + Dz + E}{(z-z_1)^3}\right) + 2RS \int \frac{dz}{(z-X)^2}$$

$$= R \ell n \left(\frac{z^3 + Cz^2 + Dz + E}{(z-z_1)^3}\right) - \frac{2RS}{(z-X)} \tag{35}$$

For L<0, Eq. 20 will have three unequal real roots (7)

$$\text{Let } \cos\phi = \frac{-b/2}{(-a^3/27)^{1/2}} \tag{36}$$

Then the three roots of Eq. 20 are given by

$$z_4 = 2(-a/3)^{1/2} \cos(\phi/3) - C/3 \tag{37}$$

$$z_5 = 2(-a/3)^{1/2} \cos((\phi+2\pi)/3) - C/3 \tag{38}$$

$$z_6 = 2(-a/3)^{1/2} \cos((\phi+4\pi)/3) - C/3 \tag{39}$$

Thus,

$$I_2 = \int \frac{z+k}{(z-z_4)(z-z_5)(z-z_6)}\, dz$$

$$= \int \frac{(k+z_4)dz}{(z_5-z_4)(z_6-z_4)(z-z_4)} + \int \frac{(k+z_5)dz}{(z_4-z_5)(z_6-z_5)(z-z_5)} + \int \frac{(k+z_6)dz}{(z_4-z_6)(z_5-z_6)(z-z_6)}$$

$$= \frac{(k+z_4)\ \ell n\,(z-z_4)}{(z_5-z_4)(z_6-z_4)} + \frac{(k+z_5)\ \ell n\,(z-z_5)}{(z_4-z_5)(z_6-z_5)} + \frac{(k+z_6)\ \ell n\,(z-z_6)}{(z_4-z_6)(z_5-z_6)} \tag{40}$$

Finally, then, integration of Eq. 1, on the assumption that resistance coefficients and layer discharges along the reach are constant yields

$$fx/(8h) = -\frac{1}{F_o^2}\{z^4/4 - (3+C)z^3/3 + [3-D+C(3+C)]z^2/2$$

$$+ (3D-A-E+2CD-3C-3C^2-C^3)z + \frac{F}{3}\ell n\,(z^3+Cz^2+Dz+E)$$

$$+ \frac{F}{3}(3G-2C)\,I_2\} + \text{constant} \qquad (41)$$

with I_2 given by Eq. 32 when L>0, by Eq. 35 when L=0 and by Eq. 40 when L<0.

Taking into account that the sign of x will depend on the direction of integration along the interface the result shown above may, after considerable manipulation, be shown to agree with the two limiting cases C_Q=0 and C_Q=1. The former result is given as Eq. 16 in Ref. 1 and as Eq. 1 in Ref. 8. The latter result is given as Eq. 17 in Ref. 1.

The work of Polk et al (8) indicates that in practice values of α range from 0.23 up to 0.45, with variations of α not having a substantial effect on wedge length. Figure 2 of Ref. 1 indicates that if F_o is less than 0.25 a wedge will exist for C_Q = 1.0. For purposes of illustrating the sensitivity of wedge geometry to variations of C_Q in the range $0 \leq C_Q \leq 1.0$ using Eq. 41 an intermediate value of α = 0.3 and a value of F_o = 0.2 have been selected. Figure 2 shows the results for C_Q = 0, 0.2, 0.4, 0.6, 0.8 and 1.0. Evidently the sensitivity is greatest for the lower range of C_Q values. The lower range is shown in more detail in Fig. 3 with C_Q = 0, 0.05, 0.10, 0.15, 0.20 and 0.25. Finally, Fig. 4 shows C_Q = 0, 0.01, 0.02, 0.03, 0.04 and 0.05. It should be noted that the curve for C_Q = 0 was calculated using Eq. 16 in Ref. 1 and the curve for C_Q = 1.0 was calculated using Eq. 17 in Ref. 1. The curves for intermediate values were calculated using Eq. 41.

Next, the sensitivity of wedge geometry to variations of α in the range 0.20 to 0.45 for $F_o = 0.2$ and three different values of C_Q, 0, 0.1 and 0.2 was examined as illustrated in Figs. 5, 6 and 7. The sensitivity is seen to decline as C_Q increases. However, it is worth noting that the geometry does appear more sensitive to variations of α for low values of C_Q than the semi-logarithmic plotting in Figs. 11 and 12 of Ref. 8 might lead one to presume.

For completeness, the sensitivity of the wedge geometry to variations of F_o is depicted in Figs. 8, 9 and 10 for three different values of C_Q with α fixed at 0.3.

It should be noted that the fx/(8H) scales on Figs. 5, 6 and 7 are more compressed than for the other figures. Taking this into account it is clear, however, from a comparison of Figs. 4 and 5 that the wedge geometry is far more sensitive to minor variations of C_Q close to zero than it is to variations of α.

CONCLUSIONS

Equation 41 is the closed form result of integrating Eq. 1 along the interface between two fluids of different density when there is a constant net discharge in both layers and it is assumed that resistance coefficients do not vary along the interface. Equation 41 may be adapted to situations where these features vary (e.g. due to entrainment) by breaking the flow into short reaches over which these quantities may be treated as constant.

Figures 2, 3 and 4 illustrate the sensitivity of wedge geometry to minor variations of C_Q when C_Q is close to zero, particularly in comparison with the sensitivity to α shown in Figs. 5, 6 and 7. This should be of particular interest to laboratory researchers who generally find it impossible to measure the very low velocities in arrested laboratory wedges with sufficient accuracy to define the interface on the basis of zero average velocity and therefore resort to measurement of density profiles for wedge definition, assuming that C_Q will remain sufficiently close to zero to use the solution for $C_Q = 0$. Clearly the sensitivity of wedge geometry to minor variations of C_Q at values of C_Q close to zero is sufficiently high that such an assumption may result in substantial errors.

LIST OF REFERENCES

1. Bata, G. L., "Recirculation of Cooling Water in Rivers and Canals," Journal of the Hydraulics Division, ASCE, Vol. 83, No. HY3, Proc. Paper 1265, June 1957, pp. 1-27.

2. Brocard, D., Jirka, G. H., and Harleman, D.R.F., "Buoyancy-Driven Circulations in Side Arms of Cooling Lakes," Meeting Preprint 2628, ASCE National Convention, Denver, Colorado, Nov. 3-7, 1975.

3. Dick, T. M., and Marsalek, J., "Thermal Wedge Between Lake Ontario and Hamilton Harbour," Proc. 15th Conf. Great Lakes Res., 1972, pp. 536-543.

4. Holley, E. R. and Waddell, K. M., "Stratified Flow in Great Salt Lake Culvert," Journal of the Hydraulics Division, ASCE, Vol. 102, No. HY7, Proc. Paper 12250, July 1976, pp. 969-985.

5. Lofquist, K., "Flow and Stress Near an Interface Between Stratified Liquids," The Physics of Fluids, Vol. 3, No. 2, March/April 1960, pp. 158-175.

6. Majewski, W., "Laboratory Investigation on Heat Transfer in Thermally Stratified Flow," Paper A-25, Proc. Fourteenth Congress, International Assoc. for Hydraulic Research, Paris, 1971, pp. 207-216.

7. Mathematical Tables from Handbook of Chemistry and Physics, 11th ed., Chemical Rubber Publishing Co., Sept. 1960.

8. Polk, E. M., Benedict, B. A., and Parker, F. L., "Cooling Water Density Wedges in Streams," Journal of the Hydraulics Division, ASCE, Vol. 97, No. HY10, Proc. Paper 8446, Oct. 1971, pp. 1639-1652.

9. Schijf, J. B., and Schönfeld, J. C., "Theoretical Considerations on the Motion of Salt and Fresh Water," Minnesota International Hydraulics Convention, Minneapolis, Minn., Sept. 1953, pp. 321-334.

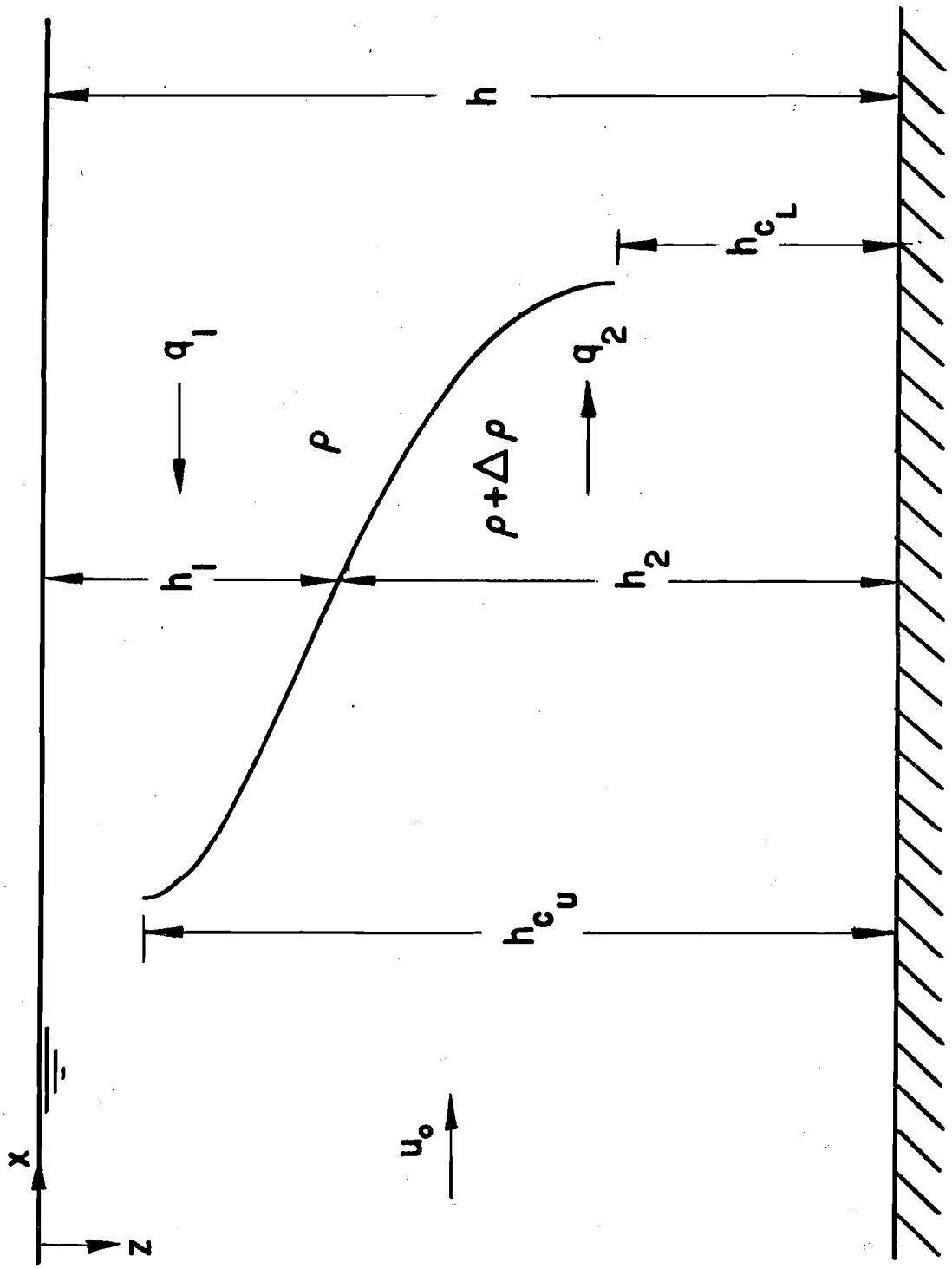

Fig. 1 Schematic View of Density Wedge

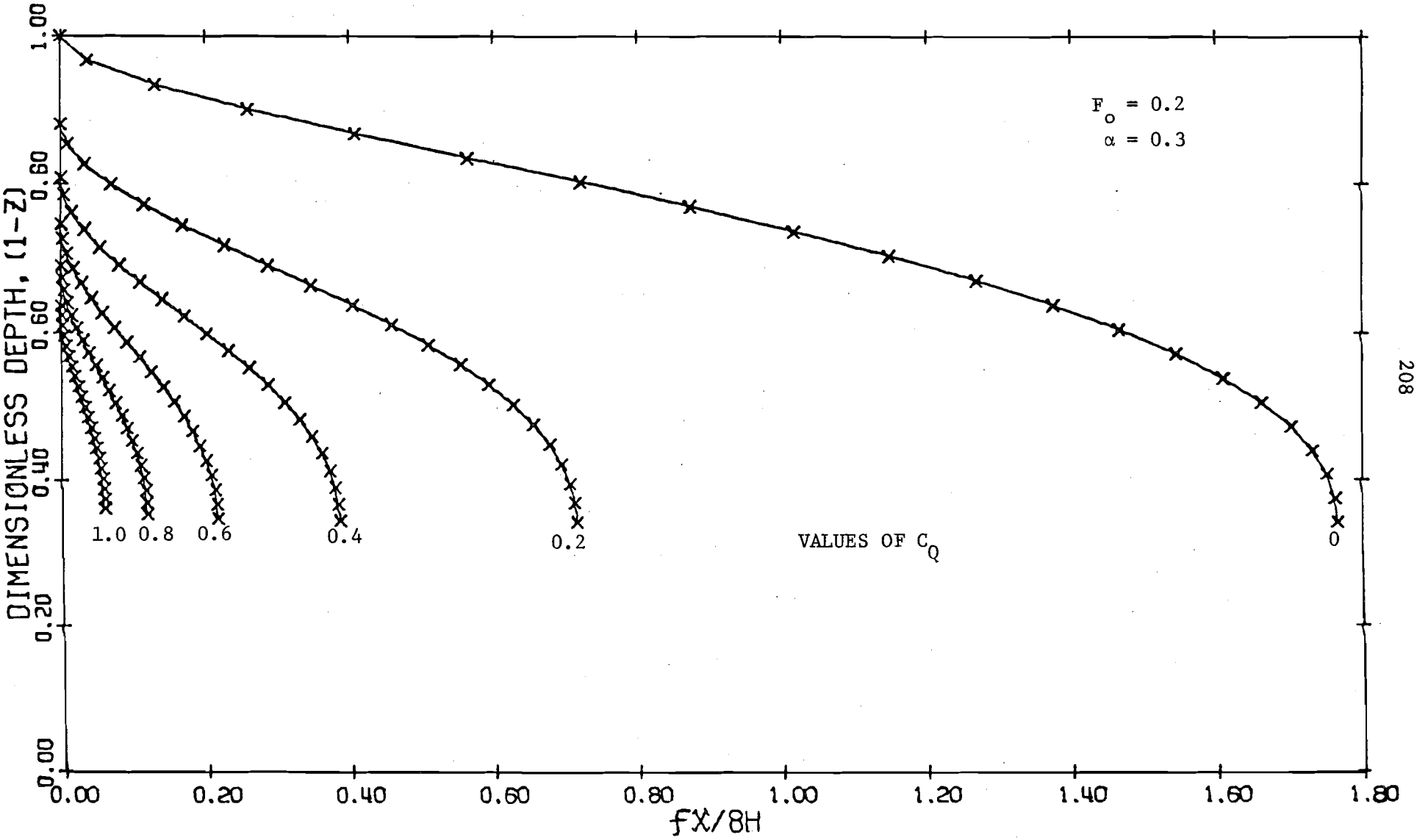

Fig. 2 Solutions for Interface Geometry for F_o = 0.2, α = 0.3 and C_Q = 0, 0.2, 0.4, 0.6, 0.8 and 1.0

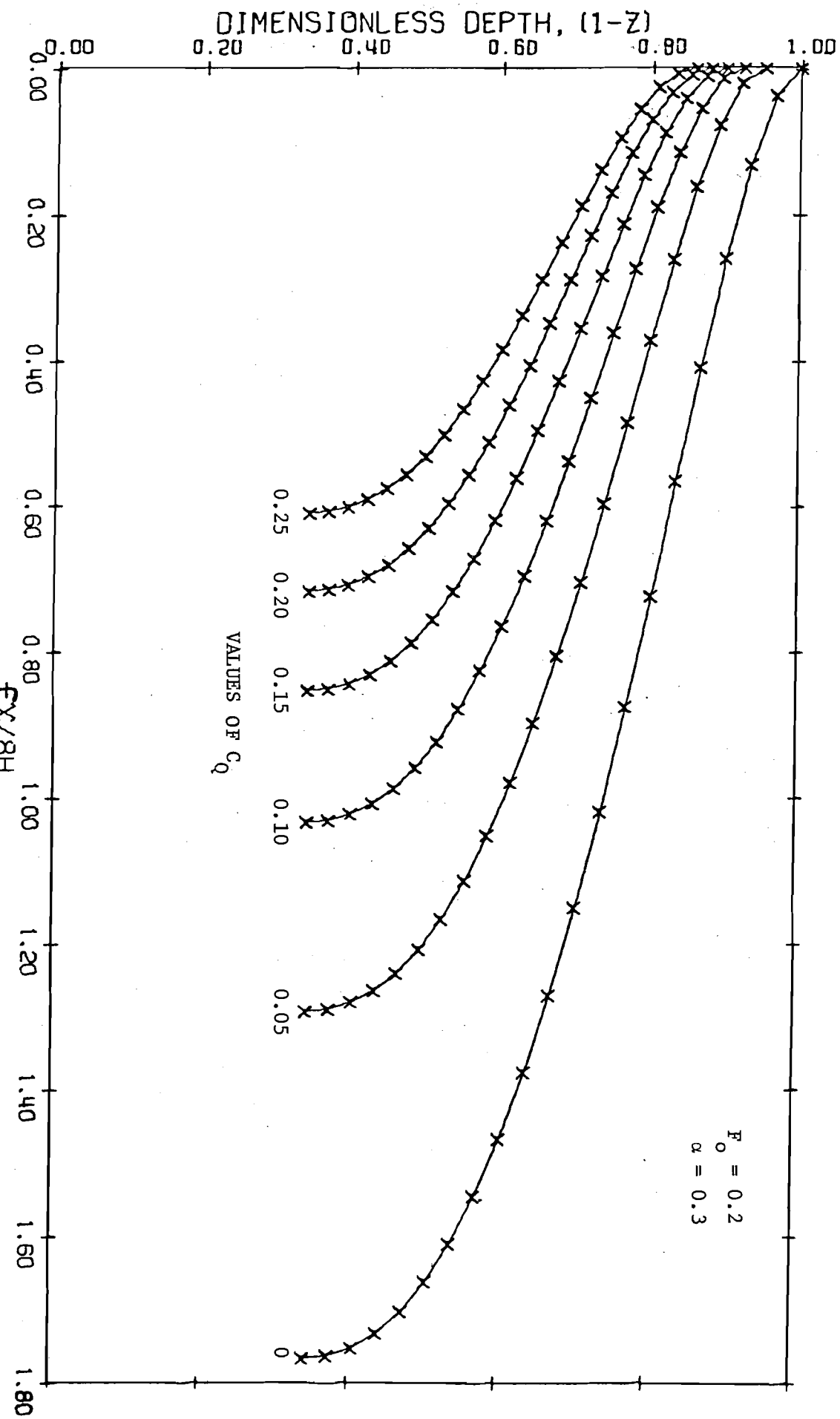

Fig. 3 Solutions for Interface Geometry for F_o = 0.2, α = 0.3 and C_Q = 0, 0.05, 0.10, 0.15, 0.20 and 0.25

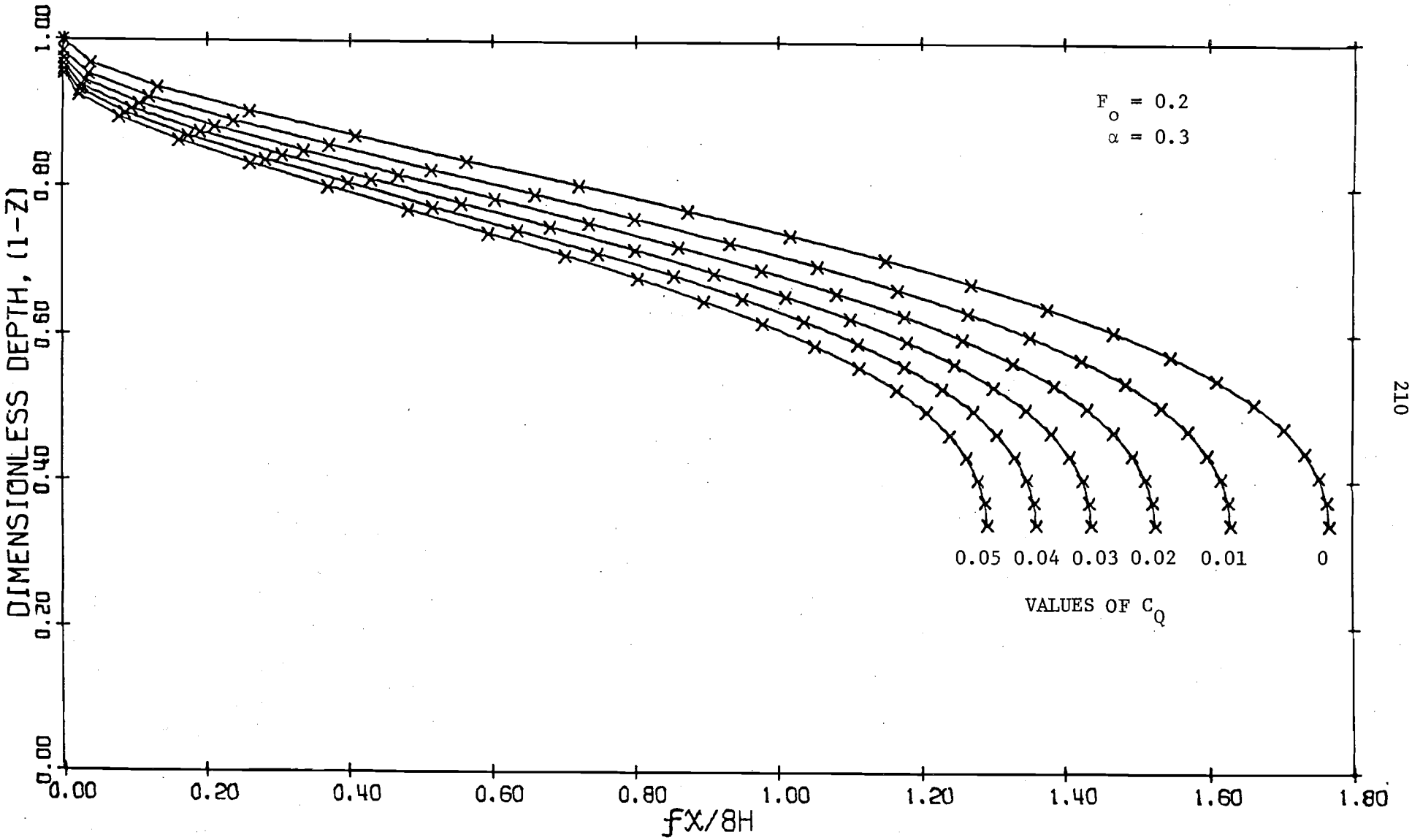

Fig. 4 Solutions for Interface Geometry for F_o = 0.2, α = 0.3 and C_Q = 0, 0.01, 0.02, 0.03, 0.04 and 0.05

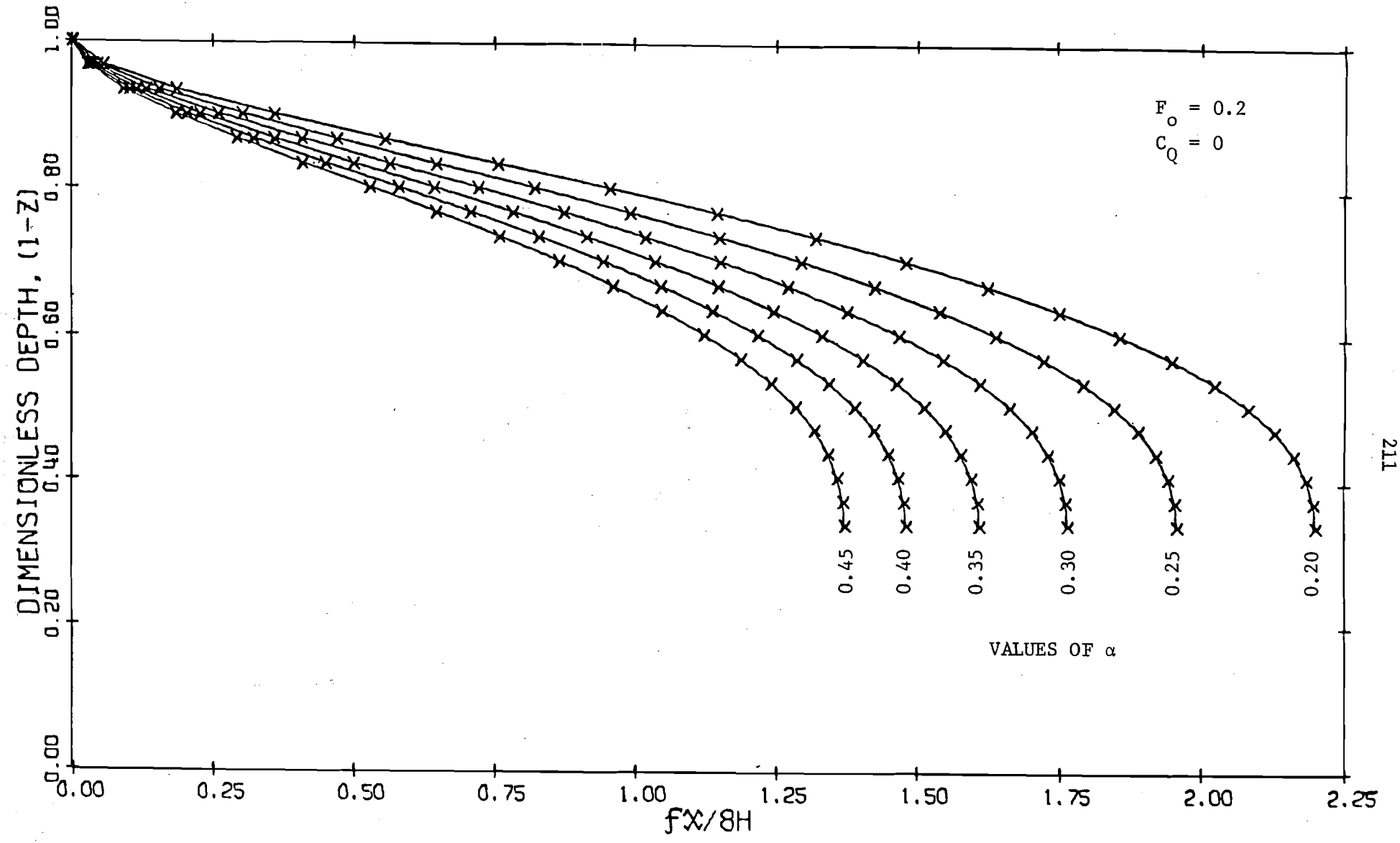

Fig. 5 Solutions for Interface Geometry for F_o = 0.2, C_Q = 0 and α = 0.20, 0.25, 0.30, 0.35, 0.40 and 0.45

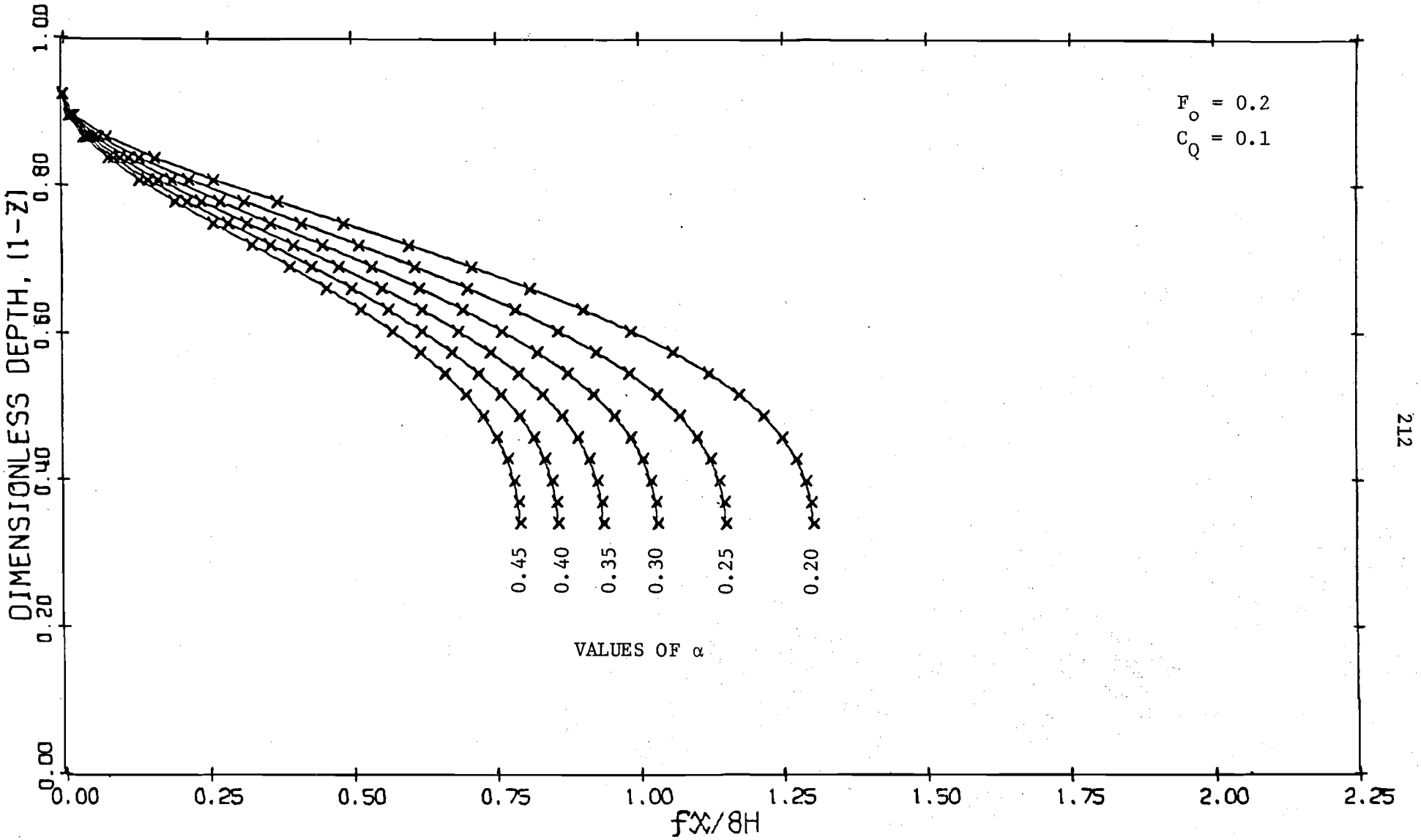

Fig. 6 Solutions for Interface Geometry for F_o = 0.2, C_Q = 0.1 and α = 0.20, 0.25, 0.30, 0.35, 0.40 and 0.45

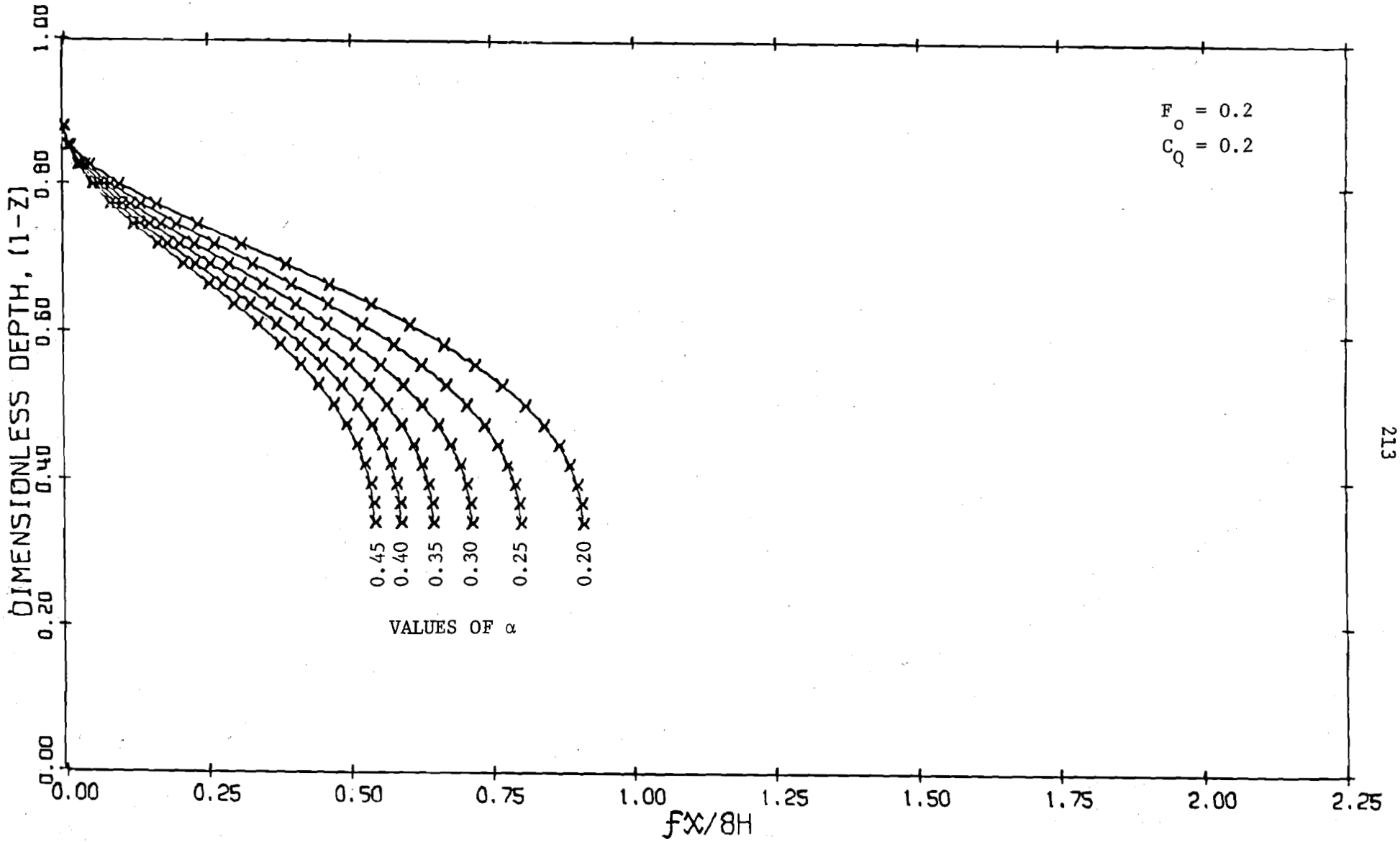

Fig. 7 Solutions for Interface Geometry for F_o = 0.2, C_Q = 0.2 and α = 0.20, 0.25, 0.30, 0.35, 0.40 and 0.45

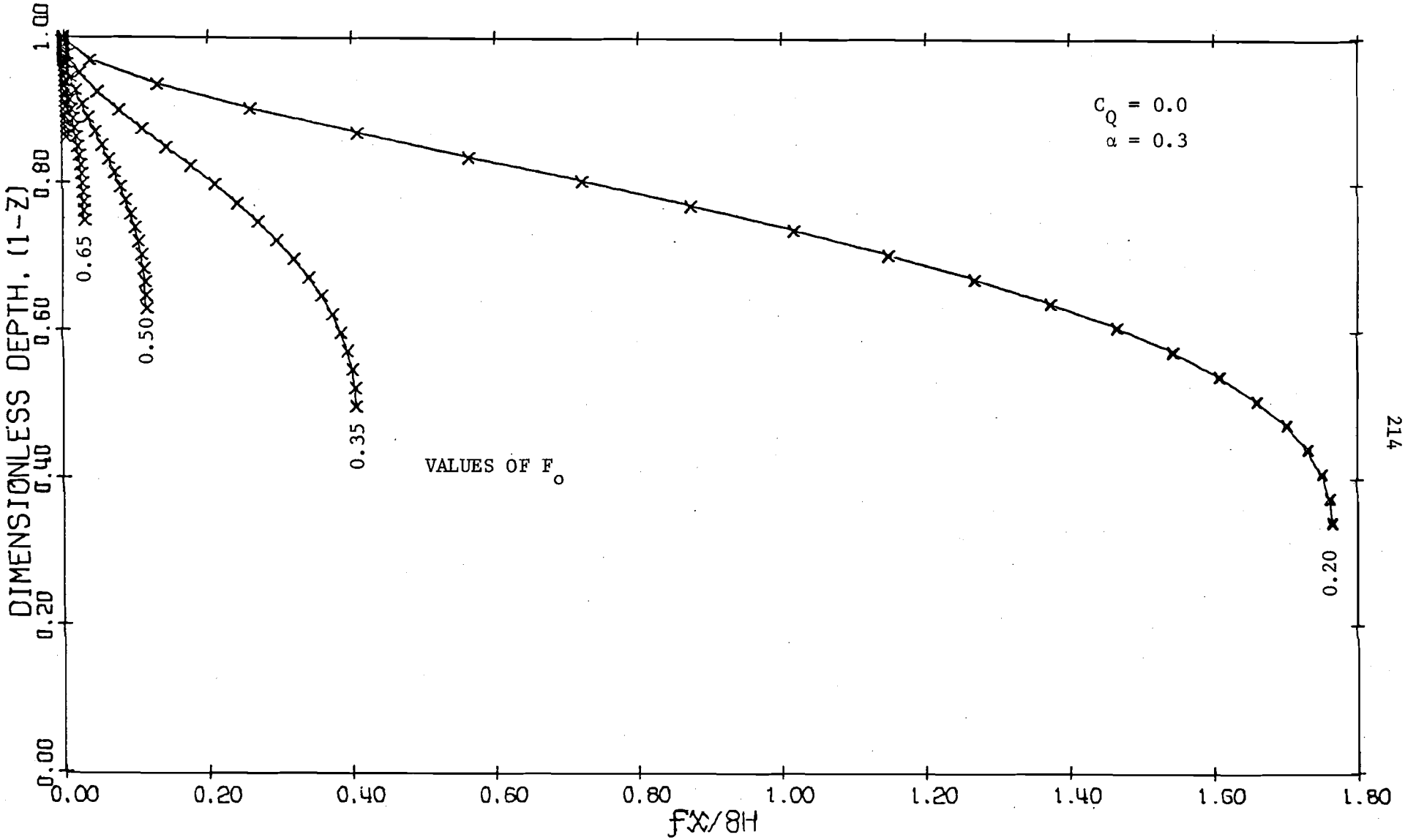

Fig. 8 Solutions for Interface Geometry for C_Q = 0.0, α = 0.3 and F_o = 0.20, 0.35, 0.50, 0.65, 0.80 and 0.95

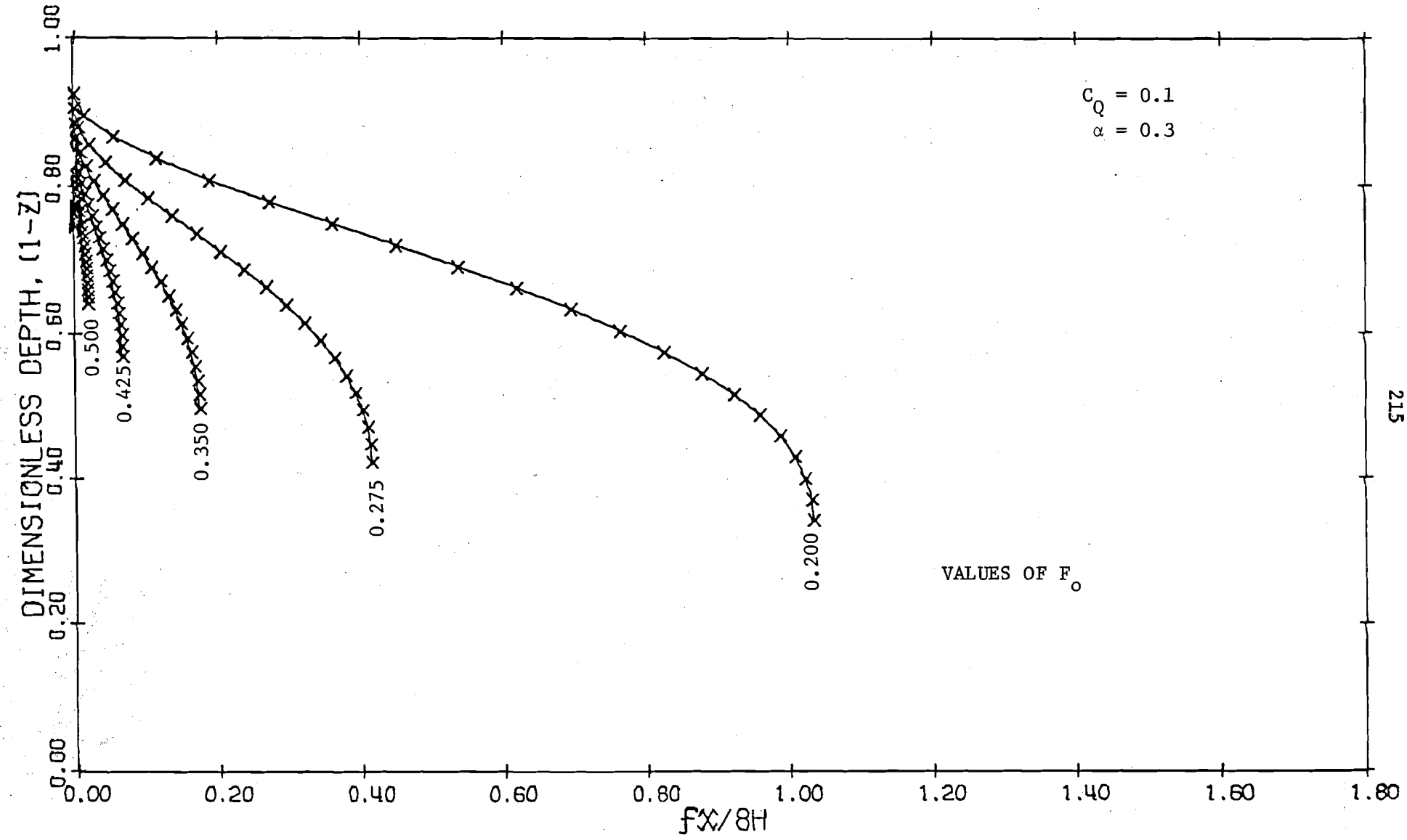

Fig. 9 Solutions for Interface Geometry for C_Q = 0.1, α = 0.3 and F_o = 0.200, 0.275, 0.350, 0.425, 0.500 and 0.575

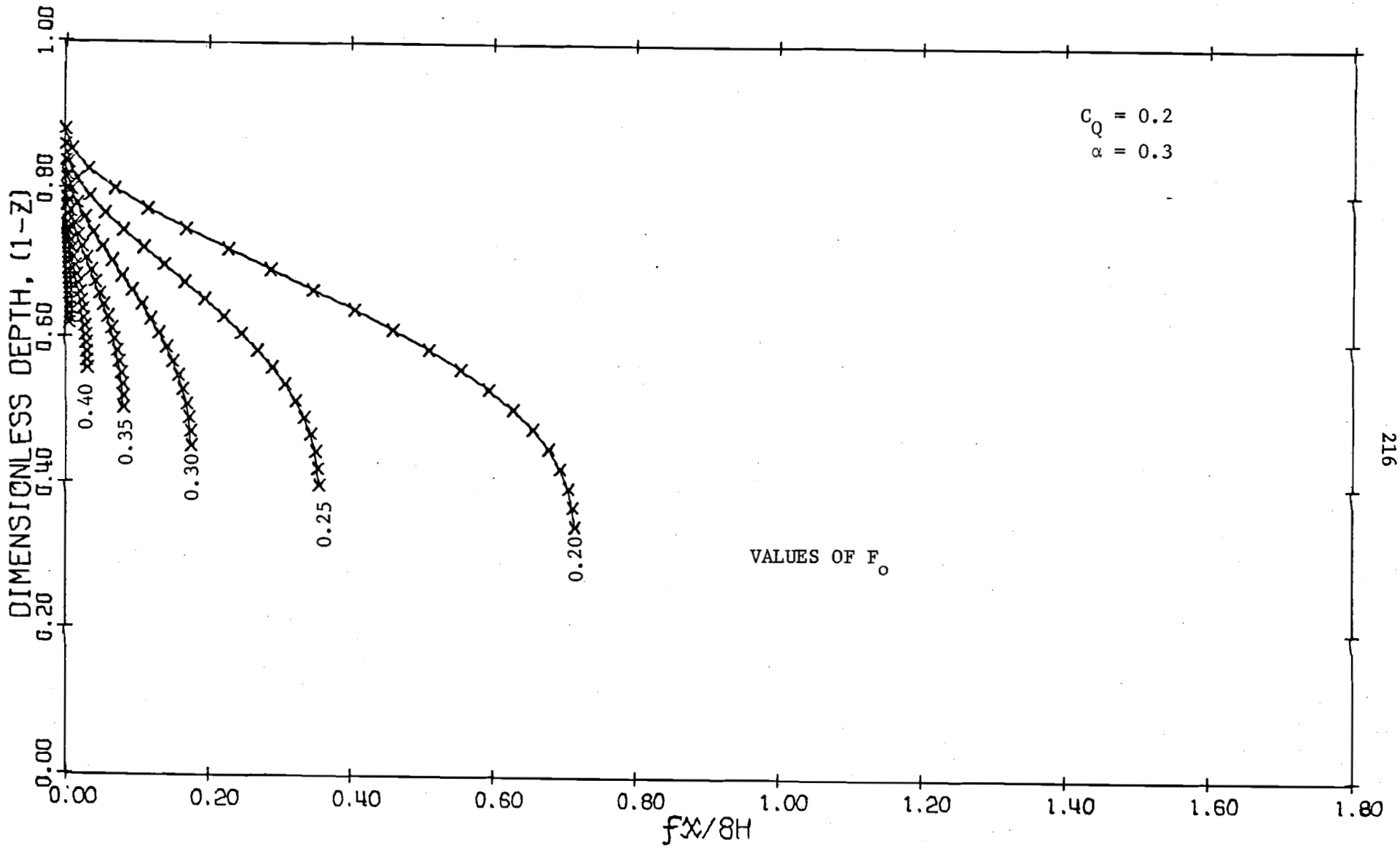

Fig. 10 Solutions for Interface Geometry for C_Q = 0.2, α = 0.3 and F_o = 0.20, 0.25, 0.30, 0.35, 0.40 and 0.45